



<https://theses.gla.ac.uk/>

Theses Digitisation:

<https://www.gla.ac.uk/myglasgow/research/enlighten/theses/digitisation/>

This is a digitised version of the original print thesis.

Copyright and moral rights for this work are retained by the author

A copy can be downloaded for personal non-commercial research or study, without prior permission or charge

This work cannot be reproduced or quoted extensively from without first obtaining permission in writing from the author

The content must not be changed in any way or sold commercially in any format or medium without the formal permission of the author

When referring to this work, full bibliographic details including the author, title, awarding institution and date of the thesis must be given

Enlighten: Theses

<https://theses.gla.ac.uk/>
research-enlighten@glasgow.ac.uk

**COILED COIL PROTEIN 1,
a novel gene downstream of FGF2
expressed in the
developing brain**

Francesca Pellicano

February 2006

A Thesis Submitted for the Degree of Doctor of Philosophy

University of Glasgow

Division of Cancer Sciences & Molecular Pathology
Faculty of Medicine, University of Glasgow
Beatson Laboratories for Cancer Research

ProQuest Number: 10753984

All rights reserved

INFORMATION TO ALL USERS

The quality of this reproduction is dependent upon the quality of the copy submitted.

In the unlikely event that the author did not send a complete manuscript and there are missing pages, these will be noted. Also, if material had to be removed, a note will indicate the deletion.



ProQuest 10753984

Published by ProQuest LLC (2018). Copyright of the Dissertation is held by the Author.

All rights reserved.

This work is protected against unauthorized copying under Title 17, United States Code
Microform Edition © ProQuest LLC.

ProQuest LLC.
789 East Eisenhower Parkway
P.O. Box 1346
Ann Arbor, MI 48106 – 1346

GLASGOW
UNIVERSITY
LIBRARY:

ABSTRACT

Fibroblast Growth Factor 2 (FGF2) plays an important role in modulating cell proliferation and differentiation in the developing central nervous system. It has been shown that FGF2 affects the transcription of several genes. In this study, a previously uncharacterised gene downstream of FGF2, named 'coiled coil protein 1' (ccp1), was identified and characterised. The expression at the tissue levels, particularly, in the brain, and cellular localization of ccp1 was investigated. In addition, functional analysis was carried out by overexpression and RNAi approaches.

Ccp1 was identified by previous microarray analysis of primary cortical neuron culture derived from mouse embryonic brains stimulated by FGF2. Microarray data showed that ccp1 was up-regulated by 2.3-fold upon FGF2 stimulation. The study in this thesis showed that FGF2 up-regulated ccp1 both at the transcript and protein levels. Ccp1 cDNA is 1697 nucleotides long and the protein size is predicted to be 180 amino acids. Bioinformatic analysis revealed ccp1 homologues in various species, including human, rat, zebrafish, and drosophila. The gene is located in mouse chromosome 1,1B and its human homolog in chromosome 2q21.2.

Next, in order to gain insight into the physiological role of ccp1 in mouse forebrains, its expression pattern was further analysed using *in situ* RNA hybridisation. Ccp1 was highly expressed early in the brain development in a ventro-lateral area of the cortex and in the specific layer of the dorsal cortex. The pattern of ccp1 expression reflects some of the aspects of the tangential and radial migration that occurs at the early stages of brain development.

A number of conserved domains are contained within the amino acid sequence of *ccp1*, including two coiled coil regions, a leucine zipper and two nuclear exporting signals (NES). These domains are related to specific protein functions and they may provide information in determining a role of *ccp1* in the cell and in animal development. Analysis of enhanced green fluorescent protein (EGFP)-tagged *ccp1* expressed in cells demonstrated that *ccp1* was localised to the cytoplasm in a punctate pattern.

Finally, *ccp1* function was investigated using a retroviral overexpression system and RNAi *in vitro*. *Ccp1* overexpression induced cell proliferation in the absence and presence of serum. Silencing of *ccp1* expression by RNAi decreased cell proliferation, which provided further evidence for the role of *ccp1* in this process. Incorporation of the S phase marker, 5-Bromo 2-Deoxyuridine (BrdU), has indicated that *ccp1* enhances G₁-S transition. To address the signalling mechanism by which *ccp1* induces proliferation, involvement of 'Mitogen-Activated Protein Kinase' (MAPK) pathway was investigated. The addition of the 'MAPK or ERK Kinase' (MEK) inhibitor, U0126, blocked cell proliferation in cells overexpressing *ccp1* in the presence of serum. The data suggested that MAPK pathway may be at least partially responsible for the *ccp1*-induced cell proliferation.

The data presented in this thesis form the bases for functional study of *ccp1 in vivo* in the future, and provides novel insights into the mechanism of cell proliferation by growth factors.

CONTENTS

ABSTRACT	ii
CONTENTS	iv
LIST OF FIGURES	x
LIST OF TABLES	xii
DECLARATION	xiii
ACKNOWLEDGEMENTS	xiv
ABBREVIATIONS	xv
CHAPTER 1	1
INTRODUCTION	1
1.1 Identification and characterization of ccpl	2
1.1.1 Preliminary microarray experiments and identification of ccpl	2
1.2 The brain development	4
1.2.1 Development of the Central Nervous System (CNS).....	4
1.2.2 Development of the cortex	5
1.2.3 Radial migration.....	5
1.2.4 Proteins expressed by cells known to migrate radially.....	7
1.2.5 Tangential migration	8
1.2.6 Proteins expressed by cells known to migrate tangentially.	9
1.2.7.Types and functions of brain cells.....	11
1.3 Fibroblast growth factors and their receptors	13
1.3.1 Gene family of FGFs and FGFRs.....	13
1.3.2 Expression of FGFRs and FGF.	14
1.3.3 Functions of FGFs and FGFRs.....	16
1.3.4 Function of FGF2 during brain development.....	20
1.3.5 FGFs and FGFRs in the brain.....	21
1.3.6 Pathologies related to FGFR mutations.....	22
1.4 Growth factor regulation of cell proliferation	25
1.4.1 Cell proliferation and cell cycle	25
1.4.2 Growth factors signalling and proliferation through MAPK pathway	26

1.4.3 Negative feedback of MAPK	28
1.5 Characteristic domains identified within ccp1 sequence and cellular compartments where ccp1 may localise.....	29
1.5.1 The coiled coil domain	29
1.5.2 The leucine zipper	32
1.5.3 The Nuclear Exporting Signal (NES).....	33
1.5.4 The endosomes lysosomes pathway	34
CHAPTER 2.....	37
MATERIALS and METHODS.....	37
2.1 Materials	38
2.1.1 Chemicals and tissue culture media	38
2.1.2 Plasmid Vectors	38
2.1.3 Ccp1 cDNA.....	38
2.1.4 Cells	38
2.1.5 Mice	39
2.2 Methods.....	40
2.2.1 Cell culture	40
2.2.1.1 Brain dissection.....	40
2.2.1.2 Primary cortical neuron culture (CNC).....	40
2.2.1.3 Immortalised oligodendrocytes progenitor culture BC30.....	41
2.2.1.4 Other cells.....	41
2.2.1.5 Cell treatment.....	41
2.2.1.6 Cell transfection.....	41
2.2.2 Preparation of DNA and RNA	42
2.2.2.1 Small scale preparation of plasmid DNA	42
2.2.2.2 Large scale preparation of plasmid DNA.....	42
2.2.2.3 Total RNA extraction from cell culture	43
2.2.2.4 Total RNA extraction from tissue.....	44
2.2.2.5 Poly A-RNA extraction from cell culture	44
2.2.2.6 Quantification of nucleic acids	44
2.2.3 Gene manipulation	44
2.2.3.1 Reverse transcriptase reaction (RT).....	44
2.2.3.2 Polymerase Chain reaction (PCR)	45
2.2.3.3 Automated DNA sequencing	46
2.2.4 Cloning techniques	46

2.2.4.1 Ligation and transformation.....	46
2.2.4.2 Identification of recombinant positive clones.....	47
2.2.4.3 TA cloning.....	47
2.2.4.4 Expression vectors construction.....	47
2.2.4.5 pdEGFP-N-ccp1, pEGFP-C-ccp1, pDsRed-N-ccp1 and pDsRed-C-ccp1 vectors construction....	48
2.2.5. Northern Blotting.....	49
2.2.5.1 Preparation of probes for Northern Blotting.....	49
2.2.5.2 Northern electrophoresis and blotting.....	49
2.2.5.3 Northern hybridisation.....	50
2.2.5.4 Stripping Northern blots.....	50
2.2.6 Multiple Tissue Northern blot.....	51
2.2.7 Western blotting.....	51
2.2.7.1 Protein quantification.....	51
2.2.7.2 Blotting and transfer.....	52
2.2.7.3 Probing and Detection.....	52
2.2.7.4 Western signal detection.....	53
2.2.7.5 Stripping Membranes to re-probe.....	53
2.2.8 Heterologous expression and purification of recombinant proteins.....	53
2.2.8.1 Expression vector construction.....	53
2.2.8.2 Transformation of BL21 (DE3)pLysS <i>E. coli</i> cells.....	54
2.2.8.3 Heterologous expression of recombinant proteins.....	54
2.2.8.4 Purification of the recombinant protein.....	55
2.2.8.5 Gel electrophoresis.....	55
2.2.8.6 Electro-elution of the protein.....	55
2.2.9 Antibody generation.....	56
2.2.9.1 Hybridoma production (Beatson antibody facility).....	56
2.2.9.2 Polyclonal antibody production.....	56
2.2.10 Cellular localisation.....	57
2.2.10.1 Cell immunostaining.....	57
2.2.10.2 Chloroquine treatment.....	58
2.2.11 Generation of stable cell lines over-expressing ccp1.....	58
2.2.11.1 Retrovirus system and vector pLPC/ccp1 construction.....	58
2.2.11.2 Retrovirus vector pLPC-ccp1/ GFP-N (GFP-C) construction.....	59
2.2.11.3 Retrovirus generation and recipient cells infection.....	59
2.2.11.4 Stable cell lines selection.....	61
2.2.12 RNA interference (RNAi).....	61
2.2.13 Functional assays.....	62

2.2.13.1 Proliferation assay.....	62
2.2.13.2 Apoptosis assay.....	62
2.2.13.3 Wound assay.....	63
2.2.13.4 Statistics.....	63
2.2.14 Histology.....	63
2.2.15 In situ Hybridization.....	64
2.2.15.1 Transcription of Riboprobes.....	64
2.2.15.2 Dot Blot Method.....	65
2.2.15.3 Hybridization.....	65
2.2.16 Immunohistochemistry.....	66
2.2.17 Microarray analysis.....	66
Table 2.6 Restriction enzymes.....	75
Table 2.7 Buffers.....	76
CHAPTER 3.....	77
RESULTS.....	77
3.1 Identification and characterization of ccp1 gene.....	78
3.1.1 Characterization of the novel gene, coiled coil protein 1 (ccp1).....	80
3.1.2 Ccp1 genomic structure and its chromosomal location.....	82
3.1.3 Ccp1 protein sequence was conserved between species.....	82
3.1.4 Primary CNC treatment with FGF2 and heparin.....	83
3.1.5 Ccp1 expression level was up-regulated upon FGF2 stimulation.....	84
3.1.6 Ccp1 was predominantly expressed in the heart and liver in adult mouse.....	86
3.1.7 Ccp1 gene encoded a protein.....	86
3.1.8 Expression of ccp1/His fusion protein as an antigen.....	87
3.1.9 Purification of the ccp1/His fusion protein.....	89
3.1.10 Generation of antibodies against ccp1.....	90
3.1.11 Ccp1 polyclonal antiserum was not suitable for immunocytochemistry.....	91
3.2 Ccp1 expression during brain development.....	93
3.2.1 Ccp1 transcript was detected in all regions of the embryonic brain.....	94
3.2.2 Expression of ccp1 in the adult brain.....	94
3.2.3 Expression pattern of ccp1 in the embryonic brain.....	95
3.2.4 Ccp1 may follow the radial migration.....	95
3.2.5 Ccp1 may follow tangential migration.....	96
3.3 Cellular localisation of the ccp1 protein.....	98

3.3.1 Ccp1 was localised to cytoplasmic vesicles when transiently expressed as a Myc-tagged fusion protein.	98
3.3.2 Ccp1 protein transiently expressed with fluorescent protein-tags was also localised to cytoplasm and showed vesicular structure.	100
3.3.3 Chloroquine treatment indicated that ccp1 was localised to lysosomes.	101
3.3.4 Expressed ccp1 did not localise in endosomes or autophagy vesicles.	101
3.3.5 Transiently expressed ccp1 localised to lysosomes.	102
3.3.6 Ccp1 positive vesicles did not co-localise with cytoskeletal components.	103
3.3.7 Generation of cell lines stably expressing ccp1 by retrovirus system.	104
3.3.8 Stably expressed ccp1 was localised to the cytoplasm and to the nucleus.	106
3.3.9 Putative nuclear exporting signal (NES) domains might affect ccp1 cellular localization.	107
3.4 The function of ccp1 <i>in vitro</i>	109
3.4.1 Cellular ccp1 overexpression caused morphological changes.	109
3.4.2 No significant change in wound healing closure was observed in MEF stably expressing ccp1.	110
3.4.3 Ccp1 stable expression induced an increase in cell number.	110
3.4.4 No significant change in apoptosis was observed in MEF stably over-expressing ccp1.	111
3.4.5 Ccp1 promoted BrdU incorporation in MEF and SK-N-SH cells.	112
3.4.6 BrdU incorporation was inhibited when ccp1 expression was knocked down by RNAi in SK-N-SH cells.	112
3.4.7 MEK inhibitor, U0126, inhibited the ccp1-induced cell proliferation.	113
3.4.8 Effects of growth factor stimulation on ccp1-induced cell proliferation.	115
3.4.9 Levels of ERK phosphorylation in ccp1 expressing cells in the presence and absence of FGF2 stimulation.	116
3.4.10 Sprouty, a negative regulator for MAPK pathway, was up-regulated in ccp1-positive MEF. ..	117
CHAPTER 4	119
CONCLUSIONS and DISCUSSION	119
4.1 Conclusions	120
4.2 Discussion	123
4.2.1 Ccp1 function in relation to its cellular localisation and domains in the amino acid sequence.	123
4.2.1.1 Coiled coil regions in ccp1	123
4.2.1.2 The leucine zipper domain in ccp1	124
4.2.1.3 NES in ccp1	125
4.2.1.4 FGF signalling and ccp1 in vesicle compartments.	126
4.2.1.5 Phosphorylation and myristoylation sites in ccp1.	127

4.2.2 Ccp1 induces cell proliferation <i>in vitro</i>	128
4.2.2.1 Reorganisation of the cellular cytoskeleton	128
4.2.2.2 Regulation of the cell cycle.....	129
4.2.2.3 Signalling involved in the proliferative effect of ccp1.....	130
4.2.2.4 Regulation of MAPK signalling	132
4.2.3 Ccp1 in the brain	134
4.2.3.1 Effect of ccp1 in progenitor proliferation	134
4.2.3.2 Function of ccp1 in post-mitotic cells.....	136
4.3 Future research direction	137

REFERENCES

PUBLICATIONS

LIST OF FIGURES

- Figure 1.1 Selection of the genes of interest.
- Figure 1.2 The ERK/MAPK cascade and the negative-feedback
- Figure 1.3 Dimerization, autophosphorylation and signalling mechanism of receptor tyrosine kinase
- Figure 2.1 Plasmid map of pCR II-ccp1 4.0 vector
- Figure 2.2 Plasmid map of pcDNA4-ccp1/Myc-His,C and of pET28b -ccp1/His vectors
- Figure 2.3 Plasmid map of pEGFP-ccp1/EGFP-C1, pd2GFP-ccp1/EGFP-N1 and pDsRed-ccp1/Red-N1 vectors
- Figure 2.4 Plasmid map of pDsRed-ccp1/Red-N1 vector
- Figure 2.5 Plasmid map of pLPC-ccp1 vector
- Figure 3.1.1 Selection of the genes of interest.
- Figure 3.1.2 The nucleotide sequence of ccp1 and its predicted protein sequence
- Figure 3.1.3 Schematic view of the ccp1 gene structure and protein product
- Figure 3.1.4 Comparison of ccp1 primary structure across species
- Figure 3.1.5 Cortical neuron culture was treated with different concentration on FGF2.
- Figure 3.1.6 Ccp1 was up- regulated upon FGF2 treatment.
- Figure 3.1.7 Ccp1 expression in adult mouse tissues
- Figure 3.1.8 Construction of pcDNA4- ccp1/Myc(His) vector
- Figure 3.1.9 Ccp1/Myc fusion protein was expressed as 27.6 kDa band.
- Figure 3.1.10 Characterization of ccp1 protein expressed in bacteria
- Figure 3.1.11 Purification of the expressed ccp1/His protein
- Figure 3.1.12 Characterization of ccp1 polyclonal antiserum
- Figure 3.1.13 Polyclonal and monoclonal antibody.

- Figure 3.1.14 Ccp1 polyclonal antiserum did not show specificity in immunocytochemistry experiments.
- Figure 3.2.1 Ccp1 transcript was detected in all regions of the embryonic brain.
- Figure 3.2.2 Ccp1 is expressed in human and mouse adult brain.
- Figure 3.2.3 Expression pattern of ccp1 in the developing mouse brain
- Figure 3.2.4 Expression of ccp1 in the dorsal cortex
- Figure 3.2.5 Ccp1 expression in the embryonic brain was similar to those of GABAergic neurons.
- Figure 3.3.1 Transiently expressed ccp1 was localises in vesicle-like structures.
- Figure 3.3.2 Transiently expressed ccp1/Myc fusion protein was localised to cytosolic vesicles in various cell type.
- Figure 3.3.3 Fluorescently-tagged ccp1-fusion proteins localised to cytosolic vesicles.
- Figure 3.3.4 Ccp1 vesicle-like structures are disrupted by chloroquine treatment.
- Figure 3.3.5 Ccp1 did not localise in endosomes or autophagy vesicles.
- Figure 3.3.6 Transiently expressed ccp1/Myc localised to lysosomes.
- Figure 3.3.7 Ccp1 did not align with the cytoskeletal components.
- Figure 3.3.8 Stable expression of ccp1 in MEF by retrovirus approach.
- Figure 3.3.9 Ccp1 stably expressed in MEF localised mainly to the cytoplasm.
- Figure 3.3.10 Two putative nuclear exporting signals (NES) are present in ccp1 amino acid sequence.
- Figure 3.4.1 Ccp1 overexpression in MEF caused morphological changes.
- Figure 3.4.2 Wound healing closure was not induced by ccp1 expressing MEF.
- Figure 3.4.3 Ccp1 expression caused an increase in cell number
- Figure 3.4.4 Apoptosis was not induced by ccp1 in stably expressing MEF.
- Figure 3.4.5 Ccp1 induced cell proliferation in stably expressing system.
- Figure 3.4.6 Cell proliferation was inhibited when ccp1 expression was knocked down in SK-N-SH cells.
- Figure 3.4.7 Cell proliferation promoted by ccp1 was reduced by addition of MEK inhibitor.

- Figure 3.4.8 Effects of growth factor stimulation on ccp1-induced cell proliferation.
- Figure 3.4.9 Regulation of ERK1/2 phosphorylation in ccp1 expressing MEF upon FGF2 stimulation
- Figure 3.4.10 Sprouty was up-regulated in ccp1-positive MEF.
- Figure 4.1 Hypothesis of mechanism of ccp1-induced cell proliferation.

LIST OF TABLES

- Table 1.1 Expression of fibroblast growth factors in the developing central nervous system
- Table 1.2 Functions of the main FGF and FGFR family members
- Table 1.3 The major phenotypes observed in FGF and FGFR knockout mice
- Table 1.4 Genetic alterations of FGFRs in human cancers
- Table 2.1 Features of plasmid vectors and their uses
- Table 2.2 Primers and PCR conditions
- Table 2.3 Primers sequences
- Table 2.4 Details of antibodies and conditions used in the Western blotting
- Table 2.5 Details of antibodies and conditions used in the immunohistochemistry
- Table 2.6 Restriction enzymes
- Table 2.7 Buffers
- Table 3.1 List of the NCBI and Ensemble GeneBank accession numbers of the sequences used in this study
- Table 3.2 Nucleotide sequences at the exon-intron boundaries of ccp1

DECLARATION

I declare that this thesis is based upon results obtained from investigations performed by myself and that the entire thesis is my own composition. Any work other than my own has been clearly acknowledged in the text with reference to the relevant investigators and contributors. This thesis has not been previously presented, in whole or in part, for the award of any higher degree.

ACKNOWLEDGEMENTS

I would firstly like to thank my supervisor, Dr Tomoko Iwata for enabling me to undertake my PhD, for her support throughout my studentship and mainly for teaching me how to become a good scientist.

I would like to thank Rachel, who helped me a lot every day with her enjoyable mood, even when everything was going wrong.

Big thanks to Fay for her friendship and moral support.

Thanks to Suzanne, for teaching me several laboratory techniques.

Thanks to Eyal and Sue, for the helpful and interesting conversations about my project.

Thanks must go to my friends and colleagues at the Beatson Institute for Cancer Research, in particular to Claire, Francois, Alex, Blanca, Edina, Alessandra, Mercedes, Laura, Diane, Sam, Helen, Dan, Stuart, Gaby and Iain, for the help and the great laughs.

On a more personal note, thanks go to my parents and my sister Mari. They always believed in me and supported my choices.

Thanks to Vignir, for his incredible patience and for making every single day of my PhD sunnier, even in Glasgow.

Thank you

ABBREVIATIONS

A	Adenine
AA	Amino Acids
ATP	Adenosine Triphosphate
BCIP	5-Bromo 4-Chloro-3 Indolyl Phosphate
BLAST	Basic Local Alignment Search Tool
bp	base pair
BrdU	5-Bromo 2-Deoxyuridine
BSA	Bovine Serum Albumin
°C	Degrees centigrade
C	Cytosine
CC	Coiled Coil
cDNA	complementary DNA
CDS	Coding Sequence
CNC	Cortical Neuron Culture
CNS	Central Nervous System
CP	Cortical Plate
CR cells	Cajal-Retzius cells
DAB	3, 3'-Diaminobenzidine
DEPC	Diethyl Pyrocarbonate
DIG	Digoxigenin
dH ₂ O	distilled water
DIV	Day In Vitro
Dlx	Distal-less homeobox gene
DMEM	Dulbecco's Modified Eagle's Medium
DMSO	Dimethyl Sulphoxide
DNA	Deoxyribonucleic Acid
DTT	Dithiothreitol
<i>E.coli</i>	<i>Escherichia coli</i>
ECL	Enhanced Chemiluminescence
EDTA	Ethylenediaminetetraacetic Acid
EGFP	Enhanced Green Fluorescent Protein
ERK	Extracellular-signal Regulated Kinase
EST	Expressed Sequence Tag
EtBr	Ethidium Bromide
FACS	Fluorescence Activated Cell Sorting
FGF	Fibroblast Growth Factor
FBS	Fetal Bovine Serum
G	Guanine
g	gram
GABA	γ-Aminobutyric Acid
GAD	Glutamic Acid Decarboxylase
GAPDH	Glyceraldehydes-3-Phosphate Dehydrogenase
HCl	Hydrochloric Acid
HEPES	N-2-Hydroxyethylpiperazine-N'-2-Ethanesulfonic Acid
H	Hippocampus

h	hour/s
HRP	Horseradish Peroxidase
HS	Horse Serum
IgG	Immunoglobulin-G
IMAGE	Integrated Molecular Analysis of Genomes and their Expression
IPTG	Isopropyl β -D-Thiogalactoside
IZ	Intermediate Zone
kb	kilobase
kDa	kiloDalton
l	litre
LB	Luria-Bertani medium
LGE	Lateral Ganglionic Eminence
LMB	Leptomycin B
M	Molar concentration
MEK	MAPK or ERK Kinase
MGE	Medial Ganglionic Eminence
MZ	Marginal Zone
min	minute/s
mRNA	messenger Ribonucleic Acid
MW	Molecular Weight
NaCl	Sodium Chloride
NBT	Nitro Blue Tetrazolium
NES	Nuclear Exporting Signal
MAPK	Mitogen-Activated Protein Kinase
ON	Overnight
ORF	Open Reading Frame
PAGE	Polyacrylamide Gel Electrophoresis
PBS	Phosphate-Buffered Saline
PCR	Polymerase Chain Reaction
pH	negative log of hydrogen concentration
PP	Preplate
RAF	Rabbit Fibrosarcoma Protein
RAT	Ratadione
RNA	Ribonucleic Acid
RT	Reverse Transcriptase
RT	Room Temperature
SDS	Sodium Dodecyl Sulphate
sec	second/s
SP	Subplate
SSC	Sodium Chloride/Sodium Citrate
SVZ	Subventricular Zone
T	Thymine
Tbr1	T-brain-1
TBS	Tris-Buffered Saline
TBST	Tris-Buffered-Saline-Tween
TEMED	NNN'N'-Tetramethylethylenediamine
Tris	Tris-(hydroxymethyl) Aminomethane
UTR	Untraslated Region
UV	Ultra Violet
VZ	Ventricular Zone

CHAPTER 1

INTRODUCTION

1.1 Identification and characterization of ccp1

Fibroblast Growth Factors (FGFs) and their receptors (FGFRs) are proteins that have important roles in development, angiogenesis and tumorigenesis (75). FGFs regulate proliferation, differentiation and migration of cells and are expressed in many tissues and different cell types (75). A major role for FGFs has been demonstrated in embryonic brain development (89,106, 119, 157, 158). FGFs have been shown to directly affect the transcription of several genes, such as proto-oncogenes, homeobox genes, and growth factors and their receptors (74). In order to understand the molecular basis of FGFs function during the brain development, I hypothesised that a particular set of genes may be downstream of FGF2. The aim of this thesis is to identify and characterise a novel gene downstream of FGF2 that I named coiled coil protein 1 (ccp1).

1.1.1 Preliminary microarray experiments and identification of ccp1

To identify the genes downstream of FGF2 in cortical cells during embryonic development, a microarray was performed using cortical neuron culture (CNC). Microarray experiments were previously carried out in the laboratory before this PhD project had commenced. CNC were treated with FGF2 in the presence of heparin for 4 h, and the expression of the genes was compared to those in the absence of FGF2. A microscopic glass chip containing 15,247 unique cDNA clones in the National Institute of Aging (NIA) mouse 15K clone set (<http://lgsun.grc.nia.nih.gov>) was used

(276). The study showed more than 500 genes with altered expression levels after FGF2 stimulation by more than 1.5 fold (283). 324 genes were shown to be up-regulated and 225 were down-regulated. The genes were categorized with known function based on the information on the NIA gene ID list. In contrast, more than half of the identified genes did not show any homology to genes with annotation or known function. In this project, 39 genes were initially selected from the list based on the intensity of the induction, novelty of the genes, as well as their characteristics in correlation with FGF functions. Based on the interest on an uncharacterised gene, I decided to focus on only one gene, which I named *coiled coil protein 1* or *ccp1* (see Chapter 3.1 for screening details).

1.2 The brain development

1.2.1 Development of the Central Nervous System (CNS)

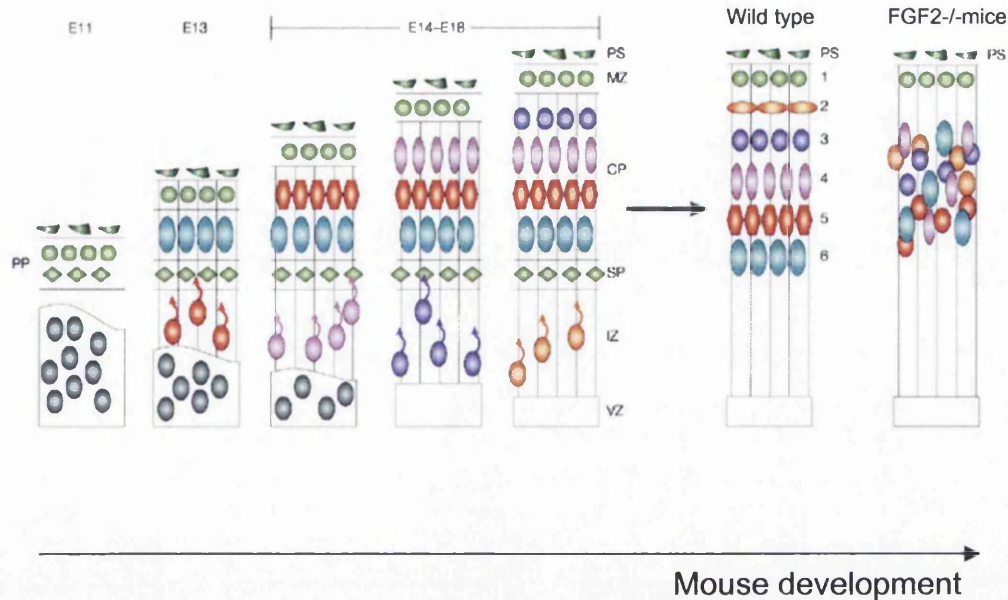
The CNS is one of the most complex organs. In vertebrates, the CNS derives from the neural plate, an epithelial region that originates from the ectoderm (1). At the end of the gastrulation, the neural plate starts to fold in itself in a process called neurulation and it forms the neural tube, a structure that is designated to give rise to the brain and the spinal cord. The rostral (front) part of the neural tubes develops into the brain and the rest of the neural tube develops into the spinal cord. The neural tube is originally constituted by three different regions, the forebrain (or prosencephalon), the midbrain (or mesencephalon) and the hindbrain (or rhombencephalon). The forebrain differentiates into secondary vesicles, consisting of the optic vesicles, the telencephalic vesicles (or telencephalon) and the diencephalon. The telencephalon will form the cerebral cortex, the basal telencephalon and the olfactory bulb, while the diencephalon will form the thalamus and the hypothalamus. The telencephalon is composed of dorsal (pallium) and ventral (subpallium) domains. The pallium is subdivided in the cerebral cortex and the hippocampus, while the subpallium is subdivided into the basal ganglia that consist in proliferative regions named medial ganglionic eminence (MGE), lateral ganglionic eminence (LGE), and caudal ganglionic eminence (CGE) (2). The LGE give rise to the striatum, while the MGE to the globus pallidus and the CGE to the amygdaloid of the limbic region. The midbrain differentiates into the tectum and, finally, the hindbrain differentiates in the cerebellum, the pons and the medulla oblongata (1).

1.2.2 Development of the cortex

The mammalian telencephalon is the seat of all higher brain functions, including the sensory and motor processing (1). It originates from a sheet of germinal cells that differentiate into neurons and glial cells at precise timing of the development. The typical laminar structure arises through a series of histogenetic processes involving neuronogenesis followed by neuronal migration. The process of cell death is also known to contribute the regulation on cortical cell number (3, 4). Cell migration is one of the important processes during the development of the CNS (1). Two types of neuronal migration identified so far are the radial and the tangential migration (5). Studies have demonstrated that some cortical neurons arise in the proliferative zone of the dorsal telencephalon (6, 7), while other neurons arise in the ventral telencephalon (8-10).

1.2.3 Radial migration

In the neocortex, the major component of radially migrating cells is a class of projection neurons that express the excitatory neurotransmitter, glutamate (5). The formation of the neocortex occurs in mice between embryonic day 11 and 18 (E11 and E18) and it is composed of six layers of neurons that have distinct morphological and functional identities (11, 12). It has been shown that cortical progenitors in the ventricular zone (VZ) undergo 11 cell cycles between E11 and E17 during neurogenesis and the timing of cell cycle exit is closely correlated to their destination in the cortical layers (13). The development of the layers involves the migration of



Adapted from Gupta *et al*, 2002

Figure 1.1 Neocortical-layer formation

The neocortical-layer formation occurs mainly by migration along radial glia. At E11, the preplate (PP) is established by a postmitotic wave of neurons that has migrated from the ventricular zone (VZ) to the pial surface (PS). By E13, a second postmitotic neuronal wave has migrated through the intermediate zone (IZ) and split the PP into the marginal zone (MZ) and subplate (SP), creating the cortical plate (CP). During E14–E18, subsequent waves of neurons expand the CP in an inside-out fashion, as each wave of neurons passes its predecessors to settle underneath the MZ. Fgf2 knockout mice show neuronal defects in the cerebral cortex. Mutant mice show a general decrease in neuronal cell number and a group of neuronal precursors fail to migrate from the place of origin to their target layers II and III. IZ, intermediate zone; MZ, marginal zone; PS, pial surface; VZ, ventricular zone. (Adapted from Gupta *et al*, 2002).

neurons at a distance from their birth-place to final destination (14, 15) (Fig 1.1). Around E11, the neocortex consists of a layer of progenitor cells. The first group of post-mitotic neurons leaves the VZ towards the pial surface of the brain forming the preplate (PP). At E13, a second group of neurons that forms the cortical plate (CP), splits the PP into the superficial marginal zone (MZ) and a deeper subplate (SP) (16). Experiments using [³H]-Thymidine-incorporation (17) have shown that layers II–VI of the cerebral cortex are produced during E14-E18 in an 'inside-out' manner, in which neurons that are generated early form the deepest layers, whereas later-born cells migrate past the existing layers and form the superficial layers. Consequently, the MZ and SP contain the earliest-generated neurons of the cerebral cortex. The SP is separated from the VZ by the intermediate zone (IZ), a layer that will eventually contain the afferent and efferent axons of the cortex (white matter). As the CP emerges, the subventricular zone (SVZ), another layer of proliferating cells, is formed between the VZ and IZ. At adult stages, the SP degenerates (1).

In the radial migration, neural progenitors migrate using the radial glia as scaffold, which have an elongated shape with processes attached between the VZ and the pial surface (3, 18). It has been reported that, when the radial glia cells stop functioning as support for new migrating neurons, they differentiate into astrocytes (19, 20). In addition, it has been shown that some neurons, especially at early stages, migrate by extending and then retiring their processes from the VZ to the pial surface independently from the radial glia, following a process called somal translocation (16, 21). Neurons following the somal translocation migrate through the IZ but they are not associated with radial glial processes. It has been hypothesised that neurons

destined to migrate radially follow (a) the somal translocation during the early stages of corticogenesis, when the cerebral wall is thin and (b) the glia-guided migration during the later stages of cortical formation, when the cerebral wall is thicker (16, 22).

1.2.4 Proteins expressed by cells known to migrate radially.

In this study, several layer markers were used to investigate migration of ccp1-positive cells in the brain. To study the radial migration, two genes expressed by projection neurons, reelin and T-brain-1 (Tbr1) were used as layer markers. These genes are important for radial migration during development (12). Mutations in their sequences have been identified to be responsible for abnormal cortical layer formation (12).

Reelin

Reelin is a protein secreted by the Cajal-Retzius (CR) cells, a group of cells located in the MZ (23). Reeler mice are naturally occurring mutants that present an autosomal recessive mutation of the reelin gene (24). These mice show abnormalities in the cortical layer formation (24). Reelin mediates its response by binding to its receptor, Very Low Density Lipoprotein Receptor (VLDLR) and ApoE Receptor 2 (ApoER2). Consequent phosphorylation of the downstream molecule Disabled1 (DAB1) is observed (25, 26). Reelin mutation in humans causes lissencephaly with cerebellar hypoplasia (LCH). Patients affected by lissencephaly present abnormal layering of the cortex, which is caused by migration defect (27, 28).

T-brain-1 (Tbr1)

Tbr1 is a transcription factor and a member of the T-box gene family (29). It is expressed by early-born cortical neurons designated to form the cortical layer VI (29). Since Tbr1 is expressed only by post-mitotic neurons, it is likely to have a role in neuronal differentiation (29). Tbr-1 mutant mice showed severe disruption of the laminar organization, a deficiency in CR cells, and hypoplasia of the olfactory bulb (30). Furthermore, Tbr1 mutant mice show abnormal organization of the cortical layers and disrupted axonal connection (31).

1.2.5 Tangential migration

A sub-set of cells that originate in the basal ganglia migrate tangentially to the developing cortex (32) (Fig 1.2). These cells constitute the class of interneurons and express the inhibitor neurotransmitter GABA (33). Interneurons arise in the subpallium, in particular in the two major regions of the basal ganglia, the LGE and the MGE (32, 34). From these regions, post-mitotic interneurons, avoiding the striatal region, migrate towards the dorsal cortex superficially to the MZ and IZ and deeply to the SVZ (8, 10, 35). Interneurons start to migrate from the MGE to reach the IZ around E12 (10). Later, a second group of cells leave the LGE (around E14) to reach the SVZ and the olfactory bulb (34, 36). Once the interneurons reach the cortex, they can also migrate radially and locate in defined layers, similar to the projection neurons (37, 38). Interneurons may move both toward and away from the VZ (35, 39). Migrating interneurons may be guided and orientated by a series of chemo-repulsive and chemo-attractive factors, whose identity and mechanism of action is

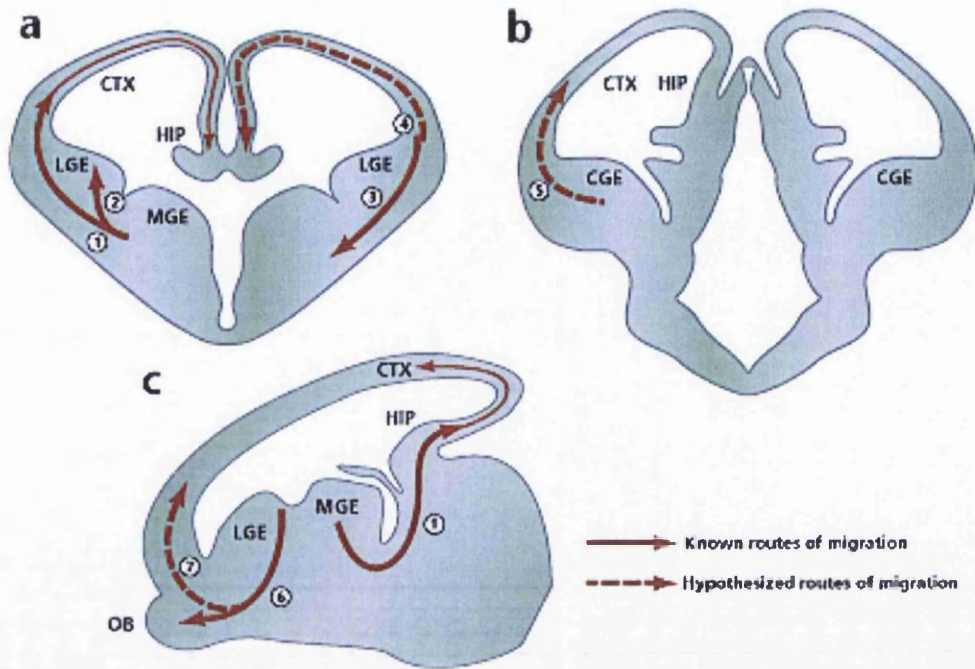


Figure 1.2 Detailed overview of the known and hypothesized routes of tangential cell migration.

The embryonic telencephalon is shown in coronal (a, b) and sagittal (c). Well characterized routes of migration are shown as a solid arrow; less well characterized routes are shown by a dashed arrow. Key to migratory routes: (1) MGE to neocortex and hippocampus (2) MGE to LGE (3) cortical-striatal boundary to ventrolateral telencephalon (lateral cortical stream) (4) LGE to neocortex and hippocampus (5) CGE to dorsal telencephalon (6) LGE to olfactory bulb (rostral migratory stream) (7) Retrobulbar region to marginal zone^{75, 76}. HIP, hippocampus.

still unclear (5). One known chemo-repulsive molecule is Slit1/2, a molecule secreted in the VZ of the basal ganglia that repels the interneurons from the subpallium towards the cortex (40). Netrin1 and the family of Semaphorin inhibit neural migration from the MGE to the cortex, creating a path between exclusion zones for migrating cells (41, 42).

1.2.6 Proteins expressed by cells known to migrate tangentially.

Several genes have been identified as being exclusively expressed by tangentially migrating interneurons. These genes are used as tools to better understand and characterise interneurons and their migration processes from the basal ganglia to the cortex. In this study, three genes, the Distal-less homeobox gene 2 (Dlx2), calbindin, and Glutamic Acid Decarboxylase 65 and 67 (GAD 65/67), were used to investigate whether ccp1 expressing cells follow the tangential migration.

Distal-less homeobox gene (Dlx)

The Dlx-homeobox gene family is a group of transcription factors. Four members (Dlx 1, 2, 5 and 6) are specifically expressed by interneurons and their precursors (8, 43). Dlx1/2 is expressed at E11-12 in the progenitor cells of the LGE and MGE (34, 43). Dlx1/2 is later found in the dorsal region of the cortex. Dlx1 and Dlx2 show similar expression patterns in the forebrain (43). Dlx2-knockout mice do not show any significant brain phenotype (44), suggesting a redundant effect by the Dlx family members. In mice lacking both Dlx2 and Dlx1, late born neurons do not differentiate and interneurons fail to migrate from the basal ganglia to the cortex (8). This effect results in the accumulation of tangentially migrating neurons in the VZ of the basal

ganglia and a decrease of the GABAergic neurons in the dorsal cortex, hippocampus and olfactory bulb (30, 34, 45).

Calbindin

Calbindin is a member of the calmodulin superfamily of calcium binding proteins (CBP) (46). The main function of calbindin in rat dorsal root ganglion neurons is to buffer calcium levels and to protect cells from degeneration and excito-toxicity (47). Calbindin is a well-known marker for mature GABAergic neurons (48). At E12.5, the calbindin positive-cells localise to the mantle of the MGE and the developing cortex (49).

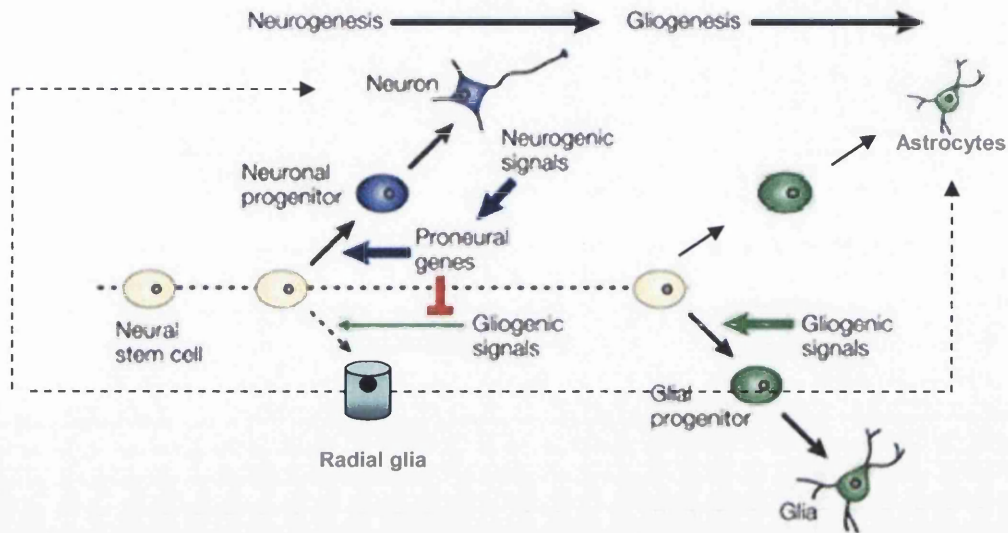
Glutamic Acid Decarboxylase 65 and 67 (GAD 65/67)

GAD is an enzyme that synthesizes the inhibitory neurotransmitter, GABA, from L-glutamate, and therefore it is a marker for GABAergic interneurons (50-52). In the adult brain, GAD exists in two major isoforms, GAD65 and GAD67, named according to their molecular masses (50). GAD65 is a membrane protein whereas GAD67 is soluble and distributed in the cytoplasm (53). GAD65 is the predominant GABA synthetic enzyme in rat and mouse brains (54), whereas GAD67 is the major form in the human brain (55). *In vitro*, GABA is known to inhibit DNA synthesis and to affect migration and neurite outgrowth (56-58). Knockout mice for GAD65 have been generated (59). Brain abnormality was not observed in the GAD65 knockout mice, probably due to compensation from GAD67 (59). Mutant mice lacking both GAD65 and GAD67 die immediately after birth due cleft palate, however, the embryonic brain did not present any abnormalities (60).

1.2.7 Types and functions of brain cells

The developing forebrain consists of different type of cells that are usually classified into two categories, neurons and glia. Function of neurons is to receive, conduct, and transmit impulses in the nervous system. Glial cells are subdivided into radial glia, astrocytes and oligodendrocytes. Glial cells are more abundant than neurons: they constitute 90% of the brain's substance. Of these cells, the astrocytes are the most numerous (1). Radial glia cells function as scaffolding during the radial migration of neurons. As discussed earlier, neurons have been shown to attach to radial glial fibres and to slide along these fibres (3). Radial glial also function as neural progenitors (19). Astrocytes are star-shaped cells that provide physical and nutritional support for neurons. Astrocytes have been considered the as 'brain glue', providing an inert scaffold necessary for neuronal distribution and interactions. They also regulate the chemical content of extra-cellular space (1). It has been shown that astrocytes express voltage-gated channels suggesting an involvement in intercellular communication (61). Finally, oligodendrocytes provide the insulation to neurons in the CNS by producing myelin sheaths (62). These cells wrap around axons concentrating the propagation of the action potentials along the axon at regular, discontinuous sites, called nodes of Ranvier. The myelin functions as an internodal insulator and facilitates the current flow increasing the action potential conduction speed (1).

A common multipotent progenitor cell gives rise to (a) the astrocytes, (b) the radial glia, and (c) the progenitors for oligodendrocytes and neurons (63) (Fig 1.3). Astrocyte differentiation in the telencephalon involves factors including BMP2/Smads, LIF/STAT and FGF2 (64). In radial glia differentiation, Pax6 plays an



Modified from Nature Reviews Neuroscience 3; 517-530 (2002)

Figure 1.3 Model of neuronal fate

The developing forebrain is formed by different type of cells that are usually classified in two categories, neurons and glia. Radial glia cells function as scaffolding during radial migration of the neurons and also function as neural progenitors. Neural stem cells are multipotent and can generate all neural cell types; that is, neurons, astrocytes and oligodendrocytes. Generally, neural stem cells first generate neurons, and later produce glia.

essential role (65). Oligodendrocyte differentiation occurs in the ventral telencephalon and involves the signalling molecule Shh and the bHLH transcription factors Olig1 and Olig2 (66-68). Neurons arise during the embryonic stages, while the most of the glia is produced after birth (69). Several factors have been recently implicated in the differentiation process of the neural progenitors in the telencephalon. Some of these factors include Notch, its downstream effectors, Hes, and the homeodomain factor, Emx2 (70-73).

1.3 Fibroblast growth factors and their receptors

1.3.1 Gene family of FGFs and FGFRs

Fibroblast Growth Factors (FGFs) are a family of at least 22 polypeptides (74). They constitute a group of factors that act during tissue development and regeneration (75). Roles of FGFs include organ development, angiogenesis, wound healing and tumorigenesis (75). FGF actions are mediated by activation of receptors on the cell surface (75). Three classes of cell surface receptor have been identified for FGFs: (1) high-affinity receptors (termed FGFR1-4), (2) low-affinity receptors (heparan sulphate-containing proteoglycans), and (3) cysteine-rich FGFRs (CFRs) (76). Both FGFs and FGFRs have been found in many species, including vertebrates, fruit flies, worms and sea urchin (77-81). FGFRs are single-pass transmembrane proteins. The extracellular domain consists of a signal peptide, an immunoglobulin (Ig)-like motifs (Ig loops) and an acid box. Most forms of FGFR have two or three Ig-like domains. The intracellular region includes a conserved kinase domain, which is split by the kinase insert region, and a carboxy tail domain (82).

Different FGF family members activate the receptors to different extents, depending on their ability to bind each receptor type (83). One FGF-molecule simultaneously binds two adjacent receptors and the binding occurs in cooperation with heparan sulphate proteoglycan (HSPG), which is either soluble or cell surface-bound (84, 85). Binding of the extracellular FGF ligand to FGFR leads to dimerization of the receptor and initiates the intermolecular autophosphorylation of

tyrosines (86). Dimers are formed between FGFRs of the same type (homodimerization) and between different FGFRs (heterodimerization) (87). FGFRs transmit extracellular signals to various cytoplasmatic signal transduction pathways through tyrosine phosphorylation. Signalling pathways known to be involved in the FGFRs activation include phosphatidylinositol 3' kinase (PI3-kinase), MAPK, Stat1 and Stat3 and PLC- γ (88).

1.3.2 Expression of FGFRs and FGF.

The expression pattern of the FGF family is variable, from almost ubiquitous, such as FGF2, to very restricted (75). Expression of FGFs in the developing CNS is listed in Table 1.1 (89).

FGFRs expression is regulated at the level of transcription, translation and post-translation (90, 91). FGFR1 is widely expressed in the mesenchyme of limb buds and in the developing spinal cord (92, 93). FGFR2 is expressed in diverse epithelial tissues, such as the skin (93). FGFR3 is mainly expressed in the growth plate chondrocytes of developing bone (93). Finally, FGFR4 is highly expressed in several tissues of endodermal and mesodermal origin (94, 95), such as skeletal muscles (92) and adult liver (96). All the four receptors are present in the developing brain at different stages and in specific regional patterns (89, 93, 97-101).

Table 1.2 Expression of FGFs in the developing central nervous system (89)

FGF	Timing	Location
FGF1	E11 onwards	Telencephalon, diencephalon, mesencephalon, metencephalon, spinal cord
FGF2	< E9 onwards	Telencephalon, diencephalon, mesencephalon, spinal cord
FGF3	E8–E11	Otocyst, hindbrain
FGF4	–	–
FGF5	–	–
FGF6	–	–
FGF7	E14.5–E15.5	Lateral ventricle
FGF8	E8.5–E12.5	Telencephalon, diencephalon, midline, midbrain–hindbrain boundary
FGF9	E10–E14	Spinal cord motor neurons
FGF10		Otocyst
FGF15	E8–E14	Telencephalon, diencephalon, mesencephalon, metencephalon, spinal cord
FGF16	–	–
FGF17	E9–E16	Telencephalon, midline, midbrain–hindbrain boundary
FGF18	E10–E15.5	Telencephalon, midbrain–hindbrain boundary

1.3.3 Functions of FGFs and FGFRs

The functions of the FGF family are diverse. FGFs play a key role in the regulation of many critical processes, such as cell differentiation, migration and mitogenesis (74, 88). Functions of the FGF and FGFR family members are summarised in Table 1.2. Several members of the FGF family have been disrupted or mutated in mice, which have shown a broad range of phenotypes, from early embryonic to adult defects. In contrast, some of the knockout mice did not show any obvious phenotype, probably due to the FGF functional redundancy. The major phenotypes observed in FGF and FGFR knockout mice are summarised in Table 1.3.

Table 1.3 Functions of the FGF and FGFR family members

Gene	Function	References
FGF1	Modulates early cell migration, proliferation and initial differentiation in neuronal cells <i>in vitro</i> ; induces morphogenesis in primary murine fibroblasts and stimulates fibroblast migration; inhibits cell attachment to multiple ligands and cytoskeletal organization; regulates angiogenesis.	(89, 102-104)
FGF2	Modulates proliferation in the developing nervous system; stimulates the differentiation of the neuroepithelial cells into mature neurons and glia and the early migration and proliferation of ganglion cells; has a neurotrophic and mitogenetic activity in fibroblast and pre-endothelial cells during embryogenesis; regulates blood pressure.	(75, 89, 103, 105-109)
FGF4	Induces differentiation, proliferation and migration of murine aortic endothelial and in mesenchymal cells; regulates limb development during embryogenesis.	(110-112)
FGF5	Functions as an inhibitor of hair follicle growth.	(113)
FGF6	Regulates muscle regeneration.	(114)
FGF7	Functions as a paracrine mediator of epithelial cell growth.	(115-117)
FGF8	Regulates patterning of forebrain and midbrain during embryogenesis; regulates the anterior-posterior axis formation; regulates nephrogenesis.	(118-120)
FGF9	Induces glial cell proliferation and motoneuron survival; regulates chondrocyte proliferation, differentiation and apoptosis.	(121-123)
FGF10	Regulates caudal neuronal tube and limb development.	(118, 124, 125)
FGF17	Regulates midbrain-hindbrain patterning.	(126)
FGF18	Regulates midbrain-hindbrain patterning.	(127)
FGFR1	Regulates cell proliferation and migration during the axial organization of early post-implantation embryos; stimulates mesodermal and neuroectodermal development.	(97, 128, 129)
FGFR2	Regulates proliferation, differentiation and	(97, 130-132)

apoptosis in cells; stimulates the differentiation and the maintenance of the inner cell mass.

FGFR3 Negatively modulates endochondral bone growth, (133) (134-137)
inhibiting chondrocyte proliferation and
differentiation; controls the development of the
cortex, by regulating proliferation and apoptosis of
cortical progenitors. Promotes the differentiation
of oligodendrocytes and myelination at early
postnatal stages.

FGFR4 Promotes muscle progenitor differentiation. (138)

Table 1.4 The major phenotypes observed in Fgf and Fgfr knockout mice

FGF knockout mice			
Gene	Survival	Phenotype	References
Fgf1	Viable	Morphologically normal	(139)
Fgf2	Viable	Mild cardiovascular, skeletal, neural	(106, 139, 140)
Fgf3	Viable	Mild inner ear, skeletal	(124)
Fgf4	Lethal at E5.5	Inner cell mass proliferation	(112)
Fgf5	Viable	Long hair	(113)
Fgf6	Viable	Subtle, muscle regeneration	(141)
Fgf7	Viable	Hair follicle growth	(115, 116)
Fgf8	Lethal at E8.5	Gastrulation defects, CNS development, limb development	(142, 143)
Fgf9	Lethal	Lung mesenchyme, XY sex reversal	(144)
Fgf10	Lethal at P0	Development of multiple organs	(125)
FGF17	Viable	Cerebellar development	(127)

Fgfr knockout mice			
Gene	Survival	Phenotype	References
Fgfr1	Lethal at E9.5	Growth retardation, defect of mesodermal patterning	(128, 145)
Fgfr2	Lethal at E10.5	Mutant embryos died a few hours after implantation	(132)
Fgfr3	Viable	Bone over growth inner ear defect	(133, 146)
Fgfr4	Viable	Morphologically normal	(147)
Fgfr3/Fgfr4	Viable	Neonatal growth retardation, lung abnormalities.	(147)

1.3.4 Function of FGF2 during brain development

FGF2 plays an important role during the development of the CNS (148, 149). *In vitro*, FGF2 has a mitogenic activity in specific neural cell types (150). FGF2 was shown to promote differentiation and long-term survival of neurons in culture in a concentration-dependent manner (108, 151-155). FGF2 is also an inhibitor of oligodendrocyte proliferation and differentiation during remyelination (156). It has been shown that microinjection of FGF2 into the cerebral ventricles at the beginning of neurogenesis produces permanent increases in cortical volume and number of neurons, an effect that is maintained until the adult stages (155). Furthermore, *in vitro* experiments showed that FGF2 treatment increases the number of both glutamate- and GABA-containing neurons (155), two major neurotransmitters expressed by projection neurons and interneurons, respectively, of the cortex. *Fgf2* knockout mice show neuronal defects in the cerebral cortex, hippocampal commissure and spinal cord (106, 139). Mutant mice show a general decrease in neuronal cell number (155). FGF2 has a function before the onset of cortical neurogenesis, since *Fgf2* knockout mice show a 60% reduction of proliferating cells within the dorsal pseudostratified ventricular epithelium (PVE) at early stages as E10.5 (157). Furthermore, a group of neuronal precursors fail to migrate from the place of origin to their target layers II and III (106). The development of the basal telencephalon and the number of neurons within the basal ganglia do not present abnormalities in the absence of FGF2 (157). The FGF family is composed of at least 22 polypeptides (74), which could all potentially interact with the same FGFRs (75). Therefore, the fact that *Fgf2* knockout

mice present such a dramatic brain phenotype suggests that FGF2 by itself may play a major role in regulating corticogenesis (155).

Similar to Fgf2 null mouse, Fgf1-Fgf2 double knockout mice showed abnormal organization of neurons of the frontal motor cortex (139).

1.3.5 FGFs and FGFRs in the brain

Several FGFs and FGFRs are expressed within the developing CNS. They have multiple roles during the embryonic development, including cell proliferation and apoptosis as well as regulating areal patterning (89). Some FGFs, such as FGF1 and FGF2 are more involved in regulating cell proliferation, while others, such as FGF8, regulate mainly areal specification (106, 119, 157, 158).

The FGFRs are expressed in partly overlapping areas of the embryonic neuroepithelium, however, with distinct patterns and intensities (97, 159). The expression pattern of each receptor becomes more distinct in the adult stages, which may indicate their role in specific populations of cortical cells (160). For example, in the developing choroids plexus, FGFR1 and FGFR4 are expressed only at early stages, suggesting a role in the early stages of the development (101). On the contrary, FGFR2 is present throughout development of the choroids plexus (101). Interestingly, FGFR3 has been observed only in the cell nuclei in the choroids plexus, probably playing a role in the intracrine signalling (101).

FGFR1 null mice are lethal prior to the formation of the mature CNS (161). To investigate the role of FGFR1 signalling in the telencephalon, FGFR1 conditional knockout mice have been crossed with Foxg1-Cre mice (162). Foxg1-Cre allows Cre-

lox recombination specific to the telencephalon. The *Foxg1:Fgfr1^{flox/flox}* mice show abnormal formation of the olfactory bulb suggesting a key role for FGFR1 in patterning and morphogenesis of the telencephalon (162).

FGFR2 null mice display failure of early post-implantation development (132). FGFR2 conditional knockout mouse has been generated using Cre-mediated RNAi strategy but the brain phenotype has not been investigated to date in these mice (163).

No obvious brain phenotype was originally reported in the FGFR3 null mice (133). However, FGFR3 has been recently been implicated in glia differentiation. It has been shown that FGFR3 represses glial fibrillary acid protein (GFAP) expression in grey matter astrocytes in the adult spinal cord (137) and promotes the differentiation of oligodendrocytes and myelination at early postnatal stages (164). Recently, it has also been shown that FGFR3 controls the development of the cortex, by regulating proliferation and apoptosis of cortical progenitors (135).

1.3.6 Pathologies related to FGFR mutations

FGFRs have been implicated in multiple pathological processes, including skeletal disorders and tumorigenesis (165, 166). The skeletal disorders can be classified into two groups, the dwarfing chondroplasia syndromes and the craniosynostosis syndromes. The dwarfing chondroplasia syndromes include Achondroplasia (ACH), Hypochondroplasia (HCH), Thanatophoric dysplasia types I and II (TDI and TDII), and Severe Achondroplasia with Developmental Delay and Acanthosis Nigricans (SADDAN) (167-171). The phenotypes of HCH, ACH and TD display progressively increasing clinical severity (169, 172-174). Point mutations in FGFR3 have been

associated with these diseases (175). These conditions result from mutations that render the FGFR3 constitutively active (175). Patients affected by these conditions are characterised by a disproportionate shortening of the proximal segment of limbs, a relatively large skull and increased spinal curvature (169, 170).

The majority of craniosynostosis syndromes are associated with mutations in FGFR2. These disorders are characterized by premature fusion of the sutures of the skull, causing an abnormal head shape (169). The craniosynostosis syndromes include Apert syndrome (AS), Beare-Stevenson cutis gyrata, Crouzon syndrome (CS), Jackson-Weiss syndrome (JWS), and a non-syndromic craniosynostosis (NSC) (168-171, 176). The FGFR1 is also involved in autosomal dominant craniosynostosis syndromes such as the Pfeiffer syndrome (PS), characterized by craniofacial abnormalities (177).

Malformation of the cerebral cortex is also a condition associated with TDII (178). The malformation is characterized by enlargement of the temporal lobe and hippocampal dysplasia (178, 179).

Loss of function mutations in FGFR1 are associated with the autosomal dominant form of Kallmann syndrome (KAL) (180). KAL is a rare genetic condition in which the gonadotrophin releasing hormone (GnRH)-synthesizing neurons fails to migrate from the olfactory epithelium, causing hypogonadotropic hypogonadism (181).

Finally, the mutations found in severe skeletal dysplasia have been also identified in certain types of cancer, including multiple myeloma, cervix carcinoma and bladder carcinoma (165). Table 1.4 summarizes the known types of cancers associated with altered expression of FGFRs (182).

Table 1.5 Genetic alterations of FGFRs in human cancers

Gene	Alteration	Reference
FGFR1	8P11 myeloproliferative syndrome (EMS), breast cancer, prostate cancer, astrocytoma, pancreatic adenocarcinoma	(183-187)
FGFR2	Prostate cancer, astrocytoma, gastric cancer	(186-188)
FGFR3	Transitional cell carcinoma of bladder, thyroid carcinoma, cervical carcinoma, colorectal cancer, peripheral T cell lymphoma, multiple myeloma	(189-195)
FGFR4	Pancreatic adenocarcinoma, head and neck squamous cell carcinoma	(185, 196)

1.4 Growth factor regulation of cell proliferation

1.4.1 Cell proliferation and cell cycle

Cell proliferation is the basic biologic process that results in an increase in the number of cells. The rate of cell number depends on (a) the time the cells take to complete a cell cycle of division, (b) the fraction of cells within the population undergoing cell division (growth fraction), and (c) the rate of cell loss from the population due to terminal differentiation or cell death (197).

Cells divide by progressing through a sequence of phases that constitute the mitotic cycle (or the cell cycle). The cell division cycle is composed of two functional phases, S (for Synthesis) and M (for Mitosis), and two preparatory gap phases, G_1 and G_2 . During the S phase the DNA is synthesized, whereas during the M phase the parent cells divide into two daughter cells. G_1 and G_2 phases are necessary for checkpoints and for the synthesis of cellular constituents. The cells that do not proliferate usually enter a phase called G_0 . The length of time that a typical human cell takes to complete the S phase lasts between 12 and 24 h, whereas the length of M phase is about 1 h and the G_2 phase lasts for about 2-3 h. The length of G_1 phase is variable and can last from about 6 h to several days or longer.

The cell cycle is rigorously regulated. The M phase cannot start unless the S phase has been completed, and vice versa (198). At the end of the cell cycle, the daughter cells, in the G_1 phase, either start another cycle or arrest in a quiescent G_0 phase, depending, on external conditions. If these conditions are not adequate, the cell arrest in G_0 before it reinitiates cell cycle. Neuronal and skeletal muscle cells are in

terminally differentiated G_0 and the expression of cell cycle regulators is permanently off. Liver cells, in contrast, are in G_0 phase but they can re-enter the cell cycle after tissue damage.

1.4.2 Growth factors signalling and proliferation through MAPK pathway

Proliferation of mammalian cells is strictly regulated by extracellular signals, such as mitogens present and the supply of nutrients. They largely exert their effects on cells during G_1 phase of the cell cycle (199). Binding of a growth factor to its receptor can trigger activation of the tyrosine-kinases (200). The signal is then transduced from the cytoplasm to the nucleus by a heterogeneous group of molecules known as second messengers. Binding of the extracellular FGF ligand to FGFR leads to dimerization of the receptor and initiates the intermolecular autophosphorylation of tyrosines (86). The phosphotyrosines either stimulate the intrinsic catalytic activity of the receptors or serve as high-affinity recruitment sites for the binding of downstream signalling proteins (201).

One of the major pathways modulated by growth factor signalling and known to promote cell proliferation is the MAPK pathway (202) (Fig 1.4). Binding of FGF to its receptor triggers cell cycle progression through different pathways, including the MAPK signalling (88). The MAPK family is composed of protein kinases that are highly conserved in evolution and play central roles in signal transduction in the cell. The MAP kinases are protein-serine/threonine kinases activated in response to a variety of growth factors and are known to regulate cell growth, death and differentiation (203).

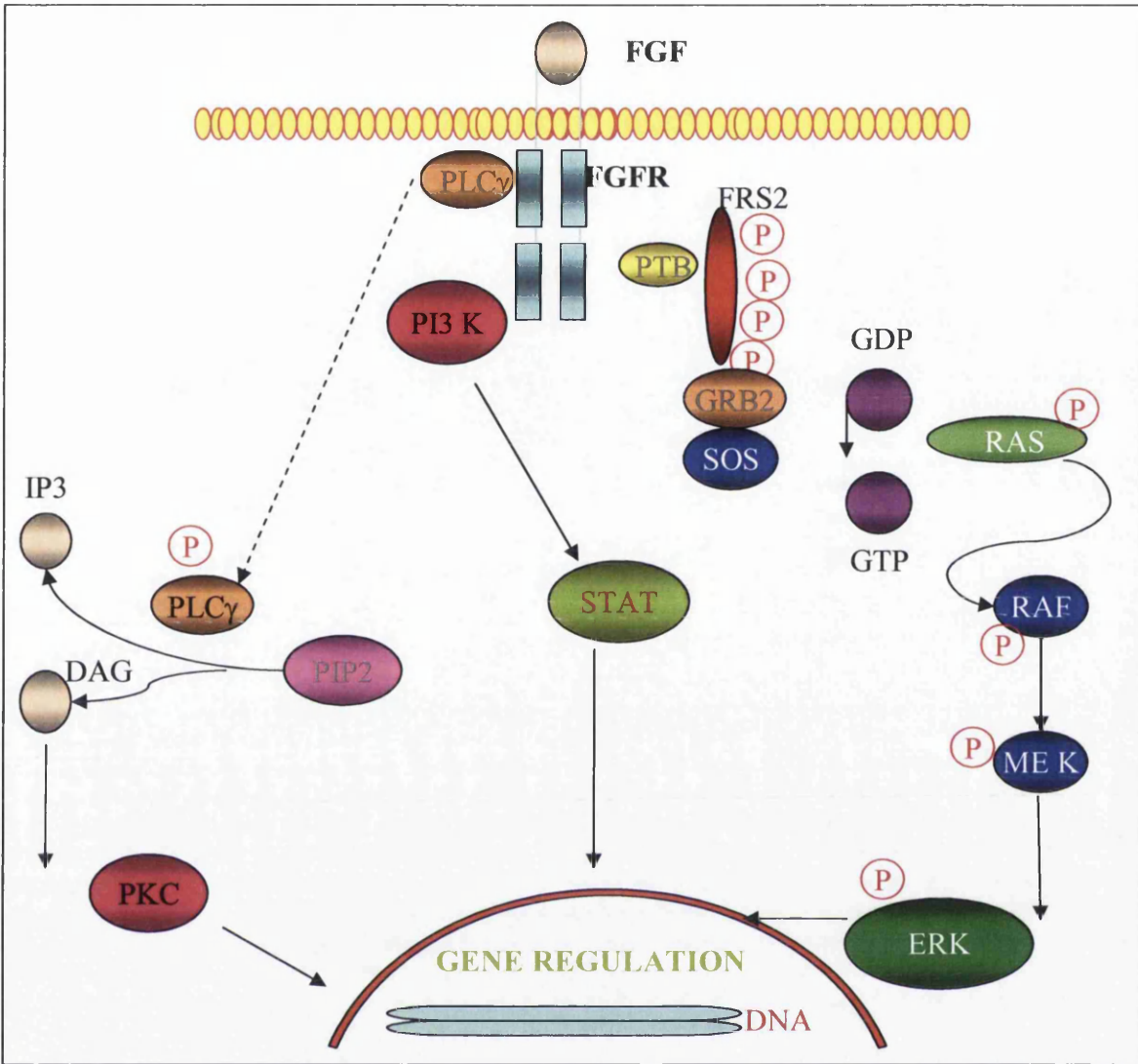


Figure 1.4 *Dimerization, autophosphorylation and signalling of FGF/FGFR*

Schematic diagram showing several FGF signalling pathways and how they interact to form a signalling network. Binding of the extracellular FGF ligand to FGFR leads to dimerization of the receptor and initiates the intermolecular autophosphorylation of tyrosines. The ERK/MAPK cascade is one of the best known for its key role in mediating the transduction of signals from FGFRs. Other pathways involve PI3-kinase, Stat1/3 and PLC γ .

Autophosphorylation of receptor protein tyrosine kinases results in their association with adaptors, which contain modular protein-protein interaction domains, such as Shc and 'Growth factor Receptor Binding 2 protein' (GRB2). This mediates protein-protein binding, such as between the SH2 domains of the modular proteins and the FGFR (204). Association of GRB2 with activated receptors localises 'son-of-sevenless protein' (SOS) to the plasma membrane and it stimulates guanine nucleotide exchange, resulting in activation of RAS, a GTP-binding protein (205). Activation of RAS leads to activation of the 'rabbit fibrosarcoma protein' (RAF) serine-threonine kinase (206). Three isoforms of RAF have been identified so far, A-RAF, B-RAF, and RAF-1. RAF-1 is widely distributed in the body and expressed in most cultured cells, whereas the other isoforms are more restricted in the expression. For example, B-RAF is expressed specifically in neuronal tissues (207). When activated, RAF phosphorylates and activates the protein MEK. MEK selectively activate ERK1/2 by phosphorylation of both threonine and tyrosine residues (208, 209). ERK1 and ERK2, proteins of 44 and 42 kDa respectively, share 83% amino acid identity and are expressed in various type of tissues (207). Once activated, ERK translocates to the nucleus, where it phosphorylates various targets, including other protein kinases and transcription factors. For example, ERK phosphorylates and regulates transcription factors such as Myc, a protein that promotes cell cycle entry by regulating the expression of cyclin D (210).

The family-named 'immediate-early genes' expression is also induced by growth factor stimulation (197). These genes are induced through the regulation of a sequence, which is recognized by a complex of transcription factors including the

serum response factor (SRF) and ELK-1 (212). ERK is known to phosphorylate and activate ELK-1, providing a direct link between MAP kinase family and immediate-early gene induction (212).

1.4.3 Negative feedback of MAPK

MAPK signalling events are precisely regulated to ensure a physiologically appropriate biological effect. One of the mechanism by which MAPK signalling is regulated involves a negative-feedback loop through Sprouty (SPRY) (213) (Fig 1.5). SPRY expression is induced by MAPK signalling upon growth factor stimulation, such as FGFs (214, 215). SPRY proteins undergo phosphorylation in response to growth-factor stimulation (216-218). Its phosphorylation site functions as a binding site for the SH2 domain of the adaptor molecule GRB2 (217). FGFs induce interaction of SPRY with GRB2, preventing GRB2 from binding to either 'FGF-receptor substrate-2' (FRS2) or 'SH2-domain-containing protein tyrosine phosphatase-2' (SHP2) (217). The SH2-dependent recruitment of complexes of GRB2 and SOS to FRS2 and SHP2 is a fundamental step in the MAPK signalling to lead RAS activation. Therefore, the sequestration of GRB2 by SPRY blocks the signalling events downstream of RAS (217).

Other inhibitors of MAPK signalling have been identified, including PYST1/MKP3, Sprouty-related 1/2 (Sprad-1/2), and the 'Similar expression to FGF gene' (Sef) (219-221).

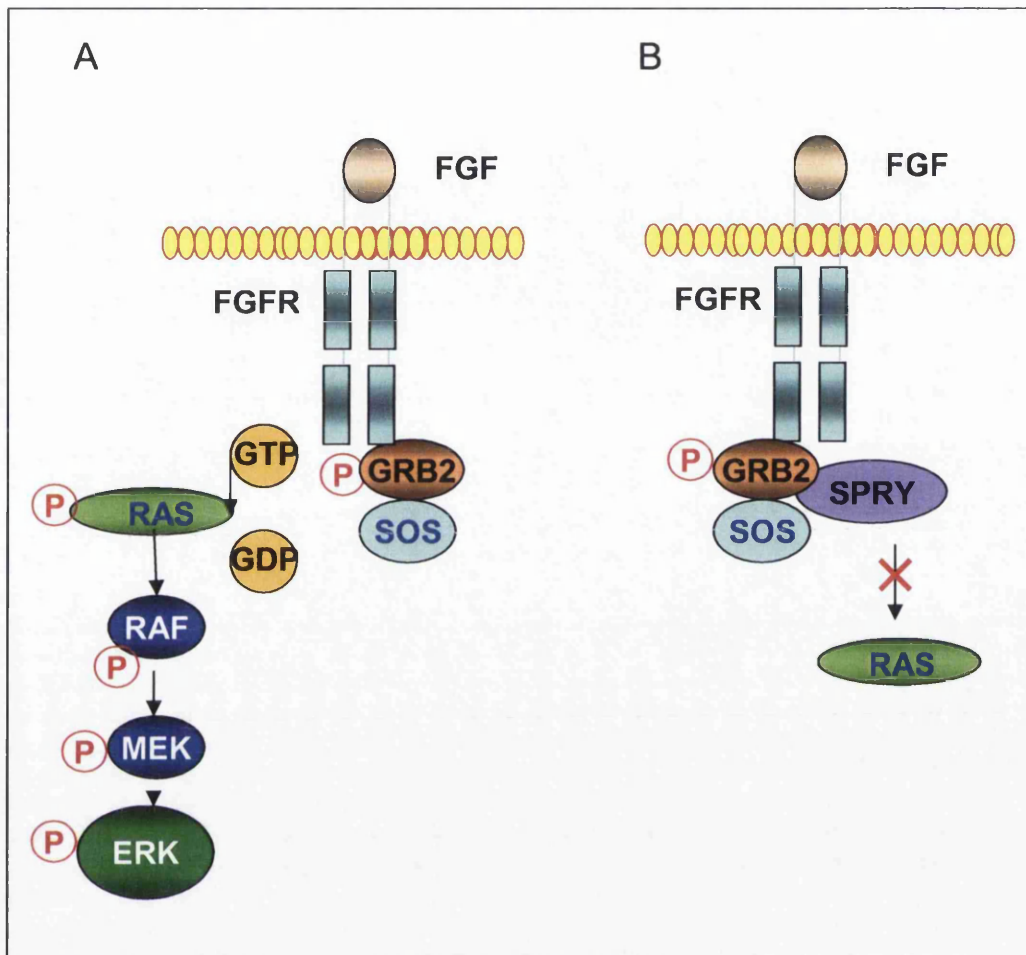


Figure 1.5 *The MAPK cascade and its negative-feedback.*

(A) The members of the MAP kinase family are ERK1/2, MEK and RAF, which are coupled to growth factor receptors by a GTP-binding, RAS. Once activated, ERK translocates to the nucleus, where it phosphorylates various targets (B) FGF stimulation leads to GRB2-SOS complex formation, which is recruited to the phosphorylated tyrosine residues on FRS2 or SHP2. This recruitment event results in the activation of RAS. When Sprouty (SPRY) is activated, it generates a binding site for GRB2-SOS complex preventing RAS activation.

1.5 Characteristic domains identified within ccp1 sequence and cellular compartments where ccp1 may localise

Proteins contain several functional domains that may be related to specific protein functions, such as DNA binding, enzyme activity, and other important cellular processes. The protein motif search tools have predicted specific domains within the ccp1 amino acid sequence (Chapter 3.1). In this section, the domains that have been identified in ccp1 amino acid sequence are introduced, including the coiled coil region, the leucine zipper and the nuclear exporting signal (NES). Furthermore, when transiently expressed, ccp1 localised in vesicle-like structures identified as lysosomes (Chapter 3.3). Here, an overview of the main endosomal/lysosomal pathway is presented.

1.5.1 The coiled coil domain

Coiled coil domains are known to form a stable superhelix structures when two or three α -helices bound around each other (222). These structures allow oligomerisation and binding to other proteins possessing coiled coil domains. Two-stranded, three-stranded, and four-stranded versions of coiled coils are known to be possible (223). In the coiled coil domain, the amino acids are positioned to form a heptad repeat pattern in which the first and fourth amino acids are hydrophobic and

the fifth and the seventh are charged or polar (222, 224). The interactions between amino acids at these heptad positions are essential for the formation of the coiled coil structure. The specificity of these interactions and the amount of packing space required for the residues at each position vary depending on the oligomerization state of the coiled coil (223).

A large number of coiled coil proteins with diverse functions have been identified. They are roughly categorised into four functional groups, (a) cytoskeletal proteins, such as keratin and vimentin, (b) motor proteins, such as myosin, kinesins, and dyneins, (c) proteins important for vesicular transport, such as synaptobrevin, syntaxin and SNAP-25, and (d) transcription factors, such as fos and jun.

Cytoskeletal proteins

The cytoskeleton of eukaryotic cells contains three filament moieties: microtubules, actin-containing microfilaments and intermediate filaments (IFs) (225). One of the most common families of IFs is that of the keratins and vimentin. Keratin filaments are elongated molecules that contain a coiled coil domain (197). The protein α -keratin was the first protein in which the coiled coil structural motif was identified (226). The coiled coil structure defines the elongated shape of IF molecules, which form heterodimers and, subsequently, interact with other IFs to form tetrameric subunits (227). The interconnected network of IFs gives mechanical stability to the cell and is involved in processes such as cell division and cell motility (228).

Motor proteins

In eukaryotic cells, different organelles often move in the cytoplasm using macromolecular complexes located on microtubules and actin filaments (229, 230).

Specific motor proteins, such as myosin, kinesins, and dyneins, mediate these movements (231). Myosin is known to move along actin and kinesins along microtubules (232). In the nervous tissue, both kinesin and dyneins show a function in anterograde and retrograde axonal transport respectively (232, 233). The motor protein dynein and its binding partner dynactin are essential for nuclear migration in fungus (234). The Lis1 gene is known to be involved in function as nuclear translocation and mitosis together with the cytoplasmatic proteins dynein and tubulin (235, 236). Recently, more proteins that interact with motor proteins have been identified by yeast two-hybrid and biochemical analyses (237). One of these proteins is NUDEL, a coiled coil protein fundamental for neurofilament assembly and neuron cytoskeleton integrity *in vitro* (238). NUDEL is known to interact with dynactin and Lis1 (239-241), indicating that NUDEL is required for active transport along microtubules.

Proteins important for vesicular transport

During the endocytic traffic, the cargo vesicles recognise the target membrane through specific surface markers. The SNAP receptor (SNAREs) family is a class of protein that control this recognition process (242). SNARE proteins are known to form complexes through their coiled coil regions (243). In neurons, most vesicles and protein complexes are generated in the cell body and are then transported along axons (244). The SNARE family has been well characterised in neurons, where it mediates synapse connections (245). Well studied SNARE family members in the neuronal cells include SNAP-25 and Synaptobrevin (242). Another protein is Syntabulin,

which connects syntaxin-containing vesicles to microtubules, ensuring their anterograde transport (246).

Transcription factors

Transcription of DNA is a cellular process that involves specific interactions between DNA and DNA-binding proteins. Many transcription factors contain coiled coil regions that are fundamental for specific recognition between molecules (247). An example of transcription factors containing coiled coil regions are the GCN4 proteins (223, 248, 249). Fos and jun proteins (which are part of the AP-1 transcription factors) are associated preferentially to form a heterodimer that binds to DNA, and thereby modulates transcription of a wide variety of genes in response to mitogenic stimuli. It is reported that incorrect coiled coil pairing may result in oncogenic activity. In this functional category, coiled coil pairing must therefore be very specific in order to avoid unfavourable modulation of transcription.

1.5.2 The leucine zipper

The leucine zipper is a periodic repetition of leucine residues at every seventh position that facilitates dimerisation between two peptides as well as the binding of the DNA chain (250). The leucine zipper can fold as a parallel, two-stranded coiled coil (251, 252). A leucine zipper consists of two α -helices, one from each monomer. Transcription factors containing a leucine-zipper bind DNA as dimers. The α -helices of two proteins are held together by hydrophobic interactions between leucine residues, which are located on one side of each helix. Examples of leucine zipper containing proteins are the B-ZIP class of transcription factors (253). The B-

ZIP family includes the activator protein-1 (AP-1), the cyclic AMP response element binding protein (CREB) and CCAAT/enhancer binding proteins (C/EBP) (254-256).

1.5.3 The Nuclear Exporting Signal (NES)

A NES is a short sequence that determines the nuclear transport from the nucleus to the cytoplasm through the nuclear pore complexes (NPC) (257). In contrast to small proteins (< 40 kDa) that can freely diffuse through the pore, larger proteins require a NES. These protein signals are recognised by specific soluble receptors, karyopherins, which are able to interact with the NPC (258). When the cargo and the karyopherins form a complex, they translocate through the NPC with an active transport using the energy provided by RAN, a GTPase of the RAS family (259).

There are several type of NES, but the most common NES is the leucine-rich NES domain (260). It is composed of a leucine-rich region. The accepted consensus is LX₂₋₃LX₂₋₃LXL, although many of the known leucine-rich NES deviate from this generally accepted consensus (261). Only 36% of the sequences known so far contain a NES domain that fit the consensus (257). The leucine-rich NES was first identified within the protein kinase inhibitor (PKI) and the HIV Rev protein (262) (263).

The receptor 'Chromosome Region Maintenance 1' (CRM1) has been identified as the export receptor for proteins containing leucine-rich NES (264, 265). CRM1 was originally identified as a protein responsible for maintaining the chromosome structure of the *Scizosaccharomyces pombe* (266). Later, CRM1 was associated to the nuclear exporting process (264, 265). Recognition of the NES domain by CRM1 is

inhibited by the fungicide leptomicin B (LMB) and ratjadone (RAT) (264, 267). LMB binds to a single sulfhydryl group of CRM1 inhibiting its activity (268).

At least 75 proteins containing a leucine-rich NES have been identified so far (257), including MEK (269), the tumor suppressor protein p53 (270), Smad1 (271) and Cdc25A (272). Activation of MAP Kinases leads to their nuclear translocation and phosphorylation of DNA-binding proteins that are mainly transcriptional regulators (273). MEK contains a NES and it is mainly localised to the cytoplasm (274). Nuclear localisation of ERK is transient, since, after its activation, it is immediately re-localised to the cytoplasm to prepare for the next stimulation. Since ERK does not contain a NES, its relocation to the cytoplasm is likely to be mediated by a protein anchor, which has been hypothesised to be MEK (275).

1.5.4 The endosomes lysosomes pathway

When transiently expressed, ccp1 fusion protein localised in a vesicle-like structure similar to endosomes or lysosomes. During the course of this study, the ccp1-positive structures were identified as lysosomes (Chapter 3.3).

Cells are known to elaborate internal membrane system that allows them to internalised macromolecules by a process called endocytosis (197). After endocytosis, most membrane proteins return to the cell surface to be recycled up to several hundred times, whereas other membrane components are delivered to late endosomes or to lysosomes in order to be degraded (197). There are different types of endocytosis that can transport molecules to several destinations within the endosomal system. A well-known endocytic process is the one of the internalization of receptors

and their ligands by clathrin-coated pits (334). However, non-clathrin mechanisms are also known, although their mechanism is still not fully understood. Endosomes are commonly classified in early endosomes or sorting endosomes, late endosomes and recycling endosomes. After entering the cytoplasm, the endocytotic vesicles lose its clathrin coat and fuse each other or with pre-existing endosomes (334). They appear tubular-vesicular structures and have a luminal pH of 6.0. Early endosomes uptake material for only about 5–10 minutes and then translocate along microtubules, stop fusing with newly endocytosed vesicles and become more acidic (197). At this step, early endosomes acquire acid hydrolases and take on the properties of late endosomes. These changes in sorting endosomes are called as maturation (334). The fusion of coated-pit-derived primary endocytic vesicles with sorting endosomes is regulated in part by early endosome antigen 1 (EEA1) and Rab5 (334). EEA1 is a phosphoinositide-binding protein containing zinc finger like domains in the amino and carboxyl terminal (295). Rab proteins are a family of small GTPase regulatory proteins (334). Late endosomes are formed as the pH continues to drop to 5-6 and they acquire the surface marker Rab7. Late endosomes are not able to digest all the material, therefore they form a dynamic network together with lysosomal structures, the end point of endocytosis and site of protein degradation (197). Lysosomes are membrane-bound vacuoles, which play a critical role in cellular metabolism that act as sites for digestion of foreign materials and for specialized autolytic cellular processes (197). Membrane-associated glycoproteins have an important role in normal lysosomal function and they can be used as marker for a late endosome or a

lysosome, for example the heavily glycosylated lysosomal associated membrane proteins (LAMPs) (299, 300).

Receptors such as LDL-receptor (LDLR) and transferrin receptor (TfR), are continuously internalized, delivered to early endosomes and finally recycled back to the plasma membrane via recycling endosomes (296). The TfR is included in the class of ligand transport receptors that are internalized and clustered in coated pits (293). The TfR binds the serum transport protein transferrin (Tf) and mediates the uptake of iron into the cell (293).

CHAPTER 2

MATERIALS and METHODS

2.1 Materials

2.1.1 Chemicals and tissue culture media

The chemicals and tissue culture media used in this study were all purchased from Sigma or Invitrogen, unless indicated in the text.

2.1.2 Plasmid Vectors

A list of plasmid vectors used during this study is presented in table 2.1, detailing specific applications and characteristics.

2.1.3 Ccp1 cDNA

The original *ccp1* cDNA was obtained from the National Institute on Aging (NIA) mouse 15 K cDNA clone set (source: Max-Planck, Martinsried, Germany). The original cDNA was cloned in NotI/SalI site of the ampicillin-resistant pSport1 vector (Life Technologies) (276).

2.1.4 Cells

Human embryonic kidney HEK293, human neuroblastoma SK-N-SH cells, human osteosarcoma U2OS cells and primary MEF were obtained from colleagues at the Beatson Institute. Immortalized rat oligodendrocytes progenitors, OPC/*c-myc/bcl-2* cell line or BC30, were a gift from Dr. Sue Barnett (277).

2.1.5 Mice

CD1 mice were obtained from Charles River, UK. All procedures using mice were performed in accordance with the Project Licence (PPL 60/3060) and Personal Licence (60/9362) under the Home Office Animal (Scientific Procedures) Act 1986.

2.2 Methods

2.2.1 Cell culture

2.2.1.1 Brain dissection

Female pregnant mice were sacrificed at different stages of gestation by neck dislocation. Embryos were collected from the uterus and immediately sacrificed by decapitation. Mice heads were kept in warm PBS containing 100 U/ml of penicillin-streptomycin (Pen-strep) until dissection was performed. The forebrain was dissected out from mouse embryos. The tissue was incubated in trypsin solution (0.25% trypsin/1 mM EDTA) for 15 min and dissociated by polished Pasteur pipettes.

2.2.1.2 Primary cortical neuron culture (CNC)

The cells were allowed to attach in Minimum Essential Media (MEM, Gibco)-HS (MEM, 0.6% glucose, 2 mM glutamine and 10% horse serum). After 4 h, the medium was replaced with N2-MEM (MEM, 1.25 mM pyruvic acid, 0.6% glucose, 2 mM glutamine, 0.1% egg albumin, 20 nM progesterone, 100 μ M putrescine, 30 nM selenium dioxide, 0.1 mg/ml transferrin) and cultured ON at 37°C in 5% CO₂. The cells were grown in 10 cm dishes or in glass cover-slips inserted into 24-well tissue-culture plates. All the dishes and cover-slips were coated overnight (ON) with 1 mg/ml poly-L-Lysine (SIGMA).

2.2.1.3 Immortalised oligodendrocytes progenitor culture BC30

BC30 were maintained in Dulbecco's MEM (D-MEM, Gibco) supplemented with 60% SATO mix, 40% BIO4 cells supernatants, 43 mM Insulin, 65.5 mM transferrin, and 2 mM glutamine. SATO mix consists of 2.8% bovine serum albumin (Miles SCI, Pentex), 0.45 M putrescine, 180 μ M T4, 227 μ M T3, 0.9 mM progesterone (Sigma), and 1 mM sodium selenite. Cells were maintained at 37°C in 5% CO₂.

2.2.1.4 Other cells

Human neuroblastoma SK-N-SH, human HEK 293, mouse Phoenix packaging cells and primary mouse fibroblast MEF cells were maintained in D-MEM, 10% foetal bovine serum (FBS) and 2 mM glutamine. Cells were maintained at 37°C in 5% CO₂.

2.2.1.5 Cell treatment

Cells were starved in media without serum for 4 to 24 h and treated with different concentrations of recombinant h-FGF2 (1-10 ng/ml) and heparin (1-0.001 μ g/ml) depending on the experiment. Cells were observed daily and used from 1 to 6 days in vitro (DIV).

2.2.1.6 Cell transfection

Cells were plated at 90% confluence in 6-well or 24-well tissue-culture plates. Transfections were performed using Lipofectamine 2000 reagent according to the manufacturer's instructions (Invitrogen) using the appropriate plasmid. 2 or 0.5 μ g/dish of DNA was used when 6 or 24-well tissue-culture plates were used, respectively. Non-transfected cells and empty vectors were used as negative controls.

Cells were used for the experiments after 24 h and processed depending on the protocol. See table 2.1 for expression vectors used in the transfections.

2.2.2 Preparation of DNA and RNA

2.2.2.1 Small scale preparation of plasmid DNA

Preparation of DNA from small quantities of bacterial culture was performed using the QIAprep Spin Miniprep Kit (Qiagen) as per manufacturers' instructions. Bacterial cultures were prepared as explained in section 2.2.4.1. Briefly, 5 ml of overnight culture was pelleted at 2500 rpm for 10 minutes and the supernatant discarded. The pellet was subjected to alkaline lysis followed by neutralisation then centrifugation at 13000 rpm to remove cell debris. Supernatant was transferred to a spin filter containing a silica-gel membrane to which DNA was specifically adsorbed in the presence of high salt. Following a wash step to remove salts, DNA was eluted in 50 µl of distilled water. DNA was examined by electrophoresis in 1% (w/v) agarose gel that contained TAE buffer with 0.5 µg/ml ethidium bromide (EtBr). The 100 bp and 1 kb (New England Biolabs) markers were used.

2.2.2.2 Large scale preparation of plasmid DNA

Maxi-preparation of plasmid DNA was performed using the Qiagen Plasmid Maxiprep kit as per manufacturers' instructions. Briefly, 50 µl glycerol stock or 500 µl fresh overnight culture was added into 5 ml LB media containing an appropriate antibiotic and incubated ON in an orbital shaker at 37°C. The following day cultures were expanded in 500 ml of LB media with appropriate antibiotic and incubated overnight in an orbital shaker at 37°C. The bacteria were harvested by centrifugation

at 4000 rpm for 10 min and alkaline cell lysis performed. Crude cell lysate was cleared by centrifugation and then loaded onto an anion exchange column, which selectively binds plasmid DNA under appropriate low-salt and pH conditions. Following wash steps in medium salt buffer plasmid DNA was eluted in high salt buffer then precipitated by adding 0.7X volume of isopropanol and centrifugation at 4000 rpm for 30 min at 4°C. The DNA pellet was washed with 5 ml of 70% ethanol then centrifuged again at 4000 rpm for 15 min. Finally, the pellet was air-dried at 37°C for 10 to 15 min and re-dissolved in a suitable volume of water.

2.2.2.3 Total RNA extraction from cell culture

Total RNA was isolated from cells using RNazol (Biogenesis). The cells were harvested in 1.6 ml RNazol/10 cm dish. RNA was extracted using 200 µl of chloroform/ml lysate. The lysate was centrifuged at 12,000 g for 15 min at 4°C. This separates the mixture into 3 phases: a lower red, phenol-chloroform phase (containing protein), an interphase (containing DNA) and a colourless upper aqueous phase (containing RNA). The aqueous phase was transferred to a fresh tube and precipitated with 1:1 volume of isopropanol. After centrifugation, the RNA pellet was washed with 1 ml of 75% ethanol/ml lysate. The sample was allowed to stand for 10 min at room temperature (RT) and then centrifuged at 12,000 g for 10 min at 4°C. The supernatant was removed and the RNA pellet was washed once by adding 1 ml of 75% (v/v) ethanol prepared with diethyl pyrocarbonate (DEPC) water. The sample was vortexed and then centrifuged at 7,500 g for 5 min at 4°C. The RNA pellet was briefly air-dried and re-suspended in an appropriate volume of DEPC water. RNA

was examined by electrophoresis in 1% (w/v) agarose gel that contained TAE buffer with 0.5 µg/ml EtBr and the remaining RNA was aliquoted and stored at –80°C.

2.2.2.4 Total RNA extraction from tissue

Tissue dissected from embryonic body was homogenised using an EZ-Gen Homogenizer (Omni International) in 1 ml of RNAzol. From this step, the same protocol described in the previous section was followed.

2.2.2.5 Poly A-RNA extraction from cell culture

Poly A-RNA was isolated from cells using Micro-FastTrack 2.0 kit (Invitrogen) according to the manufacturer's instructions.

2.2.2.6 Quantification of nucleic acids

Nucleic acid concentrations were estimated by spectrophotometry at A_{260}/A_{280} (Eppendorf BioPhotometer), where an optical density (OD) of 1 at 260 nm corresponds to 50 µg/ml of double-stranded DNA and 40 µg/ml of single-stranded DNA and RNA. Readings were zeroed with the solution in which the samples had been diluted. The ratio of A_{260}/A_{280} provided an estimate of nucleic acid purity. Values between 1.8 and 2.0 indicated pure preparations.

2.2.3 Gene manipulation

2.2.3.1 Reverse transcriptase reaction (RT)

RNA extracted from cells or tissue was reverse-transcribed using SuperScript II (Invitrogen). 2 µg of total RNA was added into a reaction containing 500 ng of Random examers to a final volume of 12 µl water. The reaction was heated to 70°C

for 10 min, and then placed on ice to denature the secondary structure of the RNA. To each reaction the following mix was added: 1X first strand buffer, 0.1 M DTT, 25 mM MgCl₂ and 10 mM of dNTPs (Invitrogen). After 5 min incubation at 25°C, 200 Units (U) of Superscript II Reverse Transcriptase (Invitrogen) was added and the reaction incubated at 25°C for 10 min and 42°C for 50 min. Final reaction volume was 20 µl. The reaction was terminated by 15 min incubation at 70°C, and the RNA/DNA duplex degraded by the addition of 2 U of RNase-H (Invitrogen) for 20 min at 37°C.

2.2.3.2 Polymerase Chain reaction (PCR)

Standard PCR protocols were used for amplification of cDNAs. 2 µl of template cDNA were used per reaction. Each reaction contained 1X PCR buffer (minus MgCl₂), 1.5 mM MgCl₂, 0.2 mM each dNTP, 0.2 µM forward and reverse primers and 1.25 U Taq DNA polymerase (Biotaq, Bioline), in a final volume of 25 µl. Cycling was performed in thin-walled dome-topped 0.2 ml PCR tubes in an PTC-200 Peltier thermal cycler. Initial denaturation was at 94°C for 2 min, followed by 25-30 cycles of 94°C, 30 sec; 58°C, 30 sec; 72°C, 1 min, and final extension at 72°C for 5 min. PCR product was examined by electrophoresis in 1.5% (w/v) agarose gel that contained TAE buffer with 0.5 µg/ml EtBr. Primers used were obtained from TAGN, Newcastle Ltd, as a purified pellet. Some primers were designed in order to incorporate specific restriction enzymes at the 5' and 3' of ccp1 CDS (Table 2.2, 2.3 for primers details). Prior to use, the primers were diluted using water to appropriate concentrations and, once diluted, stored at -20°C.

2.2.3.3 Automated DNA sequencing

Automated sequencing was performed at the Beatson Laboratories. The templates (0.5-1 µg) and primers (3.2 pmol) were supplied. A single-stranded reaction was used with a PCR mix containing fluorescently labelled di-deoxynucleotides. Samples were run on an agarose gel and the nucleotides detected on a Beckman CEQ 2000 sequencer. Analysis was carried out by Beckman CEQ 8000, and the sequence data viewed and further analysed using SeqMan II. See Table 2.2-2.3 for the list of primers used.

2.2.4 Cloning techniques

2.2.4.1 Ligation and transformation

Following agarose gel purification, cDNAs were ligated into the appropriate vectors. Each 10 µl mixture contained 6.5 µl sterile water, 1 µl ligation buffer (10X), 50 ng linearised vector, 100 ng DNA insert and 4 U of T4 DNA ligase (Invitrogen). These reactions were carried out overnight at 15°C. Transformation was performed using 2 µl of ligation product. Plasmid DNA was added to a thawed vial of DH5α competent *E. coli* cells and, after gently mixing with a pipette tip, was incubated on ice for 30 min. Cells were then heat-shocked through incubation at 42°C for 45 sec and immediately cooled on ice for 2 min. 250 µl of SOC medium (Invitrogen) was added to the competent cells before incubating at 37°C for 1 h with agitation. Selection of transformed cells was then achieved by plating 100–200 µl of culture on LB/agar (15 g/L bacto-agar in LB broth) that contained antibiotic selection (30 µg/ml kanamycin or 50 µg/ml ampicillin). Transformed colonies were identified by incubating plates

ON at 37°C. Individual colonies were then selected and grown ON at 37°C (with continuous shaking) in 5 ml LB containing the appropriate antibiotic. Plasmid DNA extraction was carried out using Qiagen plasmid mini or maxi kits, following the manufacturer's instructions.

2.2.4.2 Identification of recombinant positive clones

After DNA quantification, digestion of isolated plasmid DNA was carried out in a 10 µl volume containing 6 µl sterile water, 1 X of buffer, 200 ng of DNA and the appropriate restriction enzyme. DNA digestion took place at 37°C ON. 1 µl of the digestion product was analysed by agarose-gel electrophoresis. See Table 2.6 for the list of enzymes used and their applications.

2.2.4.3 TA cloning

Following RT-PCR, the cDNA was ligated into pCRII vector (TA cloning kit, Invitrogen). The same procedure described in the above section was followed, except that INVα F' competent *E. coli* cells (Invitrogen) were used instead of DH5α *E. coli* cells.

2.2.4.4 Expression vectors construction

A list of plasmid vectors used during this study is presented in Table 2.1, detailing specific applications and characteristics. See Table 2.6 for the list of enzymes used and their applications.

2.2.4.5 pdEGFP-N-ccp1, pEGFP-C-ccp1, pDsRed-N-ccp1 and pDsRed-C-ccp1 vectors construction

pdEGFP-N, pEGFP-C, pDsRed-N and pDsRed-C vectors (Clontech) were used to express *ccp1* in the cells. EGFP, or enhanced green fluorescent protein, is a red-shifted variant of GFP showing brighter luminescence in mammalian systems (278). Red is the *Discosoma* sp. red fluorescent protein. *Ccp1* CDS was generated by RT-PCR as explained in the section 2.2.3.2 (Table 2.2-2.3 for primers details). The PCR fragments were first cloned in pCRII vector and sequenced using the primers SP6 and T7. After confirmation of the fragment identities, they were digested with *EcoRI* and *Sall* restriction enzymes and cloned in the expression vectors. The vectors pdEGFP-N, pEGFP-C and pDsRed-C were from Clontech. The vectors pDsRed-N was engineered in the laboratory. Specific primers were designed in order to amplify the Red-CDS (F-pRed and R-pRed) flanked by the *BamHI* and *NotI* restriction enzymes and missing the STOP codon. As a template, the pDsRed-C vector was used. The PCR fragment was sequenced using the primers Sp6 and T7 and cloned in the pCRII vector. At the same time, the pdEGFP-N vector was digested with *BamHI* and *NotI* restriction enzymes in order to eliminate the GFP tag and ligated with the Red-CDS fragment. *Ccp1* CDS was cloned in the pDsRed-N vector using the *EcoRI* and *Sall* restriction enzymes.

2.2.5. Northern Blotting

2.2.5.1 Preparation of probes for Northern Blotting

The DNA probe was prepared by digesting the plasmid in a 10 µl volume containing 6 µl sterile water, 1 X of buffer, 200 – 500 ng of DNA and the appropriate restriction enzymes (Table 2.6). DNA digestion took place at 37°C ON. DNA was examined by electrophoresis in 1% (w/v) agarose gel that contained TAE buffer with 0.5 µg/ml EtBr. The 100 bp and/or 1 kb (NewEngland Biolabs) markers were used. DNA was visualised by UV illumination at 302 nm or 365 nm. DNA fragments were excised from the gel using a scalpel blade and the DNA extracted using the Qiagen Gel Extraction kit according to the manufacturers' instructions. The DNA was eluted in 30 µl of water.

2.2.5.2 Northern electrophoresis and blotting

All equipment and surfaces used for gel preparation were cleaned with RNaseZap™ (Ambion) and rinsed with DEPC water. The NorthernMax Kit (Ambion) was mainly used following the manufacturer instructions. When buffer produced in laboratory were used the following protocol was used. A 1% agarose-formaldehyde/1X 3-N-morpholino-propanesulfonic acid (MOPS) gel and 1X MOPS was used as running buffer diluted from a 10X stock. The total RNA (10 µg) or Poly A-RNA (2µg) and 2 µg of RNA marker (Invitrogen) were mixed with 5 µl RNA loading buffer, 1X MOPS and 20% formaldehyde and incubated at 65°C for 15 min, then on ice for 1 min. After loading the samples, the gel was run at a constant 50 V for 3 h. The gel was washed twice for 15 min using 20X SSC to remove formaldehyde. The part of

the gel containing the marker and the positive control were stained in 1X running buffer containing 0.5 $\mu\text{g}/\mu\text{l}$ EtBr ON. The DNA was visualised by UV illumination at 302 nm or 365 nm. RNA was transferred from the agarose gel to a positively charged nylon membrane (Hybond-N⁺; Amersham). The following materials were assembled as follows: Three pieces of Whatmann 3 MM paper soaked in 2X sodium chloride/sodium citrate (SSC) were placed on top of a 5 cm stack of paper towels, the membrane and the gel (upright). 3 pieces of wet Whatmann paper were stacked on top and the transfer was left ON. The RNA was cross-linked using a UV Stratalinker 2400 (Stratagene) for 1200 $\mu\text{joules} \times 100$.

2.2.5.3 Northern hybridisation

20 ng of the probe DNA, denatured at 100°C for 5 min was labelled with [α ³²P]-dCTP using Rediprime II (Amersham) and purified with Probe QuantTM G50 Micro Columns (Amersham). Following pre-hybridisation in 6x SSC, 5x Denhardt's, 0.5% SDS at 65°C for 1 h, hybridisation was performed with the labelled probe at the final concentration of 500,000 cpm/ml at 65°C ON. The membrane was washed twice in 2x SSC, 0.1% SDS, at RT for 10 min, once in 1x SSC, 0.1% SDS, at 60°C for 10 min, and finally in 0.1x SSC, 0.1% SDS, at 60°C for 10 min. Hybridisation was visualised and quantified by Molecular Imager FX (Biorad).

2.2.5.4 Stripping Northern blots

Blots were stripped with boiling 0.1% (w/v) SDS until the solution was cold and for a few minutes in 2X SSC. The membranes were stored at -20°C.

2.2.6 Multiple Tissue Northern blot

Multiple Tissue Northern blotting was performed using mouse adult poly A-RNA derived from adult mouse tissues and from adult human brain, according to the manufacturer's instructions (Clontech). Hybridisation was performed at 42°C. β -actin hybridisation was performed for normalization of the loading.

2.2.7 Western blotting

2.5×10^6 cells/well were plated in 6-well plates. Cells were lysed in 100 μ l/6-well of Laemmli sample buffer (BIO-RAD) and one fifth of lysate was analysed on 10-12% SDS-PAGE followed by immobilisation on nitrocellulose membranes (Hybond ECL, Amersham).

2.2.7.1 Protein quantification

Proteins from whole cell extracts were quantified using BCA/ CuSO_4 protein assay (Pierce). Standards were made up with 8, 100, 200, 400, 1000 and 2000 μ g/ml of Bovine Serum Albumin (BSA) made up to 200 μ l with water. For each sample, serial dilutions of cell extract were added up to 200 μ l with water. For each sample 200 μ l of protein assay buffer (50 parts of buffer A and 1 part of buffer B) were added. This was incubated for 30 min at 37°C. The optical density of the standards was measured at 562 nm and a standard curve created. The OD of samples was then measured to give the protein per ml of cell extract.

2.2.7.2 Blotting and transfer

20 µl aliquots of the lysated extracts were denatured at 90°C for 10 minutes on a heating block. Proteins were separated on 7.5-12% SDS-PAGE followed by immobilisation on nitrocellulose membranes (Hybond ECL, Amersham) using semi-dry or dry blotting apparatus. 6 pieces (1 in the dry transfer) of 3 MM Whatman blotting papers were soaked in transfer buffer and placed onto the conductive plate of a semi-dry or dry blotting apparatus. The Millipore filter with the gel facing upwards was placed on top of the blotting paper followed by a further 6 pieces (1 in the dry transfer) of 3 MM Whatman blotting papers soaked in transfer buffer. Transfer was performed at 100 V constant for 1 h. After transfer the blotting the filter was blocked for at least 1 h at RT in TBS-T containing 10% non-fat dried milk (Marvel).

2.2.7.3 Probing and Detection

Primary antibodies were diluted with 10 % Marvel in TBS-T, added to the blots and incubated on a rocker for 2 h at RT or ON at 4°C. After probing with the primary antibody, filters were washed 2 times for approximately 10 min each with TBS-T. Horse Radish Peroxidase (HRP) conjugated secondary antibody appropriate to the species of the primary antibody (Table 2.4) was diluted in 10% Marvel in TBS-T and incubated with the blots for 1 hour at RT on a shaker. Following probing with the secondary antibody, filters were washed 2X for approximately 10 minutes each with TBS-T.

2.2.7.4 Western signal detection

Chemilluminescence detection using the ECL™ Western blotting analysis system (Amersham Pharmacia) or SuperSignal West Femto Maximum Sensitivity Substrate (Perbio) was performed by adding equal volumes of reagent 1 and reagent 2 to the membrane, incubating at RT for 1-5 min and then exposing the blot to ECL film (Amersham Pharmacia) for different lengths of time before developing using an X-OMAT 3000RA film processor. After developing membranes were washed in PBS-T and stored in Saran wrap at 4°C.

2.2.7.5 Stripping Membranes to re-probe

Before re-probing, membranes were stripped of bound primary and secondary antibodies by submerging in 2% SDS, 64.5 mM Tris-HCl and 100 mM β-mercapto-ethanol for 1 hour at 50°C. Membranes were then rinsed in TBS-T and re-blocked in 10% Marvel in TBS-T.

2.2.8 Heterologous expression and purification of recombinant proteins

2.2.8.1 Expression vector construction

pET28b-His expression vector (Novagen) introduced an N-terminal polyhistidine tag to facilitate subsequent protein purification through nickel-beads. The vector was prepared as described in the section 2.2.4.1. See Table 2.6 for enzymes used in this protocol.

2.2.8.2 Transformation of BL21 (DE3)pLysS *E. coli* cells

For the purpose of protein expression, pET28b-His vector containing the insert was propagated in BL21(DE3)pLysS (Novagen) cells. DE3 designation means that the strain of bacteria carries the gene for T7 RNA polymerase, which is inducible by IPTG, whereas the pLysS produces T7 lysozyme to reduce basal level expression of the gene of interest in the event of *ccp1* being toxic. Plasmid DNA (50-200 ng in 1 μ l) was added to a thawed 50 μ l aliquot of BL21(DE3)pLysS competent *E. coli* cells, gently mixed with a pipette tip and incubated on ice for 10 min. Cells were then heat-shocked through incubation at 42°C for 45-50 sec and immediately cooled on ice for 2 min. 250 μ l SOC medium (Invitrogen) were added, and the cells incubated at 37°C for 1 h in a shaker. Selection of transformed cells was then performed by plating these cultures on LB/agar (15 g/L bacto-agar in LB broth) that contained 15 μ g/ml kanamycin at 37°C. Individual colonies were then selected and grown overnight in 5 ml LB containing 15 μ g/ml kanamycin, continuously shaking at 37°C.

2.2.8.3 Heterologous expression of recombinant proteins

BL21(DE3)pLysS transformed colonies were grown to exponential phase (OD_{600} 0.4-0.6) whilst shaking at 37°C in 100 ml LB medium containing 15 μ g/ml kanamycin. Expression through the T7 promoter of the pET28b-His vector was induced ON both at 25°C and 37°C, through the addition of 1-0.1 mM isopropyl β -D-thiogalactoside (IPTG). Samples were collected after 1, 2, 4, 6 and 24 h. Bacteria were then harvested by centrifugation at 6000 g for 20 min at 4°C and the cell pellets stored at -70°C until required.

2.2.8.4 Purification of the recombinant protein

3 g of bacterial pellet were lysated in 15 ml of BugBuster reagent (Novagen) and 25 U of Benzonase Nuclease (Novagen). The His Bind Kits (Novagen) was used to purify the protein from the insoluble fraction following the manufacturer's instruction. 6 M Urea was used as denaturant. The final protein concentration was determined using the ABC kit from Perbio, following the manufacturer's instructions.

2.2.8.5 Gel electrophoresis

4 ml of the protein lysated at the concentration of 1 mg/ml and 500 µl of Laemmli Sample Buffer (BIO-RAD) were loaded in a 10 % SDS-PAGE gel and run at 120 V for 2.5 h. The band corresponding to the right molecular size was cut from the gel and, after fractionating, inserted in a dialysis bag (Medicell International Ltd, MW 12-14 KDa).

2.2.8.6 Electro-elution of the protein

The dialysis bag was previously prepared by heating in 2% Sodium bicarbonate and 1mM EDTA at 80°C for 30 min. The bag was washed several times in distilled water. At this step the gel fragments and 6 ml of elution buffer (0.2 M Tris-Acetate, 1% SDS, 100 mM dithiothreitol, DTT) were inserted into the bag already closed at the extremities. The protein was electro-eluted at 120 V for 3 h in running buffer (50 mM Tris-Acetate, 0.1% SDS). At the end, the protein solution was recovered and centrifuged for 1 h using a centricon tube (Amicon, MW 3 KDa), in order to desalt and concentrate the solution.

The protein concentration was determined by eye-comparison running the solution in a 10% SDS-PAGE gel next to protein samples whose concentration was known.

2.2.9 Antibody generation

5 ml of protein solution (antigen) at the concentration of 0.6 mg/ml was given to the Antibody Facilities of the Beatson Laboratories in order to generate monoclonal and polyclonal antibodies against ccp1/His recombinant protein.

2.2.9.1 Hybridoma production (Beatson antibody facility)

An outbred strain of mice CD-1 (Harrlan-UK) was immunised at 4 week intervals subcutaneously with 25 µg ccp1/His recombinant protein. The protein was emulsified with equal quantities of Freund's adjuvant. Complete adjuvant was used for the first immunisation and then incomplete for subsequent immunisations. Test bleeds were taken after the 2nd, 3rd and 4th immunisation and tested by ELISA assay on plates coated with the immunising protein. The best responding mouse was selected and splenocytes were prepared. The splenocytes were fused with SP2/0-Ag14 mouse myeloma cells using polyethylene glycol (Roche) following the method of Lane & Harlow (Antibodies a laboratory Manual CSH Press 1988). Hybridomas were grown for 10 days then assayed by ELISA. ELISA positive hybridomas were further screened by Western blot analysis and positive hybridomas were single cell cloned by limiting dilution.

2.2.9.2 Polyclonal antibody production

New Zealand White rabbits were immunised with 50 µg ccp1/His recombinant protein at 4 week intervals. The protein was emulsified with equal quantities of

Freunds adjuvant. Complete adjuvant was used for the first immunisation and then incomplete for subsequent immunisations. Test bleeds were taken after the 2nd and 3rd immunisation and tested by ELISA assay on plates coated with the immunising protein. The rabbits were exsanguinated after the 4th immunisation.

2.2.10 Cellular localisation

2.2.10.1 Cell immunostaining

500,000 cells/well were plated on cover-slips inserted in 24-well tissue-culture dishes and transfected with the expression vectors listed in the Table 2.1, following the protocol detailed in the section 2.2.4.1. After 24 h, cells were fixed with 3.7% formaldehyde in PBS and permeabilised in 0.5% Triton X-100 for 20 min each. Blocking solution (0.2% gelatine and 0.1% Triton X-100 in PBS) was applied for a further 20 min. Incubation with the primary antibody was performed ON at 4°C and the secondary antibody for 1 h at RT (Table 2.5 for the list of antibodies used in this study). Filamentous actin structures were visualised after incubation for 1 h at RT with Texas Red-cojugated phalloidin (1:250, Molecular probes). Endoplasmatic reticulum was visualised using specific stain solution (1 mg/ml, Chemicon). Autophagy vesicles were visualised with Monodansyl-cadaverin (MDC, Sigma) as described in (279). Briefly, the cells were incubated with 1 nM MDC in PBS at 37°C for 10 min. After incubation in antibodies, the cells were washed with PBS and mounted on slides using DAPI (4, 6 diamino-2-phenylindole, Vectashield). The slides were analysed by fluorescence microscopy using Zeis Axioplan 2 and the computer program ISIS. Leica confocal SP2 was used and, based on the scanning 14 serial

sections of 0.6 μm , three-dimensional image of the cell were build up. Excitation and emission were: for DAPI (blue) 359 nm and 461 nm; for Texas Red (red) 596 nm and 615 nm; for FITC (green) 494 nm and 520 nm.

2.2.10.2 Chloroquine treatment

500,000 cells/well in 24-well tissue culture dishes with cover-slips were transfected for 24 h in the presence of 25, 100 and 500 μM of chloroquine (Sigma). Cells were immunostained as above.

2.2.11 Generation of stable cell lines over-expressing ccp1

2.2.11.1 Retrovirus system and vector pLPC/ccp1 construction

The retrovirus expression vector pLPC was obtained from Dr S. Lowe. The vector is a derivative of pBabePuro (280) and has been modified by Dr S. Lowe: the SV40 promoter driving puro was deleted to put puro under the control of the LTR (this region contains all signals necessary for gene expression, including the enhancer, promoter, transcription initiation, transcription terminator and polyadenylation signal). The CMV promoter and multi-cloning site was inserted downstream of puro. pLPC and ccp1 CDS were ligated together following the protocol detailed in the section 2.2.5.1. See Table 2.6 for enzymes used in this study. The vector pLPC/EGFP was obtained from L. Bell, Beatson Institute.

2.2.11.2 Retrovirus vector pLPC-ccp1/ GFP-N (GFP-C) construction

pLPC vector was cut with HindIII (XhoI) restriction enzyme at 37°C for 3 h. The linearised vector was blunted using 0.2 mM dNTPs, 1X buffer, 5U of T4 Polimerase (Epicentre) at 12 °C for 15 min and 65°C for a further 15 min. After the blunting reaction, the vector was purified using the Qiagen PCR purification kit and cut ON with the enzyme BamHI (EcoRI) at 37°C. The vector was dephosphorilated using Shrimp Alkaline Phosphates (Promega) at 37°C for 10 min and 65°C for 15 min. The vector was purified using the Qiagen PCR purification kit. In parallel, pd2EGFP-N (pEGF-C)/Ccp1 was cut with AgeI (NotI) restriction enzyme for 3 h at 37°C, blunted as above and purified with Qiagen PCR purification kit. The linearised vector was cut with BamHI (EcoRI) restriction enzyme and the ccp1/EGFP fragment was isolated by agarose gel purification. The pLPC linearised and the ccp1/EGFP fragments were ligated together as explained in section 2.2.4.1. In order to eliminate the plasmid that was not blunted, the ligation product was cut with HindIII (XhoI) restriction enzyme. The product was transformed in DH5α *E.coli* and, after bacterial culture and miniprep, the presence of the insert was tested by restriction enzyme digestion, using StuI and BamHI (EcoRI and Nhe) enzymes.

2.2.11.3 Retrovirus generation and recipient cells infection

As packaging cell line (specially-engineered cell lines that express the viral genes and produce vector virus), phoenix cells were chosen. The cells were obtained from Dr K. Ryan. The choice of packaging cells depends on the desired host range, or tropism, of the virus. For infection, retroviruses require a highly specific cell to interact with a protein on the surface of the viral particle. Tropism can be categorized by the range of

host cells that can be infected: Ecotropic (ecos = home), containing the EcoR receptor, in which virus replicate only in cells from the natural host or closely related species; xenotropic (xenos = foreign) virus replicate efficiently only in cells of foreign origin, not the host; amphotropic (amphos = both) virus replicate in cells of both the natural host and foreign origin. Phoenix is a second-generation retrovirus producer line for the generation of helper free ecotropic and amphotropic retroviruses. The lines are based on the 293T cell line. Ecotropic phoenix lines (capable to infect only cells containing Eco receptor, including mouse, rat and rabbit cells) were created by placing into 293T cells constructs capable of producing gag-pol, and envelope protein for ecotropic viruses. Retroviral expression vector provided the packaging signal psi and a target gene. 2,000,000 cells/well phoenix packaging cells were plated in a 10 cm dish and transfected with 5 µg of vectors pLPC/EGFP, pLPC-ccp1/EGFP-C and pLPC-ccp1/EGFP-N using Lipofectamine 2000 as explained in section 2.2.1.5. Cells were incubated ON in 20% FBS media in order to allow virus production. Primary MEF cells were plated at the density of 2,500,000 cells/well in a 10 cm dish and infected with the Phoenix-supernatant filtered and containing 10 mg/ml of polibrene. The infection was repeated three times at intervals of 12 h each. After the last infection, cells were cultured for 1 week in media containing 25 mg/ml of puromycin in order to select the cells that have been infected. As a control non-infected MEF were selected with the same antibiotic. The same experiment was carried out using SK-N-SH. Since SK-N-SH cells are human cells, the cells were transfected with the pWZLneo-EcoR expression vector.

2.2.11.4 Stable cell lines selection

The surviving cells were plated in a 15 cm-tissue culture dishes and single colonies were grown for one week. The singles clones were picked using cloning rings and grown individually in 10 cm dishes.

2.2.12 RNA interference (RNAi)

RNAi approach was used as tool to suppress gene expression based on a phenomenon in which the introduction of double-stranded RNA (dsRNA) causes degradation of the complementary mRNA (281). Upon introduction the cells with small interfering RNAs (siRNAs) by normal transfection, a RNA-induced silencing complex (RISCs) is assembled. The siRNA strands guide the RISCs to complementary RNA molecules, where they cleave and destroy the cognate RNA. SK-N-SH were plated at 90% confluence in 6-well. Transfection was performed using Lipofectamine 2000 reagent in Optimem media (Gibco) according to the manufacturer's instructions (Invitrogen). 50 nM/well of pre-designed and annealed siRNA (Ambion) was used, RNAi 1, sense 5'-aguugaagccuuugacuuctt-3', anti sense 5'-gaagucuaaggcucaacut-3'. As negative controls, silencer siRNA were used, respectively. Non-transfected cells were also used as negative controls. After 24 h, cells were harvested and RNA was extracted and used for RT-PCR as described in the sections 2.2.2.3 and 2.2.3.1. The primers used were F-338 and R-1096.

2.2.13 Functional assays

2.2.13.1 Proliferation assay

Proliferation KIT I from Roche was used for the proliferation assay and the manufacturer protocol was followed. Briefly, cells were grown on cover-slips coated at a density of 500,000 cells/well in a 24-well tissue-culture dish. 5-bromo-2-deoxyuridine (BrdU) labelling medium (10 μ M BrdU) was added for 60 min. The cover-slips were washed 3 times with PBS, fixed with ethanol fixative (50 mM glycine, 70% of 100% ethanol) for 20 min at -20°C and again washed 3 times with PBS. Anti BrdU (1:10 in incubation buffer: 66 mM Tris, 0.66 mM MgCl₂, 1 mM 2-mercaptoethanol) was added and incubated for 30 min at 37°C. The cover-slips were washed 3 times with PBS and incubated with the anti mouse Ig-fluorescein (1:10 in incubation buffer) for 30 min at 37°C. After washing in buffer, the cover-slips were mounted using Vectashield containing DAPI and analysed by fluorescence microscopy using Zeis Axioplan 2 and the computer program ISIS.

2.2.13.2 Apoptosis assay

TUNEL enzyme and TUNEL labelling mix from Roche were used for apoptosis assay and the manufacturer protocol was followed. Briefly, cells were grown on cover-slips coated at the density of 500,000 cells/well in a 24-well tissue-culture dish. The culture medium was aspirated and the cover-slips washed 3 times with PBS. Cells were fixed with 4% paraformaldehyde for 1 h at RT. After washing in PBS, the cover-slips were incubated with permeabilization solution (0.1% TritonX-100 in 0.1% sodium citrate) 2 min at 4°C. The cover-slips were washed 3 times with PBS

and covered with the 1X labelling mix and deoxynucleotidyl transferase enzyme (5 μ l) and incubated 1 h at 37°C. After washing in PBS, the cover-slips were mounted with Vectashield containing DAPI and analysed by fluorescence microscopy using Zeis Axioplan 2 and the computer program ISIS.

2.2.13.3 Wound assay

Cells were plated at the density of 1×10^5 cells/well in a 6-well tissue culture plate. For treatment, the cells were serum-starved for 24 h. A wound was made on the monolayer using a P200 pipette tip and pictures were taken at 4, 6, 8, 24 h. The cells were fixed and stained with 50% methanol, 10% acetic acid, 0.25% Comassie blue for 10-15 min.

2.2.13.4 Statistics

Student's T-test was performed to test the significance of difference in numerical data as appropriate. The t-test assessed whether the means of two groups were statistically different from each other. The data in the text represents "mean \pm standard error (SEM)". SEM also represents the error bars in the graphs. In the BrdU and TUNEL assays, 6 pictures for each samples were taken, analysed and % mean of the values obtained was calculated. Each ccp1-entity was compared to each control entity.

2.2.14 Histology

After dissection, the tissue was fixed in 4% paraformaldehyde ON at 4°C, processed, and embedded in paraffin. Sections (8 μ m) were cut using a microtome and mounted on siliconated glass slides by the Techonology Service at the Beatson Laboratories. The sections were de-waxed in histoclear (Fisher) and re- and dehydrated in graded

ethanol. For the Haematoxylin and Eosin staining (H&E) sections were stained with haematoxylin for 4 min and rinsed with water. Slides were immersed briefly in 1% cloridric acid in 70% ethanol followed by Scott's Tap Water (Surgipath) for 1 min, then washed in water and counter-stained with eosin for 30 sec.

2.2.15 In situ Hybridization

2.2.15.1 Transcription of Riboprobes

The DIG RNA labelling Kit (SP6/T7) from Roche was used. Ccp1-DNA to be transcribed consisted of part of the CDS and the 3' UTR. Ccp1 was originally cloned into the vector pSPORT1 containing promoters for SP6 and T7 RNA polymerases adjacent to the polylinker. 15 µg of DNA template were linearised using *Sall* (SP6 riprobe generation) and *NotI* (T7 riprobe generation) restriction enzymes in a total volume of 100 µl at 37°C for 2 h. The samples were extracted in phenol/chloroform twice and precipitated in 100% ethanol at -80°C for 30 min. The samples were centrifuged at 13 rpm for 30 min and the pellets washed with 70% ethanol. The pellets were re-suspended in 11 µl of DEPC water. RNA polymerase was used to produce "run-off" transcripts. Digoxigenin (DIG)-UTP was used as a substrate and incorporated into the ccp1 transcript every 20-25th nucleotide. The rprobes were transcribed using 1 µl of cut DNA, 1X DIG RNA labelling mix, 1X transcription buffer, 1 U of RNase inhibitor and 1 U T7 or SP6 RNA polymerase. Samples were incubated at 37°C for 2 h and RNase free DNaseI was added to the rest and incubated at 37°C for 15 min. 0.3 M Sodium acetate and 300 µl of 100% ethanol in DEPC water were added to each sample and stored ON at -20°C. The transcripts were then

centrifuged at 13 rpm for 30 min and the supernatant removed. The pellet was washed with 70% ethanol and centrifuged for 10 min. The pellet was air dried for 10 min and re-suspended in 100 µl of water.

2.2.15.2 Dot Blot Method

In order to check that the probes are correctly labelled, a dot blot experiment was performed. 1 µl of each sample was dotted onto a Hybond-N⁺ (Amersham) membrane and cross-linked for 12 sec using the UV-crosslinker. The membrane was washed 1% blocking reagent (Boeringer Mannheim) in DIG1 (20 mM Tris base, 80 mM Tris HCl, 150 mM NaCl₂), for 30 min. Anti-DIG-AP conjugate (1:5000, Roche) was applied to the membrane for 45 min. The bound antibody conjugate was visualised by colour detection using 5 mg/ml of 5-Bromo 4-cholro-3 indolyl phosphate (BCIP) and 7.5 mg/ml of Nitro blue tetrazolium (NBT) from Sigma. Phosphatase activity was detected by a colour reaction. Ccp1-probes signals were were used at the dilution of 1:50 in hybridization buffer.

2.2.15.3 Hybridization

In situ hybridization was performed using standard procedures. Sections were washed in 0.2 M cloridric acid and then washed in 0.3% triton X100 on a shaker for 15 minutes each. The sections were covered with 100 µg/ml Proteinase K solution for 30 minutes in a moist chamber at 37°C and then fixed in 2% paraformaldehyde solution for 5 minutes at RT. After 2h of incubation in pre-hybridization solution (2X SSC, 20% formaldehyde in water) the slides were incubated in hybridization buffer (0.1 mM Tris, pH 7.5, 12.5X Denhardt's solution, 2X SSC, 0.5 % SDS, 50% formamide,

10% dextran sulphate, 0.25 mg/ml of salmon sperm DNA) containing the probes diluted 1:50. Hybridization was carried out ON at 37°C. Anti-Digoxigenin-alkaline phosphatase conjugate (1:2000, Anti-DIG-AP, Roche) was applied in DIG1 buffer (20 mM Tris base, 80 mM Tris HCl, 150 mM NaCl₂), 25% normal swine/horse serum for 1 h at RT. The antibody conjugate was detected using 5 mg/ml of BCIP and 7.5 mg/ml NBT.

2.2.16 Immunohistochemistry

The sections were deparaffinized in HistoClear (Fisher) and dehydrated in graded ethanol. The sections were boiled twice for 5 min in 0.01 M Citric Acid (pH 6). Endogenous peroxidases were inhibited by a wash in cold 0.3% hydrogen peroxide in methanol for 20 min. Sections were blocked for 1 h at RT in 10% normal horse serum, 0.5% bovine albumin, and 0.3% Triton X-100. The primary antibody was applied ON at 4°C and the secondary for 1 h at RT. The immunoreactivity was visualised by Vectastain IgG ABC kit or Impress Kit (Vector Laboratories) and DAB (Dako) in the presence of Nickel. See Table 2.5 for antibodies used.

2.2.17 Microarray analysis

CNC were treated with 50 ng/ml FGF2 in the presence of 10 µg/ml heparin for 4 hours, and the expression of genes were compared to those in the absence of FGF2. Seventeen features representing housekeeping genes in the array (GAPDH, HPRT and S16, S9, and S8 ribosomal proteins) gave average value of Ratio of Medians (ROM), 1.20 ± 0.28 , which was confirmed to be acceptable. Total RNA was

extracted from cells in the growing phase by using RNA Clean (Hybaid) according to the manufacturer's instruction and further purified with RNeasy mini kit (Qiagen). Direct labelling of 20 µg of total RNA primed with Oligo(dT) was performed in the presence of Cy-5 and Cy-3-dUTP (Amersham Pharmacia Biotech) using SuperScript II (Invitrogen). The Cy5- and Cy3-labelled cDNA samples were then mixed and purified with GFX DNA purification kit (Amersham Pharmacia Biotech). The samples were added with 1.2 µg of salmon sperm DNA and 5 µg of Poly-A and dried in SpeedVac at 60°C. The high-density glass microarray chips were prepared at the EMBL core facility by spotting the PCR products prepared from the NIA 15k cDNA mouse clone set (Tanaka et al., 2000; Cortes-Canteli et al., 2004). Array slides were pre-hybridized in 6x SSC, 0.5% SDS, 1% BSA at 42°C for 1 h and incubated in a boiled water for 2 min shortly prior to hybridisation. The cDNA samples were resuspended in 15 µl of hybridisation buffer (50% formamide, 6x SSC, 0.5% SDS and 5x Denhardt's) and denatured by incubating at 95°C for 2 min. Hybridisation was at 42°C for 16 h. The slides were washed for 10 min each with 2x SSC, then with 0.5x SSC, 0.1% SDS, followed by 0.1x SSC, 0.1% SDS, at RT. Scanning was performed with GenePix 4000B (Axon). The data acquisition and initial data analysis was performed with GenePix Pro 3.0 and the data tables were analysed further in Excel in order to obtain the gene list. Quality control was performed, firstly by eye, to confirm scanner alignment and absence of significant bubbles and scratches. Scatter plots were further used to eliminate the unacceptable hybridisation data. The multiple spike-in controls RNA template were added to the sample upon direct labelling, and the successful labelling and hybridisation was confirmed in each hybridisations.

GenePix Pro program calculates the Normalisation Factor of each hybridisation, based on the premise that the arithmetic mean of the ratios from every feature on the given array should be equal to 1. Normalisation was therefore performed by multiplying the Factor to ROM in each gene. The program also identifies features that did not give good alignment to the expected spotted area as “flagged” spots, indicative of the impaired-quality hybridisation of the specific genes. To generate the list, we have removed all flagged genes from the list. Finally, the genes that passed all these criteria were sorted by ROM and those that showed more than ± 1.5 fold changes were selected from each data table. Only those genes that appeared in all 3 experiments were selected in the final list and average ROM value was calculated. Gene functions were categorised based on the information given in the NIA mouse 15k cDNA clone gene ID list at the first instance and modified when necessary. The original microarray data has been deposited to GEO database (Accession No. GSE2066).

Table 2.1 Features of plasmid vectors and their uses

Vector (Source)	Selection	Description
pSPORT (Stratagene)	ampicillin resistance	Vector containing the NIA 15K clone set
pCR [®] II (Invitrogen)	ampicillin resistance	Used as a holding vector for sequencing after initial propagation.
pCDNA4/Myc-Hys, C (Invitrogen)	kanamycin resistance	Protein expression in mammalian cells
pd2EGFP-N1 (Clontech)	kanamycin resistance	Protein expression in mammalian cells
pEGF-C1 (Clontech)	kanamycin resistance	Protein expression in mammalian cells
pDsRED-N1 (constructed in the laboratory)	kanamycin resistance	Protein expression in mammalian cells
pDsRED-C1 (Clontech)	kanamycin resistance	Protein expression in mammalian cells
pLPC (gift from Dr Ryan)	puromycin resistance	Retroviral expression vector. It is a derivative of pBabePuro
pWZLneo-EcoR (gift from Dr Ryan)	neomycin resistance	EcoR protein expression in mammalian cells
pET28b (Novagen)	ampicillin resistance, N-terminal His-tag, T7-tag	Protein expression in <i>Escherichia coli</i> . Transcription of DNA inserts driven by the isopropyl β -D-thiogalactoside (IPTG)-inducible T7 promoter

Table 2.2 Primers and PCR conditions

Primers	Annealing T	Cycles	Applications	Usage
F-338	58°C	30	Cloning in pCRII	Ccp1 5' UTR, CDS and part of the 3' UTR amplification
R-1096	58°C	30	Cloning in pCRII	Ccp1 5' UTR, CDS and part of the 3' UTR amplification
F-338-EcoRI	58°C	30	Cloning in pCDNA4/Myc-His	Ccp1 CDS amplification; <i>EcoRI</i> incorporation at the 5' end of the CDS
R-850-NotI *	58°C	30	Cloning in pCDNA4/Myc-His	Ccp1 CDS amplification; <i>NotI</i> incorporation at the 3' end of the CDS; stop codon missing
F-338- EcoRI + 1AA	58°C	30	Cloning in pdEGFP-N, pEGFP-C and pDsRed-C	Ccp1 CDS amplification; <i>EcoRI</i> incorporation at the 5' end of the CDS; 1 AA was added to the sequence to obtain the exact reading frame
R-850-SalI	58°C	30	Cloning in pEGFP-C and pDsRed-C	Ccp1 CDS amplification; <i>SalI</i> incorporation at the 3' end of the CDS
R-850-SalI + 2 AA*	58°C	30	Cloning in pdEGFP-N	Ccp1 CDS amplification; <i>SalI</i> incorporation at the 3' end of the CDS; 2 AA were added to the sequence to obtain the exact reading frame
R-850-SalI + 1 AA*	58°C	30	Cloning in pET28b	Ccp1 CDS amplification; <i>SalI</i> incorporation at the 3' end of the CDS; 1 AA was added to create the exact reading frame
F-pRed	55°C	25	Cloning in pdEGFP-N	pRed sequence amplification
R-pRed	55°C	25	Cloning in pdEGFP-N	pRed sequence amplification
F-GAPDH	64°C	30	Loading control	GAPDH amplification
R-GAPDH	64°C	30	Loading control	GAPDH amplification

* Stop codon omitted

Table 2.3 Primers sequences

Ccp1-primers	Sequence
F-338	5'-ATTGGCTGTCATGCACATGGC-3'
R-1096	5'-CACACGTCACCTGTCATGCCCTGA-3'
F-338-EcoRI	5'-5"TTGAATTCACCATGGCGGTCCAGGCTCTGCGAGAGGAGT T -3'
R-850-NotI *	5'-GGGCGGCCGCGGCAG CCCAGG -3'
F-338- EcoRI + 1AA	5'-T TGAAT TCAATGGCGGTCCAGGCTCTGCGAGAGGAGT T -3'
R-850-SalI	5'-GTCGACTCAGGCAGGCCCAGG -3'
R-850-SalI + 2 AA*	5'-CCCGTCGACTTGGCAGGCCCAGG -3'
R-850-SalI + 1 AA*	5'-CCCGTCG CTGGCAGGCCCAGG -3'

Other primers	Sequence
F-pRed	5'- TTGGATCCA ATGGCCTCCTCCGAGGACGTCATC -3'
R-pRed	5'- GGGCGGCCGCTTCACAGGAACAGGTGGTG -3'
T7 Primer	5'-AATACGACTCACTATAG-3'
SP6 Primer	5'-ATTTAGGTGACACTATAG 3'
F-pLPC	5'CTATATAAGCAGAGCTCTCTGGCTAAC-3'
R-pLPC	5'-CTAGATGCATGCTCGAGCGGCCCCAG-3'
R-BGH	5'-CCTCGACTGTGCCTTCTA -3'
F-GAPDH	5'-ACCACAGTCCATGCCATCAC-3'
R-GAPDH	5'-TCCACCACCCTGTTGCTGTA-3'

* Stop codon omitted

Table 2.4 Details of antibodies and conditions used in the Western blotting

Primary antibody	IgG class	Source	Dilution
Anti-ccp1 79a	Rabbit	Beatson antibody facility	1:500
Anti-ccp1	Mouse monoclonal	Beatson antibody facility	undiluted
Anti-myc 9E10	Mouse monoclonal IgG1	Beatson antibody facility	1:1000
Anti-GFP	Rabbit polyclonal	Abcam	1:4000
Anti-actin	Mouse monoclonal IgG1	Sigma	1:2000
Anti-ERK	Rabbit polyclonal	Cell Signalling	1:1000
Anti-phospho-ERK	Rabbit polyclonal	Cell Signalling	1:1000
Anti-lamin A/C	Goat polyclonal	Santa Cruz	1:1000

Secondary antibody	IgG class	Source	Dilution
Conjugated horseradish peroxidase	Mouse IgG	Transduction Lab	1:5000
Conjugated horseradish peroxidase	Rabbit	Transduction Lab	1:20000

Table 2.5 Details of antibodies and conditions used in the immunohistochemistry

1° antibody	IgG class	Source	Dilution
Anti-ccp1 79a	Rabbit polyclonal	Beatson antibody facility	1:100
Anti-myc 9E10	Mouse monoclonal IgG1	Beatson antibody facility	1:100
Anti-c-myc	Rabbit polyclonal	Santa Cruz	1:100
Anti-β-tubulin	Mouse monoclonal IgG1	Sigma	1:100
Anti- Transferrin receptor	Mouse monoclonal IgG1	Zimed laboratories	1:100
Anti-GFP	Rabbit polyclonal	Abcam	1:4000
Anti-Lamp2	Mouse monoclonal IgG1	BD Bioscience	1:100
Anti-EEA1	Mouse monoclonal IgG1	BD Bioscience	1:100
Anti-Vinculin	Mouse monoclonal IgG1	Chemicon	1:100
Anti-Dlx 2	Rabbit polyclonal	Chemicon	1:200
Anti-glutamate decarboxilase 65/67	Rabbit polyclonal	Chemicon	1:200
Anti Reelin	Mouse monoclonal IgG1	Chemicon	1:500
Anti-FGFR3	Rabbit polyclonal	SantaCruz	1:200
Anti- calbindin	Rabbit polyclonal	Chemicon	1:1000
Anti-A2B5	Hibridoma	gift from Dr Sue Barnett	1:10
Anti-Map2	Mouse monoclonal IgG1	Sigma	1:500
Anti-Tuj1	Mouse monoclonal IgG2α	Covance	1:500

Secondary antibody	Class	Source	Dilution
FITC-conjugated	Mouse IgG1	Cambridge Bioscience	1:100
TRITC -conjugated	Mouse IgG1	Cambridge Bioscience	1:100
FITC-conjugated	Anti Rabbit	Cambridge Bioscience	1:100
Texas red	Mouse IgG1	Molecular Probes	1:400

Table 2.6 Restriction enzymes

Enzyme	Source	Plasmid cut	Application
NotI	BioLabs	pSPORT1/ccp1	Northern blots-probes
Sall	Invitrogen		preparation
EcoRI	Invitrogen	pCRII/ccp1	Check fragment insertion
NotI	BioLabs		
NotI	BioLabs	pCRII/ccp1	Check fragment insertion
Sall	Invitrogen		
EcoRI	Invitrogen	pCDNA4/Myc-Hys/ccp1	Expression vector
NotI	BioLabs		preparation and checking of fragment insertion
BamHI	Invitrogen	pd2EGFP-N1/ccp1	Elimination of GFP
NotI	BioLabs		
EcoRI	Invitrogen	pET28b/ccp1	Expression vector
Sall	Invitrogen		preparation and checking of fragment insertion
EcoRI	Invitrogen	pLPC/ccp1	Retrovirus vector preparation
XhoI	Invitrogen		and checking of fragment insertion
Sall	Invitrogen	pSPORT1/ccp1	Sp6 riprobe production for in situ hybridisation
NotI	BioLabs	pSPORT1/ccp1	T7 riprobe production for in situ hybridisation

Table 2.7 Buffers

Buffers	Composition
Agarose gel buffer (TAE)	40 mM Tris-base, 1 mM acetic acid, 1 mM EDTA, pH 8.5
Luria-Bertani Medium (LB)	10 g/l bacto-tryptone, 5 g/l bacto-yeast extract, 10 g/l NaCl
10X MOPS	0.2 M MOPS, 50 mM Sodium acetate, 10 mM EDTA
SDS/PAGE running buffer	25 mM Tris-base, 192 mM glycine, and 0.1% (w/v) SDS, pH 8.3
SDS/PAGE sample buffer	0.5 M Tris-base, 10% or 25% (v/v) glycerol, 10% (w/v) SDS, 0.05% 2 β -mercaptoethanol, 0.05% (w/v) bromophenol blue, pH 6.8
TBS	200 mM Tris, pH 7.6, 137 mM NaCl
TBS-T	200 mM Tris, 137 mM NaCl, 0.1% Tween 20
Western blot transfer buffer	25 mM Tris, 192 mM glycine, 20% (v/v) methanol
Electro-elution running buffer	50 mM Tris-Acetate, 0.1% SDS

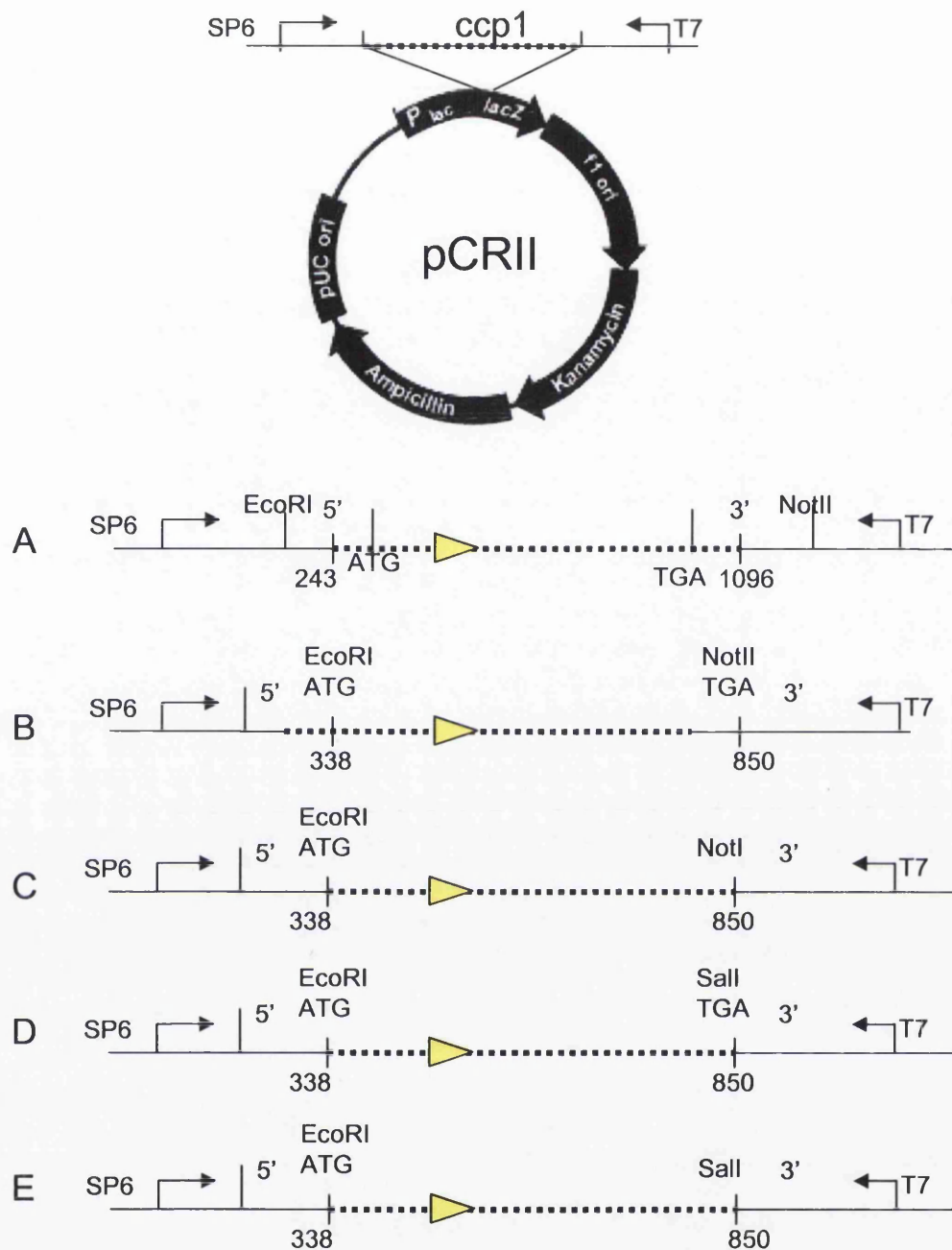


Figure 2.1 Plasmid map of pCR II-ccp1

Ccp1 CDS and part of the 3' UTR were amplified the using RT-PCR. Several fragments were generated: (A) A 853 bp PCR product generated using primers F243 and R1096. (B) A 512 bp PCR product generated using primers F338-EcoRI and R850-Not. (C) 512 bp PCR product generated using primers F338-EcoRI and R850-NotI. (D) A 512 bp PCR product generated using primers F338-EcoRI and R850-Sall. (E) A 512 bp PCR product generated using primers F338-EcoRI and R850-Sall + 2 AA.

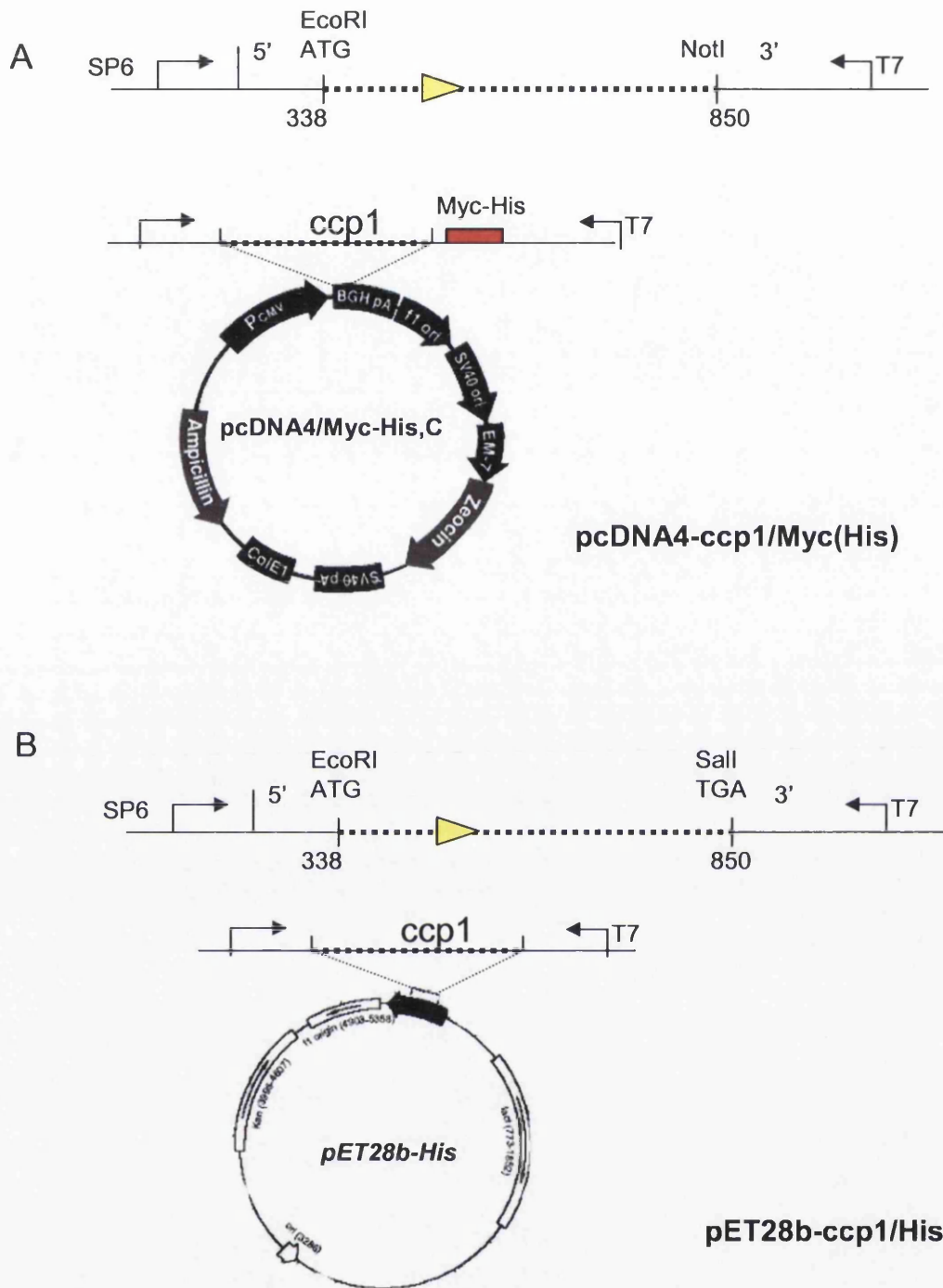


Figure 2.2 Plasmid map of *pcDNA4-ccp1/Myc(His)* and of *pET28b-ccp1/His* vectors

(A) Ccp1 CDS was digested with *EcoRI* and *NotI* restriction enzymes and ligated into the complementarily digested *pcDNA4/Myc-His, C* expression vector. (B) Ccp1 CDS was digested with *EcoRI* and *Sall* restriction enzymes and ligated into the complementarily digested *pET28b* expression vector.

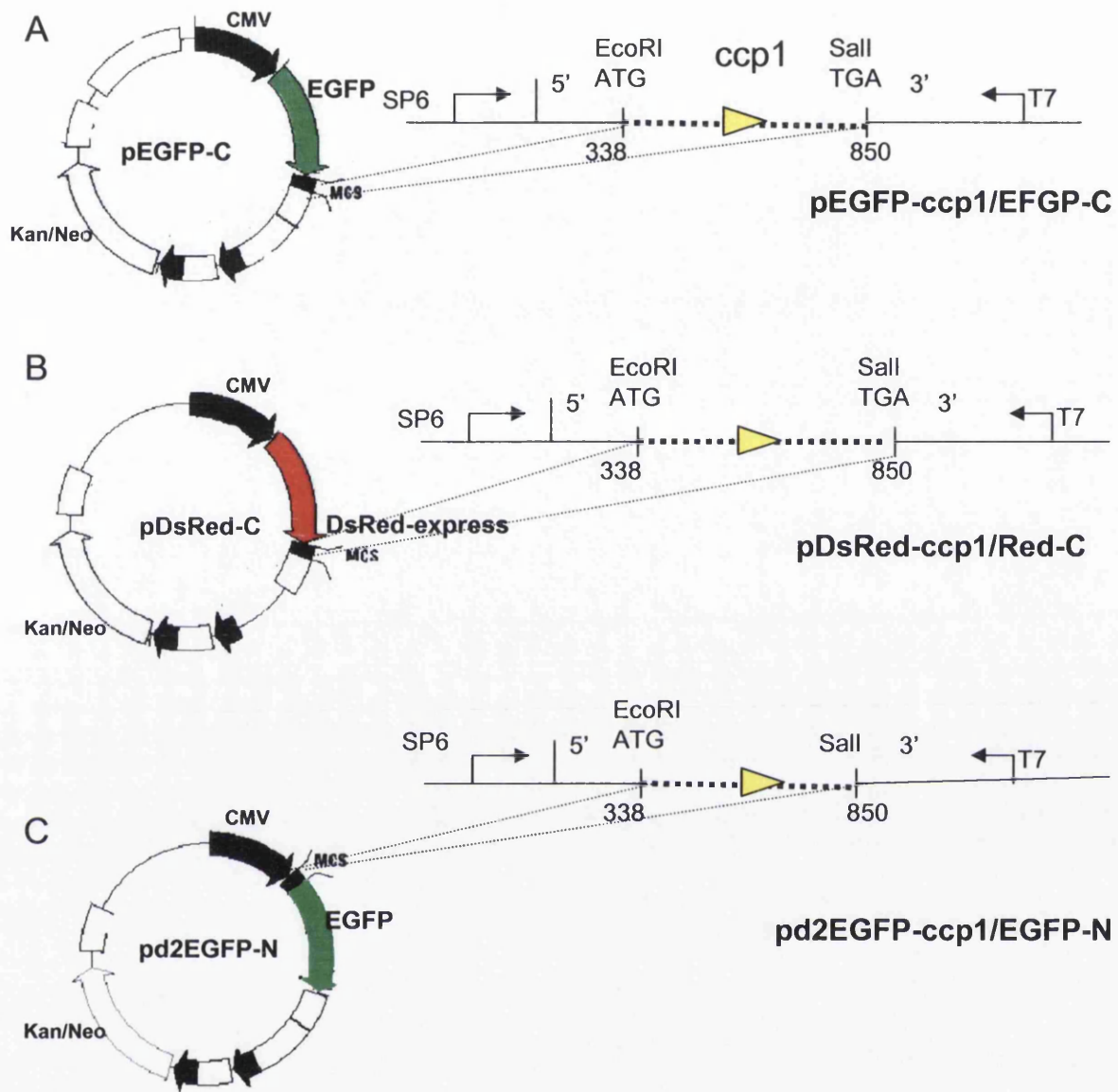


Figure 2.3 Plasmid map of pEGFP-ccp1/EGFP-C, and pDsRed-ccp1/Red-C and pd2EGFP-ccp1/EGFP-N vectors

(A-C) Ccp1-CDS was ligated into pEGFP-C, pDsRed-C and pd2EGFP-N expression vectors. The vectors contained a (A) EGFP at the N-terminus, a Red tag (B) at the N-terminus and a (C) EGFP tag at the C-terminus.

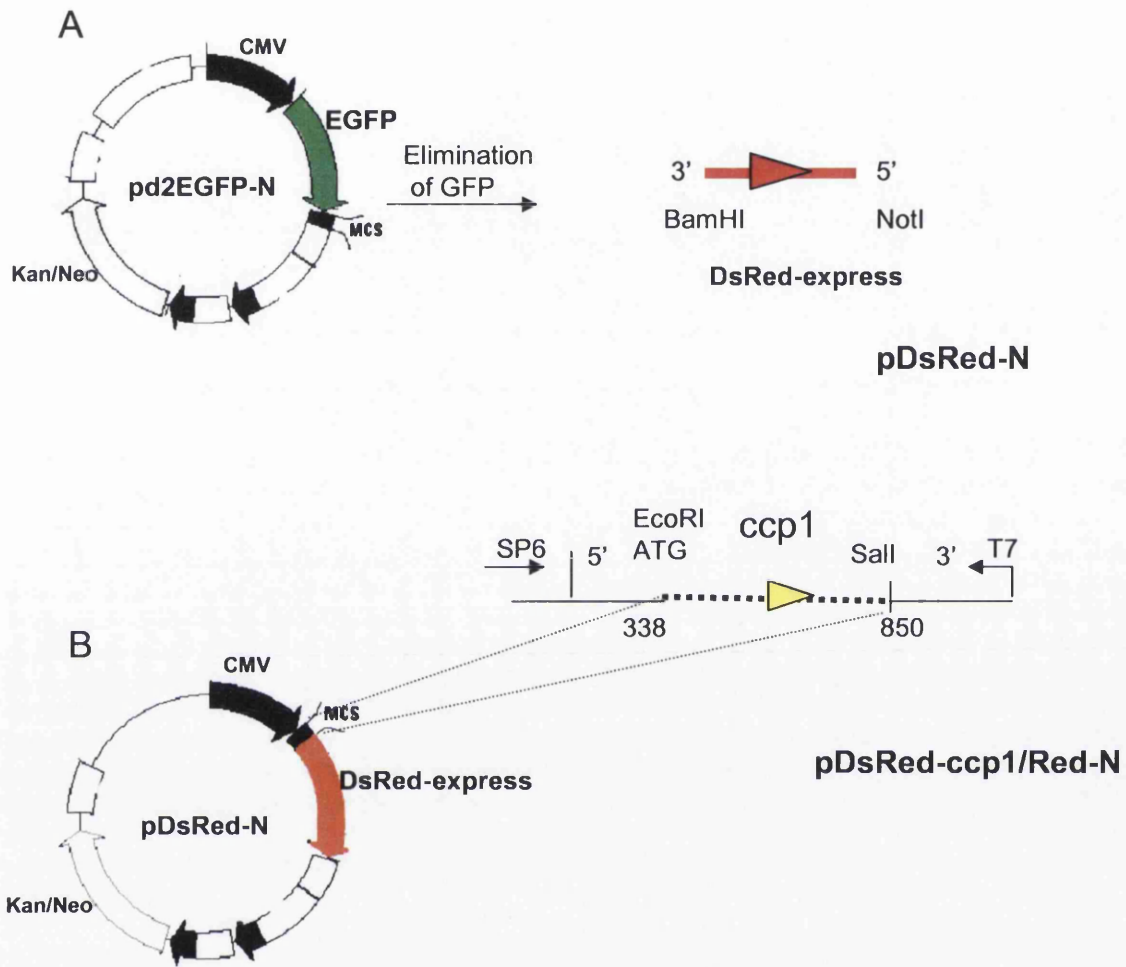


Figure 2.4 Plasmid map of pDsRed-ccp1/Red-N vector

(A) The EGFP-sequence was cut out from the vector pd2EGFP-N and substituted with DsRed fragment. (B) The final vector contained ccp1-CDS tagged with DsRed at the N-terminus.

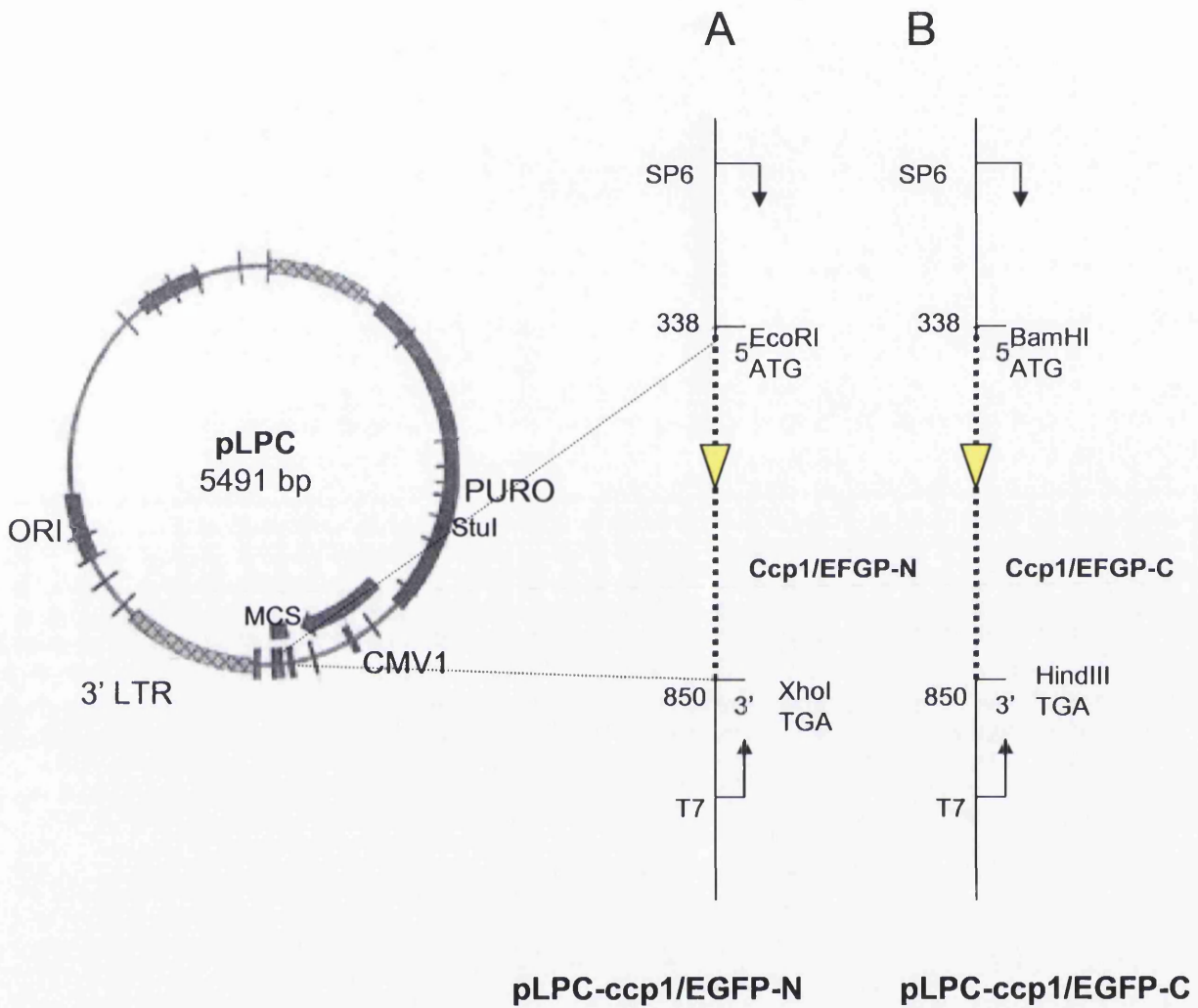


Figure 2.5 Plasmid map of pLPC-ccp1/EGFP-N and pLPC-ccp1/EGFP-C vector

The retroviral vector pLPC was ligated together with the fragments ccp1/EGFP-N (A) and ccp1/EGFP-C (B).

CHAPTER 3

RESULTS

3.1 Identification and characterization of *ccp1* gene

FGF2 is expressed in the telencephalic neuroepithelium and is known to modulate cell proliferation and differentiation and long-term survival of neurons in culture (106, 282). FGFs have been shown to directly affect the transcription of several genes (74). To identify the genes downstream of FGF2 in cortical cells during embryonic development, a microarray was previously performed using cortical neuron culture (CNC). A microscopic glass chip containing 15,247 unique cDNA clones in the National Institute of Aging (NIA) mouse 15K clone set (<http://lgsun.grc.nia.nih.gov>) was used (276). The study showed more than 500 genes with altered expression levels after FGF2 stimulation by more than 1.5 fold (283). 324 genes were shown to be up-regulated and 225 were down-regulated. Genes were categorized with known function based on the information on the NIA gene ID list. In contrast, more than half of the identified genes did not show any homology to genes with annotation or known function. At the beginning of this thesis, 39 genes were selected from the list based on the intensity of the induction, novelty of the genes, as well as their characteristics in correlation with FGF functions. In order to determine the identity of the corresponding bacterial clones, first the original plasmids were sequenced and compared with the 3' and 5' sequences provided by the NIA website. The genes were blasted against NCBI databases and identified the name, if known and provided details, including accession number, predicted protein size, coding sequences size and base composition. First, 14 genes were chosen and analyzed by northern blotting in order to study the expression level upon FGF2 stimulation. The *ccp1* cDNA probe

was prepared from the NIA mouse 15k cDNA clone set (pSport1-H3104E08) that contained a part of the coding sequence and 3' un-translated region (UTR). To test the expression of the genes in the embryonic brain and the specificity of the probe, first northern blotting was performed using total RNA extracted from brain tissue from E14.5 mice (CD1 background). Only the genes that gave good quality results in the northern blotting were selected for the further analysis. The list included *Protein phosphatase 1*, *TRIM8*, *gene 29a* (Riken, XM_129811), *gene 31* (NOID, AK034517), *gene 35* (Riken, XM_133378) and *formin binding protein 3*. Next, northern blotting was performed using RNA extracted from CNC treated with or without FGF2 for 4 h in the presence of heparin at 1 DIV. GAPDH hybridisation was performed to normalize the level of expression. 4 genes were selected for further investigation: *TRIM8*, *gene 29a*, *gene 31* and *formin binding protein 3* (Fig. 3.1.1). *In situ* hybridisation was also performed on the selected genes using CD1 mice coronal section obtained from whole E12.5 body and E14.5 cortex (Fig. 3.1.1, B, E, H, K). The genes showed specific staining in the embryonic body and in the dorsal cortex. Gene 29a was highly expressed in the ventricular zone of the cortex (Fig. 3.1.1, F), whereas *TRIM8* and *formin binding protein 3* (Fig. 3.1.1, C, L) were more restricted in the cortical plate. Gene 31 expression was diffuse in the cortex thickness (Fig. 3.1.1, I).

Based on the quality of the data and my interest in an uncharacterized Riken clone gene 29a, was chosen as subject of this study. The gene is a previously uncharacterised Riken clone encoding a putative 180 amino acid (AA) protein was identified and characterised. The amino acid sequence predicted two coiled coil

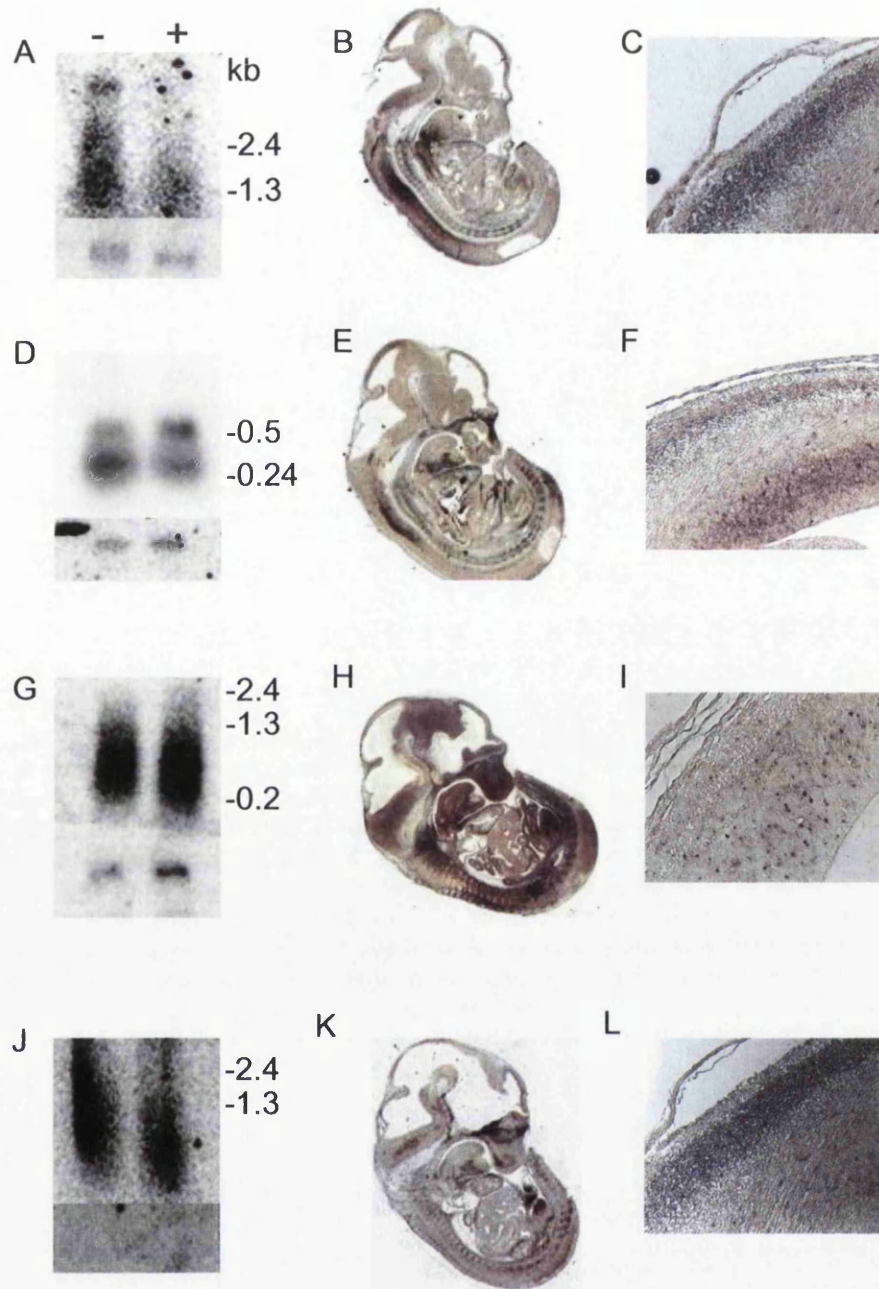


Figure 3.1.1 Selection of the genes of interest.

In order to select the gene of interest, a number downstream genes of FGF2 were analysed by northern blotting: TRIM 8 (A, B, C); novel gene 29 (ccp1) (D, E, F); novel gene 31 (G, H, I); formin binding 3 (J, K, L). First, the genes were analysed by northern blotting using 2 μ g of RNA extracted from E14.5 CNC treated with 50 ng/ml FGF2 and 10 μ g/ml heparin (+) or heparin alone (-). Normalization with GAPDH is reported below each northern-sample (A, D, G, J). Secondly, the genes were analysed using non radioactive in situ hybridization in E12.5 sagittal sections of the body (B, E, H, K) and in E14.5 coronal section of the cortex (C, F, I, L).

domains, therefore the gene was named 'coiled coil protein 1' (*ccp1*). The *ccp1* gene was characterised at the molecular level as follows. Firstly, *ccp1* gene structure was characterised using information available from the databases. Secondly, Northern blotting was performed to analyse regulation of *ccp1* expression upon FGF2 stimulation in cell lines and in primary cortical neurons. Thirdly, expression vector of the *ccp1* gene was constructed and its expression was examined. Finally, monoclonal and polyclonal antibodies were raised against the bacterially expressed *ccp1* protein and characterised for the detection of both expressed and the endogenous *ccp1* proteins using Western blot.

3.1.1 Characterization of the novel gene, *coiled coil protein 1 (ccp1)*

Using a blast search against the NCBI database, a novel gene, Riken clone 2310061I09 (NIA clone ID; H3104E08, GeneBank accession #; XM_129811) was characterised. Based on the NCBI GeneBank information, the gene is 1697 bp long and encodes a putative protein composed of 180 AA (Fig. 3.1.2 and 3.1.3). Various protein motif search tools available at the ExPASy Proteomics Server (<http://www.expasy.org>), including SMART (Simple Modular Architecture Research Tool) and the Protein Information Resource (PIR), have predicted specific domains within the sequence (Fig. 3.1.2). Two coiled coil domains (CC1 and CC2) at amino acid positions 3-38 and 154-175 were present in the sequence. A coiled coil domain is known to form a stable superhelix structure when two or three α -helices bind around each other (222). This structure renders opportunities for oligomerisation as

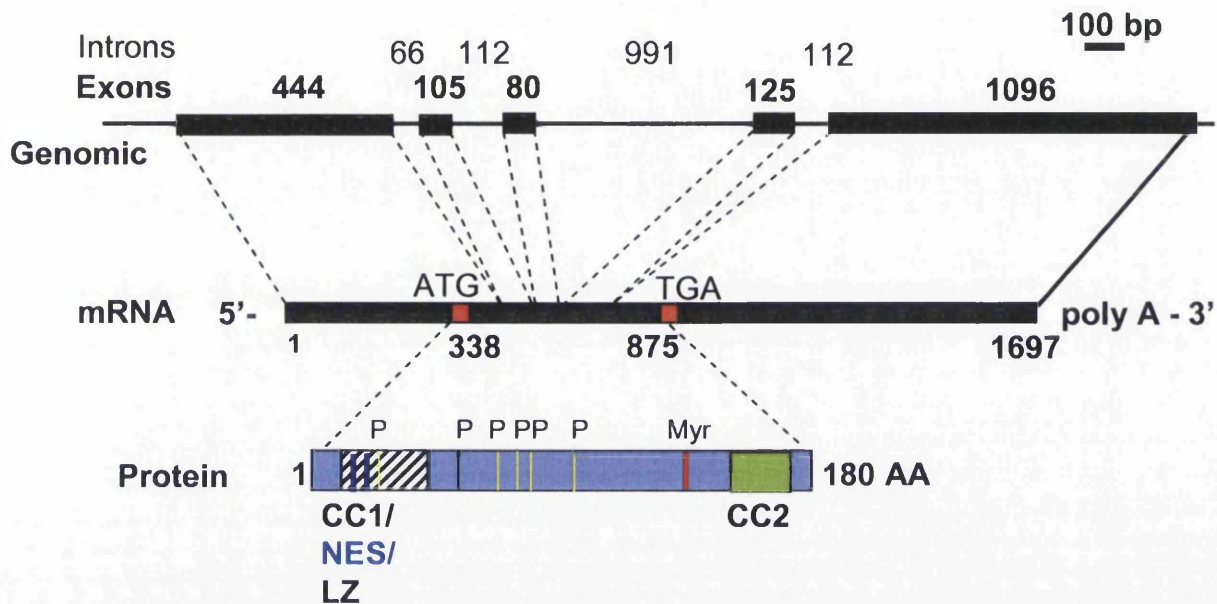


Figure 3.1.3 Schematic view of the *ccp1* gene structure and protein product

Ccp1 genomic sequence is composed of 5 exons and 4 introns. *Ccp1* is transcribed into a mRNA of 1.7 kb size. The gene product is predicted to be 180 AA. There are two coiled-coil regions in the protein at 3-38 AA and 154-175 AA, with a leucine zipper motif and two NES domains present within the first CC region (LZ/CC1 and CC2). Domain flanked by the two coiled coil regions contained putative phosphorylation sites for protein kinase C and casein kinase II (P), as well as an N-myristoylation site (Myr).

well as the binding of other proteins with a coiled coil domain. Based on this particular feature, the gene was named '*coiled coil protein 1 (ccp1)*'.

A leucine zipper structure was also predicted at the N-terminus of the protein within the CC1 domain (CC1/LZ) based on the presence of 4 leucine-repeats with 6 amino acid residue intervals. The leucine zipper is a periodic repetition of leucine residues at every seventh position that facilitates dimerisation between two peptides as well as the binding of the DNA chain (250).

Two putative NES domains were also found in the N-terminus of *ccp1*. NES is a short sequence that determines the nuclear transport of the host protein through the nuclear complex from the nucleus to the cytoplasm (257). NES is composed of a leucine rich region with the accepted consensus, LX₂₋₃LX₂₋₃LXL (261). Many of the known nucleoplasmatic shuttle proteins are involved in signal transduction and cell cycle regulation (284).

Other motifs were also detected in the *ccp1* sequence, including putative phosphorylation sites by protein kinase C (position 80, 100, and 134) and casein kinase II (position 19, 61, and 90). Both of these enzymes are serine/threonine kinases and the putative patterns are [ST]-X-[RK] and [ST]-X₂-[DE], respectively. A potential N-myristoylation site (position 145) was also present. N-terminal myristoylation is a lipid anchor modification of eukaryotic and viral proteins targeting them to membrane locations (285). The pattern for a putative myristoylation site is G-{EDRKHPFYW}-X₂-[STAGCN]-{P}.

3.1.2 *Ccp1* genomic structure and its chromosomal location

To assess *ccp1* genomic structure, alignment between cDNA sequence and the mouse genomic database was performed (see Table 3.1 for GeneBank accession numbers). Comparison of the cDNA and the genomic sequence allowed identification of the boundaries between exons and introns (ag-gt sequences) (Table 3.2). The gene is composed of 5 exons and was spaced with relatively short introns sized between 66 to 991 bases. *Ccp1* was localised in mouse chromosome 1,1B. In addition, human homologue of *ccp1* was located in human chromosome 2q21.2.

3.1.3 *Ccp1* protein sequence is conserved between species.

To determine whether *ccp1* sequence was conserved between species, a blast search of the protein sequence was performed in NCBI database. It revealed several putative homologues of *ccp1* across species (Fig 3.1.4). Alignment of the mouse primary sequence revealed a high similarity with the rat (97.2% similarity and 83.3% identity) and the human sequence (83.3% similarity and 78.9% identity). The sequence was well-conserved throughout the entire protein, however some divergence was found in the two coiled coil domains, as well as the localised regions in the middle portion (position 46-61 and 121-129).

The NES sequences were similar between mouse and human. The mouse *ccp1* sequence contained the NES consensus LX_3LX_2KXL and LX_2LX_2LXA , while the human *ccp1* contained LX_3LX_2LXL and LX_2LX_2LXA (position 6-17 and 18-26, both in mouse and human sequences). Similarity was also present in zebrafish (37.2% homology and 30.6% identity) and drosophila (31.9% homology and 19.5% identity)

Table 3.1 The Accession Numbers of the *ccp1* sequences

Type	Species	Accession Number
cDNA	Mouse	XM_129811 (NCBI)
Genomic	Mouse	NT_039170 (NCBI)
Protein	Human	NP_115733 (NCBI)
Protein	Mouse	XP_129811 (NCBI)
Protein	Rat	XP_343552 (NCBI)
Protein	Drosophila	NP_649550 (NCBI)
Protein	Zebrafish	ENSDARP00000042663 (Ensembl)

Table 3.2 Nucleotide sequences at the exon-intron boundaries of *ccp1*.

Alignment between the genomic and cDNA sequences (NT_039170 and XM_129811) was performed to identify boundaries of the exons of the *ccp1* gene in the mouse. Sequences of the exons and introns of mouse *ccp1* gene are in upper and lower case, respectively. The GT/AG sequence was conserved in all exon-intron boundaries (bolded).

Exon	3' splice donor	5' splice donor	Exon size (bp)	Intron size (bp)	Domain
1		GGTGGAGGAG gt gggccacg	444	66	5' UTR CDS
2	tctcccc ag GGTTGGCTCT	TGCGTGCCAG gt gagcgccc	105	112	CDS
3	tttttccc ag CGAGGCCCAG	AGCGAAGCAT gt aagtctcc	80	991	CDS
4	tttctttc ag CTCTGCGCAG	TTCCGGGATG gt gagtttta	125	112	CDS
5	ctctcacc ag GCCTACAGCT		1096		CDS 3' UTR

Mouse-	MAVQALREELDSKCLQLLSDLEELEAKRAALNARVEEGWLSLAKARYAMGAK	52
Human-	--AL--A--LV--G--G--TV-----	52
Rat-	-E-----	52
Zebrafish-	LDE-LL.....LFMEQ--A--E--QR-SLI---F-I-----S-N--	43
Drosophila-	MSIQRSEKE-AGQLLDDLY-DMFHLVEEHTQC	32
Mouse-	SVGPLQYASRMEPQVCVRASEAQDGPQTFRVIKADAQTPEEVGPSEASLRRR	114
Human-	-----H-----H-----E--K-K-VR-GVHA-----R--G-----	114
Rat-	-----N-----	114
Zebrafish-	Q-SA-----E-Q-L-H-ETRNMIYHFLTGLRRRVHTKQKEVKEGEQETDEV	95
Drosophila-	RINLERCNASGAILLARTRFQHGGSQCVSTAQIPTENSA-FNALCRVVDSTD	84
Mouse-	KGPTKTKELGSAVVPQDPLNWFILVPHSLRQAQASFRDGLQLAADIASLQT	156
Human-	-----P-PE-SEA-----	156
Rat-	-----S-----	156
Zebrafish---TDSPTPEHR--K-----QN-K---SA-KE-	131
Drosophila-	GVCIERQAVDKSKGFVE--H--SV-P-M--N-VNK-K-CIE-V-ESTN--R	136
Mouse-	RINWGQSQLRGLQKKLKELDPGPA	180
Human-	--D---R-----E---Q-E--A-	180
Rat-	-----L-----R-----	180
Drosophila-	QLGEA-DSITKLRRSALLS	155

Figure 3.1.4 Comparison of *ccp1* primary structure across species

Alignment was carried out using Mega Align version 5.05 (DNA Star). High similarity was found in rat (97.2% homology and 83.3% identity) and human sequences (83.3% homology and 78.9% identity). Less similarity was found with zebrafish (37.2 % homology and 30.6% identity) and drosophila (31.9% homology and 19.5% identity) sequences. The coiled coil regions and the NES are conserved in mouse, human, and rat sequences (shadowed) but not in drosophila and zebrafish. Gene accession numbers are listed in the Table 3.1.

sequences. The two coil coiled regions, the NES and the leucine-zipper motif (CC1/LZ/NES and CC2) were conserved within the mammalian species but absent in drosophila and zebrafish sequences.

3.1.4 Primary CNC treatment with FGF2 and heparin.

Ccp1 was identified as a downstream gene of FGF2. Therefore, FGF2 has been routinely used as stimulatory ligand in the experiment. In order to determine the optimal concentration of FGF2 to use in the treatment of CNC, a time and a concentration course was performed. E14.5 CNC were cultured and at 1 DIV treated them with different concentrations of recombinant FGF2 (1-10 ng/ml) and heparin (1-0.001 μ g/ml). The cells were observed daily (Fig 3.1.5). When the cells were treated only with FGF2 (10 ng/ml) (Fig 3.1.5, A-C) or with a smaller concentration of heparin (0.1 μ g/ml) (Fig 3.1.5, J-L), no changes were detected in comparison with the mock treated cells (Fig 3.1.5, M-O). At 1 DIV, high concentrations of heparin (10 μ g/ml) lead to the formation of neuronal clusters that become bigger at 3 and 5 DIV (Fig 3.1.5, D-F). Because any were detected, 10 ng/ml FGF2 and 0.1 μ g/ml heparin did not cause changes in cell phenotype, Therefore, these concentrations of the ligands for cell treatments longer than 24 h. For treatment no longer than 4 h the concentration of 50 ng/ml of FGF2 in the presence of 10 μ g/ml of heparin was used based on the ligand concentration used in the microarray experiments and the literature search carried out in the laboratory before the commencement of this project.

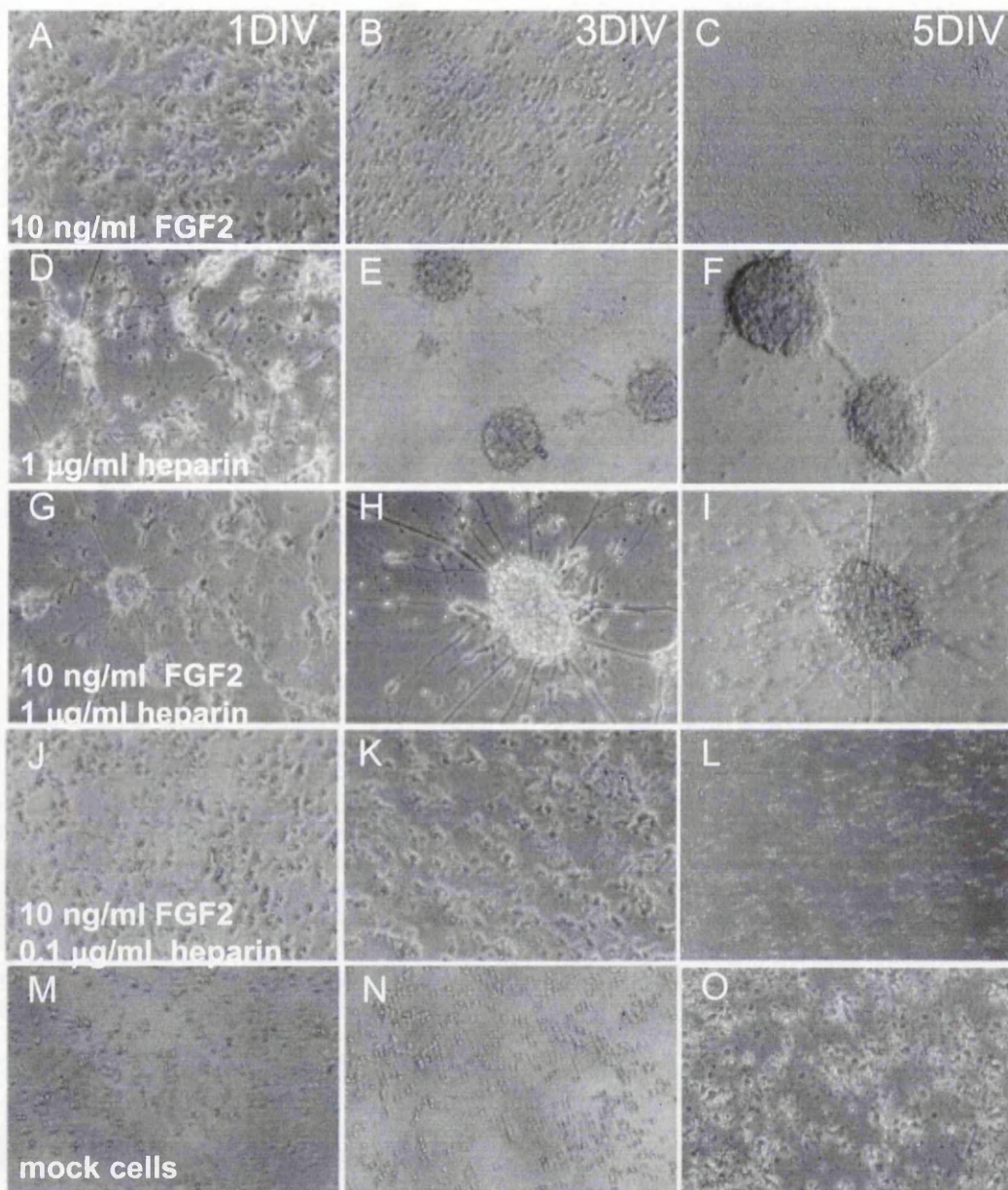


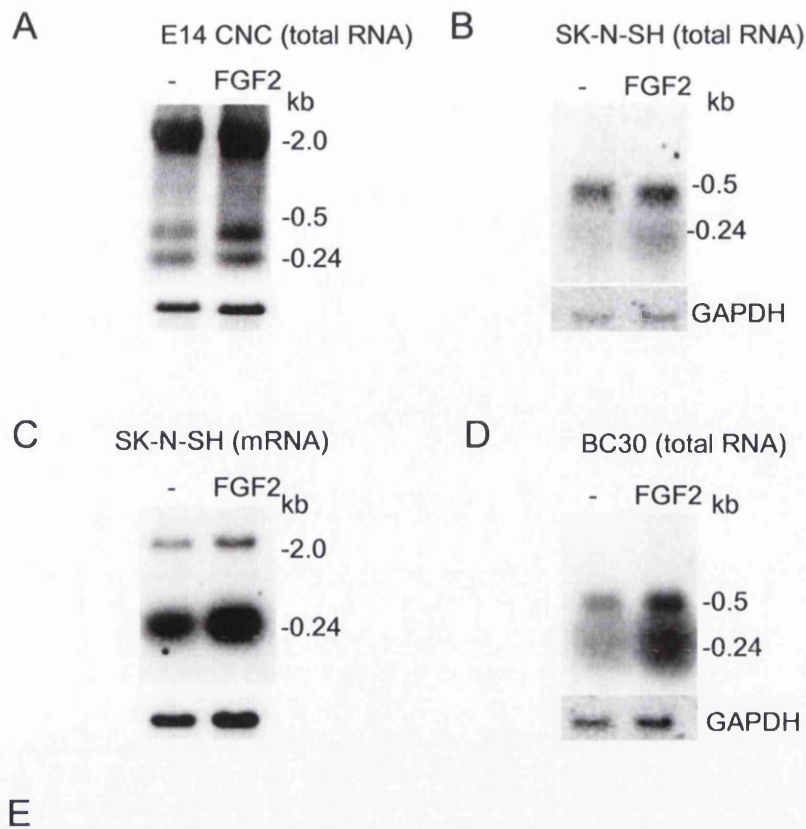
Figure 3.1.5 Cortical neuron culture was treated with different concentration on FGF2.

Mouse E14 CNC were treated at 1 DIV using different concentration of FGF2 and heparin for 5 days: 10 ng/ml of FGF2 (A-C); 1 mg/ml of heparin (D-F); 10 ng/ml of FGF2 and 1 µg/ml of heparin (G-I); 10 ng/ml of FGF2 and 0.1 µg/ml of heparin (J-L); mock treated cells (M-O). Cells were observed at 1DIV (A, D,G, J, M), 3 DIV (B, E, H, K, N) and 5 DIV (C, F, I, L, O) after the treatment.

3.1.5 *Ccp1* expression level was up-regulated upon FGF2 stimulation.

The microarray data showed that *ccp1* was up-regulated upon FGF2 stimulation by 2.3 fold in E14.5 CNC. To assess whether the regulation is a cell specific process, Northern blotting was performed using the RNA extracted from different cell types (Fig 3.1.6). In the previous microarray experiment, CNC were serum starved for 24 h and stimulated for 4 h with 50 ng/ml of FGF2 in the presence of 10 µg/ml of heparin. As a control, cells were treated only with heparin. E14.5 CNC were treated as above and Northern blotting was performed (Fig 3.1.6, A). The *ccp1* cDNA probe was prepared from the cDNA vector in the NIA mouse 15k cDNA clone set (pSport1-H3104E08) that contained a part of the coding sequence and 3' un-translated region (UTR). After hybridisation, *ccp1* transcript with an expected size of 2.0 kb (kilobases) was observed, together with shorter fragments of 0.24 and 0.5 kb. The 2.0 kb band showed the strongest signal, whereas the 0.24 and 0.5 kb bands showed a similar intensity. The bands were further quantified using the Quantity One 4.2.3 program (Biorad), taking account of the level of glyceraldehyde-3-phosphate dehydrogenase (GAPDH) control hybridisation (Fig 3.1.6, E).

Next, the analysis was performed using total RNA extracted from a neuroblastoma line, SK-N-SH cells, under the same condition of FGF2 stimulation. The two fragments of 0.24 and 0.5 kb were detected (Fig 3.1.6, B). After quantification, the 0.24 kb band showed stronger up-regulation (1.9 fold) in comparison with the 0.5 kb band (1.3 fold) (Fig 3.1.6, E). In this experiment, 2.0 kb *ccp1* transcript was below the level of detection. NorthernMax kit (Ambion) kit used in Fig 3.1.6, A, may have allowed more efficient hybridisation than in Fig 3.1.6, B.



kb	Cell type RNA Treatment Panel	E14 CNC Total RNA FGF2 (A)	SK-N-SH Total RNA FGF2 (B)	SK-N-SH Poly A -RNA FGF2 (C)	BC30 Total RNA FGF2 (D)
2		+1.1		+1.9	
0.5		+1.4	+1.3		+1.2
0.24		+3.6	+1.9	+1.4	+1.2

Figure 3.1.6 *Ccpl* expression level was up-regulated upon FGF2 treatment.

Northern blotting was performed using cells treated with 50 ng/ml of FGF2 in the presence of 10 µg/ml heparin (FGF2) and with heparin alone as control (-) for 4 h. (A) Three transcripts of 2.0, 0.5 and 0.24 kb were observed in the CNC total RNA. (B) Two transcripts of 0.5 and 0.24 kb were observed in SK-N-SH total RNA. (C) In poly-A RNA, two transcripts of 2.0 and 0.24 kb were observed. (D) Two transcripts of 0.5 and 0.24 kb were observed in BC30 total RNA. (E) By normalizing the band intensity based on the hybridisation with GAPDH and quantification, the bands showed a regulation upon FGF2 stimulation.

The experiment was carried out using poly-A RNA from SK-N-SH stimulated as above. A band of approximately 2.0 kb was indeed detected, together with the shorter fragment of 0.24 kb (Fig 3.1.6, C). Upon FGF2 stimulation, the 2.0 kb band was up-regulated by 1.9 fold, whereas the 0.24 kb band was up-regulated by 1.4 fold (Fig 3.1.6, E).

Finally, in total RNA extracted from immortalised oligodendrocyte progenitors BC30, the two fragments of 0.24 and 0.5 kb were detected (Fig 3.1.6, D). Both bands showed up-regulation by 1.2 fold after FGF2 stimulation (Fig 3.1.6, E).

All together, *ccp1* showed a modest up-regulation upon FGF2 stimulation in accordance with the microarray data. This regulation was observed both in CNC and in cell lines. Interestingly, three different transcripts were detected. Since the transcript size of *ccp1* was expected to be 2.0 kb, the smaller fragments of 0.24 and 0.5 kb may be alternative splice variants. However, RT-PCR amplification using primers flanking the entire CDS did not produce any PCR product corresponding to this fragments (see *ccp1*-CDS amplification, Fig 3.1.8). This observation do not imply that these bands are not alternative splicing products and more work should be done for conclusive results. The 0.5 kb band was not detected in the Northern blot using poly-A RNA, indicating that the corresponding alternative splice variant may not contain the poly-A signal. Since the smaller bands were detected in all the cell types analysed, they are unlikely to be degradation products.

3.1.6 Ccp1 was predominantly expressed in the heart and liver in adult mouse.

In order to analyse *ccp1* expression in adult tissues, Northern blotting was performed using the probe generated above and the 'Poly-A RNA adult mouse Multiple Tissue Blot' (Clontech) (Fig 3.1.7). A 2.0 kb single band was observed in the heart, liver, kidney and testis. Lower levels of expression were also observed in brain and lung. Expression in the spleen and muscles was under detection level. Hybridisation with β -actin was performed to confirm equal sample loading.

3.1.7 Ccp1 gene encoded a protein.

In order to test whether *ccp1*, originally a Riken cDNA 2310061I09 clone, encodes a protein, transient expression was performed using a vector containing the *ccp1* cDNA in mammalian cells. Ccp1 was expressed as a fusion protein with a Myc tag, in order to enable a detection using an antibody against Myc. The bacterial clone encoding *ccp1* obtained from the NIA mouse 15k set (pSPORT-H3104E08) contained only a part of the coding sequence and the 3' UTR (nucleotide 453-1697). In order to obtain the full length clone, a 858 base pair (bp) long *ccp1* sequence, including part of the 5' UTR, the coding region (CDS) and a part of the 3' UTR, was amplified using RNA extracted from primary E14.5 CNC as a template (Fig 3.1.8, A). Next, the region of the *ccp1* CDS (562 bp) was amplified using the previous 858 bp fragment as a template (Fig 3.1.8, B-C). Ccp1 was then cloned into pCRII vector and its sequence was confirmed by sequencing. Finally, the 562 bp fragment was cloned into the expression vector pcDNA4/Myc-His (Invitrogen), allowing the fusion of *ccp1* to a Myc tag at the C-terminus, resulting in pcDNA4-*ccp1*/Myc(His).

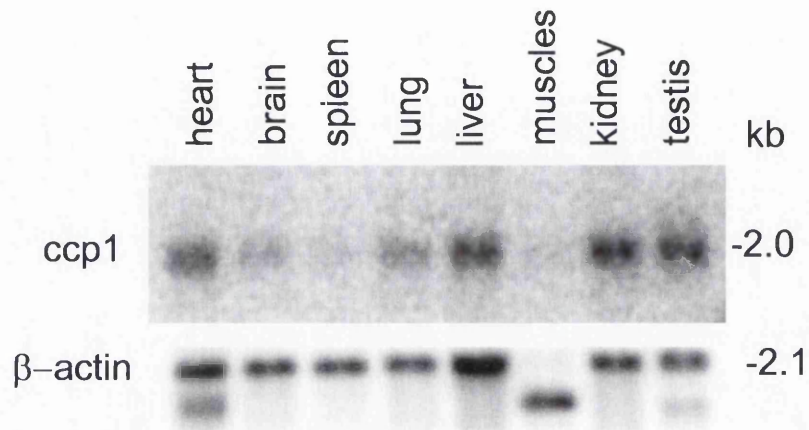


Figure 3.1.7 *Ccp1* expression in adult mouse tissues

A multiple tissue northern blot (Clontech) was hybridised with *ccp1* cDNA probe. A single band corresponding to the 2.0 kb transcript was observed. *Ccp1* was highly expressed in the heart, liver, kidney, and testis, less in the brain and lung. Expression in the spleen and muscles was under detection level. β -actin hybridisation was used as loading control.

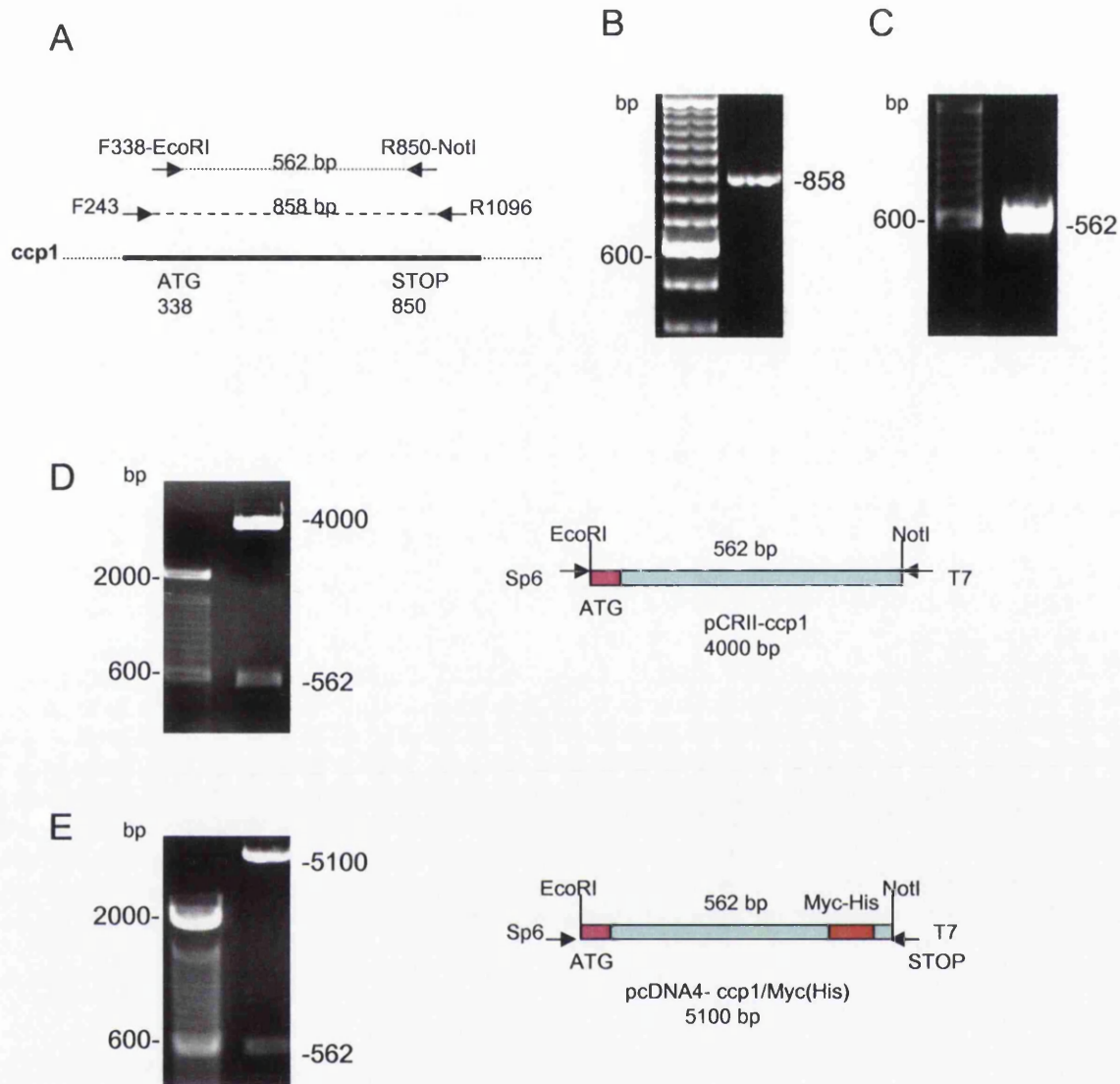


Figure 3.1.8 Construction of pcDNA4- ccp1/ Myc(His) vector

RT-PCR was carried out to amplify *ccp1* CDS. (A) Schematic view indicating the location of the primers used is shown. (B) RT-PCR was carried out to amplify a fragment containing part of the 5' UTR, the CDS and part of the 3' UTR. The product size was 858 bp (C). A fragment of 562 bp containing the CDS was amplified. (D) The 562 bp fragment was inserted into pCRII vector generating the intermediate pCRII-*ccp1* vector. (E) The 562 bp fragment was then re-ligated in the expression vector pcDNA4-Myc(His).

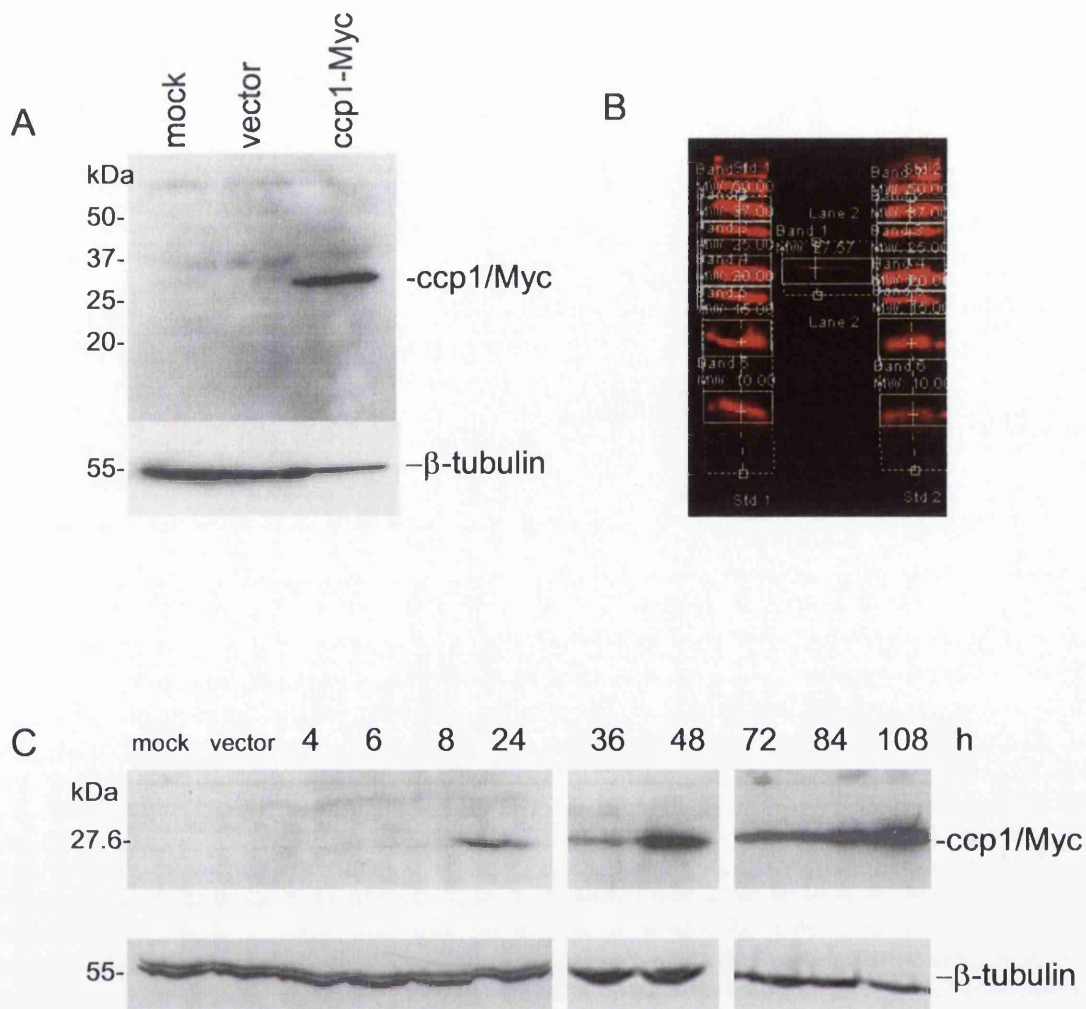


Figure 3.1.9 *Ccp1/Myc fusion protein was expressed as 27.6 kDa band.*

Ccp1 was expressed as a fusion protein with the Myc tag in HEK293 cells and detected with an antibody against Myc (9E10). (A) A single 28-kDa band was detected in cells transfected with the pcDNA4-ccp1/Myc(His). Cells were also transfected with only vector (vector) or mock-treated (mock). Immunoblot with β -tubulin was shown as a loading control. (B) The protein size was precisely determined by the Odyssey infrared imaging system (LI-COR) as 27.6 kDa. (C) Ccp1 expression vector was transfected for the time indicated. Expression of ccp1-Myc was detectable 24 h after the transfection and the level of the ccp1-Myc was maintained without any obvious degradation at 108 h. 12.5% SDS-PAGE.

HEK293 cells were transiently transfected with the pcDNA4-ccp1/Myc(His). After 24 h, expressed ccp1 fusion protein was analysed by Western blotting using antibody against Myc, 9E10 (Fig. 3.1.9, A). The number of amino acids in the fusion protein were 209 (ccp1 sequence, 180 AA; Myc sequence, 10 AA; His sequence, 6 AA; extra AA in the expression vector, 13 AA). Using the value of 112 kilo Dalton (kDa) as average molecular weight for each amino acid, the protein was expected to be 24 kDa. The Western blotting indeed revealed a single protein band of about 27 kDa (Fig 3.1.9, B).

For precise analysis of the protein size, the Odyssey infrared imaging system (LI-COR) was used. The LI-COR program calibrates the molecular weight of a given band by identifying the set of standards used in the molecular weight markers. Lysates from HEK293 cells transfected by pcDNA4-ccp1/Myc(His) were blotted and incubated with primary antibody against Myc (9E10). Ccp1 protein was visualised using the anti-goat Alexa Fluor secondary antibody. The analysis determined the ccp1 fusion protein size as 27.6 kDa (Fig 3.1.9, B).

Expression of ccp1 fusion protein was further examined by allowing cells to express up to 108 h. Expression of ccp1/Myc protein was detectable 24 h after the transfection and the level of the ccp1/Myc was maintained without any obvious degradation up to 108 h (Fig 3.1.9, C).

3.1.8 Expression of ccp1/His fusion protein as an antigen

In order to produce specific monoclonal and polyclonal antibodies against the ccp1, ccp1 fusion protein was expressed and purified as an antigen to be injected into mice

and rabbits. In order to express ccp1 protein in a large quantity, the pET system (Novagen) was used. Ccp1 was cloned in pET28b-His, a vector that allows expression of the inserted gene as a His tagged fusion protein under control of the strong bacteriophage T7 promoter (pET28b-ccp1/His). Ccp1 insert was sequenced to confirm that no mutations had occurred during the PCR amplification.

For bacterial expression, pET28b-ccp1/His expression vector was transformed in *E. coli* strain, BL21(DE3)pLysS. Bacterial cells were harvested and lysed. The lysate was then separated into the soluble (s) from the insoluble (i) phases by centrifugation. Both the soluble and insoluble phases of each sample were analysed by SDS-PAGE gel-comassie stained. As a negative control, the soluble and insoluble fraction of proteins from bacterial lysates before the addition of IPTG were analysed (Fig 3.1.10, A). First, bacterial cells were incubated with 0.1 mM IPTG for 24 h at 25°C (Fig 3.1.10, B) and at 37 °C (Fig 3.1.10, C). Ccp1/His protein was detected as a 23 kDa band in the insoluble fraction in both samples with similar intensity. Then, in order to determine the optimal time course for ccp1/His expression, the bacterial cells were incubated with 1 mM IPTG at 25°C (Fig 3.1.10, D) and at 37 °C (Fig 3.1.10, E).

At 25°C, ccp1/His protein expression was detectable in the insoluble fraction after 6 h of induction (Fig 3.1.10, D). At 37°C, ccp1/His expression reached maximum level after 4 h. However, no expression of ccp1/His was detected after 6 h (Fig 3.1.10, E). In order to confirm if the expressed 23 kDa band was indeed the ccp1/His protein, Western blotting was performed using an anti-His antibody on the insoluble fractions generated after 4 h of 1 mM IPTG induction at 37°C. A band of 23 kDa was detected in the sample, whereas no band was detected in the negative control

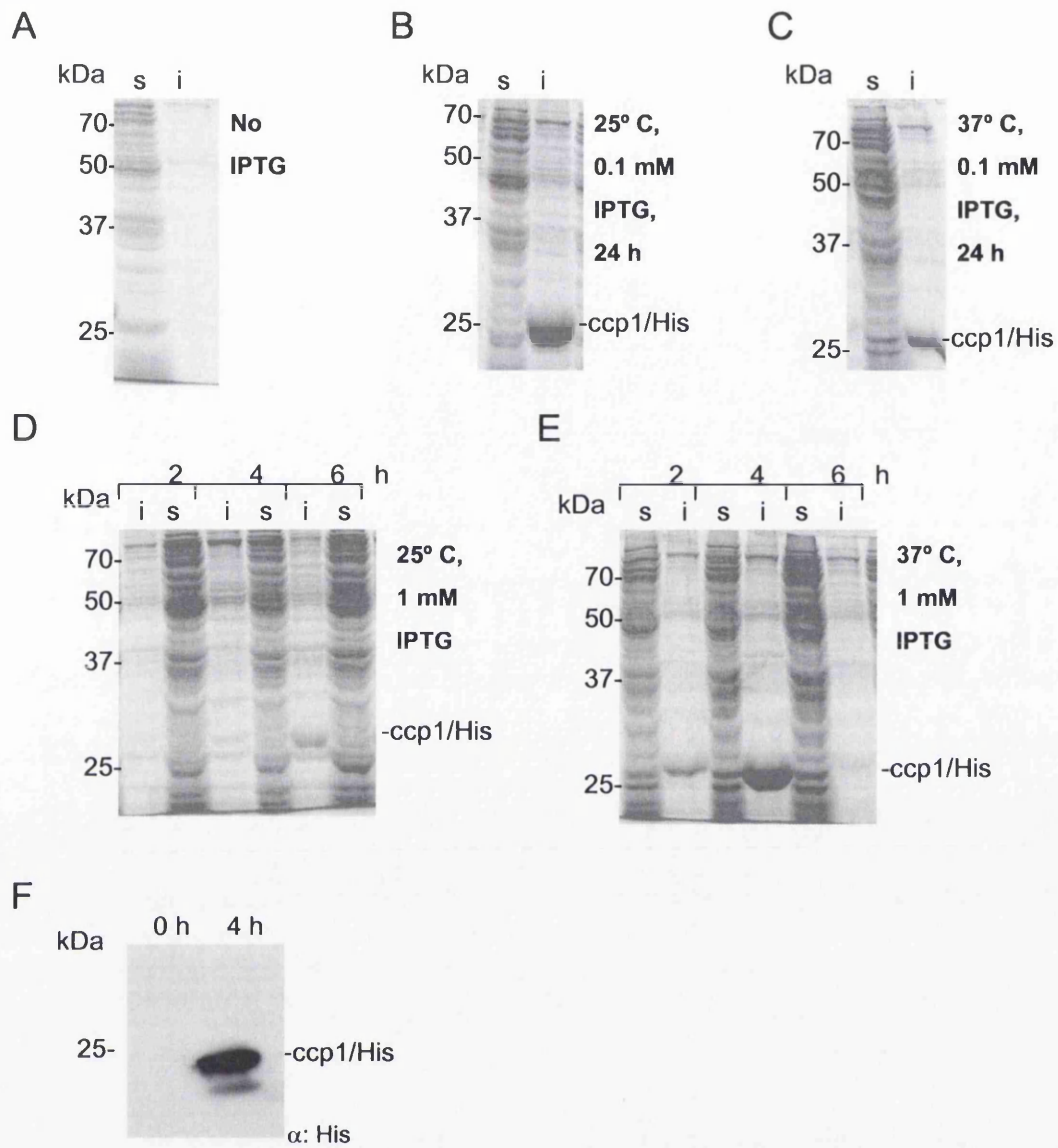


Figure 3.1.10 Characterization of *ccp1* protein expressed in bacteria

Ccp1 protein was expressed as a fusion protein with His-tag at the C terminus in *E. coli* strain BL21(DE3)pLysS. The soluble (s) and the insoluble (i) fraction of the expressed protein were analysed before IPTG induction (A), after induction at 25°C (B) or at 37 °C (C) using 0.1 mM IPTG for 24 h. Ccp1/His was detected as a 23 kDa band in the insoluble fraction. Ccp1/His was induced at 25°C (D) and 37°C (E) using 1 mM IPTG from 2 to 6 h. Protein were detected by comassie staining. (F) In order to confirm the identity of the band, western blotting was carried out using anti-His antibody on the samples induced at 37°C. 12.5 % SDS-PAGE gels.

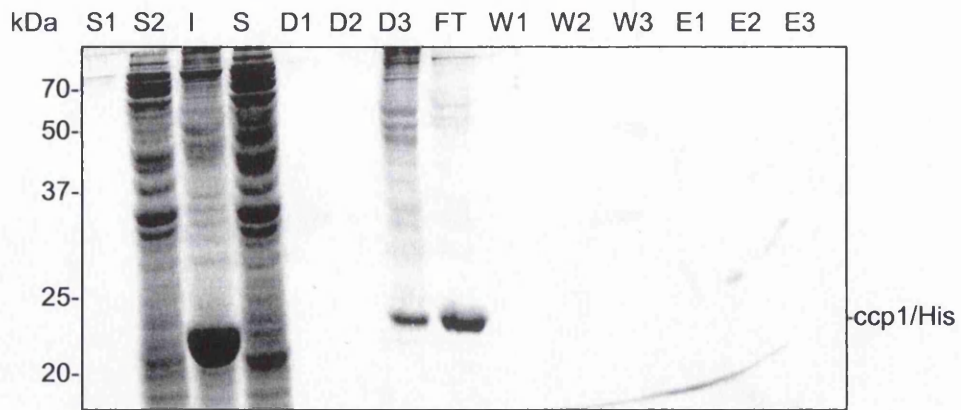
(Fig 3.1.10, F), showing that the protein expressed was indeed ccp1/His protein. As the strongest level of ccp1/His protein expression was detected at 4 h of 1 mM IPTG induction at 37°C, these conditions were used to produce the ccp1/His protein required for antibody generation.

3.1.9 Purification of the ccp1/His fusion protein.

In order to purify the ccp1/His protein suitable for injection to animals, Ni (Nickel)-charged beads were firstly used. Since ccp1/His protein was detected in the insoluble fraction, the protein was purified following a denaturing protocol using a batch method. The protein was washed twice in lysis buffer without addition of urea (Fig 3.1.11, A; D1, D2) or using 6 M urea (D3) and mixed with Ni-charged beads. Then the protein complex was packed into a column and the flow through (FT) was collected. The protein lysate in the column was washed with binding solutions (W1, W2) and with washing buffer (W3). Finally, the elution was performed with increasing concentration of imidazole (E1, 100 mM; E2, 250 mM; E3, 1 M). Unexpectedly, after analysis in comassie-stained gel, ccp1/His protein was observed in the flow through fraction (FT), indicating that the protein did not bind the beads (Fig 3.1.11, A). Ccp1/His protein was also partly eliminated during the solubilisation process together with the discard (Fig 3.1.11, A; D3).

As an alternative method, electro-elution was used to purify ccp1/His protein. The protein lysate was first separated on a 12.5% SDS-PAGE gel. The band was excised from the gel and extracted using a dialysis bag in an electrophoretic chamber. The protein solution was finally desalted and concentrated by centrifugation in

A



B

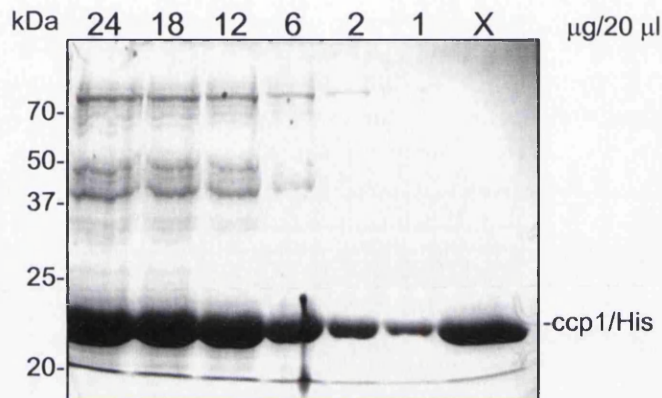


Figure 3.1.11 Purification of the bacterially expressed *ccp1/His* protein

(A) Samples were analysed during the purification of *ccp1* protein in a Nickel-agarose chromatography column. S1: no IPTG induction, insoluble fraction; S2: no IPTG induction, soluble fraction; S: insoluble and I: soluble fraction after IPTG induction; D1, D2, D3: discards obtained from the solubilisation process; FT: flow through; W1, W2, W3: washing; E1: elution with 100 mM imidazole; E2: elution with 250 mM imidazole; E3: elution with 1M imidazole. See text for explanation. (B) *Ccp1/His* protein was purified using electro-elution. The concentration of the protein sample was determined by comparison with a series of diluted samples with known concentration. *Ccp1* concentration was determined as 0.6 mg/ml. Proteins were visualised using comassie staining.

Centricon tubes. The resulting protein solution contained only the ccp1/His protein, as shown in a SDS-PAGE gel (Fig 3.1.11, B). In total, 3 mg of ccp1/His recombinant protein were purified at a concentration of 0.6 mg/ml.

3.1.10 Generation of antibodies against ccp1.

Monoclonal and polyclonal antibodies were generated by the Antibody Facility at the Beatson Laboratories. The specificity of the anti-rabbit polyclonal ccp1-antiserum was tested using different dilutions between 1:500-1:10000. 10 µg of protein extracted from HEK293 cells transiently expressing ccp1/Myc fusion protein were used for this analysis (Fig 3.1.12, A). A few weak background bands were detected at lower dilutions (1:500-2000). Increasing the antiserum dilution to 1:10000, the signal at the band at 27.6 kDa corresponding to ccp1/His protein was weaker but more specific. Next, the sensitivity of the ccp1-antiserum was tested using known amount of ccp1/His protein between 2-20 ng at 1:1000 dilution. The antiserum detected as little as 10 ng of ccp1/His protein (Fig 3.1.12, B). Based on these results, 1:10000 dilution of the antiserum was used in the Western blot experiments when expressed ccp1 was analysed. Instead, 1:1000 dilution of the antiserum was used when the endogenous ccp1 was detected.

To facilitate the detection of endogenous ccp1 protein, primary MEF were treated with FGF2 for 24 h and cell lysates were analysed by Western blotting (Fig 3.1.13, A). Endogenous ccp1 up-regulated upon FGF2 by 2.1 fold. Protein lysates extracted from HEK293 and from HEK293 cells transiently expressing ccp1/Myc fusion protein were also analysed. Ccp1 polyclonal antiserum recognised the

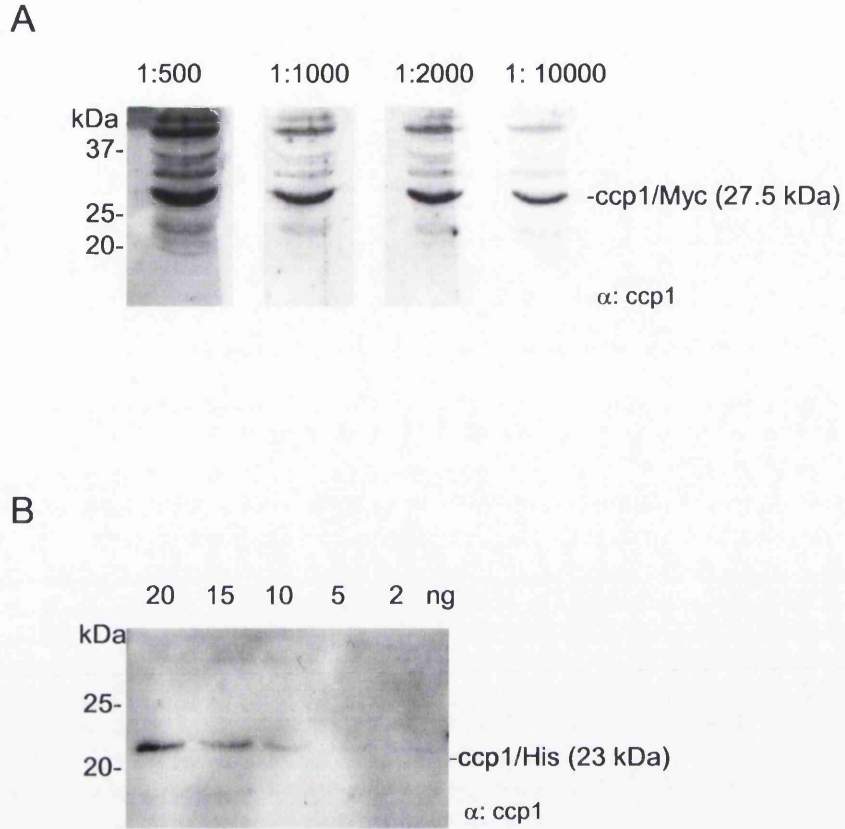


Figure 3.1.12 Characterization of ccp1 polyclonal antiserum

Titration of the polyclonal antiserum against endogenous ccp1 was carried out. (A) Protein lysate extracted from HEK293 cells transiently expressing ccp1/Myc fusion protein were analysed using dilutions of the ccp1 polyclonal sera. (B) The sensitivity of the antiserum was tested using dilutions of ccp1/His protein. The polyclonal antiserum detected as little as 10 ng of ccp1/His protein. 12 % SDS-PAGE gels.

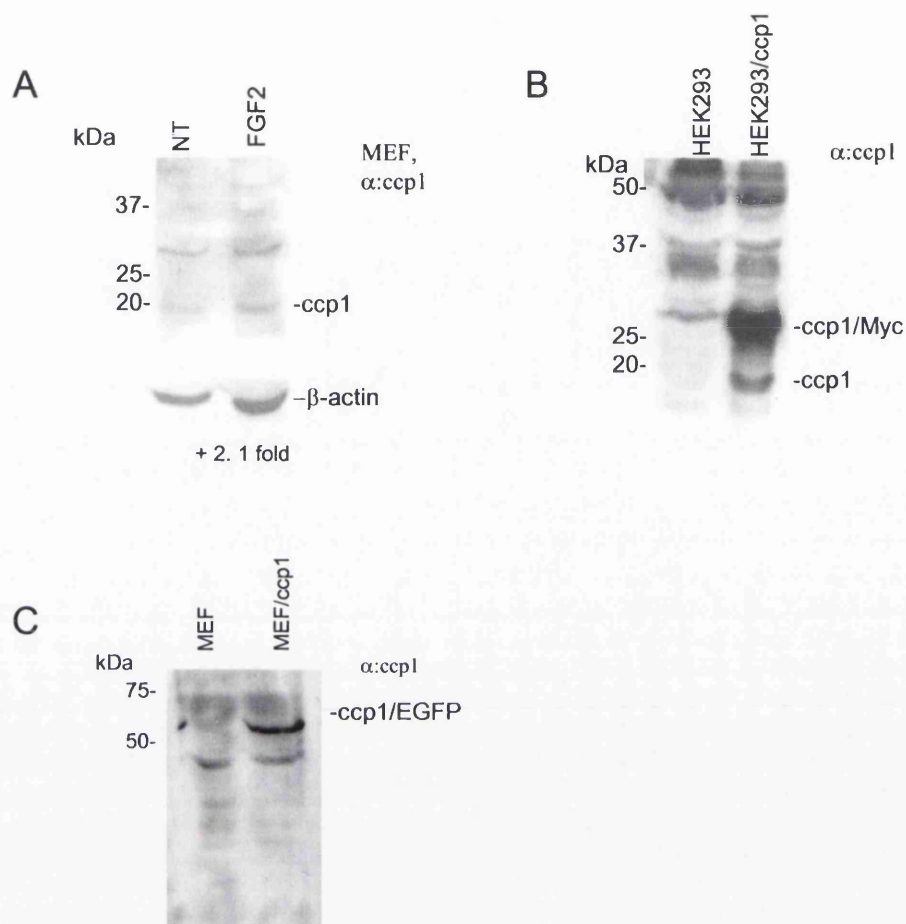


Figure 3.1.13 Polyclonal and monoclonal antibody.

(A) Western blotting was carried out on MEF cells treated with 50 ng/ml of FGF2 and 10 μ g/ml of heparin for 24 h. Endogenous ccp1 was detected at 19 kDa by ccp1-polyclonal antiserum. After normalization with β -actin, it was up-regulated by 2.1 fold upon stimulation. (B) Transiently expressed ccp1/Myc fusion protein in HEK293 cells was detected at 23 kDa by ccp1-polyclonal antibody. (C) Stably expressed ccp1/EGFP fusion protein in MEF cells was detected at 55 kDa by ccp1-monoclonal antibody. The samples were analysed in 7.5 % SDS-PAGE gels. The ccp1 polyclonal antiserum was used at 1:1000 dilution; the monoclonal antibody was used undiluted.

ectopically expressed protein at 27.6 kDa as well as a small but strong band at 19 kDa (Fig 3.1.13, B). The endogenous *ccp1*, expected at 19 kDa was not detected in HEK293. Therefore, the 19 kDa band observed in the HEK293 transiently expressing *ccp1*/Myc protein may be a cleavage product. Protein lysates extracted from MEF and from MEF cells stably expressing *ccp1*/EGFP fusion protein (see Chapter 3.3.7) were analysed using *ccp1*-monoclonal antibody. The antibody recognised the ectopically expressed protein at 55 kDa (Fig 3.1.13, C). The endogenous *ccp1*, expected at 19 kDa was not detected.

3.1.11 Ccp1 polyclonal antiserum was not suitable for immunocytochemistry.

In order to test whether the generated antiserum recognised *ccp1* at the cell level, immunocytochemistry was performed. MEF were stained using increasing dilutions of the polyclonal *ccp1*-antiserum (Fig 3.1.14, A-C). The pre-immune sera showed a similar pattern to that observed in the cells stained with *ccp1* antiserum (Fig 3.1.14, D-F). *Ccp1*-polyclonal antiserum did not show specificity, since the pre-immune sera obtained from the rabbit before the immunization gave a similar result. Furthermore, the *ccp1* antigen used to inject the rabbits was used to inhibit the specific antiserum-antigen interaction. The purified *ccp1* protein was added at the concentration of 0.5, 1, and 5 mg/ml to the *ccp1* antiserum diluted at 1:1000 (Fig 3.1.13, G-E). Up to 1 mg/ml of inhibitory peptide did not inhibit *ccp1*-antiserum stain. These data indicate that *ccp1*-polyclonal antiserum is not specific and it is not suitable for immunocytochemistry.

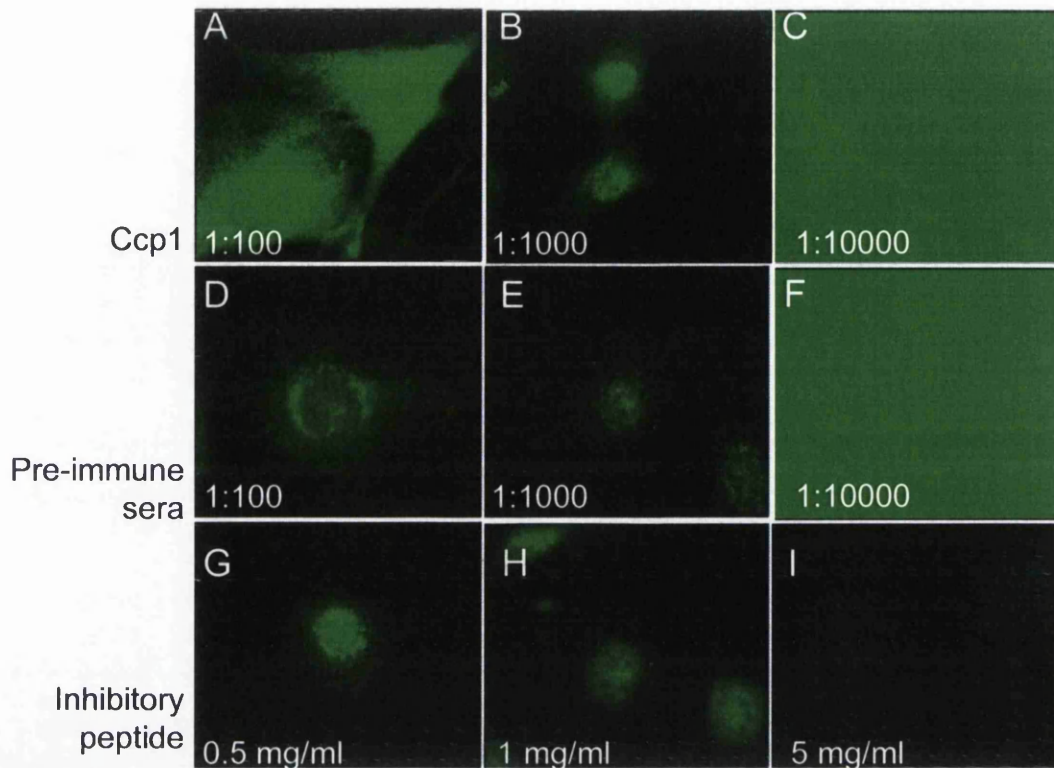


Figure 3.1.14 Ccp1 polyclonal antiserum did not show specificity in immunocytochemistry experiments.

In order to test whether the polyclonal ccp1-antiserum recognises ccp1 in the cells, immunocytochemistry was performed using MEF. (A-C) Cells were stained using increasing dilution of ccp1 polyclonal antiserum. (D-E) Cells were treated with increasing dilution of pre-immune sera, which showed similar staining pattern to the ccp1 antiserum. (G-I) Ccp1 antigen, used to arise the antiserum, was used as an inhibitory peptide for ccp1 antiserum diluted at 1:1000. Scale bar: 25 μ m.

Finally, anti-ccp1 monoclonal antibody was characterised by immunocytochemistry. MEF cells were stained using un-diluted antibody. However, no fluorescent signal was detected in the cell (data not shown). Ccp1 monoclonal antibody was therefore not suitable for immunocytochemistry experiments.

3.2 Ccp1 expression during brain development

The FGF family plays an important role during the development of the CNS (89, 148, 149). Among the family members, FGF2 is known to be a mitogenic factor in specific neural cell types and to promote differentiation and survival of neurons in culture (151-153, 286). Neuronal abnormalities were observed in FGF2 knock-out mice in the cerebral cortex, hippocampal commissure, and spinal cord (106). In particular, FGF2 knock-out mice presented abnormal formation of the cortex layer and showed a general decrease in neuronal cell number (155). The fact that FGF2 knock-out mice present such a dramatic brain phenotype suggests that FGF2 plays a key role in regulating corticogenesis (155).

As described in Chapter 3.1, *ccp1* was originally identified as a gene downstream of FGF2 in CNC derived from the cortices at E14.5. This chapter firstly describes overall expression of *ccp1* in different regions of the embryonic and adult brain using Northern Blotting and RT-PCR. Secondly, *ccp1* expression patterns in the developing forebrain was examined by *in situ* hybridisation. *Ccp1* showed a unique pattern of expression with regional variation which was altered during the embryonic development. The pattern reflected some of the aspects of radial and tangential migration (16).

3.2.1 Ccp1 transcript was detected in all regions of the embryonic brain.

In order to identify the regions of *ccp1* expression in the embryonic brain, RT-PCR was performed using total RNA extracted from embryonic telencephalic vesicles, striatum, diencephalon, mesencephalon, rhombencephalon and spinal cord (Fig 3.2.1). As it has been shown in Chapter 3.1 by Northern blotting, *ccp1* transcript was highly expressed in heart in adult mouse tissues. Therefore, the expression of *ccp1* in embryonic heart was also analysed in comparison to the brain regions. GAPDH was used as a control for the starting amount of total RNA used in the experiment. *Ccp1* transcript was detected throughout the embryonic brain regions.

3.2.2 Expression of *ccp1* in the adult brain

To investigate whether *ccp1* is expressed in various regions of the adult brain, Northern blotting was performed using a poly-A RNA blot (Clontech) derived from different regions of the human brain, including cerebellum, cerebral cortex, medulla, spinal cord, occipital lobe, frontal lobe, temporal lobe and putamen (Fig 3.2.2, A). Although weak, the band corresponding to the 2.0 kb transcript was detected throughout the brain regions. After stripping the membrane, β -actin hybridisation was carried out as a loading control, which showed a similar amount of RNA loaded in the samples.

Ccp1 expression was also analysed by RT-PCR. A 12-weeks old CD1 mouse was sacrificed and the following regions of the brain were dissected out: piriform cortex, frontal cortex, cerebellum, thalamus, medulla, spinal cord and olfactory bulb. *Ccp1* was expressed in all parts of the brain, however, its expression was not detected

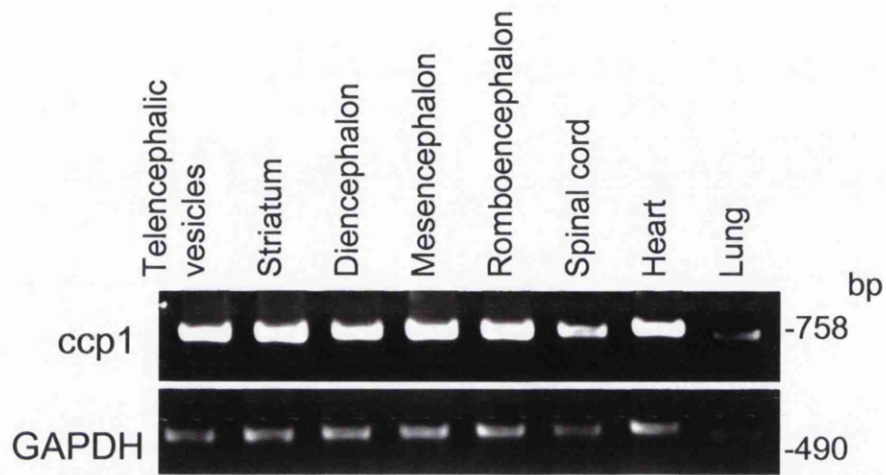


Figure 3.2.1 Ccp1 transcript was detected in all regions of the embryonic brain.

In order to determine which region of the embryonic brain expresses *ccp1*, RT-PCR was performed using RNA extracted from E16.5 mouse embryo brains. *Ccp1* was detected in all areas examined including the spinal cord. RNA extracted from adult mouse heart and lung was included for comparison. Amplification of *GAPDH* was used as a control.

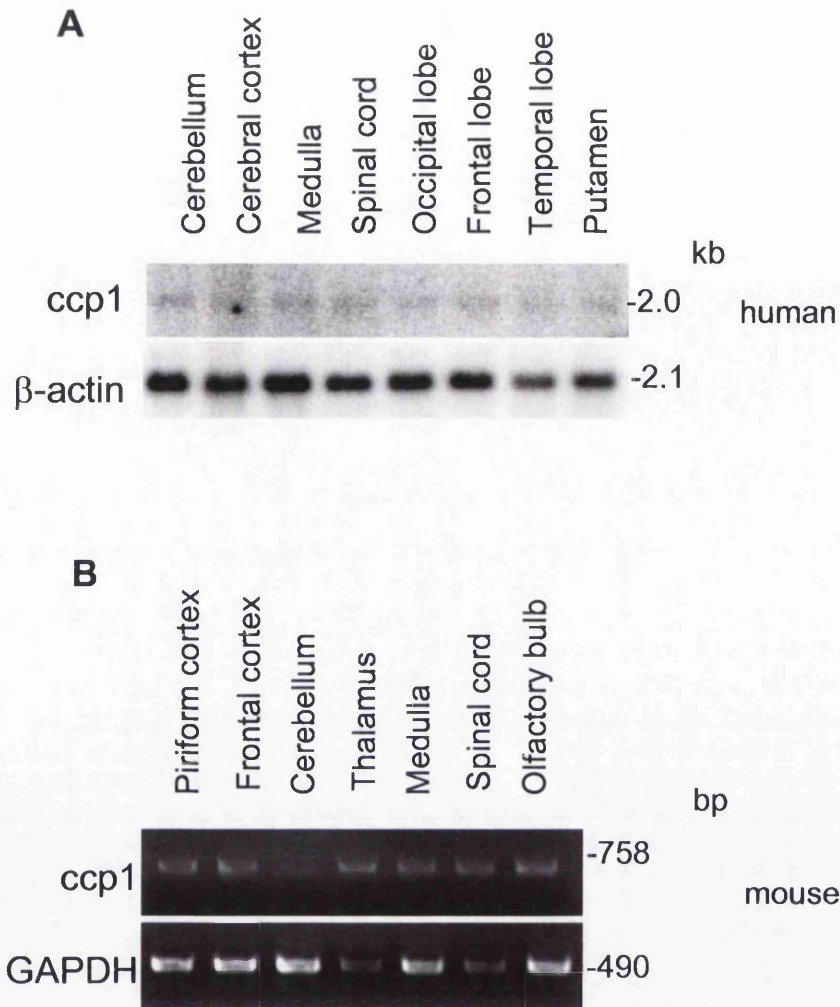


Figure 3.2.2 *Ccp1* is expressed in human and mouse adult brain.

(A) Multiple Tissue Northern blot containing adult human brain mRNAs showed a single band corresponding to the *ccp1* 2.0-kb transcript. Hybridization of the same blot was performed with β -actin to confirm equal sample loading. (B) RT-PCR showed *ccp1* expression in all the brain regions analysed, except the cerebellum. GAPDH amplification was used as control.

in cerebellum (Fig 3.2.2, B). This observation was in contrast to that in the adult human cerebellum (Fig 3.2.2, A).

3.2.3 Expression pattern of *ccp1* in the embryonic brain

In order to examine the spatial expression pattern of *ccp1* in mouse embryonic forebrain during development, *in situ* hybridisations with DIG-labelled probes were performed (Fig 3.2.3). The expression of *ccp1* was detected strongly at E13.5 in a ventro-lateral area of striatum and lateral cortex (Fig 3.2.3, A). At E15.5, some of the *ccp1*-positive cells appeared to shift toward the CP, a region that originates in the upper part of the cortex around E14.5 stage. At this stage, *ccp1* expression was strongly observed in the superficial layer of dorsal cortex, whereas in the ventral cortex there was a decrease in its intensity (Fig 3.2.3, B). This shift in expression extended further in a dorsal manner at E16.5 (Fig 3.2.3, C).

3.2.4 *Ccp1* may follow the radial migration.

During embryonic cortex development, neuronal progenitors originate in the proliferative region, the VZ (14, 15). Once the cells exit the cell cycle, they migrate radially towards the pial surface, forming six layers of neurons in a inside-out sequence (Chapter 1.1.2) (14, 15). *Ccp1* expression was further analysed in the dorsal cerebral cortex at different stages of embryonic development. At E14.5, *ccp1* was expressed in the VZ (Fig 3.2.4, A). Some of the cells in the CP also expressed *ccp1*. At later stages, *ccp1* expression become stronger in the CP and few positive cells

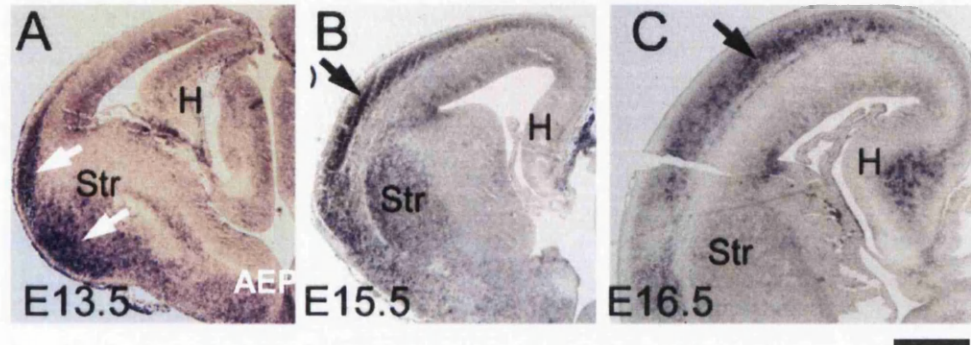
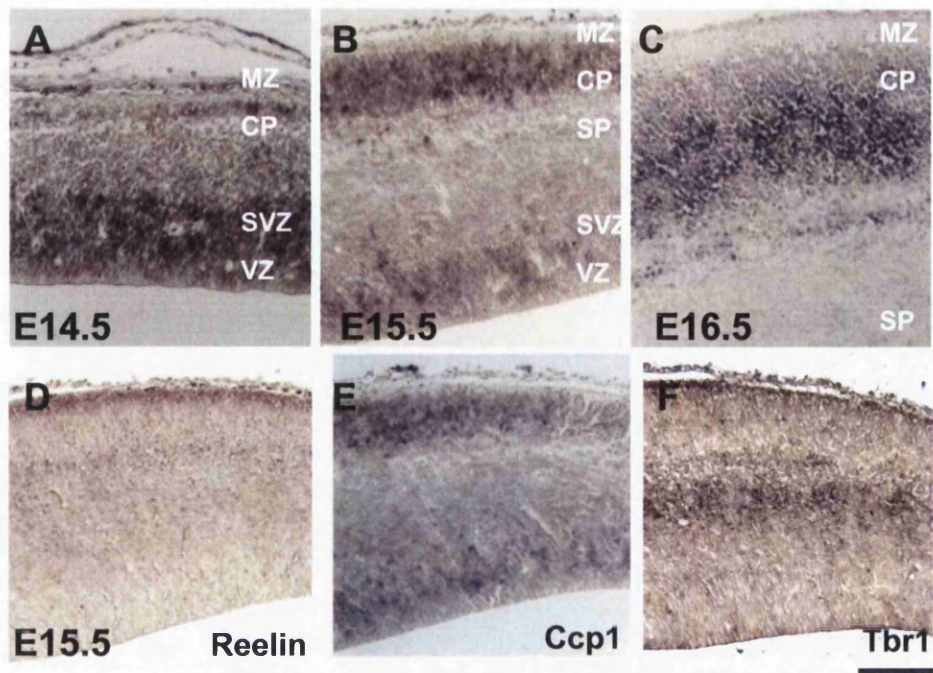


Figure 3.2.3. Expression pattern of *ccp1* in the developing mouse brain

The expression pattern of *ccp1* in the developing embryonic forebrain was examined by *in situ* hybridization. (A) *Ccp1* showed strong expression at the lateral and ventral forebrain (white arrows) at E13.5. (B) The expression gradually shifted toward dorsal cortex in E15.5. (C) Further dorsal expression was observed within the superficial area of the cortex at E16.5 (black arrows in B and C). Str; striatum, H; hippocampus. Scale bar: 800 μm .



G

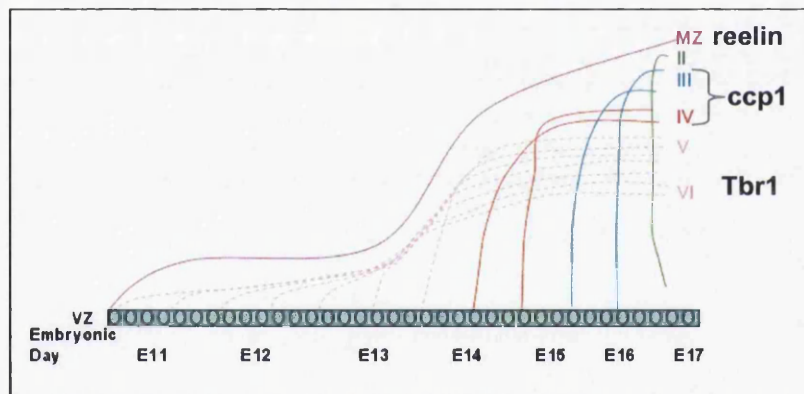


Figure 3.2.4 Expression of *ccp1* in the dorsal cortex

(A) *Ccp1* transcript was detected in the VZ at E14.5. (B) The expression shifted to CP splitting the preplate to MZ and SP at E15.5. (C) Stronger and specific staining shifted inward within the CP at E16.5. Serial coronal sections of E15.5 cortex were probed with reelin (D), *ccp1* (E) and Tbr1 (F). Reelin was detected by immunohistochemistry and *ccp1* and Tbr1 by *in situ* hybridization. (G) *Ccp1* defined a population of cortical progenitors born after reelin and Tbr1-positive cells. MZ, marginal zone; CP, cortical plate; SP, subplate, SVZ, subventricular zone; VZ, ventricular zone. Scale bar: 200 μm .

remained in the VZ. At E15.5, *ccp1* expression was localised both in the VZ and CP (Fig 3.2.4, B). At E16.5, the majority of the expression was in the deeper CP (Fig 3.2.4, C). The hybridisation with the sense probe did not show any significant staining (data not shown).

The *ccp1* expression pattern in the dorsal cortex suggests that *ccp1*-positive cells generated in the VZ and then migrate to the pial surface. To determine in which layer of the cortex *ccp1*-positive cells locate, *ccp1* expression was compared to those of layer markers. Layer markers, *reelin* and *Tbr1* were used in this study. *Reelin* is a protein produced by cells that originate in the VZ at E10.5-E11.5. This group of cells are called Cajal-Retzius (CR) cells (24) and they are the first group of migrating cells to leave the proliferative zone and migrate to the MZ, where they finally reside (287). *Tbr1* is a transcription factor expressed by the second group of cells that leave the VZ, which migrate to the surface and finally locate in the inner layer of the cortex, layer VI (31). Consecutive coronal sections from CD1 mice at E15.5 were used to analyse the expression of markers in the cortex. The comparison of *reelin* and *Tbr1* expression to *ccp1* showed that *ccp1* was expressed at a lower level than *reelin* and at higher level than *Tbr1*-positive population of cells in the CP (Fig 3.2.4, D-F).

These data suggest that *ccp1* defines a population of cortical progenitors born around E13-E14 in the VZ after CR cells and *Tbr1*-positive cells.

3.2.5 Ccp1 may follow tangential migration.

During the brain development, a class of cells that originate in the basal ganglia migrate tangentially to the developing cortex (32). As described previously, *ccp1*

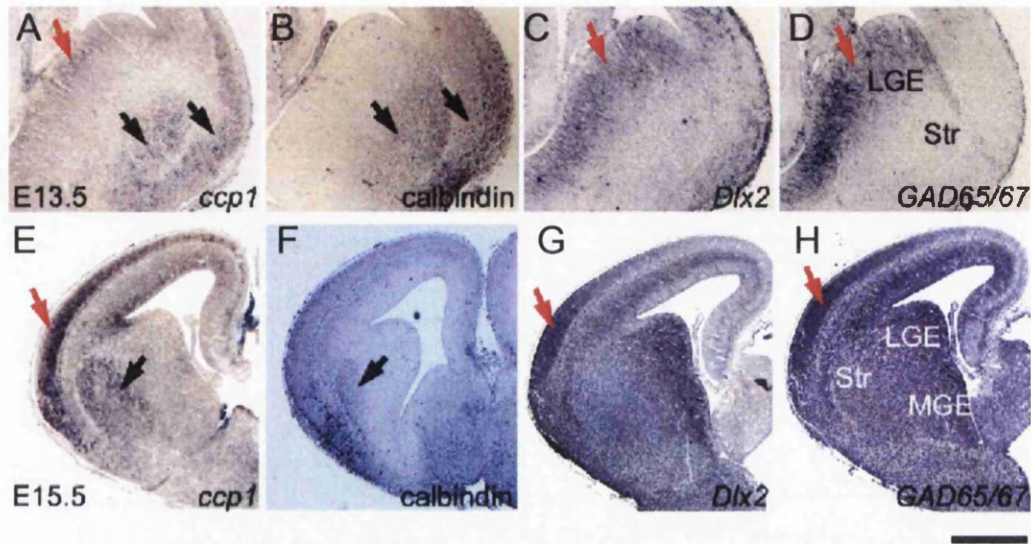


Figure 3.2.5 *Ccp1* expression in the embryonic brain was similar to those of GABAergic neurons.

Serial coronal sections deriving from E13.5 (A–D) and E15.5 (E–H) CD1 mice cortex were used to detect the expression of *ccp1* by *in situ* hybridization (A, E), calbindin (B, F), *Dlx2* (C, G) and *GAD65/67* (D, H) by immunohistochemistry. At E13.5, *Dlx2* and *GAD65/67* were expressed strongly in LGE and MGE, whereas weak expression of *ccp1* was detected in LGE (red arrows in A, C, D). At E15.5, tangentially migrating cells were marked by *Dlx2* and *GAD65/67* (red arrows in G, H). Similar staining was observed in *ccp1* (red arrow in E). Furthermore, calbindin was expressed in the striatum and lateral cortex, where *ccp1* expression was also detected at both E13.5 and E15.5 (black arrows in A, B, E, F). Str; striatum, LGE; lateral ganglionic eminence, MGE, medial ganglionic eminence. Scale bar: 200 μ m in A–D, 800 μ m in E–H.

expression during the development appeared to shift from the ventral to the dorsal telencephalon (Fig 3.2.3). Cells that migrate tangentially are known to be GABAergic interneurons (34). To see whether *ccp1*-expressing cells follow the tangential migration, the expression of *ccp1* was compared with known markers of tangentially migrating neurons, calbindin, *Dlx2* and *GAD65/67* (Fig 3.2.5). At E13.5, *ccp1* and calbindin showed a similar pattern of expression (Fig 3.2.5, A, B). Both were present in the ventro-lateral cortex and in the peri-striatum region. At E15.5, *ccp1* and calbindin were still present in the ventro-lateral cortex (Fig 3.2.5, E, F). In contrast, *Dlx2* and *GAD65/67* positive cells were strongly detected in the progenitor zones of the LGE and MGE at E13.5 (Fig 3.2.5, C, D). Some *ccp1*-positive cells were present in the LGE at E13.5 (Fig 3.2.5, A). At E15.5, *Dlx2* and *GAD65/67* positive cells migrated to the dorsal cortex and were present both in the CP, in the MZ and SVZ (Fig 3.2.5, G, H). In the MGE and LGE, some cells were still positive for *Dlx2* and *GAD65/67*, but not for *ccp1*. In summary, a particular group of *ccp1*-positive cells present at the LGE at E13.5 may migrate from the basal ganglia to the dorsal cortex, similar to *Dlx2*, *GAD65/67*.

3.3 Cellular localisation of the ccp1 protein

Ccp1 was shown to contain domain structures indicative of the localisation of ccp1 in the cell, including NES domains (Chapter 3.1.1). In this part of the study, cellular localisation of ccp1 was investigated by immunocytochemistry both in cell lines and in primary CNC. Firstly, localisation was studied by transiently expressing ccp1 as Myc tag-fusion protein. When transiently expressed, ccp1 fusion protein localised in a vesicle-like structure identified as lysosomes. In contrast, when stably expressed, the ccp1 fusion protein localised to the nucleus and to the cytoplasm in punctate spots. Cellular localisation of the endogenous ccp1 protein is still unclear. The N-terminus of ccp1 sequence presented two putative NES domains. Location of ccp1/EGFP protein was investigated upon FGF2 stimulation. Ccp1 was predominantly detected in the cytoplasm and to a lesser extent in the nucleus.

3.3.1 Ccp1 was localised to cytoplasmic vesicles when transiently expressed as a Myc-tagged fusion protein.

Since ccp1 antibody was not initially available, cellular localisation of ccp1 protein was first investigated in the expressed protein fused with a tag that could be detected by the tag-specific antibody. First, ccp1/Myc fusion protein was transiently expressed in human neuroblastoma, SK-N-SH (Fig 3.3.1). Ccp1/Myc fusion protein was visualised using anti-Myc antibody. Ccp1/Myc was localised to vesicle-like structures present in the cytosol and near the plasma membrane. Ccp1 did not appear to localise

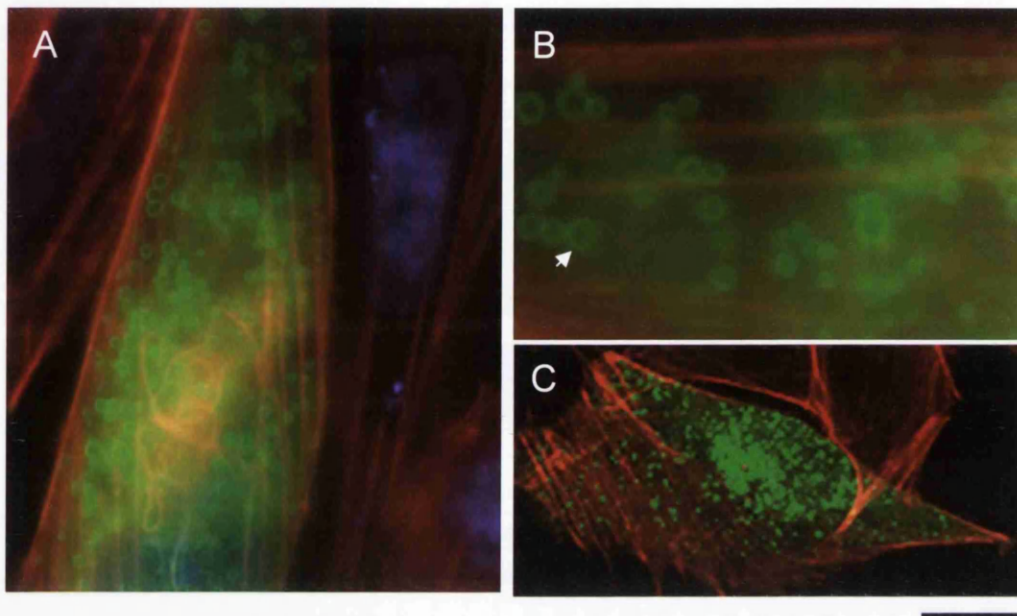


Figure 3.3.1 *Transiently expressed ccp1 was localises in vesicle-like structures.*

To localise ccp1 in the cell, ccp1/Myc fusion protein was expressed in SK-N-SH cells and visualized using antibody against Myc (9E10) (green). Filamentous actin was visualized with Texas Red-cojugated phalloidin (red). (A) Ccp1 was observed in the vicinity of the plasma membrane, as well as in cytosol. (B) Upon magnification, ccp1 localised to the surface of vesicle-like structures (arrow). (C) The cells were observed under confocal microscopy by scanning 14 serial sections through of the image and ccp1 was observed throughout the plasma membrane. Scale bar: 20 μm in A; 1.3 μm in B; 25 μm in C.

inside the nucleus. Upon magnification, ccp1/Myc was localised to the surface of the vesicles. In order to better characterize ccp1-positive vesicles, confocal microscopy was used. Based on the scanning 14 serial sections of 0.6 μm , three-dimensional image of the cell were build up and the presence of ccp1/Myc in the cytoplasm was more clearly observed.

To determine whether ccp1/Myc localisation in vesicle-like structures was specific phenomena to SK-N-SH cells, HEK293 and primary MEF were transfected by ccp1/Myc construct and its localisation was examined (Fig 3.3.2, A, B). In addition, neuronal cells, including immortalised oligodendrocyte progenitors (OPC) BC30 cell line (Fig 3.3.2, C) and primary E14 CNC (Fig 3.3.2, D) were examined. In HEK293 and in MEF, ccp1/Myc protein was observed in vesicle-like structures in the vicinity of the plasma membrane and cytosol. In BC30 and CNC, ccp1-positive vesicles were present in the cytosol, as well as in the cellular processes.

As a control, cells were transfected with vectors without insert. These cells did not show any positivity upon detection with Myc antibody (data not shown). Since the expression of Myc-fusion tag may cause artificial localisation, the fusion protein MEK/Myc and Mayven/Myc were expressed in HEK293 and SK-N-SH, respectively, and then localisation was examined (Fig 3.3.2, E, F). MEK is known to be expressed in endosomes (289) and Mayven is known to be expressed in the extremities of the cell processes (290). As expected, MEK/Myc fusion protein was localised to endosome compartments (Fig 3.3.2, E). Mayven/Myc fusion protein was localised to the extremities of the cell body, but not to vesicles structures (Fig 3.3.2, F).

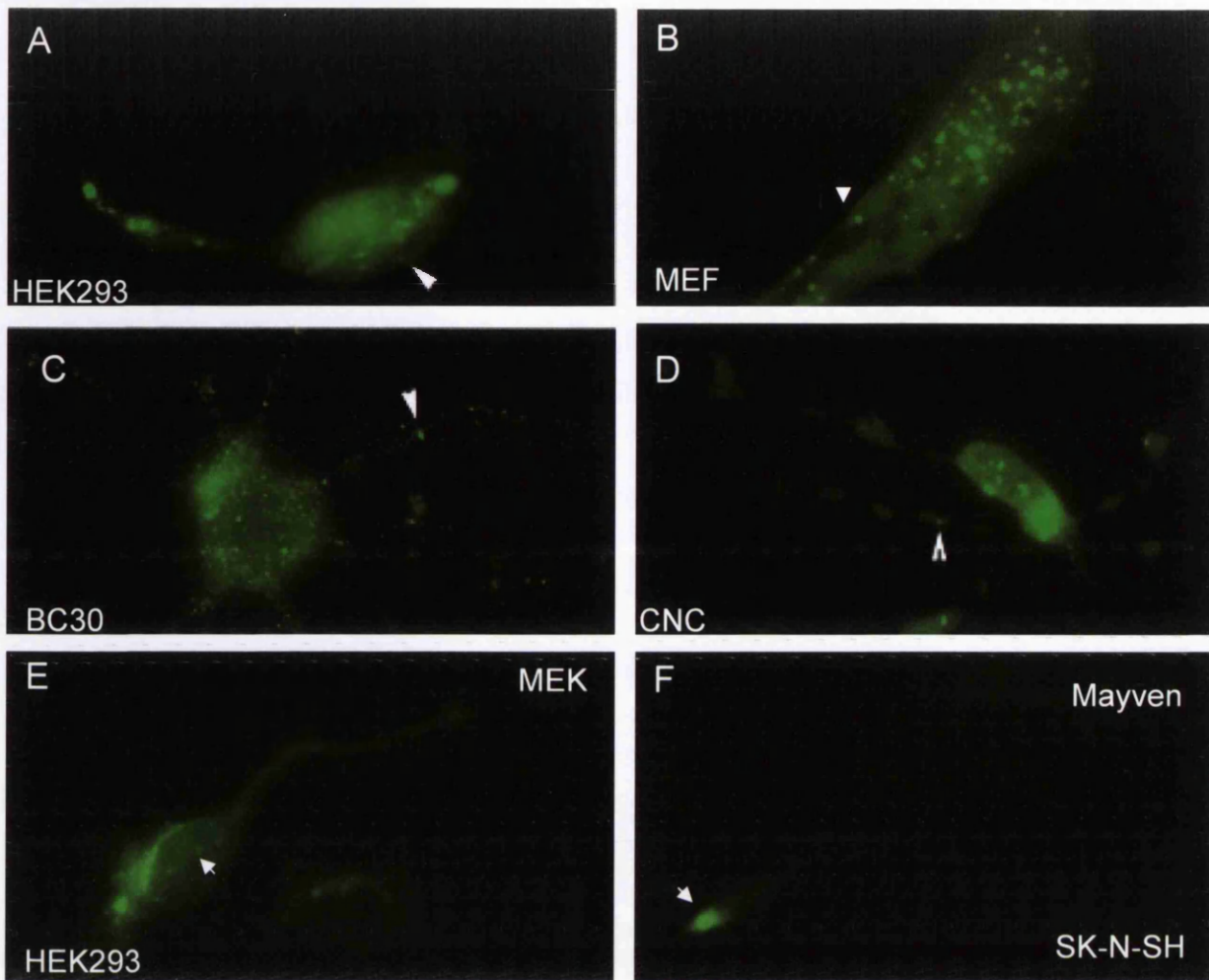


Figure 3.3.2 Transiently expressed ccp1/Myc fusion protein was localised to cytosolic vesicles in various cell types.

To examine ccp1 cellular localisation, ccp1/Myc fusion protein was transiently expressed in cell lines HEK293 (A), MEF (B), BC30 (C), and primary CNC derived from E16.5 brain (D) and detected using antibody against Myc. Ccp1/Myc was observed in the cell cytoplasm in a vesicular form (arrowheads). In BC30 and in CNC, ccp1 was also present in the processes (arrowheads). As a control for the specific staining of the Myc tag, MEK/Myc (E) and Mayven/Myc (F) fusion proteins were examined in the cells (arrows). Scale bar: 25 μ m.

3.3.2 Ccp1 protein transiently expressed with fluorescent protein-tags was also localised to cytoplasm and showed vesicular structure.

Transient overexpression of fusion-tagged proteins can result in artifactual localization within the cell. Furthermore, the position of the tag at the N- or C-terminus, may also affect the localisation of a protein in the cell. In order to address this issue, *ccp1* was fused with fluorescent tags either at the N- and C-terminus and the localisation of the transiently expressed protein was analysed. As a tag, EGFP and Discosoma sp. Red fluorescent proteins were placed at both the N and C-terminus of *ccp1*. Localisation was analysed in SK-N-SH cells and primary CNC derived from E15.5 embryos. The *ccp1*/Red-N, *ccp1*/Red-C, *ccp1*/EGFP-N and *ccp1*/EGFP-C proteins were expressed in the cells (Fig 3.3.3). As negative controls, the fluorescent proteins EGFP and Red alone were expressed.

The cells expressing *ccp1*/EGFP were stained with anti-GFP antibody. In contrast, *ccp1*/Red-C and -N fluorescence was observed under the microscope without the immunocytochemistry. *Ccp1*/EGFP-C and -N and *ccp1*/Red-C and -N were localised to the surface of vesicle-like structures in SK-N-SH (Fig 3.3.3, A-D), similar to those transiently expressed *ccp1*/Myc protein. *Ccp1*-positive vesicles were dispersed in the cytoplasm but did not localise to the nucleus. In CNC, *ccp1* vesicles were detected both in the cytoplasm and cellular processes (Fig 3.3.3, I-L). Both in SK-N-SH and CNC cells, no difference was detected in the expression of *ccp1* with tags positioned at the N- or the C-terminus. The cells expressing only the fluorescent proteins EGFP and Red showed a signal throughout the cell body.

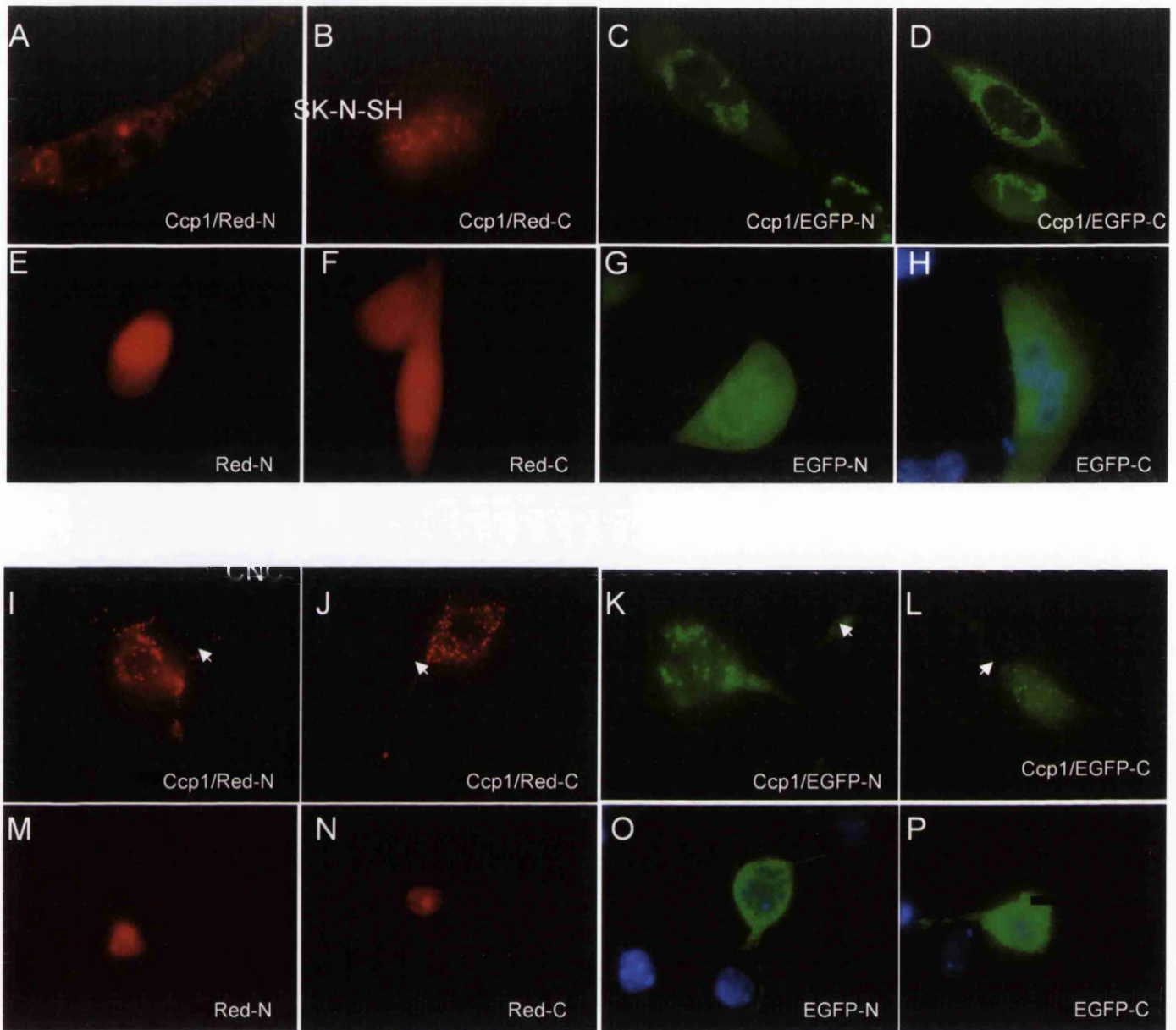


Figure 3.3.3 *Fluorescently-tagged ccp1-fusion proteins localised to cytosolic vesicles.*

Ccp1 was expressed in SK-N-SH cells (A-D) and in CNC (I-L) with fluorescent tags ccp1/Red-N (A, I), ccp1/Red-C (B, J) ccp1/EGFP-N (C, K) and ccp1/GFP-C (D, L). As a negative control, the fluorescent tags were expressed alone: DsRed (E, M, F, N), EGFP (G, O, H, P). Both in SK-N-SH and CNC, ccp1 was localised to vesicle-like structures in the cytoplasm. (I-L) Ccp1 was also present in the processes of the CNC (arrow). Scale bar: 25 μ m in A-D, I-L; 20 μ m in E-H, M-P.

3.3.3 Chloroquine treatment indicated that ccp1 was localised to lysosomes.

Chloroquine is a lyso-somotropic weak base used for the treatment of malaria and rheumatologic disorders. Chloroquine is a known inhibitor of endosomal and lysosomal functions by mechanisms thought to involve alkalinisation of endo-lysosomes (291, 292). In order to see whether the vesicles-like structures observed in cells transiently expressing ccp1 were lysosomes or endosomes, the transient ccp1/Myc expressing SK-N-SK were treated by adding 25-500 μM of chloroquine. Using in 25 μM of chloroquine, ccp1-vesicles remained intact. Using 100 μM of chloroquine some of the vesicles were disrupted. Using 500 μM of chloroquine, ccp1-positive structures were disrupted. To verify the inhibitory activity of chloroquine on endo-lysosomes compartments, SK-N-SH cells were treated with the same concentrations of chloroquine as above and stained with transferrin receptor (TfR) antibody, a marker for recycling endosomes (Fig 3.3.4, B, E, H) (293). As expected, the endosomes positive for TfR were disrupted upon treatment with 500 μM of chloroquine, similarly to the ccp1-positive structures. Therefore, chloroquine treatments indicated that expressed ccp1/Myc localised to endosomes or lysosomes.

3.3.4 Expressed ccp1 did not localise in endosomes or autophagy vesicles.

Endosomes are small membrane-bound vesicles formed by the invagination of the cell membrane (197). The endosome populations involved in recycling of vesicles to the plasma membrane have been classified in two categories, the early and the recycling endosomes (197). All internalized molecules are transported to early endosomes, also called sorting endosomes (294). Localisation ccp1/Red protein was

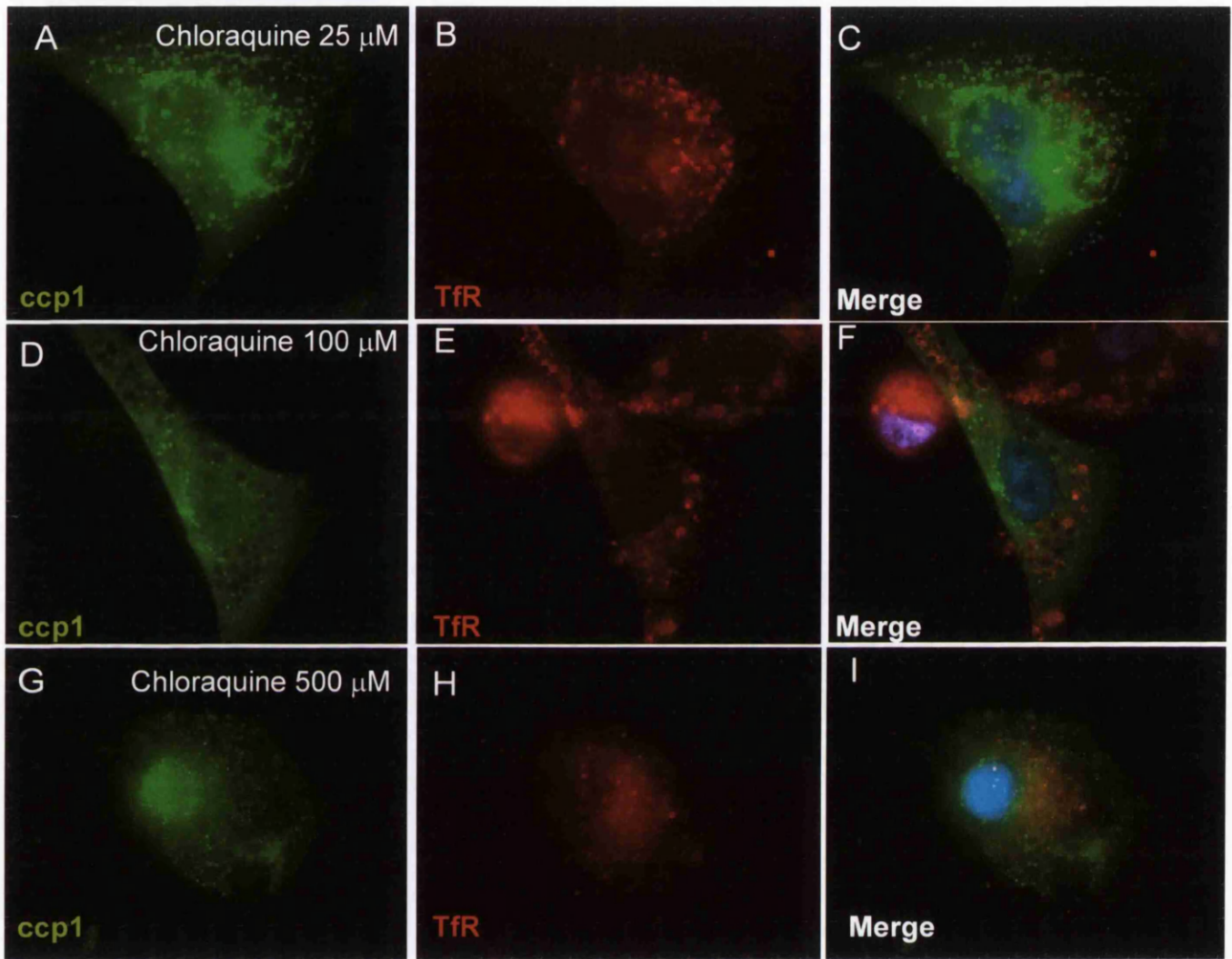


Figure 3.3.4 Ccp1 localisation to vesicle-like structures was disrupted by chloroquine treatment.

Chloroquine is an inhibitor of lysosomal and endosomal function. (A-G) SK-N-SH expressing *ccp1*/Myc were treated with increasing concentration of chloroquine. The cells were stained with antibodies against Myc (A, D, G) and Transferrin receptor (TfR), a marker for recycling endosomes (B, E, H). Upon treatment with chloroquine, structure positive with *ccp1* and TfR-positive endosomes were disrupted, indicating that expressed *ccp1* localised to endosome/lysosome structures (G, H). Scale bar: 25 μ m.

compared to that of early endosomes antigen 1 (EEA1), a marker for early endosomes (295) (Fig. 3.3.5, A, B). Ccp1/Red and EEA1 did not co-localise (Fig 3.3.5, C).

One of the known markers for recycling endosomes is TfR (293). This receptor escapes degradation by a process mediated by recycling endosomes (296). To address whether ccp1/Myc protein was localised to recycling endosomes, co-localisation study between ccp1/Myc and TfR was carried out (Fig 3.3.5, D-F). Ccp1-positive vesicles were not positive for TfR, indicating that ccp1-positive vesicles were not recycling endosomes.

The endoplasmic reticulum (ER) is an extensive network of membranes that extends from the cell membrane through the cytoplasm to the nuclear membrane (197). Using a specific 'ER stain' (Sub-cellular structure localization kit, Chemicon), ccp1/Red localisation to the ER was investigated (Fig 3.3.5, G, H) (297). Ccp1/Red did not localise to the ER.

Finally, ccp1/Red localisation in autophagy vesicles was investigated. Autophagy vesicles are double membrane structures that constitute one of the degradative cell pathways (298). To visualise autophagy vesicles, auto-fluorescent compound Monodansyl-Cadaverin (MDC) was used (279) (Fig. 3.3.5, J, K). Ccp1/Red did not localise to autophagy vesicles (Fig 3.3.5, L).

3.3.5 Transiently expressed ccp1 localised to lysosomes.

Next, localisation of the ccp1/Myc protein in lysosomes was investigated. Lysosomes are membranous vesicles characterised by low pH content and by their hydrolytic activity (197). Specific markers for low pH vesicles were used, including LysoTracker

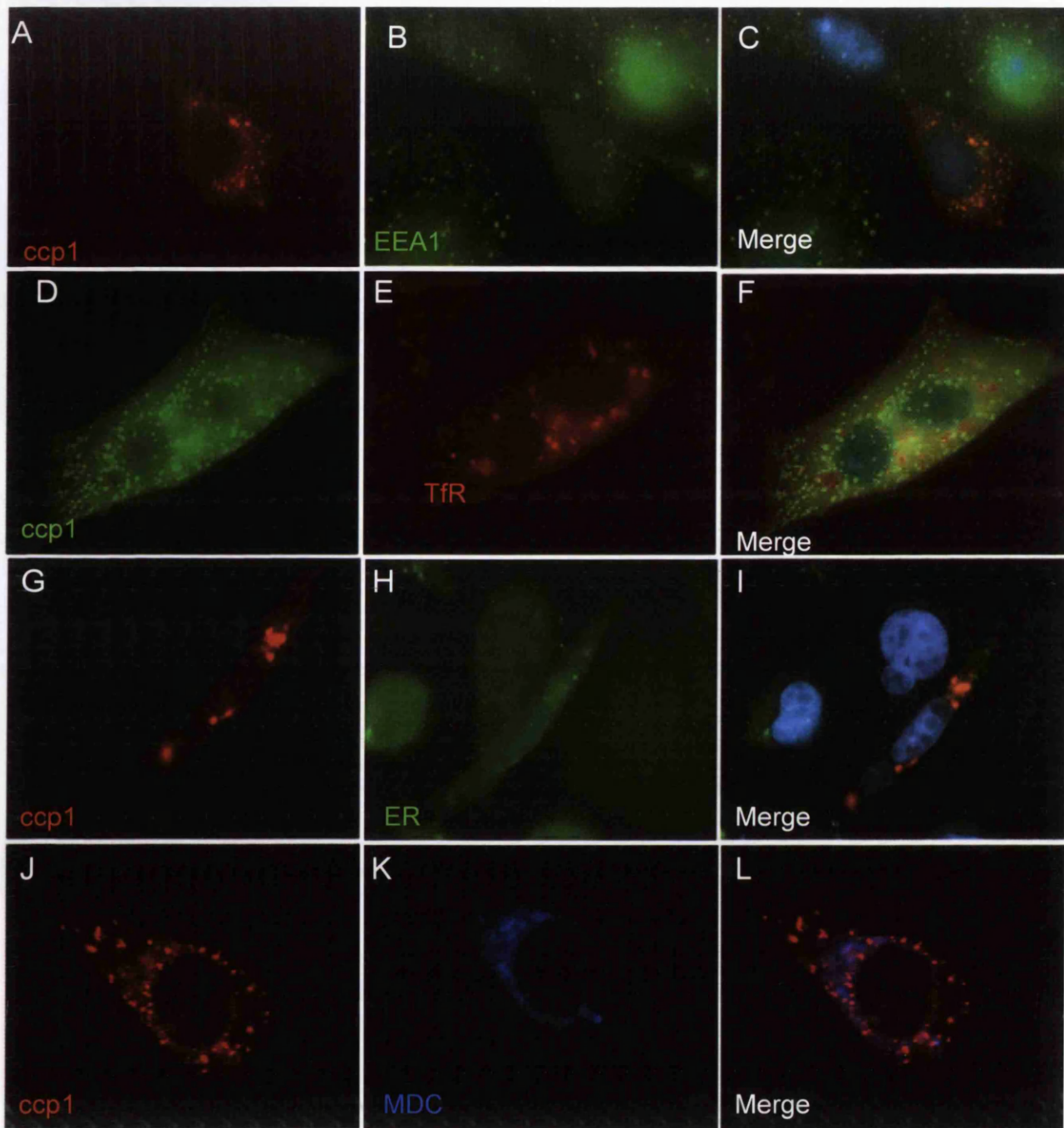


Figure 3.3.5 *Ccp1* did not localise in endosomes or autophagy vesicles.

To determine the identity of *ccp1*-positive vesicles, SK-N-SH cells transiently expressing *ccp1*/Red-N (A, G, J) and *ccp1*/Myc (D) were stained with specific markers for endosomes and cellular compartments. Anti-EEA1 (B) and anti-TfR (E) antibodies were used. The endoplasmatic reticulum (ER) was visualised with a specific stain (Chemicon) (H). Autophagic vesicles were identified with monodansilcadaverin (MDC) (K). Ccp1 did not co-localise with any of those markers tested. Scale bar 25 μ m.

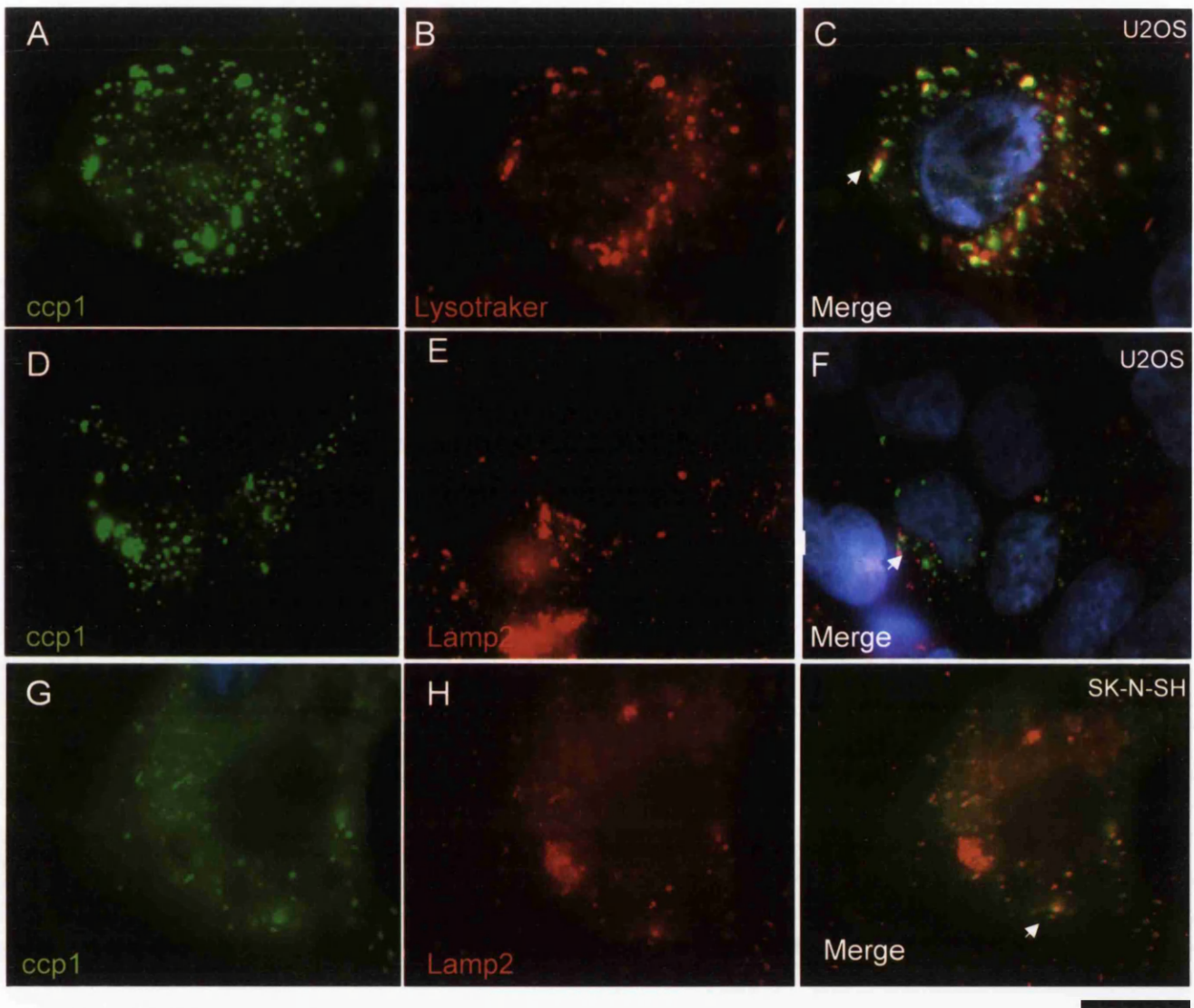


Figure 3.3.6 *Transiently expressed ccp1/Myc localised to lysosomes.*

In order to determine whether expressed ccp1/Myc localised to lysosomes, double immunostaining was performed using specific markers. Ccp1/Myc fusion protein was expressed in U2OS (A-F) and SK-N-SH cells (G-I) and visualised with anti-Myc antibody. The lysosomes were visualised with Lysotraker (B) and Lamp2 antibody (E, H). In U2OS cells, ccp1 co-localised with the Lysotraker, but little with the lysosomes marked by Lamp2 (C, F). Ccp1 co-localised with the lysosomes marked by Lamp2 in SK-N-SH cells (arrows) (I). Scale bar 25 μ m.

and antibody against 'lysosome-associated membrane protein type 2' (Lamp2). Lysotracker is a fluorescent acidotrophic probe that selectively accumulates in cellular compartments with low internal pH (299). Lamp2 is a protein that specifically localised to the lysosomal membrane (300). Since both Lysotraker and Lamp2 antibody were specific for human tissue, ccp1/Myc was transiently expressed in human osteosarcoma U2OS (Fig 3.3.6, A-D) and human neuroblastoma SK-N SH cells (Fig 3.3.6, G). In the U2OS cells, ccp1/Myc vesicles co-localised with the Lysotraker-positive structures. However, co-localisation with Lamp2 was observed only in few cases (Fig 3.3.6, F). In the SK-N SH cells, some vesicles positive for ccp1/Myc were also positive for Lamp2 (Fig 3.3.6, G-I). Ccp1 co-localisation with Lysotraker and with Lamp2 to a lesser extent indicates that transiently expressed ccp1, localised to a population of lysosome vesicles.

3.3.6 Ccp1 positive vesicles did not co-localise with cytoskeletal components.

Cellular vesicles involved the endocytic traffic are often associated with cytoskeletal components (197). To determine whether ccp1-vesicles aligned with the cytoskeletal components, ccp1/Myc expressing SK-N-SH cells were stained with specific markers for the cytoskeletal components (Fig 3.3.7, A, D, G). First, alignment between ccp1/Myc vesicles and vinculin was analysed. Vinculin is a cytoskeletal protein associated with the focal contacts and is one of several interacting proteins involved in anchoring F-actin to the membrane (301). Anti-vinculin antibody was used and vinculin was visualised at the cell periphery (Fig 3.3.7, B). Ccp1/Myc vesicles were expressed in the cytoplasm, showing no co-localisation with vinculin (Fig 3.3.7, C).

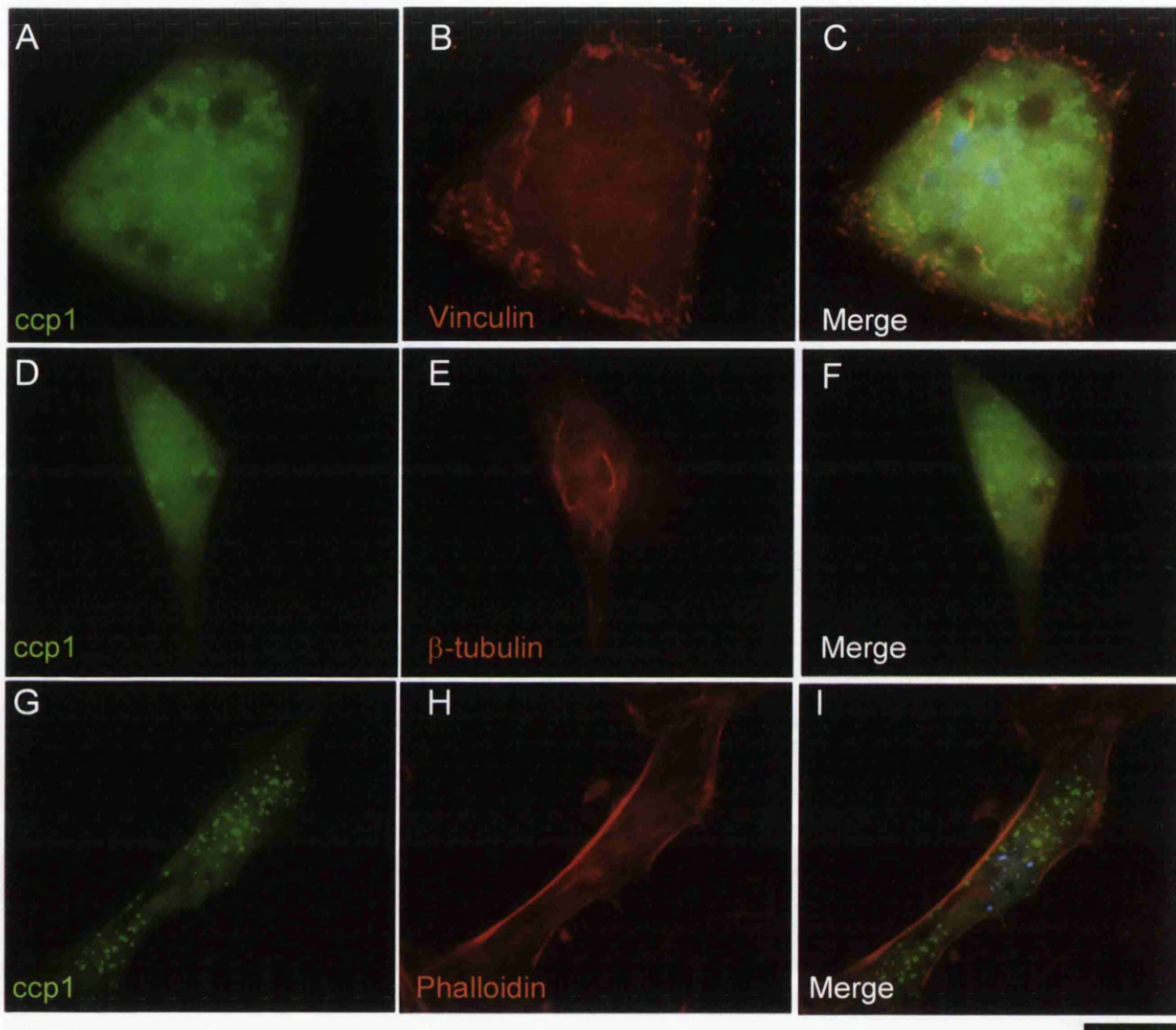


Figure 3.3.7 Ccp1 did not align with the cytoskeletal components.

To examine whether ccp1 vesicle-like structures associated with cytoskeletal components, double immunostaining was carried out. Ccp1/Myc was expressed in SK-N-SH cells and visualized using anti-Myc antibody (A, D, G), anti-vinculin (B) and β -tubulin antibodies (E). Texas red-conjugated phalloidin was used to visualize actin filaments (H). Ccp1 did not align with those structures. Scale bar: 25 μ m.

Next, alignment with α -tubulin as well as actin was analysed (Fig 3.3.7, D-F). Texas red-phalloidin (Fig 3.3.7, E) was used to visualise filamentous actin. Both tubulin and actin filaments did not show co-localisation with ccp1 (Fig 3.3.7, F, I). In conclusion, ccp1-positive vesicles did not show any association with the cytoskeletal components tested.

3.3.7 Generation of cell lines stably expressing ccp1 by retrovirus system.

In order to study the localisation and the function of ccp1 *in vitro*, cells stably expressing ccp1 were established by retrovirus approach. Ccp1 was expressed as a fusion protein with EGFP tag positioned at the N- and C-terminus using the retroviral construct pLPC (Fig 3.3.8) (280). pLPC-ccp1/EGFP and pLPC-EGFP were first transfected in ecotrophic phoenix packaging-cells, in order to produce virus particles. After 24 h, the virus-containing conditioned media of the phoenix packaging-cells was used to infect the MEF cells. Following the infection, ccp1/EGFP expression was checked by immunocytochemistry (Fig 3.3.8, A, B). Cells that incorporated ectopic ccp1 gene were then selected in 2.5 μ g/ml of puromycin for 15 days. 6 clones derived from a single cell expressing ccp1/EGFP-N were obtained. By immunocytochemistry, the clones 1-6 showed different level of ccp1/EGFP expression. Microscopic analysis showed that clone 1 and 5 presented high expression. Clone 2 and 6 showed low expression and clone 3 and 4 showed medium levels of expression (data not shown).

In order to examine the level of expression of ccp1/EGFP-N and ccp1/EGFP-C fusion proteins, Western blotting was performed (Fig 3.3.8, C). 15 μ g of protein for

each sample were analysed and the membrane was blotted using anti-GFP antibody. A strong band of 30 kDa corresponding to the EGFP-control was detected. Bands representing ccp1/EGFP-N and ccp1/EGFP-C were observed at the expected molecular weight, 55 kDa. Ccp1/EGFP-N stably expressed in MEF cells was also analysed by Western blotting using anti-ccp1 polyclonal antiserum (Fig 3.3.8, D). The MEF cells stably expressing ccp/EGFP-N showed a band of 55 kDa, corresponding to ccp1/EGFP (Fig 3.3.8, D). The same membrane was then blotted using anti-GFP and a band at the same size was observed. Following the same procedures, SK-N-SH cells stable expressing ccp1/EGFP were generated and the level of the expression was analysed using ccp1 polyclonal and GFP antibodies. Using both antibodies, a band of 55 kDa was observed (Fig. 3.3.8, E).

In order to compare the level of ccp1 expression between a transient and a stable system, 10 µg of protein lysates extracted from HEK293 cells transiently expressing ccp1/Myc, SK-N-SH, and MEF stably expressing ccp1/EGFP fusion protein were compared in a 4-12% gradient SDS-PAGE gel. Ccp1 polyclonal antiserum recognised expressed ccp1/Myc at 27.6 kDa in HEK293 (Fig 3.3.8, F). In addition, ccp1/EGFP protein was observed at 55 kDa in MEF cells. The presence of the 55 kDa band corresponding to ccp1/EGFP protein was not obvious from this gel in SK-N-SH cells. Therefore the blot using anti-GFP antibody was performed. The level of ccp1 in the transient system was much higher than in the stable system. In the MEF, a band was observed at 19 kDa, which may represent endogenous ccp1. This band was not obvious in the human SK-N-SH cells, probably due to the low level of ccp1 expression or due to a specificity of the antiserum for the mouse ccp1 protein.

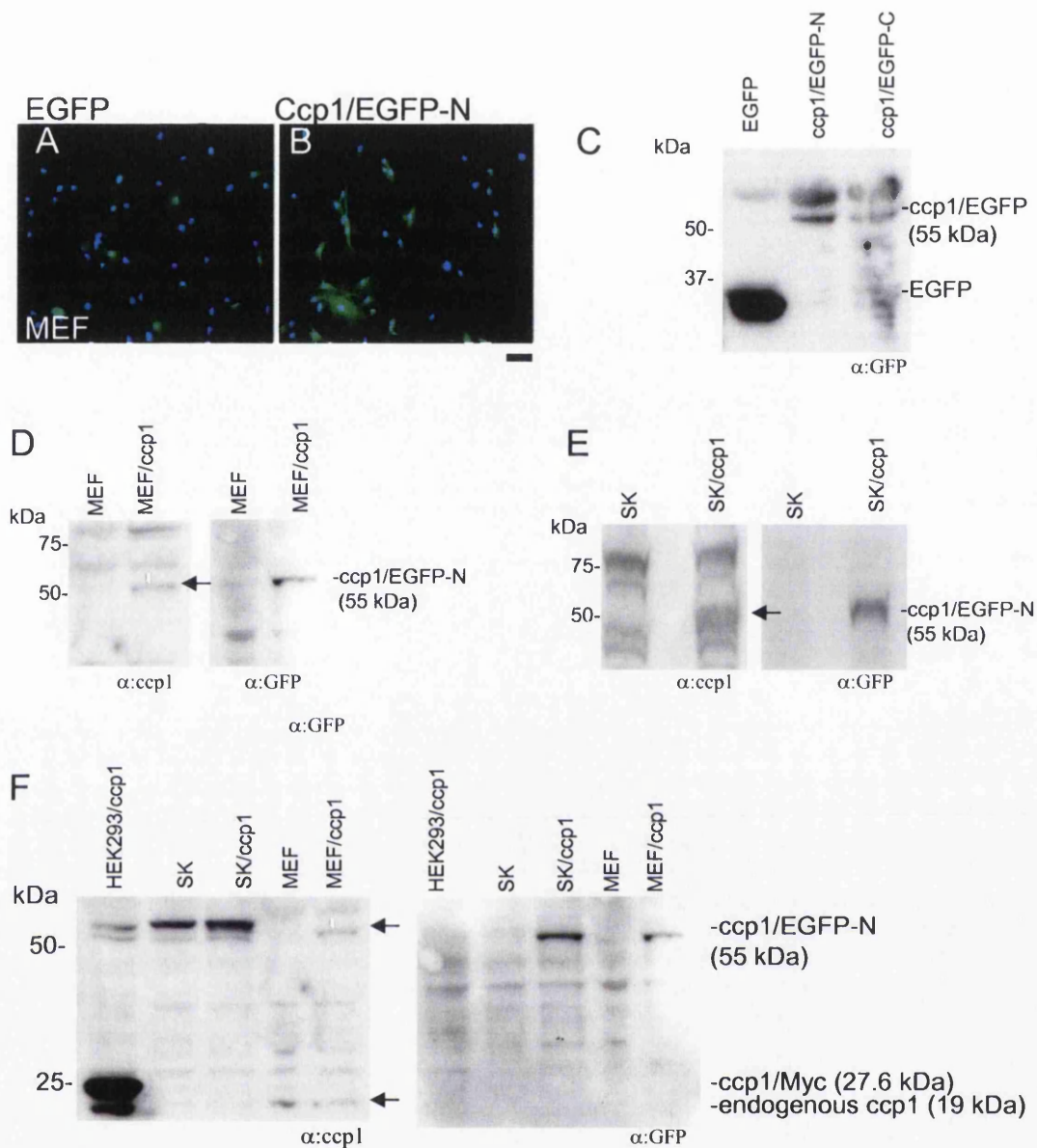


Figure 3.3.8 Stable expression of ccp1 in MEF by retrovirus approach.

Cell lines stably expressing EGFP, ccp1/EGFP-N and ccp1/EGFP-C fusion proteins were generated. (A, B) MEF expressing ccp1 were visualised with an anti-GFP antibody. (C) The level of the ccp1 expression was determined by Western blotting using anti-GFP antibody. EGFP expression was detected at 30 kDa and ccp1/GFP-N and -C were detected at 55 kDa. (D) Ccp1 stable expression was analysed and MEF cells using ccp1 polyclonal and GFP antibodies. (E) Ccp1 stable expression was analysed in SK-N-SH cells. (F) Ccp1 expression was compared in HEK293 cells transiently expressing ccp1/Myc, in SK-N-SH and in MEF stably expressing ccp1/EGFP fusion protein using ccp1 polyclonal and GFP antibodies. C, D, E: 7.5% SDS-PAGE gel. F: 4-12% SDS PAGE gradient gel. Scale bar in A, B: 25 μ m.

3.3.8 Stably expressed ccp1 was localised to the cytoplasm and to the nucleus.

Ccp1 was localised to lysosomes when transiently expressed in the cells (Fig 3.3.6). To determine whether ccp1 fusion protein shows a similar cellular localisation when stably expressed in the cells, immunocytochemistry was carried out using MEF stably expressing ccp1/EGFP-N using anti-GFP antibody. The control MEF cells expressing EGFP alone showed diffuse fluorescence throughout the cell (Fig 3.3.9, A). In a population within a single clone expressing ccp1/EGFP-N, different localisation of the ccp1 protein was observed. In some cells, ccp1/EGFP-N localised throughout the cytoplasm in punctate spots (Fig 3.3.9, B), whereas other cells showed ccp1/EGFP-N accumulated in the nucleus (Fig 3.3.9, C). A very few cells showed staining of ccp1 in aggregates (Fig 3.3.9, D).

Cells transiently expressing ccp1 showed localisation of ccp1 in a population of lysosomes (chapter 3.3.5). The punctate spots observed in cells stable expressing ccp1 were much smaller than the structures observed in the transient expressing cells. In order to determine whether the punctate spots detected in the cells stable expressing ccp1/EGFP-N were part of the lysosomes, double immunocytochemistry was carried out using LysoTracker (Fig 3.3.9, E-G) and antibody against EEA1 (Fig 3.3.9, H-J). The ccp1-positive spots did not co-localise either with LysoTracker- and EEA1-positive structures, indicating a discrepancy between ccp1 localisation observed in the transient and in the stable cell lines. It is possible that, when transiently expressed, the level of ccp1 fusion protein was high and it caused accumulation in lysosomes leading to degradation. In the stable cell lines, the level of ccp1 fusion protein was much lower (Fig 3.3.8, F).

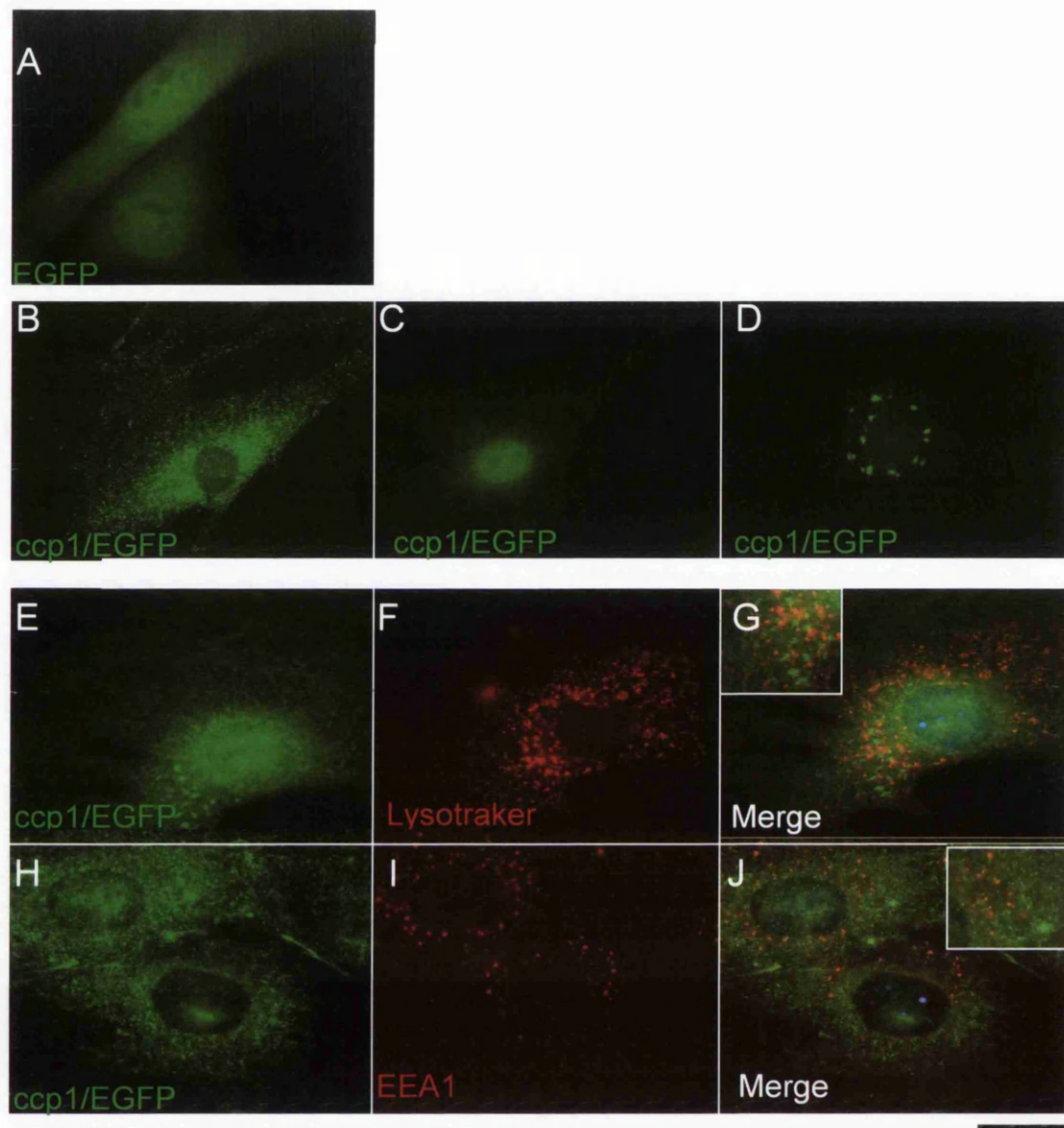


Figure 3.3.9 *Ccp1/EGFP-N* stably expressed in MEF was localised mainly to the cytoplasm.

MEF stably expressing *ccp1/EGFP-N* fusion protein were generated using a retroviral approach. Cells stably expressing EGFP did not show any major specific staining (A). Ccp1 stably expressed in MEF localised to the cytoplasm in punctate spots (B), or in the nucleus (C), or in aggregates (D). Double-immunocytochemistry was performed between *ccp1* (E, H) and Lysotraker (F) or EEA1 antibody (I) to assess whether the punctate spots were lysosomes or endosomes, respectively. Scale bar: 25 μ m.

3.3.9 Putative nuclear exporting signal (NES) domains might affect ccp1 cellular localization.

Two putative NES domains were identified in the N-terminus of the sequence (Chapter 3.1.4). As described previously, the NES is a short sequence that determines nuclear transport of the protein through the nuclear complex from the nucleus to the cytoplasm (257, 302). The NES is composed of a leucine-rich region and the accepted consensus sequence (with some variation) is $LX_{2-3}LX_{2-3}LXL$ (261). The mouse *ccp1* sequence contains two consensus sequences at residues 6-17 and 18-26, (Fig 3.3.10, A). The second NES (position 18-26) is similar to the NES of well-known proteins, including MEK (269), p120 catenin (303) and Trim27 (304) (Fig 3.3.10, B). Since *ccp1* contains a NES domain similar to MEK, which is also known to localise to cytoplasmic spots (269), co-localisation between *ccp1* and MEK was carried out (Fig 3.3.10, C-F). Although the two proteins showed a very similar punctate spots, they did not overlap upon close inspection.

In order to test the functionality of NES in *ccp1* and to determine whether the NES domains regulate *ccp1* localisation between the nucleus and the cytoplasm, sub-cellular localisation of *ccp1*/EGFP-N was examined by immunofluorescence in MEF stably expressing *ccp1*. *Ccp1*/EGFP-N was predominantly observed to the cytoplasm and partly in the nucleus (Fig 3.3.9). In order to determine if *ccp1* localisation would have been affected by a specific stimuli, such as the addition of a growth factor, the cells were treated with 50 ng/ml FGF2 in the presence of 10 μ g/ml heparin for 1-24 h (Fig 3.3.10, G-I). As a control, MEF with stable expression of EGFP were also treated and analysed. Three different conditions of *ccp1* localisation were observed,

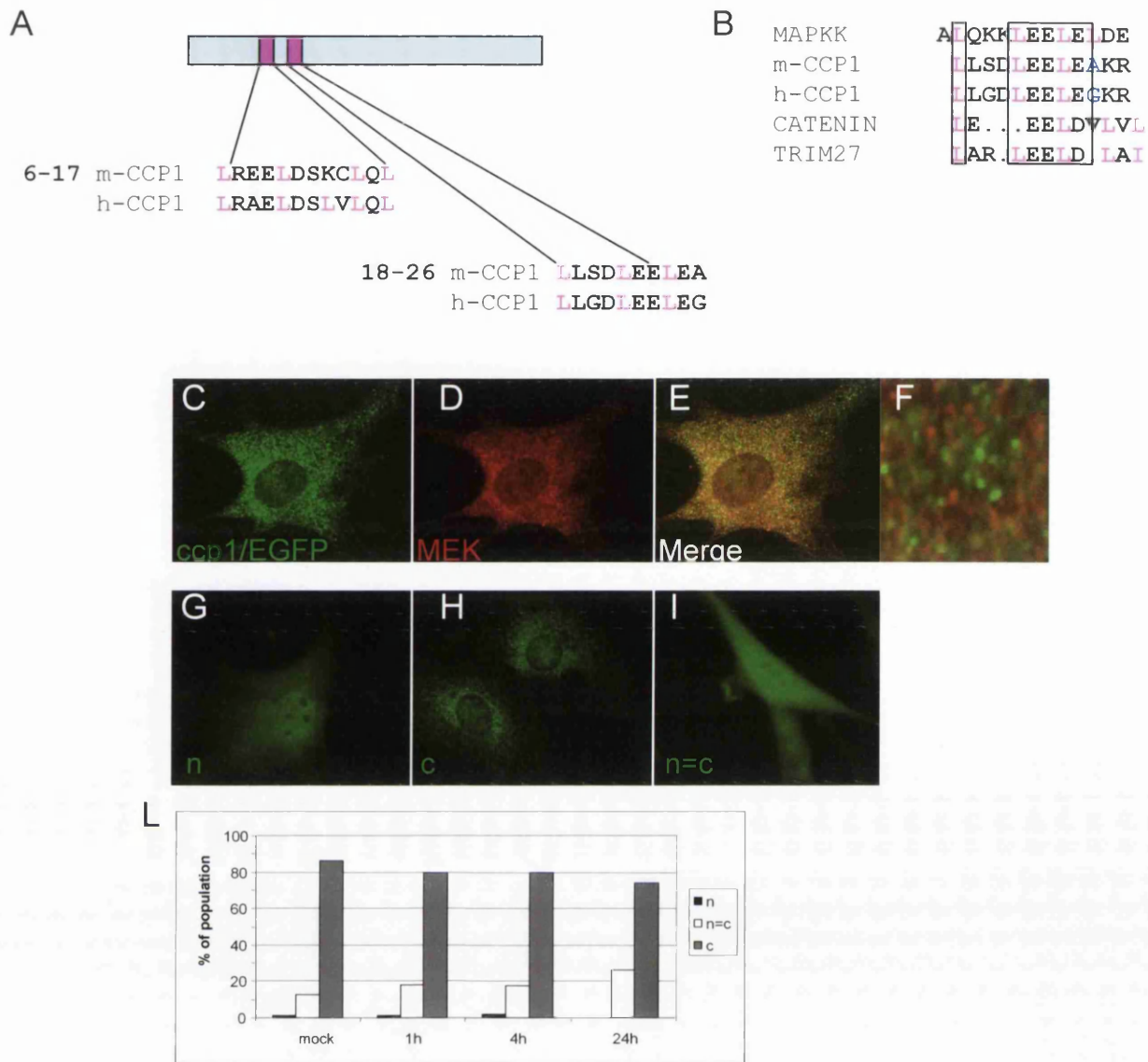


Figure 3.3.10 Two putative nuclear exporting signals (NES) are present in *ccp1* amino acid sequence.

(A) The mouse *ccp1* sequence contained the two consensus at the 6-17 and 18-26, respectively. (B) The second NES in *ccp1* (position 18-26) presented some homology to NES of well known proteins, as highlighted in the boxes. (C-E) Immunocytochemistry was performed using anti-MEK antibody in order to analyse co-localisation with *ccp1*. *Ccp1* was detected using anti-GFP antibody. (G-I) *Ccp1/EGFP-N* expressing MEF were treated with 50 ng/ml FGF2 and 10 µg/ml of heparin. *Ccp1* was observed in the nucleus (n), both in the nucleus and the cytoplasm (n=c) or in the cytoplasm (c). (L) The number of cells presenting *ccp1* in different compartments were counter-stained and reported as percentage.

in the nucleus (n), in the cytoplasm (c) and in both nucleus and cytoplasm (n=c). The total number of cells that shown ccp1/EGFP-N in the three different localisation were counted and quantified (Fig 3.3.10, L). In the mock-treated cells, ccp1 was mainly present in the cytoplasm (86%), however a small percentage of cells showed nuclear staining (about 1.3%). At 1 and 4 h of FGF2 treatment, 12.5 and 18.2% of the cells, respectively, showed ccp1/EGFP-N both in the cytoplasm and the nucleus (n=c). At 24 h of treatment, no more staining was present in the nucleus and a larger proportion of cells (26.1%) presented ccp1 both in the cytoplasm and the nucleus (n=c). These results showed that FGF2 treatment may induce movement of ccp1 between the nucleus and the cytoplasm, however further studies are required for conclusive results.

3.4 The function of *ccp1* *in vitro*

In this chapter, the function of *ccp1* was investigated *in vitro* by modifying its expression levels in cells by overexpression and by RNA interference (RNAi). Assays were performed to investigate whether *ccp1* expression influenced cell proliferation, cell death and cell migration. The results showed that *ccp1* increased cell proliferation. Furthermore, MAPK signalling, one of the major pathways activated by growth factor signalling and known to promote cell proliferation (202, 305), was investigated as a potential modulator of *ccp1*-induced proliferation.

3.4.1 Cellular *ccp1* overexpression caused morphological changes.

In order to investigate the function of *ccp1* *in vitro*, cell lines stably expressing *ccp1* were established by retrovirus approach, as described in chapter 3.3.7. The cells stably overexpressing *ccp1*/EGFP-N fusion protein were used in all the functional studies presented in this chapter. *Ccp1*/EGFP-N protein will be referred as *ccp1* protein.

MEF cells present a flat shape typical of fibroblasts (Fig 3.4.1). When *ccp1* was overexpressed in MEF, a change in cell morphology was observed (Fig 3.4.1, B). Cells expressing *ccp1* appeared smaller and had a spindle-like phenotype. Furthermore, phenotype became more prominent in cell expressing *ccp1* upon stimulation with 50 ng/ml FGF2 in the presence of 10 µg/ml heparin for 24 h. FGF2 treatment enhances changes in cell shape of MEF expressing *ccp1* (Fig 3.4.1, D).

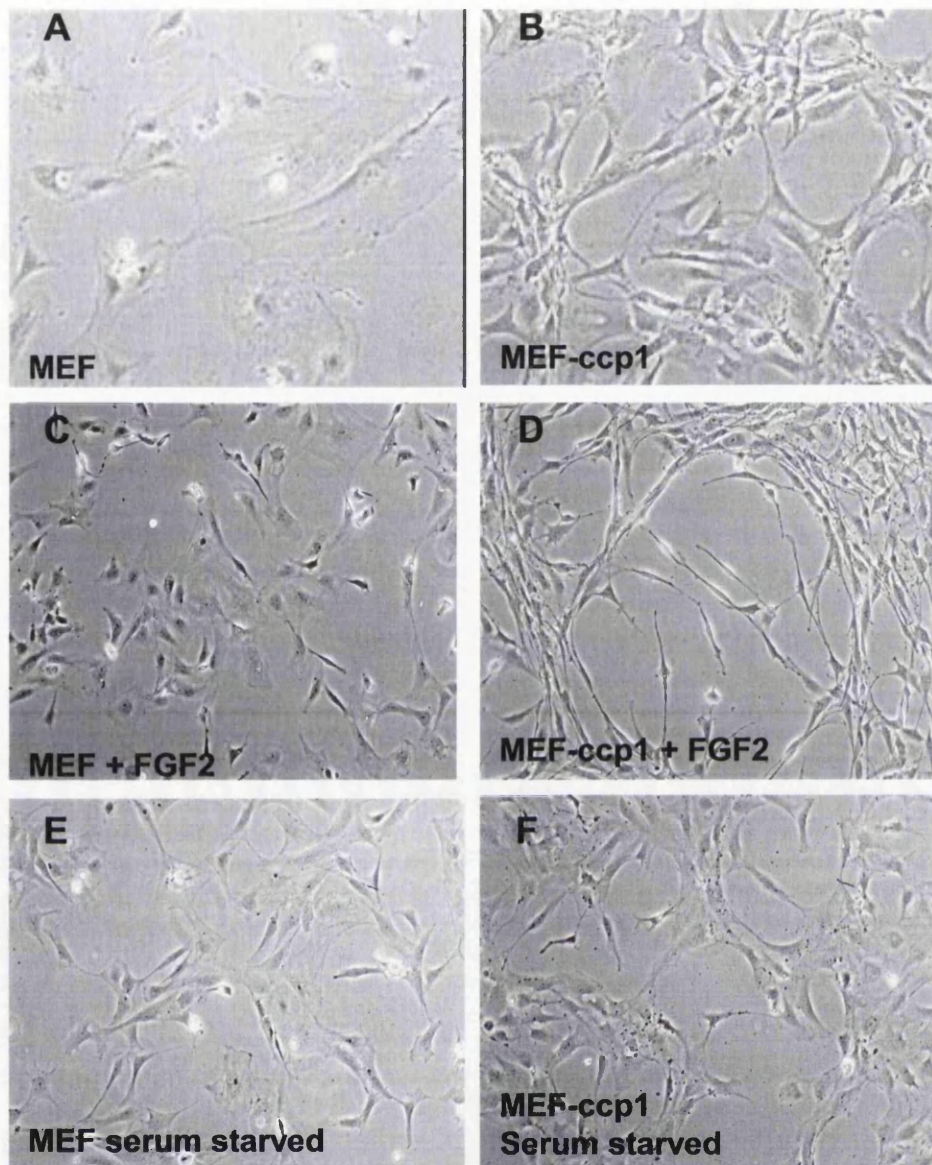


Figure 3.4.1 Stable expression of ccp1 in MEF caused morphological changes.

MEF stably expressing ccp1 were generated using a retroviral approach. (A) Normal MEF presented a typical fibroblast flat shape. (C) Upon FGF2 stimulation for 24 h, MEF presented a mild spindle shape. (B) MEF expressing ccp1 showed a change in cell morphology. Cells appeared smaller and spindle-like. (D) In the MEF stably expressing ccp1, the spindle shape become more apparent upon FGF2 stimulation. (F) Serum starvation reversed the shape changes induced by ccp1 expression.

Interestingly, serum starvation only partially reverse the shape changes of MEF expressing ccp1 (Fig 3.4.1, F). Change in the cell shape in MEF stably expressing ccp1 may indicate ccp1 role in enhancing cell proliferation.

3.4.2 No significant change in wound healing closure was observed in MEF stably expressing ccp1.

To assess whether ccp1 has a role in cell migration, wound assay was performed in MEF expressing ccp1. After the wound was made in the confluent cells, the width of the closure of the wound was measured over the time (Fig 3.4.2, A). Migration experiment was performed using single clones of MEF stably expressing ccp1, previously derived as described in Chapter 3.3.7. By Western blotting analysis, levels of the ccp1/EGFP fusion protein was analysed in 3 of the 6 single clone/cells using anti-GFP antibody (Fig 3.4.2, B). Clone 1 showed ccp1 band at the expected size of 55 kDa, whereas clone 2 and 3 showed in addition a smaller band of about 37 kDa, which may be a cleavage product. Upon assaying the wound closure in the ccp1 clones, no difference was observed in clones expressing ccp1 in comparison with the EGFP expressing controls (Fig 3.4.2, C), suggesting that ccp1 is unlikely to regulate cell migration in MEF.

3.4.3 Ccp1 stable expression induced an increase in cell number.

In order to determine whether ccp1 plays a role in cell proliferation, growth of cells were analysed in culture. Control MEF and MEF stably expressing ccp1 were

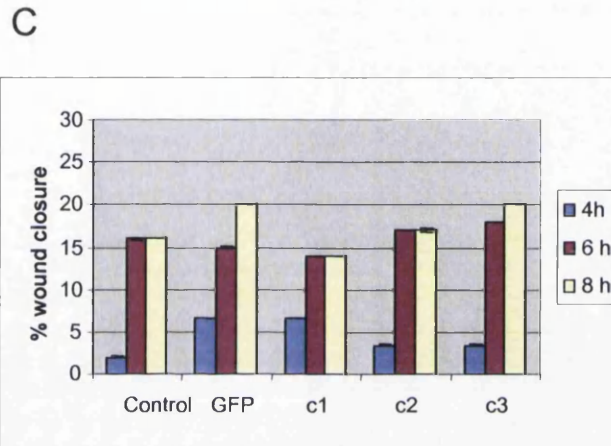
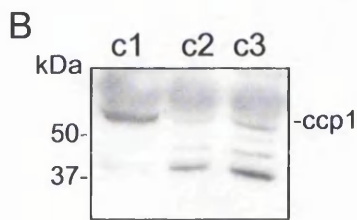
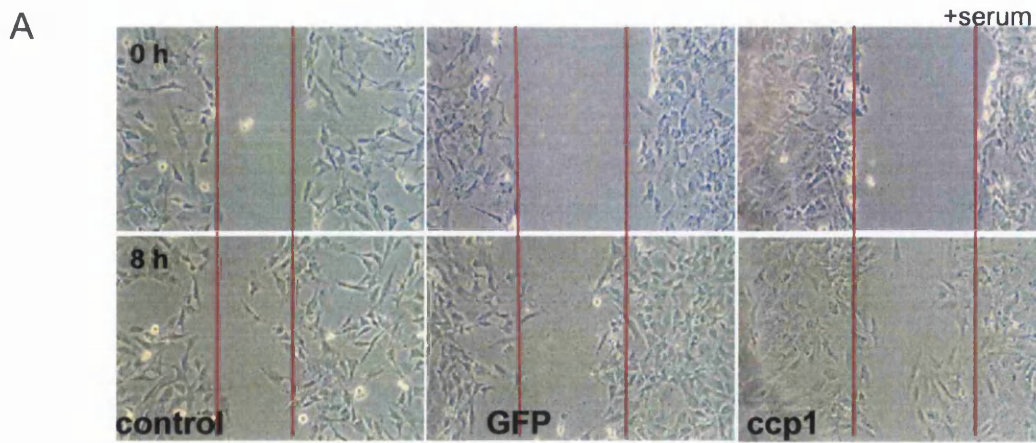


Figure 3.4.2 Wound healing closure was not induced by MEF stably expressing *ccp1*.

To investigate whether *ccp1* influenced cell migration, wound assay was carried out. (A) Monolayer of control MEF, MEF expressing EGFP and *ccp1* was scratched and photographed at 0, 4, 6, 8 and 24 h. Representative photos after 8 h are shown. (B) The clones stably expressing *ccp1*/EGFP were used. The level of *ccp1* expression was determined by western blotting in clone 1 (c1), clone 2 (c2) and clone 3 (c3). (C) Measurements were made (two in each treatment) and compared to the measurement at time 0. No significant difference in migration activity was detected between the controls and the *ccp1* positive cells.

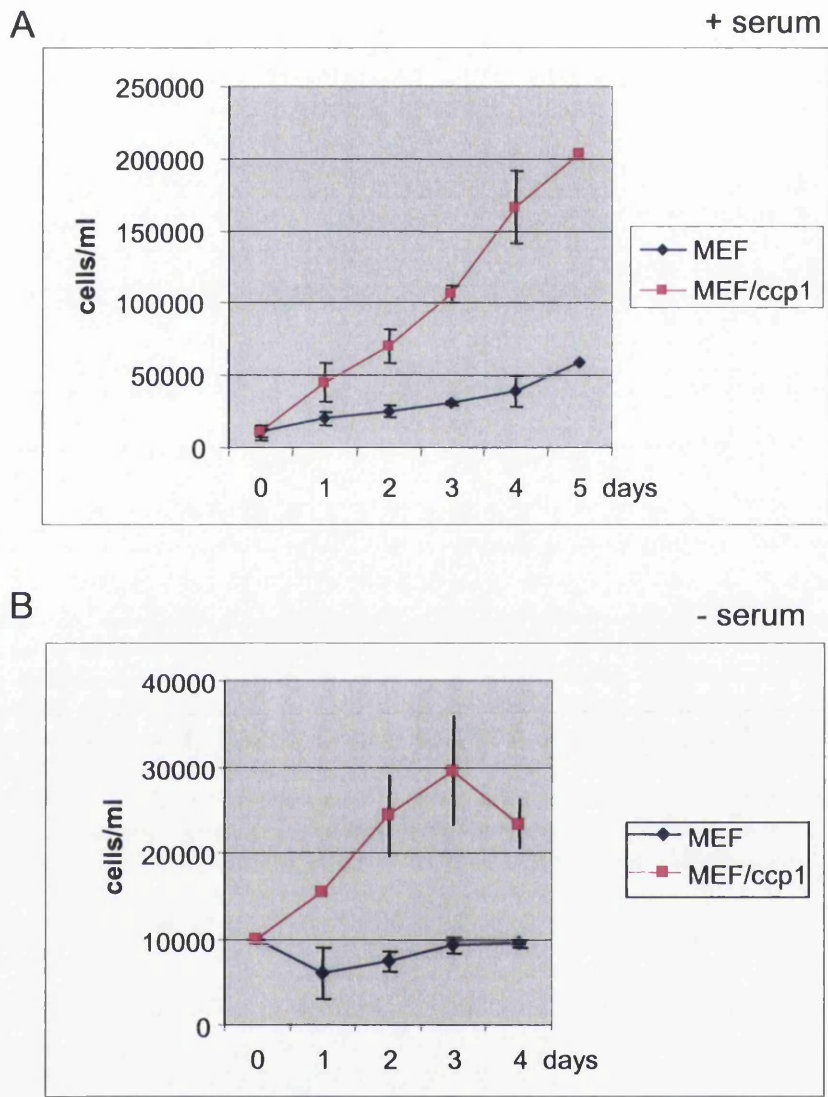


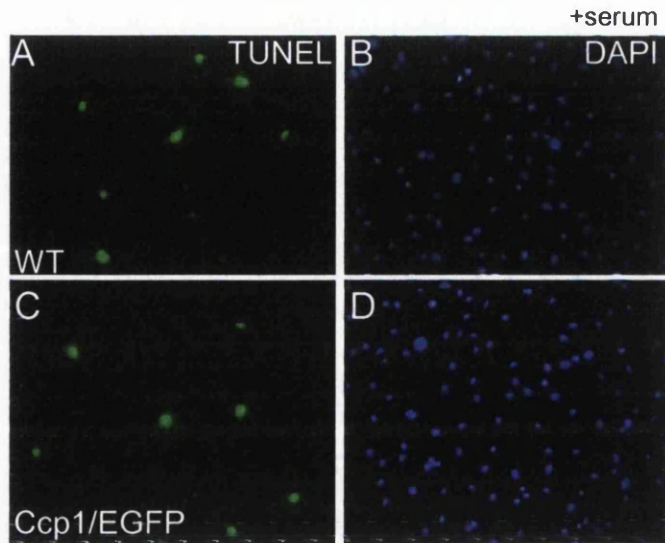
Figure 3.4.3 *Ccp1* expression caused an increase in cell number.

(A) Control MEF and MEF expressing *ccp1* were plated at the same density in the presence of serum and cell number was counted after trypsinisation. *Ccp1* caused an increase the proliferation rate in cell number. (B) In the absence of serum, three-fold increase in cell number was observed in MEF stably expressing *ccp1* in comparison to control MEF at 3 days of culture.

initially plated at the same density and cultured for up to 5 days. Cell number was counted after trypsinisation at each time point (Fig 3.4.3, A). MEF stably expressing ccp1 showed 123% increase in cell number in one day in culture. The difference between the two groups increased over days. After 5 days in culture, the cells expressing ccp1 grew 4-fold more than control MEF, indicating that expression of ccp1 promote cell proliferation. Next, cell proliferation was investigated in the absence of serum. Control MEF were cultured showed a mild increase in cell number up to 4 days (Fig 3.4.3, B). In contrast, MEF stably expressing ccp1 showed a three-fold increase in cell number at 3 days in culture. Ccp1 expression increased total cell number in both the presence and absence of serum.

3.4.4 No significant change in apoptosis was observed in MEF stably over-expressing ccp1.

In order to determine whether apoptosis is involved in the increase in cell number upon over expression of ccp1, TUNEL assay was performed in MEF stably expressing ccp1 (Fig 3.4.4). Cells were plated out at the same density and cultured for 24 h before TUNEL assay was performed. Both lines showed apoptotic cells in 7% of population and there was no change in number of apoptotic cells between the control MEF and cells expressing ccp1. (Fig 3.4.4, E). Apoptosis mediated by ccp1 has been investigated only in MEF so far. The involvement of ccp1 in cell death in neuronal cell types is not excluded.



E

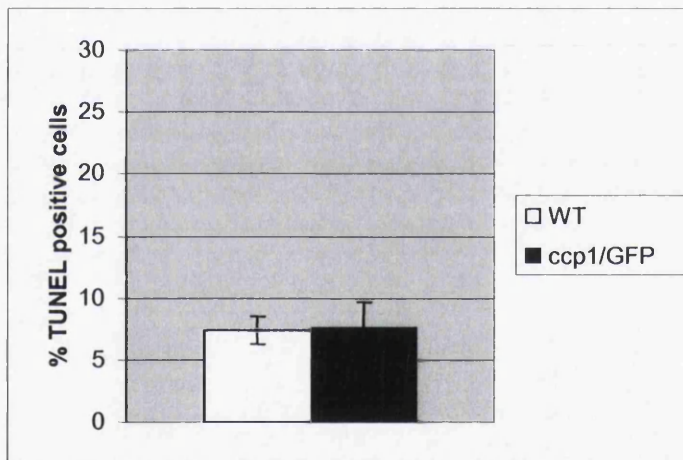


Figure 3.4.4 Apoptosis was not induced in MEF stably expressing *ccp1*.

In order to determine if *ccp1* influenced cell apoptosis, TUNEL assay was performed. (A-D) Representative photos of control cells and MEF expressing *ccp1* are shown. (B, D) The cells were counter-stained with DAPI. (E) Apoptotic cells were represented as a percentage of total cells present in a given area of cover-slips (n=5). Control and *ccp1* expressing MEF did not show any difference in the number of apoptotic cells.

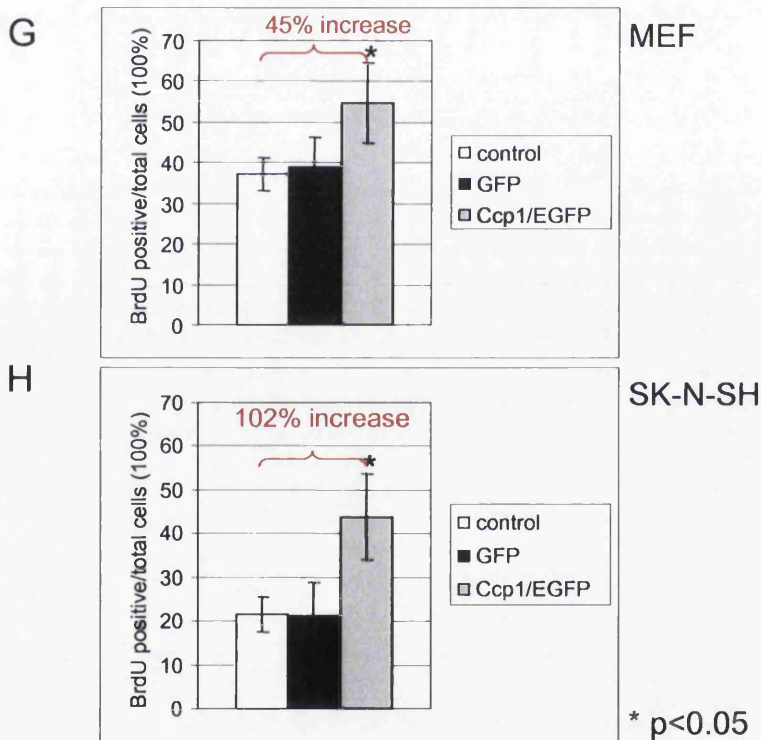
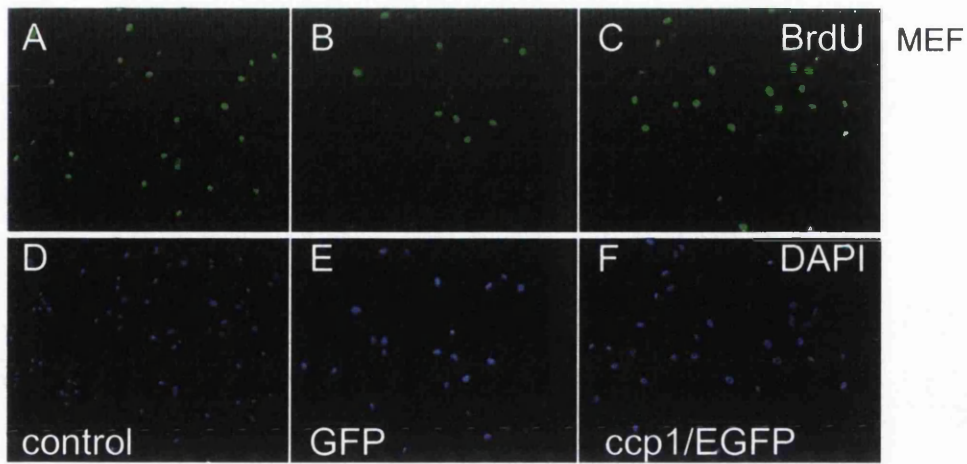


Figure 3.4.5 Ccp1 induced cell proliferation in stably expressing system.

BrdU assay was performed using MEF and SK-N-SH cells stably expressing *ccp1*. (A-C) MEF were stained with BrdU antibody. (D-F) Cells were counter-stained with DAPI. Proliferation was calculated as the percentage of BrdU-positive cells present in a given area of cover slips. (G) MEF stably expressing *ccp1* showed a 45% increase in proliferation in comparison to the controls. (H) SK-N-SH stably expressing *ccp1* showed a two-fold increase in proliferation in comparison to the controls. * The difference was statistically significant between the samples.

3.4.5 Ccp1 promoted BrdU incorporation in MEF and SK-N-SH cells.

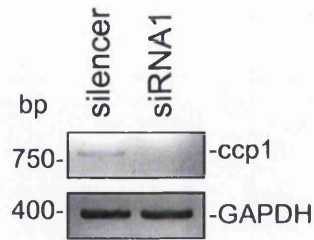
In order to determine whether the cell number increase observed above was due an increase in cells in the S phase, BrdU assay was performed in MEF and SK-N-SH cells stably expressing *ccp1* (Fig 3.4.5). Cells were cultured in 10% serum for 24 h, incubated in 10 μ M BrdU for 1 h and stained with anti-BrdU antibody (Fig 3.4.5, A-C). The presence of the cell was visualised by nuclear stain with DAPI (Fig 3.4.5, D-F). MEF expressing *ccp1* showed an increase in the number of cells in the S phase by 45% compared to that in control MEF and to MEF expressing EGFP (Fig 3.4.5, G). Similar results were obtained in SK-N-SH cells expressing *ccp1*, which showed an increase in cell proliferation by two-fold compared to the control and to the SK-N-SH stably expressing EGFP (Fig 3.4.5, H).

3.4.6 BrdU incorporation was inhibited when *ccp1* expression was knocked down by RNAi in SK-N-SH cells.

RNAi approach was used to address the *ccp1* function in cell proliferation. RNAi was used to suppress *ccp1* expression by transfecting small interfering RNAs (siRNAs). As a negative control, a silencer siRNA designed to share no significant similarity to any mouse, rat or human gene sequences, was used. At 24 h post-transfection of siRNA molecules, *ccp1* expression was analysed by RT-PCR. *Ccp1* expression was abolished in cells transfected with the siRNA1, while silencer showed no effect in the level of *ccp1* transcripts (Fig 3.4.6, A).

BrdU assays were then performed in cells lacking *ccp1* (Fig 3.4.6, B). As a control, BrdU assay was performed using mock-treated cells and cells transfected

A



B

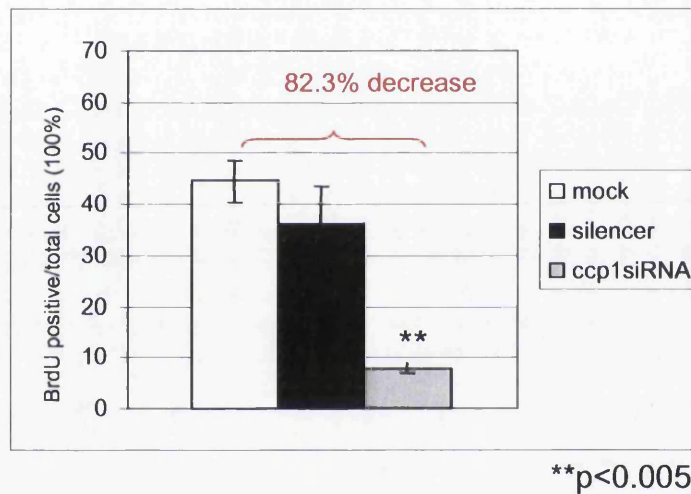


Figure 3.4.6 Cell proliferation was inhibited when *ccp1* expression was knocked down in SK-N-SH cells.

(A) Ccp1 expression was knock down in SK-N-SH cells using specific *ccp1*-siRNA (siRNA1). Ccp1 expression was assessed by RT-PCR. GAPDH amplification was shown as control. (B) BrdU assay showed that cell proliferation in cells knock down with *ccp1* decreased to 82.3% of the mock-treated cells. Cells transfected with silencer siRNA did not show significant reduction in cell proliferation.

with silencer siRNA. In the absence of *ccp1* expression, cells showed a decrease in BrdU incorporation by 82.3% compared to the mock-treated cells. The data were obtained by an experiment carried out on 6 different samples that showed similar results. This experiment has only been performed once. For conclusive evidence, three independent siRNA molecules should have been used and BrdU assay should have been performed three times, but due a technical problem related to the transfection of SK-N-SH cells, these experiments could not be carried out.

3.4.7 Ccp1 rescued MEK inhibition by U0126.

The MAPK pathway is one of the major pathways downstream of growth factor signalling involved in cell proliferation (202). In order to identify a signalling mechanism of *ccp1*-induced cell proliferation, MAPK signalling was investigated in MEF expressing *ccp1*. MEK is one of the key proteins of the MAPK signalling pathway (306) and the MEK inhibitor, U0126, was used in the BrdU assays.

First, the optimal concentration of U0126 was determined in the culture system used (Fig 3.4.7, A). MEF were plated out at the same density and treated with varying concentrations of U0126. As a control, the cells were not treated or incubated with a corresponding amount of Dimethyl Sulfoxide (DMSO), the solvent in which U0126 was dissolved. After 24 h, BrdU assays were performed. Treatment with 10 μ M U0126 resulted in a 10.4% reduction in cell proliferation in comparison to the untreated cells. 20 μ M U0126 caused a 45.3% decrease in proliferation in comparison to the untreated cells. DMSO alone did not show any effect at this concentration. 50 μ M U0126 caused a 63.4% reduction in cell proliferation, but the cells treated with

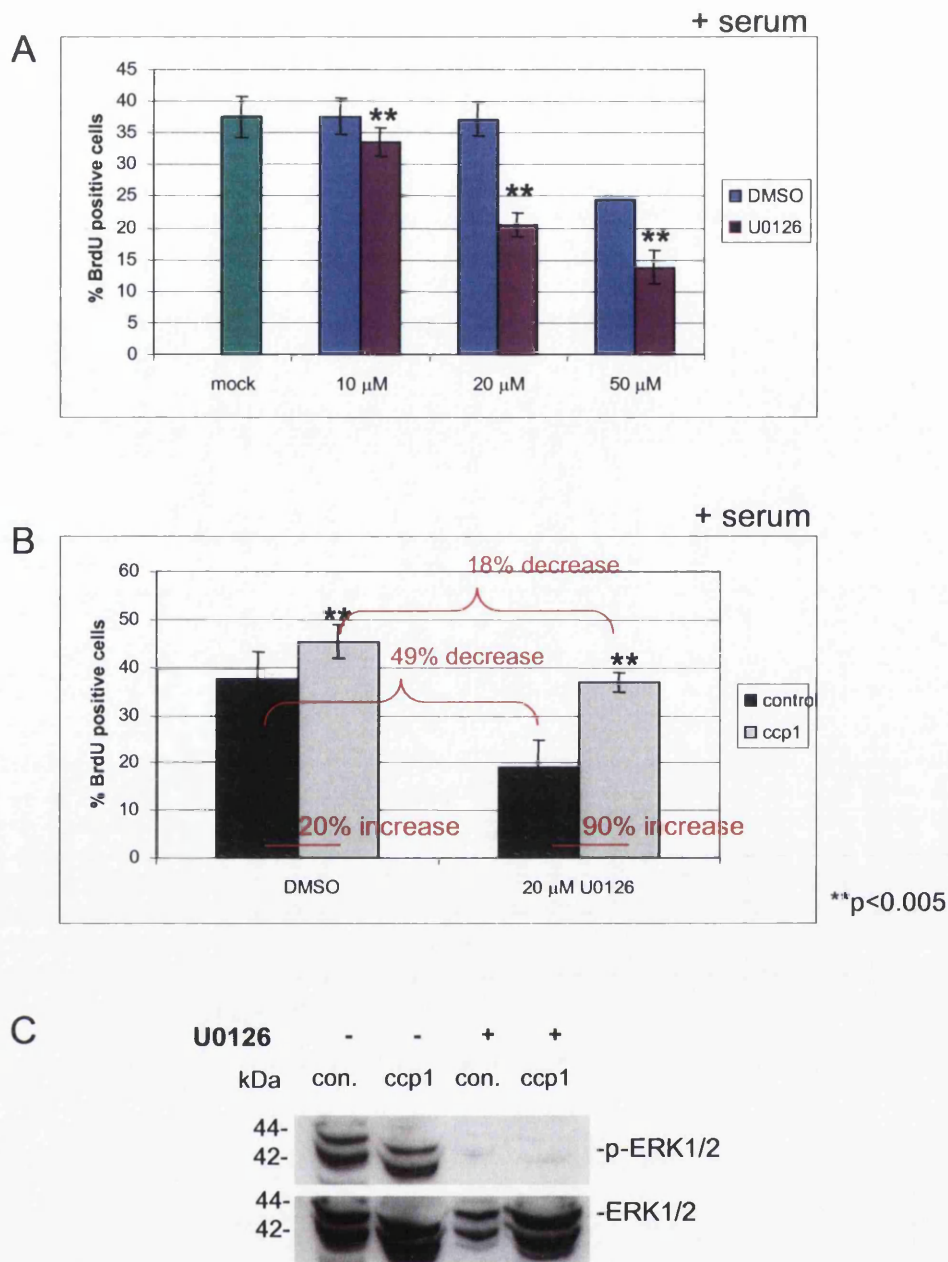


Figure 3.4.7 Cell proliferation promoted by *ccp1* was reduced by addition of MEK inhibitor.

To investigate whether *ccp1*-induced proliferation was mediated by MAPK pathway, MEK inhibitor U0126 was used. (A) To identify the concentration of inhibitor, MEF were treated with different concentrations of U0126 in the presence of serum for 24 h and BrdU assay was performed. The concentration of 20 μM was chosen. (B) Cells expressing *ccp1* were treated with 20 μM of U0126 and BrdU assay was performed. (C) Control MEF and MEF expressing *ccp1* were treated as above and Western blotting was performed to detect the level of p-ERK1/2. 7.5% SDS-PAGE gel was used.

DMSO also showed reduced proliferation (34.9%). In consideration of the toxicity of DMSO volume used when 50 μ M of U0126 was added to the culture, the concentration of U0126 at 20 μ M (lesser volume of DMSO) was chosen for the following experiments.

Control MEF and MEF expressing *ccp1* were cultured overnight in the presence of serum in the presence and absence of 20 μ M U0126. In the absence of U0126, a 20% increase in BrdU incorporation was detected in the MEF stably expressing *ccp1* compared to the control MEF (Fig 3.4.7, B). This value was somewhat lower than the data observed in figure 3.4.3, probably due the fact that, in this experiment, the cells were plated for two days before BrdU assay was performed. In the presence of U0126, both group of cells showed a decrease in cell proliferation. Control MEF showed a 49% decrease in BrdU incorporation, whereas *ccp1* expressing MEF showed a decrease of only 18.8%. This result indicates that *ccp1* rescued MEK inhibition by U0126.

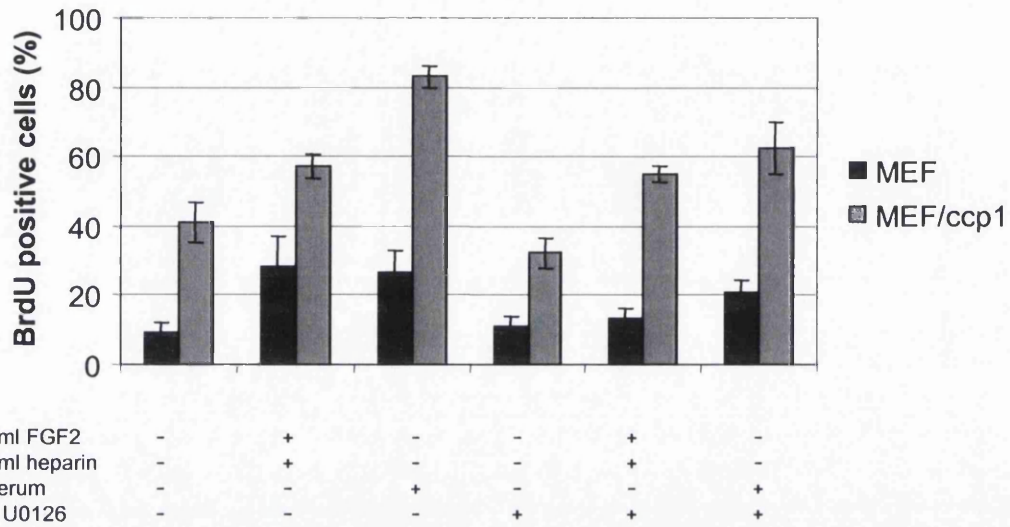
To examine whether U0126 inhibited MAPK activation, Western blotting was performed using antibody against phosphorylated ERK, one of the key protein that mediate the effect of MAPK signalling (202). The lysates were prepared from control MEF and MEF expressing *ccp1* treated with 20 μ M of U0126 for 24 h (Fig 3.4.7, C). U0126 blocked the phosphorylation of ERK in control MEF and in the MEF expressing *ccp1*.

3.4.8 Effects of growth factor stimulation on ccp1-induced cell proliferation.

In order to determine whether addition of growth factors further increases cell proliferation in cells overexpressing ccp1, Control MEF and MEF expressing ccp1 were starved overnight in order to allow all the cells to exit from the cell cycle. Cells were treated with FGF2 or serum (Fig 3.4.8, A). In order to measure the total number of proliferating cells from the same moment in which the cells were treated, BrdU was added to the culture together with the treatment and incorporation was allowed for 24 h. With no treatment, MEF expressing ccp1 showed increase in BrdU incorporation in comparison to control MEF. Similar results but more drastic were observed in the cell treated with FGF2 or serum. Furthermore, upon stimulation with serum, more cells in S phase were observed in comparison to the FGF2 treated cells. Control MEF showed 28.5% and 26.8% of cells in S phase when treated with FGF2 and serum, respectively. MEF expressing ccp1 showed 57.4% and 83.1% of BrdU positive cells in FGF2 or serum, respectively.

Next, in order to determine whether MAPK signalling has a role in ccp1 induced cell proliferation upon FGF2 addition, the cells were serum starved and treated with 20 μ M U0126 in the presence or not of 50 ng/ml FGF2 and 10 μ g/ml heparin or 10% SERUM. BrdU incorporation was inhibited in control MEF but not in MEF expressing ccp1. Similar trend was observed when FGF2 or serum were added together with U0126 (Fig 3.4.8, A). In control MEF the number of cells in S phase is similar to the samples in which only U0126 was added. On the contrary, MEF expressing ccp1 showed an increase in BrdU positive cells in the presence of FGF2 and even more in the presence of serum.

A



B

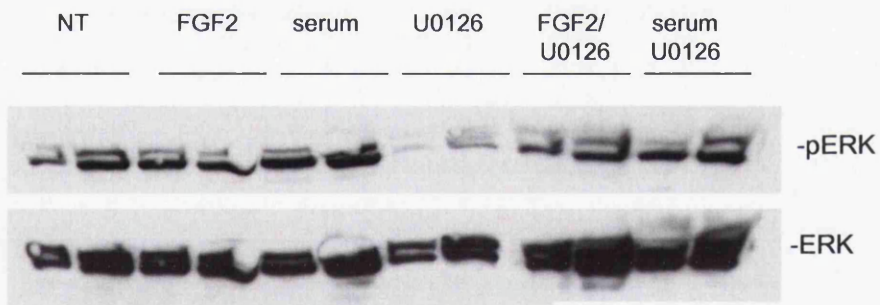


Figure 3.4.8 Effects of growth factor stimulation on *ccp1*-induced cell proliferation.

MEF expressing *ccp1* and control MEF were cultured in absence of serum for 24 h and treated with FGF2 and heparin, serum, or U0126 for 24 h. (A) BrdU assay was performed. BrdU was incorporated for 24 h. (B) Western blotting was carried out to analyse activation of ERK1/2. Blotting with ERK1/2 antibody was carried out to indicate the loading.

Western blotting was carried out to analyse phosphorylation of ERK, (Fig 3.4.8, B). Control MEF and MEF expressing *ccp1* showed a basal level of p-ERK. Addition of U0126 alone blocked ERK phosphorylation in both type of cells. When U0126 plus FGF2 or serum was added together, the level of p-ERK was still high. It is likely that after 24 h U0126 efficiency is decreased in the presence of strong mitogens as FGF2 or serum.

3.4.9 Levels of ERK phosphorylation in *ccp1* expressing cells in the presence and absence of FGF2 stimulation.

Despite an increase in cell proliferation in cells expressing *ccp1* (Fig 3.4.2), a decrease in ERK phosphorylation was observed when cultured in serum over time (steady state) (Fig 3.4.9, A), which was also observed in the previous data (Fig 3.4.7, C). Densitometry analysis showed a 60% reduction in phosphorylation of ERK in cells expressing *ccp1*.

In order to determine whether ERK phosphorylation can be induced upon FGF2 stimulation in these cells, levels of p-ERK were examined upon FGF2 stimulation over time in the absence of serum. Cells were starved overnight and treated with 50 ng/ml FGF2 in the presence of 10 μ g/ml heparin for a short time period up to 15 min (Fig 3.4.9, B). By Western blotting using anti p-ERK antibody, control MEF showed a gradual activation of ERK. A similar pattern was observed in the cells expressing *ccp1*. However, in these cells the activation of ERK was stronger after 10 min, indicating that *ccp1* increased the FGF2-induced phosphorylation of ERK. The regulation of ERK phosphorylation by *ccp1* was then examined upon FGF2

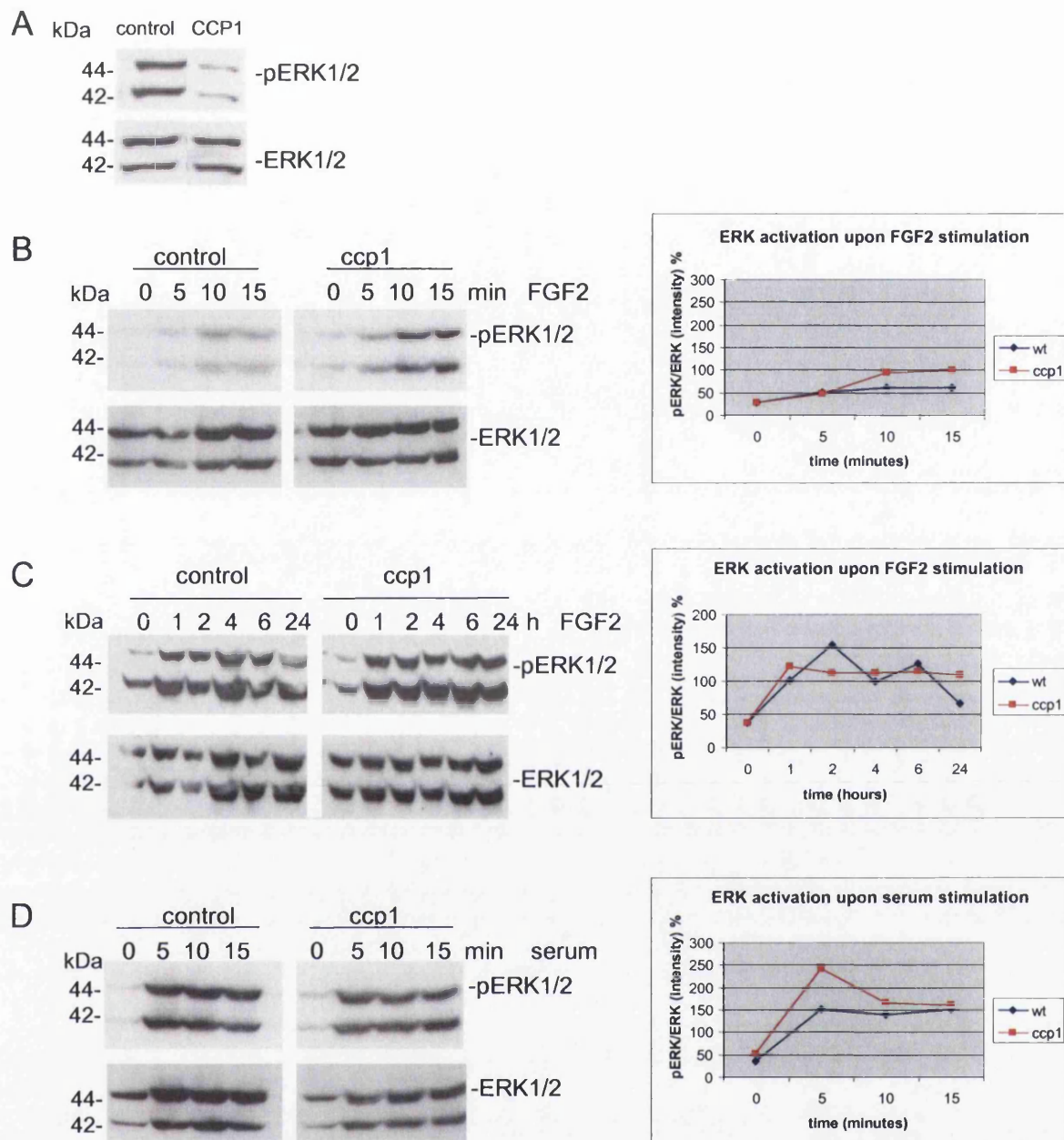


Figure 3.4.9 Regulation of ERK1/2 phosphorylation in MEF expressing *ccp1* upon FGF2 stimulation

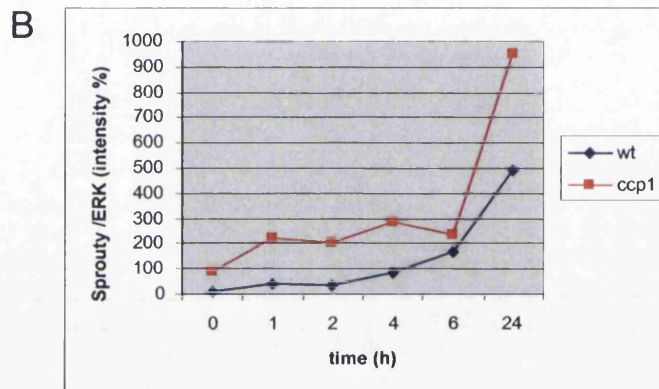
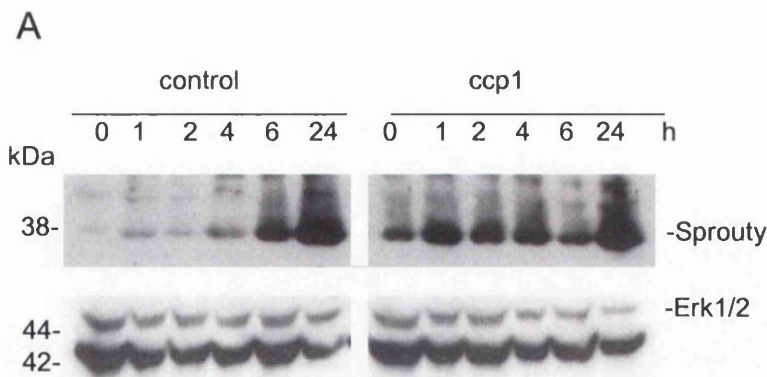
(A) MEF expressing *ccp1* showed a decrease in p-ERK1/2 by 60%. (B) Cells were cultured in absence of serum and treated with FGF2. Control MEF showed activation of ERK1/2, whereas a stronger signal was shown by the *ccp1* expressing cells. (C) Experiment was carried out for longer time frame. (D) Cells were starved and treated with 10% FBS. Analysis of ERK1/2 was performed to confirm sample loading in all the blots. Quantification of each panel by densitometry is shown in the graphs.

stimulation over a prolonged period up to 24 h (Fig 3.4.9, C). ERK phosphorylation increased after 1 h of FGF2 stimulation in the control MEF, reaching a peak at 2 h and decreased at 24 h. Similar increase in the p-ERK level was observed in MEF expressing *ccp1* at 1 h of stimulation and thereafter it remained at the constant level up to 24 h. Next, ERK phosphorylation was examined upon stimulation by the serum for up to 15 min. ERK was highly activated at 5 min in control MEF. Similar activation was also observed in MEF stably expressing *ccp1*, but phosphorylation was stronger at 5 min (Fig 3.4.9, C).

In summary, the data showed that *ccp1* overexpression caused a decrease in ERK phosphorylation in cells in the steady growing phase. However, p-ERK level can be increased by FGF2 stimulation in MEF expressing *ccp1* in comparison to the control MEF. Of note, phosphorylation of ERK was not decreased in cells expressing *ccp1* at time 0 after serum starvation. This may indicate the presence of a feedback mechanism that inhibits ERK phosphorylation in cells expressing *ccp1* maintained in the presence of serum for a long period.

3.4.10 Sprouty, a negative regulator for MAPK pathway, was up-regulated in *ccp1*-positive MEF.

Sprouty is a protein known to be a negative regulator for MAPK signalling (Chapter 1.3.3) (213, 307). In order to determine the cause of the decrease in p-ERK in MEF expressing *ccp1* in a steady growing phase, experiments were carried out to analyse the expression of Sprouty by Western blotting using a pan-Sprouty antibody (Fig 3.4.10, A). MEF expressing *ccp1* were cultured in the absence of serum overnight and



3.4.10 *Sprouty* was up-regulated in MEF stably expressing *ccp1*.

In order to investigate the cause of the decrease of p-ERK in the MEF expressing *ccp1*, the level of the expression of *Sprouty* was analysed by Western blotting. (A) MEF expressing *ccp1* were cultured in absence of serum ON and treated with 50 ng/ml FGF2 in the presence of 10 µg/ml heparin. (B) Quantification of *Sprouty* levels by densitometry is shown in the graph. In the MEF expressing *ccp1*, the level of *Sprouty* was higher than in the control MEF. 7.5% SDS-PAGE gel was used and analysis of ERK1/2 was performed to confirm sample loading.

treated with 50 ng/ml FGF2 in the presence of 10 μ g/ml heparin for up to 24 h. In the control MEF, the level of Sprouty was low at time 0 and gradually increased upon FGF2 stimulation over the time. In contrast, in the MEF expressing *ccp1*, the level of Sprouty was 100 times higher than in the control MEF at time 0 (Fig 3.4.10, B). After 24 h, the level of Sprouty was higher than in the control MEF by 2 fold. This preliminary result indicated that *ccp1* expression increased the level of Sprouty protein. This effect was amplified further by FGF2 stimulation. Expression of *ccp1* in MEF may induce Sprouty, which in turn, in the prolonged presence of growth factors, participates in negative-feedback control of ERK signalling.

CHAPTER 4

CONCLUSIONS and DISCUSSION

4.1 Conclusions

FGFs play important and multiple roles in the brain, from patterning to terminal differentiation of cortical cells (89). As FGFs exert their effect mainly through regulating their downstream genes, identifying such genes downstream of FGF2 would enhance understanding of FGF2 function during development. Relatively small numbers of such genes are currently known. In this context, genes downstream of FGF2 were screened in CNC by microarray approach. In this study, a RIKEN clone named 'coiled coil protein 1' (ccp1) was identified and characterised.

The overall findings of this thesis are summarised as follows:

- Ccp1 was identified as a novel gene downstream of FGF2.
- Ccp1 gene consists of 5 exons and it encodes a novel protein of 180 amino acids (MW: 19 kDa).
- Mouse ccp1 has homologues in human and rat. Genes with 30-40% similarity were also found in zebrafish and drosophila.
- Ccp1 is located on mouse chromosome 1,1B and its human homolog on chromosome 2q21.2.
- Ccp1 contains a number of putative domains, including two coiled coil regions, several potential phosphorylation sites, a leucine zipper, a myristoylation site, and two NES domains.

- Ccp1 was up-regulated by 2.3 fold upon FGF2 stimulation using microarray analysis.
- Ccp1 was up-regulated by FGF2 both at transcriptional and protein level.
- Ccp1 was expressed in adult mouse brain, kidney, testis, heart and skeletal muscle at both protein and mRNA levels.
- In the cortex, ccp1 was expressed in two progenitor origins in the forebrain, one in the dorsal VZ and the other in the basal ganglia.
- Studies using *in situ* RNA hybridization has shown that ccp1 was expressed in the developing brain in a specific temporal and spatial pattern that reflected some aspects of radial and tangential migration of an early-born population of cortical cells.
- In the dorsal cortex, ccp1 was localised between reelin and Tbr1-positive layers, indicating that it may be expressed in the cortical progenitors born after CR and Tbr1-positive populations.
- In the basal ganglia, ccp1 was localised in differentiating progenitors, similar to calbindin, a marker of a population of GABAergic interneurons. In the superficial area of lateral cortex, ccp1 expression was similar to Dlx2 and GAD65/67.
- In cell culture, expressed ccp1/EGFP protein localised to the cytoplasm in a punctate pattern and to the nucleus.
- Growth curve showed that ccp1 increased cell number in MEF in the presence and absence of serum.

- Overexpression studies in MEF and SK-N-SH cells showed that ccp1 increased number of cells in S phase, effect that is enhanced in the presence of serum or FGF2.
- Knockdown of ccp1 in SK-N-SH reduced number of cells in S phase.
- Cell proliferation was not suppressed in MEF expressing ccp1 when cells were stimulated with FGF2 in the absence of MAPK signalling. Ccp1 expression in the cells rescued MEK inhibition by U0126.
- A decrease in ERK phosphorylation was observed in MEF stably expressing ccp1 when cultured in serum over time. Over a short time of stimulation with FGF2, expressed ccp1 enhanced MAPK activation in the cells. Levels of Sprouty were higher in MEF expressing ccp1 and this effect was enhanced after FGF2 stimulation. The mechanism of decreased p-ERK in MEF expressing ccp1 is currently unknown.
- Ccp1 did not influence apoptosis and migration *in vitro* in MEF.

This study provides a better understanding of ccp1 gene function *in vitro* and gives solid bases for further cell biology and functional studies.

4.2 Discussion

4.2.1 Ccp1 function in relation to its cellular localisation and domains in the amino acid sequence.

With a long-term aim to understand FGF signalling and how it influences the brain development, the function of *ccp1*, a novel gene downstream of FGF2 was investigated. The function of *ccp1* has not been reported so far. In addition, *ccp1* protein does not present any similarity to known proteins. The studies carried out on *ccp1* cellular localisation, together with the presence of specific domains within the amino acid sequence, may suggest a potential role for *ccp1* protein (Chapter 3.1 and 3.3).

4.2.1.1 Coiled coil regions in *ccp1*

Protein motif searches predicted two coiled coil regions in *ccp1* (Fig 3.1.1). Several coiled coil proteins with diverse functions are known, including skeletal proteins such as keratin and vimentin, motor proteins such as myosin, kinesins, and dyneins and proteins important for vesicular transport, such as synaptobrevin, syntaxin and SNAP-25 (197, 229, 230, 242). The main function of these proteins is to organize the cytoplasm by moving different organelles and macromolecular complexes along microtubules, microfilaments and intermediate filaments by recognizing their respective cargoes through coiled coil domains (197). *Ccp1* may be involved in

organelle movement and organization of the cytoplasm by interacting with cytoskeletal or motor proteins through its coiled coil domains. In mature neurons, signalling endosomes play an important role in retrograde transport of neurotrophic signals from nerve terminals to cell bodies (308). The evidence of retrograde axonal transport of FGF2 in the specific brain regions and in spinal autonomic neurons has been reported (309, 310), however its mechanism is so far unclear. Moreover, a specific expression of *ccp1* in the developing brain that partially reflects tangential and radial migration of early-born cortical progenitors was observed. A protein complex that consists of Lis1, DCX, NudE, and NUDEL proteins has been proposed to play an essential role in the radial migration of early-born neurons involving nuclear translocation and dynamic regulation of microtubules (311). Lis1 and doublecortin (DCX) genes are identified as genes responsible for neuronal migration defects in human genetic disorder, Lissencephally (312). NudE and NUDEL are coiled coil proteins that are shown to interact with the cytoskeletal motor protein, dynein, which also contains the coiled coil domain. Ccp1 may be associated with multiple cellular proteins and may play a role in cortical neuronal migration during brain development.

4.2.1.2 The leucine zipper domain in *ccp1*

Within the first coiled coil domain of *ccp1*, a leucine zipper motif, indicative of DNA binding, has been predicted (Fig 3.1.1) (197). Leucine zipper domains often occur together with DNA-binding domains in regulatory proteins, such as eukaryotic transcription factors (247). Ccp1 may be one of these regulatory proteins.

Ccp1/EGFP fusion protein was localised to the nucleus in some cases (Fig 3.3.9). In addition, *in vitro* experiments showed that ccp1 promoted cell proliferation (Fig 3.4.2-3.4.3). Cell proliferation may be mediated by a direct ccp1-activation of target genes implicated in DNA replication in the nucleus. Several transcription factors are important components of cell proliferation control, e.g. E2F, a transcription factor that plays an important role in progression into S phase (313).

4.2.1.3 NES in ccp1

Two domains identified at the N-terminal region of ccp1 sequence showed significant similarity to NES domains (Fig 3.1.1). The presence of NES domains is known to be fundamental for the role of the protein (284). For example, Smad1, a mediator of transforming factor β (TGF- β), is known to contain a NES and its shuttling from the nucleus to the cytoplasm is shown to be essential for its transcriptional activation (271). Another protein, whose NES is known to be essential for its function, is Tob, a member of the Tob/BTG family that is known to be an anti-proliferative protein (314). It has been recently demonstrated that its cellular localisation caused by the NES, is essential for its anti-proliferative activity (315).

The NES residue at the amino acid position 18-26 in ccp1 shows high homology with the validated NES present in MEK sequence (Fig 3.3.10) (316). MEK is mainly localised to the cytoplasm because of its NES (316). Although not co-localized, MEK cytoplasmic localisation was similar to that of ccp1 (Fig. 3.3.10). Due to its small size of 19 kDa, ccp1 may shuttle from the cytoplasm to the nucleus by passive diffusion and relocates to the cytoplasm by activation of its NES, similarly to MEK

(316). Functionality of NES in *ccp1* remains unclear. Site-directed mutagenesis of amino acids in the NES domains is one of the approaches that would determine whether *ccp1* NES domains are functional. Furthermore, the use of the fungicide Leptomycin B (LMB), a direct inhibitor of the export receptor CRM1 (Chapter 1.3), would assist the analysis.

Ccp1 localisation upon FGF2 treatment was also addressed in this study (Fig 3.3.10). After 24 h of treatment, nuclear or cytoplasmic segregation of *ccp1* was less obvious and the protein was observed to be diffused throughout the cell body. Therefore, FGF2 may regulate location of *ccp1* in the cells. However, more experiments should be performed for conclusive results.

4.2.1.4 FGF signalling and *ccp1* in vesicle compartments

This study revealed that transiently expressed *ccp1* protein was localised to endo/lysosomal compartment of the cell. Endosomal system regulates the turnover of cellular membrane components by two major pathways; one leading to degradation in lysosomes and another recycling back to the plasma membrane (197). Recently, attenuation of FGF signalling was reported by down-regulation of the FGF receptor (FGFR) protein mediated by the ubiquitin ligase, Cbl (331). Ubiquitylation has been traditionally regarded as a mechanism of protein degradation by proteasomes, however the essential role of ubiquitylation regulating endocytic transport has recently been demonstrated (332). Furthermore, it was suggested that lysosomal targeting and subsequent protein degradation of receptor tyrosine kinases (RTKs) is controlled, at least partially, by sustained ubiquitylation of RTKs and Cbl binding to

RTKs (333). Ccp1 may be involved in the FGFR protein turnover, thereby providing a mechanism of negative feedback for FGF stimulation.

4.2.1.5 Phosphorylation and myristoylation sites in ccp1

Ccp1 sequence also contained putative phosphorylation sites by protein kinase C and casein kinase II (Fig 3.1.1). These potential sites have not been investigated for actual phosphorylation. Their activation and regulation may influence ccp1-function and cellular localisation. A potential N-myristoylation site was also present, but its activity has not been investigated (Fig 3.1.1).

4.2.2 Ccp1 induces cell proliferation *in vitro*.

The data presented in this thesis have indicated that expression of *ccp1* promotes cell proliferation *in vitro* (Chapter 3.4). FGF2 modulates cell proliferation both *in vitro* and *in vivo* (150, 155, 157). Being a gene downstream of FGF2, *ccp1* may regulate cell proliferation in some of the FGF2-responsive populations. However, the mechanism by which *ccp1* regulates cell proliferation is unknown.

4.2.2.1 Reorganisation of the cellular cytoskeleton

Spindle-like cell morphology became apparent in both MEF and SK-N-SH cells stably expressing *ccp1* (Fig 3.4.1). This effect was observed in the absence of FGF2 and was enhanced upon treatment with FGF2. This may be due the higher expression of endogenous *ccp1* induced by FGF2. Interestingly, serum starvation partially reversed the shape changes induced by *ccp1* expression, indicating that *ccp1* effect in cell shape is mediated by mitogens stimulation.

Ccp1 promoted cell proliferation and the change in the cell morphology may be required for this proliferative effect. Proteins such as Discs large (Dlg), Scribble (Scrib) and Lethal giant larvae (Lgl) are known to be involved in cell polarity and cell proliferation in epithelial cells (317). The molecular mechanisms by which Dlg, Scrib and Lgl proteins regulate cell proliferation is still not known, but it is has been hypothesised that the epithelial polarisation is required for this process (317). Change in cell shape is generally mediated by dynamic reorganization of the actin cytoskeleton (318, 319). Rho family of small GTPases in signal transduction

pathways is a major determinant of cell morphology and polarity and the assembly and disassembly of filamentous actin structures provides a driving force for dynamic processes (320). Ccp1 may play a role in the reorganization of the cytoskeleton, possibly interacting with skeletal proteins through its coiled coil regions.

4.2.2.2 Regulation of the cell cycle

Growth curve in the presence and absence of serum showed that the proliferating rate of MEF expressing ccp1 was higher compared to that of the control cells (Fig 3.4.2). Furthermore, incorporation of S phase marker, BrdU, in MEF and SK-N-SH expressing ccp1 indicated that ccp1 enhances G₁-S transition (Fig 3.4.3). Finally, silencing of ccp1 expression by RNAi dramatically reduced SK-N-SH cell proliferation, providing further evidence that ccp1 acts as a mitogen (Fig 3.4.4). Mitogens generally increase cell proliferation by shortening the G₁ phase of the cell cycle (197). FGF2 was shown to promote proliferation of cortical progenitor cells via a change in cell cycle kinetics simultaneously decreasing G₁ duration and increasing the proportion of proliferative divisions (321). In another study, FGF2 did not alter cell cycle parameters, but was shown to prolong capacity of cells to continue proliferating (322). How ccp1 influences the cell cycle progression is still unclear. Ccp1 may influence the G₁-S phase transition by up-regulating the transcription of cyclins, including Cyclin A, Cyclin D1 and Cyclin E. Alternatively, ccp1 may promote the degradation of cell cycle inhibitors by up-regulating transcription of ubiquitin ligases.

4.2.2.3 Signalling involved in the proliferative effect of ccp1

From this study, it appeared that ccp1 may respond to the stimulation of several mitogens other than FGF2 and that its up-regulation may coordinately activate distinct cellular pathways that lead to cell proliferation. Two different conditions were investigated, culture (a) in the presence of serum or (b) serum-starved and consequentially treated with FGF2. Both in the absence or presence of serum, MEF expressing ccp1 showed a higher number of proliferating cells in comparison to the control, suggesting a pro-proliferative effect of ccp1 (Fig 3.4.7 and 3.4.8). Furthermore, the addition of FGF2 or serum increased this effect supporting the idea that ccp1 acts as mitogen.

Finally, the involvement of MAPK signalling in ccp1-induced proliferation was investigated using the MEK inhibitor, U0126. In the constant presence of serum, U0126 only partially blocked cell proliferation in MEF expressing ccp1. This result suggests that ccp1 rescued MEK inhibition by U0126. It is likely that signalling pathways other than MAPK may be involved in ccp1-induced proliferation when the cells are cultured in media rich in mitogens (Fig 3.4.7).

Similarly, in cells serum-starved and subsequently treated with FGF2 or serum and U0126, cell proliferation decreased in control MEF but not in MEF expressing ccp1, suggesting that once again ccp1 rescued MEK inhibition by U0126. MEK inhibition did not affect ccp1 induced cell proliferation, suggesting that ccp1 may be downstream of MAPK. It is still not excluded that ccp1 induced cell proliferation is mediated by unknown pathway (Fig. 4.1) not affected by MEK inhibition. Interestingly, the western blotting analysis of the protein lysated after the treatment

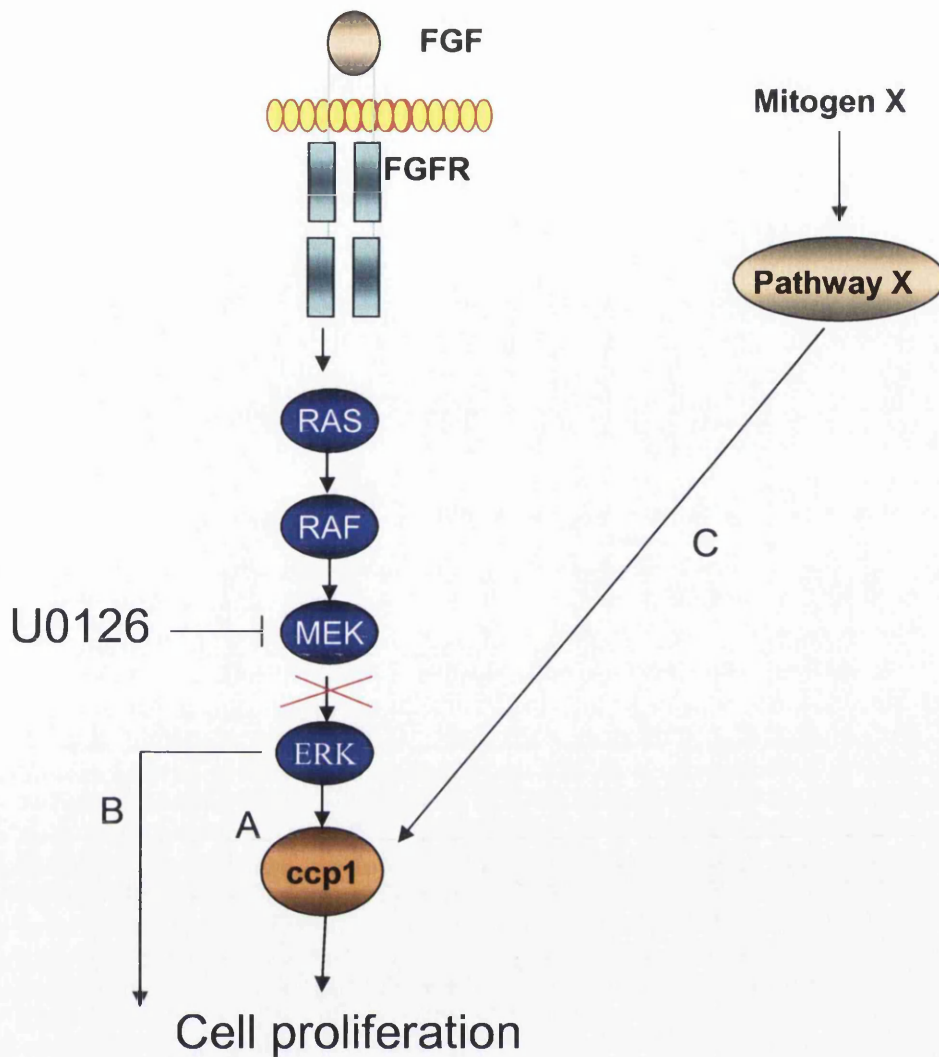


Figure 4.1 Hypothesis of mechanism of ccp1-induced cell proliferation.

Schematic diagram showing how FGF or other mitogens (named X) pathways could interact with ccp1 to form a signalling network. (A) Ccp1 may function as mediator of the signalling from the FGFRs and the MAPK, possibly associated with cellular protein complexes through its coiled coil domain. (B) MAPK is known to induce cell proliferation. (C) Nevertheless, ccp1 maybe activated through a different pathway, so far unknown, independently from MAPK.

with U0126 revealed that in the presence of mitogens, such as FGF2 and serum, phosphorylation of ERK is not inhibited, indicating that U0126 activity maybe decreased over 24 h when the strong mitogens are added to the culture.

In conclusion, binding of the extracellular FGF ligands to FGFRs leads to dimerization of the receptors and initiates the intermolecular auto-phosphorylation of tyrosines. The MAPK cascade is one of the best known for its key role in mediating the transduction of signals from FGFRs. Ccp1 may function as mediator of the signalling from the FGFRs to the MAPK, possibly associated with cellular protein complexes through its coiled coil domain. Alternatively, ccp1 may be one of the gene transcriptionally regulated by MAPK upon stimulation with FGF2. Nevertheless, ccp1 maybe activated through a different pathway, so far unknown, independently from MAPK. Other major signalling pathways downstream of FGF are PI3K and PLCgamma-PKC (179). BrdU incorporation in the presence of pathway specific inhibitors, such as wortmanin and LY294002 for PI3K, and Bisindolylmaleimide I for PKC pathways, could help to clarify ccp1 pathway.

The signalling pathway may be differently regulated depending whether (a) the cells are maintained in serum and therefore the cell cycle is continuously activated or (b) the cells are serum starved (arrest of the cell cycle) and then stimulated with mitogens (re-enter the cell cycle). How ccp1 is involved within the pathway of FGF2-MAPK signalling pathway is still unknown.

4.2.2.4 Regulation of MAPK signalling

The involvement of MAPK in *ccp1*-dependent cell proliferation was further investigated by Western blotting. Short-time stimulation with FGF2 or serum increased phosphorylation of ERK in MEF expressing *ccp1* in comparison to the control (Fig 3.4.9). This effect was not observed when the cells were treated with FGF2 over a longer period of time, probably due a maximal expression of *ccp1* both in control MEF and in MEF expressing *ccp1*.

It was shown that p-ERK was low in *ccp1*-overexpressing cells cultured in the presence of serum over the time (Fig 3.4.9). In cells maintained in media containing mitogens for a long period, *ccp1* expression may reach the maximal level and start a mechanism that lead to inhibition of phosphorylation of ERK. Sprouty is a negative regulator of MAPK signalling generally activated by growth factors such as FGFs (213, 214). Sprouty inhibits MAPK pathway exerting its function downstream of the tyrosine kinase receptor and upstream of ERK (213). It has been shown that in mouse fibroblasts, Sprouty interferes with growth factor-induced ERK activation at the level of RAS (307). Indeed, preliminary experiments showed that, upon FGF2 stimulation, cells expressing *ccp1* showed a higher level of Sprouty in comparison with the control (Fig 3.4.10). In contrast, an inhibitory effect on cell proliferation and on phosphorylation of ERK was not observed, even if the level of Sprouty was high in *ccp1*-expressing cells under these conditions (Fig 3.4.9, C). A decrease in phosphorylation of ERK was detected in cells expressing *ccp1* when cultured in serum for a long period (Fig 3.4.9, A). Level of Sprouty in this condition has to be

determined. The ability of Sprouty to regulate ERK activation is regulated by both its level of expression and phosphorylation (213). This aspect remains to be addressed.

4.2.3 Ccp1 in the brain

This study showed that *ccp1* was specifically expressed in multiple tissues including adult and embryonic brain (Fig 3.2.5). Experiments using *in situ* RNA hybridization showed that *ccp1* was expressed in the developing brain in a specific pattern that reflected some aspects of tangential and radial migration of an early-born population of cortical cells, implying specific function of *ccp1* during brain development (Chapter 3.2). Whether *ccp1* is also expressed by a different class of brain cells, such as oligodendrocytes or astrocytes, remains to be investigated.

4.2.3.1 Effect of *ccp1* in progenitor proliferation

In order to gain insight into the physiological role of *ccp1* in the brain, its expression pattern was examined. *Ccp1* was expressed by early-born neurons in the developing brain in a specific temporal and spatial pattern (Fig 3.2.1). *Ccp1* was expressed in two progenitor origins in the forebrain, one in the dorsal ventricular zone (VZ) and the other in the basal ganglia. In the dorsal cortex, *ccp1* was detected in the VZ at early embryonic day. In mice, cortical progenitors in the VZ are known to undergo 11 cell cycles between E11 and E16 during neurogenesis and the timing of cell cycle exit is closely correlated to their destination in the cortical layers (13). *Ccp1* expression was analysed using layer markers, *reelin* that labels Cajal-Retzius (CR) neurons (323) and *Tbr1*, expressed in one of the most early-born neurons (29) (Fig 3.2.4). *Ccp1* localised between *reelin* and *Tbr1*-positive layers, indicating that *ccp1* may be expressed in the cortical progenitors that are born after CR and *Tbr1*-positive

populations and migrate radially to the superficial cortex. At early stages, *ccp1* expression was also detected in the progenitor zone of the LGE. At the same stage, additional expression was also detected in the differentiating progenitors in a ventro-lateral area of the striatum, similar to calbindin, a marker of a population of GABAergic interneurons (324). In the superficial area of lateral cortex, *ccp1* expression was similar to *Dlx2* and *GAD65/67*, markers for differentiating interneurons tangentially migrating toward the dorsal cortex (43, 51). The pattern of *ccp1* expression, therefore, reflected some of the aspects of the tangential migration that occurs at the early stages of brain development (32, 325).

Lack of FGF2 caused a reduction in the total number of mature neurons and glia, suggesting a fundamental role of FGF2 in neuronal cell proliferation (155). Since *ccp1* was expressed in a subpopulation of progenitors, *ccp1* may regulate cell proliferation and neurogenesis in some of the FGF2-responsive progenitor populations.

It has been shown that there is a strong correlation between precise cell cycle regulation and determination of neuronal identity (326). Cell cycle regulator proteins such as Retinoblastoma (Rb) are known to be involved in the regulation of neuronal migration and specification of GABAergic interneurons (327). The mechanism by which Rb influences neuronal migration is not fully understood. There may be a correlation between the role of *ccp1* on the cell cycle and its high and specific expression during the brain development, as in case of Rb protein. The mechanism of *ccp1* regulation of cell proliferation and its consequence in neurogenesis are still unknown.

4.2.3.2 Function of ccp1 in post-mitotic cells

Experiments showed that some of the ccp1-positive neurons were located in a differentiated region of the cortex. The role of ccp1 in post-mitotic cells is still unknown. Ccp1 expressing cells may not migrate during the development but may be temporally and regionally switched in different regions of the cortex. Ccp1 may regulate factors that control the trajectory of tangentially migrating neurons. So far, many guidance molecules have been identified, including the Slit and the Ephrin families (328). Slit1/2 are temporally and regionally expressed and they have a repulsive role, whereas the ephrin family are permissive factors (40, 329, 330). As Slit and ephrin proteins, ccp1 may be a guidance factor for migrating neurons. In contrast, *in vitro* experiments using MEF have shown that overexpression of ccp1 did not affect cell migration and motility (Fig 3.4.10). However, ccp1 may promote cell migration in different cell types, such as neuronal cells. Furthermore, ccp1 induced cell proliferation *in vitro* and it is not excluded that this process may mask any potential activity of ccp1 in closing the wound and therefore in cell migration. Performing the same experiment using an inhibitor of cell proliferation, such as nacodazole, an inducer of G₂/M-phase block, could help to clarify whether ccp1 has a role in cell migration *in vitro*.

4.3 Future research direction

A long-term aim of this project would be to provide better understanding of potentially novel regulation of cell proliferation by *ccp1 in vitro* and during brain development. Future work would include (a) identification of *ccp1* binding partners; (b) identification of how *ccp1* regulate cell cycle phases; (c) identification of the *in vivo* function of *ccp1* using conditional knockout approach; (d) investigation of *ccp1*-function in regulating cortical progenitors proliferation using the mice generated; (e) identification of potential roles of *ccp1* in pathogenesis.

(a) Identification of *ccp1* binding partners

A way to approach *ccp1* function in the cell would be to identify its binding partners. *Ccp1* has two coiled coil regions, which is often found in the protein-protein interaction. By identifying the binding partner of *ccp1* with known function, it may be to clarify *ccp1* function. This may be achieved by using 2-hybrid screen, co-immunoprecipitation or proteomic analysis.

(b) Identification of how *ccp1* regulates cell cycle phases.

To understand how *ccp1* regulates cell proliferation, the regulation of the cell cycle progression by *ccp1 in vitro* would be addressed. BrdU incorporation assays have shown the increase of cells in the S phase in *ccp1* stable cell lines, indicating that G₁-S transition is involved. Further to this observation, fluorescence activated cell sorting

(FACS) analysis of cell lines stably expressing *ccp1* would precisely measure the cell population in each cell cycle phase. Cell cycle phase would be analysed both upon culturing cells in the presence and absence of serum. In addition, RNAi could be used to examine the effect of reduced *ccp1* protein in cell cycle progression. Mitogens increase cell proliferation by up-regulating the transcription of G1 cyclins, hence increasing the G1-cyclin dependent kinases (Cdk) activity, or that of ubiquitin ligases, promoting the degradation of cell cycle inhibitors (194). If G₁-S phase is identified as the target of *ccp1* regulation in the above study, the regulation of Cyclin A, Cyclin D1, cyclin E, and p21^{cip/waf1}, and p27^{kip1} would be further examined by Western blot. Signalling pathways involved in the increase of cell proliferation by *ccp1* would be also studied. The major signalling pathways downstream of FGF include MAPK, PI3K and PLCgamma-PKC (179). MEK inhibitor, U0126, only partially inhibited the *ccp1*-induced BrdU incorporation, indicating that *ccp1* may be associated with mechanism other than MAPK signalling pathway. BrdU incorporation in the presence of pathway specific inhibitors would be examined, such as wortmanin and LY294002 for PI3K, and Bisindolylmaleimide I for PKC pathways.

(c) Identification of the *in vivo* function of *ccp1* using conditional knockout approach

In order to characterise physiological functions of *ccp1* during development *in vivo*, it would be important to generate a mouse model in which the *ccp1* gene is deleted. As *ccp1* was expressed in multiple tissues, a conditional approach is essential to allow tissue-specific and cell-specific deletion. The *in vivo* model will allow determination of the function of *ccp1* during brain development and the function of the *ccp1*-

positive subpopulation of progenitors and neurons. This issue can be only addressed in the *in vivo* model system. *Drosophila* and zebrafish systems would not be suitable, as the homology of putative *ccp1* homologues is low.

(d) Investigation of *ccp1*-function in regulating cortical progenitors proliferation using the mice generated.

After generation of the *ccp1* null mice is available, it would be possible to analyse how *ccp1* regulate proliferation of the cortical progenitors *in vivo*. The mitotic rates of progenitor cells would be tested as well as its effect in neurogenesis by *in vivo* pulse labelling with BrdU. Furthermore, FACS and immunohistochemistry could also address the cell population in each cell cycle phase. Originally identified downstream of FGF2, *ccp1* deletion may lead to a phenotype similar to that of FGF2 knockout mice. A reduction of glutamatergic pyramidal neurons and parvalbumin-positive interneurons was observed in the dorsal cortex (103). It was also reported that some of the cortical neurons failed to target the layer II and III (103). *Ccp1* expression was observed in a subpopulation of calbindin-positive neurons. Immunohistochemistry would be performed to quantify the numbers of specific neuronal cells in the *ccp1*-null mice in comparison to control littermates in adult brains. Antibodies against Glutamate receptor 1 (GluR1) and NeuN (glutamatergic projection neuron), calbindin and parvalbumin (GABAergic interneurons) would be used.

(e) Identification of potential roles of ccp1 in pathogenesis

The last major question that should be investigated is whether ccp1 has roles in pathogenesis. Ccp1 showed to be highly expressed in the brain and in the heart. The mouse ccp1 is localised in the chromosome 1,1B and its human counterpart in the chromosome 2q21.2 (chapter 3.1). Diseases such as cerebral palsy or the coronary heart disease may be linked to genetic predisposition. A genetic form of spastic cerebral palsy maps to 2q21-q31 (OMIM%603513). Cerebral palsy is a common paediatric disorder with 1 in 250-1000 births. It affects the posture and movement caused by the abnormalities in the brain. Another genetic disease that maps in a close location to ccp1 is the coronary heart disease (CHD), located to 2q21-q22 (OMIM%608316). Coronary heart disease (CHD) is one of the most common leading causes of death in the western world. CHD is caused by several factors, including genetic and environmental. Since ccp1 chromosome location is close to spastic cerebral palsy and of the CHD and since ccp1 is expressed both in brain and heart, it maybe related to the mutation that lead to these genetic diseases. Genome linkage mapping using DNA from patients and sequencing of ccp1 would be performed to identify possible mutation that may be responsible for the occurrence of spastic cerebral palsy or CHD. In case of identification of mutations in ccp1 DNA-sequence, site directed mutagenesis would be carried out on ccp1 sequence to generate a mouse model. This approach would allow significant advances in understanding the progression and severity of the diseases. In addition, a mouse model would be an important tool for functional analysis of the brain or heart in culture, as human tissue samples are difficult to obtain.

REFERENCES

1. Bear FC, B., Paradiso M. Neuroscience, exploring the brain. 2nd ed; 2001.
2. Deacon TW, Pakzaban P, Isacson O. The lateral ganglionic eminence is the origin of cells committed to striatal phenotypes: neural transplantation and developmental evidence. *Brain Res* 1994;668(1-2):211-9.
3. Rakic P. Extrinsic cytological determinants of basket and stellate cell dendritic pattern in the cerebellar molecular layer. *J Comp Neurol* 1972;146(3):335-54.
4. Verney C, Takahashi T, Bhide PG, Nowakowski RS, Caviness VS, Jr. Independent controls for neocortical neuron production and histogenetic cell death. *Dev Neurosci* 2000;22(1-2):125-38.
5. Marin O, Rubenstein JL. Cell migration in the forebrain. *Annu Rev Neurosci* 2003;26:441-83.
6. Hatanaka Y, Murakami F. In vitro analysis of the origin, migratory behavior, and maturation of cortical pyramidal cells. *J Comp Neurol* 2002;454(1):1-14.
7. Gorski JA, Talley T, Qiu M, Puelles L, Rubenstein JL, Jones KR. Cortical excitatory neurons and glia, but not GABAergic neurons, are produced in the Emx1-expressing lineage. *J Neurosci* 2002;22(15):6309-14.

8. Anderson SA, Eisenstat DD, Shi L, Rubenstein JL. Interneuron migration from basal forebrain to neocortex: dependence on *Dlx* genes. *Science* 1997;278(5337):474-6.
9. de Carlos JA, Lopez-Mascaraque L, Valverde F. Dynamics of cell migration from the lateral ganglionic eminence in the rat. *J Neurosci* 1996;16(19):6146-56.
10. Lavdas AA, Grigoriou M, Pachnis V, Parnavelas JG. The medial ganglionic eminence gives rise to a population of early neurons in the developing cerebral cortex. *J Neurosci* 1999;19(18):7881-8.
11. Takahashi T, Goto T, Miyama S, Nowakowski RS, Caviness VS, Jr. Sequence of neuron origin and neocortical laminar fate: relation to cell cycle of origin in the developing murine cerebral wall. *J Neurosci* 1999;19(23):10357-71.
12. Gupta A, Tsai LH, Wynshaw-Boris A. Life is a journey: a genetic look at neocortical development. *Nat Rev Genet* 2002;3(5):342-55.
13. Takahashi T, Nowakowski RS, Caviness VS, Jr. The cell cycle of the pseudostratified ventricular epithelium of the embryonic murine cerebral wall. *J Neurosci* 1995;15(9):6046-57.
14. Angevine JB, Jr. Time of neuron origin in the diencephalon of the mouse. An autoradiographic study. *J Comp Neurol* 1970;139(2):129-87.
15. McConnell SK. Constructing the cerebral cortex: neurogenesis and fate determination. *Neuron* 1995;15(4):761-8.
16. Nadarajah B, Parnavelas JG. Modes of neuronal migration in the developing cerebral cortex. *Nat Rev Neurosci* 2002;3(6):423-32.

17. Berry M, Rogers AW. The migration of neuroblasts in the developing cerebral cortex. *J Anat* 1965;99(4):691-709.
18. Rakic P. Neuron-glia relationship during granule cell migration in developing cerebellar cortex. A Golgi and electronmicroscopic study in *Macacus Rhesus*. *J Comp Neurol* 1971;141(3):283-312.
19. Miyata T, Kawaguchi A, Okano H, Ogawa M. Asymmetric inheritance of radial glial fibers by cortical neurons. *Neuron* 2001;31(5):727-41.
20. Levitt P, Cooper ML, Rakic P. Coexistence of neuronal and glial precursor cells in the cerebral ventricular zone of the fetal monkey: an ultrastructural immunoperoxidase analysis. *J Neurosci* 1981;1(1):27-39.
21. Shoukimas GM, Hinds JW. The development of the cerebral cortex in the embryonic mouse: an electron microscopic serial section analysis. *J Comp Neurol* 1978;179(4):795-830.
22. Nadarajah B, Brunstrom JE, Grutzendler J, Wong RO, Pearlman AL. Two modes of radial migration in early development of the cerebral cortex. *Nat Neurosci* 2001;4(2):143-50.
23. Meyer G, Goffinet AM, Fairen A. What is a Cajal-Retzius cell? A reassessment of a classical cell type based on recent observations in the developing neocortex. *Cereb Cortex* 1999;9(8):765-75.
24. D'Arcangelo G, Miao GG, Chen SC, Soares HD, Morgan JI, Curran T. A protein related to extracellular matrix proteins deleted in the mouse mutant *reeler*. *Nature* 1995;374(6524):719-23.

25. Trommsdorff M, Borg JP, Margolis B, Herz J. Interaction of cytosolic adaptor proteins with neuronal apolipoprotein E receptors and the amyloid precursor protein. *J Biol Chem* 1998;273(50):33556-60.
26. Howell BW, Lanier LM, Frank R, Gertler FB, Cooper JA. The disabled 1 phosphotyrosine-binding domain binds to the internalization signals of transmembrane glycoproteins and to phospholipids. *Mol Cell Biol* 1999;19(7):5179-88.
27. Barkovich AJ, Koch TK, Carrol CL. The spectrum of lissencephaly: report of ten patients analyzed by magnetic resonance imaging. *Ann Neurol* 1991;30(2):139-46.
28. Hong SE, Shugart YY, Huang DT, Shahwan SA, Grant PE, Hourihane JO, et al. Autosomal recessive lissencephaly with cerebellar hypoplasia is associated with human RELN mutations. *Nat Genet* 2000;26(1):93-6.
29. Bulfone A, Smiga SM, Shimamura K, Peterson A, Puelles L, Rubenstein JL. T-brain-1: a homolog of Brachyury whose expression defines molecularly distinct domains within the cerebral cortex. *Neuron* 1995;15(1):63-78.
30. Bulfone A, Wang F, Hevner R, Anderson S, Cutforth T, Chen S, et al. An olfactory sensory map develops in the absence of normal projection neurons or GABAergic interneurons. *Neuron* 1998;21(6):1273-82.
31. Hevner RF, Shi L, Justice N, Hsueh Y, Sheng M, Smiga S, et al. Tbr1 regulates differentiation of the preplate and layer 6. *Neuron* 2001;29(2):353-66.

32. Corbin JG, Nery S, Fishell G. Telencephalic cells take a tangent: non-radial migration in the mammalian forebrain. *Nat Neurosci* 2001;4 Suppl:1177-82.
33. Rakic P. Local circuit neurons. *Neurosci Res Program Bull* 1975;13(3):295-416.
34. Anderson SA, Marin O, Horn C, Jennings K, Rubenstein JL. Distinct cortical migrations from the medial and lateral ganglionic eminences. *Development* 2001;128(3):353-63.
35. Tanaka D, Nakaya Y, Yanagawa Y, Obata K, Murakami F. Multimodal tangential migration of neocortical GABAergic neurons independent of GPI-anchored proteins. *Development* 2003;130(23):5803-13.
36. Wichterle H, Garcia-Verdugo JM, Herrera DG, Alvarez-Buylla A. Young neurons from medial ganglionic eminence disperse in adult and embryonic brain. *Nat Neurosci* 1999;2(5):461-6.
37. Fairen A, Cobas A, Fonseca M. Times of generation of glutamic acid decarboxylase immunoreactive neurons in mouse somatosensory cortex. *J Comp Neurol* 1986;251(1):67-83.
38. Peduzzi JD. Genesis of GABA-immunoreactive neurons in the ferret visual cortex. *J Neurosci* 1988;8(3):920-31.
39. Nadarajah B, Alifragis P, Wong RO, Parnavelas JG. Ventricle-directed migration in the developing cerebral cortex. *Nat Neurosci* 2002;5(3):218-24.
40. Zhu Y, Li H, Zhou L, Wu JY, Rao Y. Cellular and molecular guidance of GABAergic neuronal migration from an extracortical origin to the neocortex. *Neuron* 1999;23(3):473-85.

41. Hamasaki T, Goto S, Nishikawa S, Ushio Y. A role of netrin-1 in the formation of the subcortical structure striatum: repulsive action on the migration of late-born striatal neurons. *J Neurosci* 2001;21(12):4272-80.
42. Marin O, Yaron A, Bagri A, Tessier-Lavigne M, Rubenstein JL. Sorting of striatal and cortical interneurons regulated by semaphorin-neuropilin interactions. *Science* 2001;293(5531):872-5.
43. Bulfone A, Puelles L, Porteus MH, Frohman MA, Martin GR, Rubenstein JL. Spatially restricted expression of Dlx-1, Dlx-2 (Tes-1), Gbx-2, and Wnt-3 in the embryonic day 12.5 mouse forebrain defines potential transverse and longitudinal segmental boundaries. *J Neurosci* 1993;13(7):3155-72.
44. Qiu M, Bulfone A, Martinez S, Meneses JJ, Shimamura K, Pedersen RA, et al. Null mutation of Dlx-2 results in abnormal morphogenesis of proximal first and second branchial arch derivatives and abnormal differentiation in the forebrain. *Genes Dev* 1995;9(20):2523-38.
45. Pleasure SJ, Anderson S, Hevner R, Bagri A, Marin O, Lowenstein DH, et al. Cell migration from the ganglionic eminences is required for the development of hippocampal GABAergic interneurons. *Neuron* 2000;28(3):727-40.
46. Kallfelz FA, Taylor AN, Wasserman RH. Vitamin D-induced calcium binding factor in rat intestinal mucosa. *Proc Soc Exp Biol Med* 1967;125(1):54-8.
47. Chard PS, Bleakman D, Christakos S, Fullmer CS, Miller RJ. Calcium buffering properties of calbindin D28k and parvalbumin in rat sensory neurones. *J Physiol* 1993;472:341-57.

48. Fonseca M, del Rio JA, Martinez A, Gomez S, Soriano E. Development of calretinin immunoreactivity in the neocortex of the rat. *J Comp Neurol* 1995;361(1):177-92.
49. Pozas E, Ibanez CF. GDNF and GFRalpha1 promote differentiation and tangential migration of cortical GABAergic neurons. *Neuron* 2005;45(5):701-13.
50. Erlander MG, Tillakaratne NJ, Feldblum S, Patel N, Tobin AJ. Two genes encode distinct glutamate decarboxylases. *Neuron* 1991;7(1):91-100.
51. Feldblum S, Erlander MG, Tobin AJ. Different distributions of GAD65 and GAD67 mRNAs suggest that the two glutamate decarboxylases play distinctive functional roles. *J Neurosci Res* 1993;34(6):689-706.
52. Katarova Z, Sekerkova G, Prodan S, Mugnaini E, Szabo G. Domain-restricted expression of two glutamic acid decarboxylase genes in midgestation mouse embryos. *J Comp Neurol* 2000;424(4):607-27.
53. Makinae K, Kobayashi T, Shinkawa H, Sakagami H, Kondo H, Tashiro F, et al. Structure of the mouse glutamate decarboxylase 65 gene and its promoter: preferential expression of its promoter in the GABAergic neurons of transgenic mice. *J Neurochem* 2000;75(4):1429-37.
54. Izzo E, Auta J, Impagnatiello F, Pesold C, Guidotti A, Costa E. Glutamic acid decarboxylase and glutamate receptor changes during tolerance and dependence to benzodiazepines. *Proc Natl Acad Sci U S A* 2001;98(6):3483-8.

55. Guidotti A, Auta J, Davis JM, Di-Giorgi-Gerevini V, Dwivedi Y, Grayson DR, et al. Decrease in reelin and glutamic acid decarboxylase67 (GAD67) expression in schizophrenia and bipolar disorder: a postmortem brain study. *Arch Gen Psychiatry* 2000;57(11):1061-9.
56. Barbin G, Pollard H, Gaiarsa JL, Ben-Ari Y. Involvement of GABAA receptors in the outgrowth of cultured hippocampal neurons. *Neurosci Lett* 1993;152(1-2):150-4.
57. Behar TN, Schaffner AE, Colton CA, Somogyi R, Olah Z, Lehel C, et al. GABA-induced chemokinesis and NGF-induced chemotaxis of embryonic spinal cord neurons. *J Neurosci* 1994;14(1):29-38.
58. LoTurco JJ, Owens DF, Heath MJ, Davis MB, Kriegstein AR. GABA and glutamate depolarize cortical progenitor cells and inhibit DNA synthesis. *Neuron* 1995;15(6):1287-98.
59. Asada H, Kawamura Y, Maruyama K, Kume H, Ding R, Ji FY, et al. Mice lacking the 65 kDa isoform of glutamic acid decarboxylase (GAD65) maintain normal levels of GAD67 and GABA in their brains but are susceptible to seizures. *Biochem Biophys Res Commun* 1996;229(3):891-5.
60. Ji F, Kanbara N, Obata K. GABA and histogenesis in fetal and neonatal mouse brain lacking both the isoforms of glutamic acid decarboxylase. *Neurosci Res* 1999;33(3):187-94.
61. Volterra A, Meldolesi J. Astrocytes, from brain glue to communication elements: the revolution continues. *Nat Rev Neurosci* 2005;6(8):626-40.

62. Sherman DL, Brophy PJ. Mechanisms of axon ensheathment and myelin growth. *Nat Rev Neurosci* 2005;6(9):683-90.
63. Bertrand N, Castro DS, Guillemot F. Proneural genes and the specification of neural cell types. *Nat Rev Neurosci* 2002;3(7):517-30.
64. Lee JC, Mayer-Proschel M, Rao MS. Gliogenesis in the central nervous system. *Glia* 2000;30(2):105-21.
65. Gotz M, Stoykova A, Gruss P. Pax6 controls radial glia differentiation in the cerebral cortex. *Neuron* 1998;21(5):1031-44.
66. Tekki-Kessaris N, Woodruff R, Hall AC, Gaffield W, Kimura S, Stiles CD, et al. Hedgehog-dependent oligodendrocyte lineage specification in the telencephalon. *Development* 2001;128(13):2545-54.
67. Nery S, Wichterle H, Fishell G. Sonic hedgehog contributes to oligodendrocyte specification in the mammalian forebrain. *Development* 2001;128(4):527-40.
68. Lu QR, Cai L, Rowitch D, Cepko CL, Stiles CD. Ectopic expression of Olig1 promotes oligodendrocyte formation and reduces neuronal survival in developing mouse cortex. *Nat Neurosci* 2001;4(10):973-4.
69. Bayer SA, Altman J, Russo RJ, Dai XF, Simmons JA. Cell migration in the rat embryonic neocortex. *J Comp Neurol* 1991;307(3):499-516.
70. Malatesta P, Hartfuss E, Gotz M. Isolation of radial glial cells by fluorescent-activated cell sorting reveals a neuronal lineage. *Development* 2000;127(24):5253-63.

71. Noctor SC, Flint AC, Weissman TA, Dammerman RS, Kriegstein AR.
Neurons derived from radial glial cells establish radial units in neocortex.
Nature 2001;409(6821):714-20.
72. Nakamura Y, Sakakibara S, Miyata T, Ogawa M, Shimazaki T, Weiss S, et al.
The bHLH gene *hes1* as a repressor of the neuronal commitment of CNS stem
cells. J Neurosci 2000;20(1):283-93.
73. Heins N, Cremisi F, Malatesta P, Gangemi RM, Corte G, Price J, et al. *Emx2*
promotes symmetric cell divisions and a multipotential fate in precursors from
the cerebral cortex. Mol Cell Neurosci 2001;18(5):485-502.
74. Szebenyi G, Fallon JF. Fibroblast growth factors as multifunctional signaling
factors. Int Rev Cytol 1999;185:45-106.
75. Basilico C, Moscatelli D. The FGF family of growth factors and oncogenes.
Adv Cancer Res 1992;59:115-65.
76. Burgess WH, Maciag T. The heparin-binding (fibroblast) growth factor
family of proteins. Annu Rev Biochem 1989;58:575-606.
77. Beiman M, Shilo BZ, Volk T. Heartless, a Drosophila FGF receptor homolog,
is essential for cell migration and establishment of several mesodermal
lineages. Genes Dev 1996;10(23):2993-3002.
78. DeVore DL, Horvitz HR, Stern MJ. An FGF receptor signaling pathway is
required for the normal cell migrations of the sex myoblasts in *C. elegans*
hermaphrodites. Cell 1995;83(4):611-20.
79. Gisselbrecht S, Skeath JB, Doe CQ, Michelson AM. *heartless* encodes a
fibroblast growth factor receptor (DFR1/DFGF-R2) involved in the

directional migration of early mesodermal cells in the *Drosophila* embryo.
Genes Dev 1996;10(23):3003-17.

80. McCoon PE, Angerer RC, Angerer LM. SpFGFR, a new member of the fibroblast growth factor receptor family, is developmentally regulated during early sea urchin development. *J Biol Chem* 1996;271(33):20119-25.
81. Reichman-Fried M, Shilo BZ. Breathless, a *Drosophila* FGF receptor homolog, is required for the onset of tracheal cell migration and tracheole formation. *Mech Dev* 1995;52(2-3):265-73.
82. Johnson DE, Williams LT. Structural and functional diversity in the FGF receptor multigene family. *Adv Cancer Res* 1993;60:1-41.
83. Ornitz DM, Xu J, Colvin JS, McEwen DG, MacArthur CA, Coulier F, et al. Receptor specificity of the fibroblast growth factor family. *J Biol Chem* 1996;271(25):15292-7.
84. Kern SE, Kinzler KW, Bruskin A, Jarosz D, Friedman P, Prives C, et al. Identification of p53 as a sequence-specific DNA-binding protein. *Science* 1991;252(5013):1708-11.
85. Ornitz DM, Yayon A, Flanagan JG, Svahn CM, Levi E, Leder P. Heparin is required for cell-free binding of basic fibroblast growth factor to a soluble receptor and for mitogenesis in whole cells. *Mol Cell Biol* 1992;12(1):240-7.
86. Schlessinger J. Cell signaling by receptor tyrosine kinases. *Cell* 2000;103(2):211-25.

87. Bellot F, Crumley G, Kaplow JM, Schlessinger J, Jaye M, Dionne CA. Ligand-induced transphosphorylation between different FGF receptors. *Embo J* 1991;10(10):2849-54.
88. Thisse B, Thisse C. Functions and regulations of fibroblast growth factor signaling during embryonic development. *Dev Biol* 2005;287(2):390-402.
89. Ford-Perriss M, Abud H, Murphy M. Fibroblast growth factors in the developing central nervous system. *Clin Exp Pharmacol Physiol* 2001;28(7):493-503.
90. Ali J, Mansukhani A, Basilico C. Fibroblast growth factor receptors 1 and 2 are differentially regulated in murine embryonal carcinoma cells and in response to fibroblast growth factor-4. *J Cell Physiol* 1995;165(2):438-48.
91. Robbie EP, Peterson M, Amaya E, Musci TJ. Temporal regulation of the *Xenopus* FGF receptor in development: a translation inhibitory element in the 3' untranslated region. *Development* 1995;121(6):1775-85.
92. Kostrzewa M, Muller U. Genomic structure and complete sequence of the human FGFR4 gene. *Mamm Genome* 1998;9(2):131-5.
93. Peters KG, Werner S, Chen G, Williams LT. Two FGF receptor genes are differentially expressed in epithelial and mesenchymal tissues during limb formation and organogenesis in the mouse. *Development* 1992;114(1):233-43.
94. Partanen J, Makela TP, Eerola E, Korhonen J, Hirvonen H, Claesson-Welsh L, et al. FGFR-4, a novel acidic fibroblast growth factor receptor with a distinct expression pattern. *Embo J* 1991;10(6):1347-54.

95. Stark KL, McMahon JA, McMahon AP. FGFR-4, a new member of the fibroblast growth factor receptor family, expressed in the definitive endoderm and skeletal muscle lineages of the mouse. *Development* 1991;113(2):641-51.
96. Yu C, Wang F, Jin C, Wu X, Chan WK, McKeenan WL. Increased Carbon Tetrachloride-Induced Liver Injury and Fibrosis in FGFR4-Deficient Mice. *Am J Pathol* 2002;161(6):2003-10.
97. Orr-Urtreger A, Bedford MT, Burakova T, Arman E, Zimmer Y, Yayon A, et al. Developmental localization of the splicing alternatives of fibroblast growth factor receptor-2 (FGFR2). *Dev Biol* 1993;158(2):475-86.
98. Bansal R, Lakhina V, Remedios R, Tole S. Expression of FGF receptors 1, 2, 3 in the embryonic and postnatal mouse brain compared with Pdgfralpha, Olig2 and Plp/dm20: implications for oligodendrocyte development. *Dev Neurosci* 2003;25(2-4):83-95.
99. Marcelle C, Eichmann A, Halevy O, Breant C, Le Douarin NM. Distinct developmental expression of a new avian fibroblast growth factor receptor. *Development* 1994;120(3):683-94.
100. Ozawa K, Uruno T, Miyakawa K, Seo M, Imamura T. Expression of the fibroblast growth factor family and their receptor family genes during mouse brain development. *Brain Res Mol Brain Res* 1996;41(1-2):279-88.
101. Reid S, Ferretti P. Differential expression of fibroblast growth factor receptors in the developing murine choroid plexus. *Brain Res Dev Brain Res* 2003;141(1-2):15-24.

102. Imamura T, Engleka K, Zhan X, Tokita Y, Forough R, Roeder D, et al. Recovery of mitogenic activity of a growth factor mutant with a nuclear translocation sequence. *Science* 1990;249(4976):1567-70.
103. Ding Q, Gladson CL, Guidry CR, Santoro SA, Dickeson SK, Shin JT, et al. Extracellular FGF-1 inhibits cytoskeletal organization and promotes fibroblast motility. *Growth Factors* 2000;18(2):93-107.
104. Folkman J, Klagsbrun M, Sasse J, Wadzinski M, Ingber D, Vlodavsky I. A heparin-binding angiogenic protein--basic fibroblast growth factor-- is stored within basement membrane. *Am J Pathol* 1988;130(2):393-400.
105. Murphy M, Drago J, Bartlett PF. Fibroblast growth factor stimulates the proliferation and differentiation of neural precursor cells in vitro. *J Neurosci Res* 1990;25(4):463-75.
106. Dono R, Texido G, Dussel R, Ehmke H, Zeller R. Impaired cerebral cortex development and blood pressure regulation in FGF-2-deficient mice. *Embo J* 1998;17(15):4213-25.
107. Hossain WA, Morest DK. Fibroblast growth factors (FGF-1, FGF-2) promote migration and neurite growth of mouse cochlear ganglion cells in vitro: immunohistochemistry and antibody perturbation. *J Neurosci Res* 2000;62(1):40-55.
108. Korada S, Zheng W, Basilico C, Schwartz ML, Vaccarino FM. Fibroblast growth factor 2 is necessary for the growth of glutamate projection neurons in the anterior neocortex. *J Neurosci* 2002;22(3):863-75.

109. Doetschman T, Shull M, Kier A, Coffin JD. Embryonic stem cell model systems for vascular morphogenesis and cardiac disorders. *Hypertension* 1993;22(4):618-29.
110. Dell'Era P, Belleri M, Stabile H, Massardi ML, Ribatti D, Presta M. Paracrine and autocrine effects of fibroblast growth factor-4 in endothelial cells. *Oncogene* 2001;20(21):2655-63.
111. Moon AM, Boulet AM, Capecchi MR. Normal limb development in conditional mutants of FGF4. *Development* 2000;127(5):989-96.
112. Feldman B, Poueymirou W, Papaioannou VE, DeChiara TM, Goldfarb M. Requirement of FGF-4 for postimplantation mouse development. *Science* 1995;267(5195):246-9.
113. Hebert JM, Rosenquist T, Gotz J, Martin GR. FGF5 as a regulator of the hair growth cycle: evidence from targeted and spontaneous mutations. *Cell* 1994;78(6):1017-25.
114. Floss T, Arnold HH, Braun T. A role for FGF-6 in skeletal muscle regeneration. *Genes Dev* 1997;11(16):2040-51.
115. Andreadis ST, Hamoen KE, Yarmush ML, Morgan JR. Keratinocyte growth factor induces hyperproliferation and delays differentiation in a skin equivalent model system. *Faseb J* 2001;15(6):898-906.
116. Guo L, Degenstein L, Fuchs E. Keratinocyte growth factor is required for hair development but not for wound healing. *Genes Dev* 1996;10(2):165-75.

117. Rubin JS, Osada H, Finch PW, Taylor WG, Rudikoff S, Aaronson SA. Purification and characterization of a newly identified growth factor specific for epithelial cells. *Proc Natl Acad Sci U S A* 1989;86(3):802-6.
118. Crossley PH, Martinez S, Martin GR. Midbrain development induced by FGF8 in the chick embryo. *Nature* 1996;380(6569):66-8.
119. Fukuchi-Shimogori T, Grove EA. Neocortex patterning by the secreted signaling molecule FGF8. *Science* 2001;294(5544):1071-4.
120. Grieshammer U, Cebrian C, Ilagan R, Meyers E, Herzlinger D, Martin GR. FGF8 is required for cell survival at distinct stages of nephrogenesis and for regulation of gene expression in nascent nephrons. *Development* 2005;132(17):3847-57.
121. Miyamoto M, Naruo K, Seko C, Matsumoto S, Kondo T, Kurokawa T. Molecular cloning of a novel cytokine cDNA encoding the ninth member of the fibroblast growth factor family, which has a unique secretion property. *Mol Cell Biol* 1993;13(7):4251-9.
122. Garces A, Nishimune H, Philippe JM, Pettmann B, deLapeyriere O. FGF9: a motoneuron survival factor expressed by medial thoracic and sacral motoneurons. *J Neurosci Res* 2000;60(1):1-9.
123. Kanda T, Iwasaki T, Nakamura S, Kurokawa T, Ikeda K, Mizusawa H. Self-secretion of fibroblast growth factor-9 supports basal forebrain cholinergic neurons in an autocrine/paracrine manner. *Brain Res* 2000;876(1-2):22-30.

124. Mansour SL, Goddard JM, Capecchi MR. Mice homozygous for a targeted disruption of the proto-oncogene int-2 have developmental defects in the tail and inner ear. *Development* 1993;117(1):13-28.
125. Sekine K, Ohuchi H, Fujiwara M, Yamasaki M, Yoshizawa T, Sato T, et al. FGF10 is essential for limb and lung formation. *Nat Genet* 1999;21(1):138-41.
126. Maruoka Y, Ohbayashi N, Hoshikawa M, Itoh N, Hogan BL, Furuta Y. Comparison of the expression of three highly related genes, FGF8, FGF17 and FGF18, in the mouse embryo. *Mech Dev* 1998;74(1-2):175-7.
127. Xu J, Liu Z, Ornitz DM. Temporal and spatial gradients of FGF8 and FGF17 regulate proliferation and differentiation of midline cerebellar structures. *Development* 2000;127(9):1833-43.
128. Deng CX, Wynshaw-Boris A, Shen MM, Daugherty C, Ornitz DM, Leder P. Murine FGFR-1 is required for early postimplantation growth and axial organization. *Genes Dev* 1994;8(24):3045-57.
129. Itoh N, Mima T, Mikawa T. Loss of fibroblast growth factor receptors is necessary for terminal differentiation of embryonic limb muscle. *Development* 1996;122(1):291-300.
130. Xu X, Weinstein M, Li C, Naski M, Cohen RI, Ornitz DM, et al. Fibroblast growth factor receptor 2 (FGFR2)-mediated reciprocal regulation loop between FGF8 and FGF10 is essential for limb induction. *Development* 1998;125(4):753-65.

131. Marie PJ, Debais F, Hay E. Regulation of human cranial osteoblast phenotype by FGF-2, FGFR-2 and BMP-2 signaling. *Histol Histopathol* 2002;17(3):877-85.
132. Arman E, Haffner-Krausz R, Chen Y, Heath JK, Lonai P. Targeted disruption of fibroblast growth factor (FGF) receptor 2 suggests a role for FGF signaling in pregastrulation mammalian development. *Proc Natl Acad Sci U S A* 1998;95(9):5082-7.
133. Colvin JS, Bohne BA, Harding GW, McEwen DG, Ornitz DM. Skeletal overgrowth and deafness in mice lacking fibroblast growth factor receptor 3. *Nat Genet* 1996;12(4):390-7.
134. Naski MC, Ornitz DM. FGF signaling in skeletal development. *Front Biosci* 1998;3:D781-94.
135. Inglis-Broadgate SL, Thomson RE, Pellicano F, Tartaglia MA, Pontikis CC, Cooper JD, et al. FGFR3 regulates brain size by controlling progenitor cell proliferation and apoptosis during embryonic development. *Dev Biol* 2005;279(1):73-85.
136. Niswander L, Jeffrey S, Martin GR, Tickle C. A positive feedback loop coordinates growth and patterning in the vertebrate limb. *Nature* 1994;371(6498):609-12.
137. Pringle NP, Yu WP, Howell M, Colvin JS, Ornitz DM, Richardson WD. FGFR3 expression by astrocytes and their precursors: evidence that astrocytes and oligodendrocytes originate in distinct neuroepithelial domains. *Development* 2003;130(1):93-102.

138. Marics I, Padilla F, Guillemot JF, Scaal M, Marcelle C. FGFR4 signaling is a necessary step in limb muscle differentiation. *Development* 2002;129(19):4559-69.
139. Miller DL, Ortega S, Bashayan O, Basch R, Basilico C. Compensation by fibroblast growth factor 1 (FGF1) does not account for the mild phenotypic defects observed in FGF2 null mice. *Mol Cell Biol* 2000;20(6):2260-8.
140. Ortega S, Ittmann M, Tsang SH, Ehrlich M, Basilico C. Neuronal defects and delayed wound healing in mice lacking fibroblast growth factor 2. *Proc Natl Acad Sci U S A* 1998;95(10):5672-7.
141. Fiore F, Sebille A, Birnbaum D. Skeletal muscle regeneration is not impaired in FGF6 $-/-$ mutant mice. *Biochem Biophys Res Commun* 2000;272(1):138-43.
142. Sun X, Meyers EN, Lewandoski M, Martin GR. Targeted disruption of FGF8 causes failure of cell migration in the gastrulating mouse embryo. *Genes Dev* 1999;13(14):1834-46.
143. Shanmugalingam S, Houart C, Picker A, Reifers F, Macdonald R, Barth A, et al. *Ace*/FGF8 is required for forebrain commissure formation and patterning of the telencephalon. *Development* 2000;127(12):2549-61.
144. Colvin JS, White AC, Pratt SJ, Ornitz DM. Lung hypoplasia and neonatal death in FGF9-null mice identify this gene as an essential regulator of lung mesenchyme. *Development* 2001;128(11):2095-106.

145. Yamaguchi TP, Harpal K, Henkemeyer M, Rossant J. FGFR-1 is required for embryonic growth and mesodermal patterning during mouse gastrulation. *Genes Dev* 1994;8(24):3032-44.
146. Deng C, Wynshaw-Boris A, Zhou F, Kuo A, Leder P. Fibroblast growth factor receptor 3 is a negative regulator of bone growth. *Cell* 1996;84(6):911-21.
147. Weinstein M, Xu X, Ohyama K, Deng CX. FGFR-3 and FGFR-4 function cooperatively to direct alveogenesis in the murine lung. *Development* 1998;125(18):3615-23.
148. Dono R, Zeller R. Cell-type-specific nuclear translocation of fibroblast growth factor-2 isoforms during chicken kidney and limb morphogenesis. *Dev Biol* 1994;163(2):316-30.
149. Riese J, Zeller R, Dono R. Nucleo-cytoplasmic translocation and secretion of fibroblast growth factor-2 during avian gastrulation. *Mech Dev* 1995;49(1-2):13-22.
150. Temple S. The development of neural stem cells. *Nature* 2001;414(6859):112-7.
151. Petroski RE, Grierson JP, Choi-Kwon S, Geller HM. Basic fibroblast growth factor regulates the ability of astrocytes to support hypothalamic neuronal survival in vitro. *Dev Biol* 1991;147(1):1-13.
152. Ghosh A, Greenberg ME. Distinct roles for bFGF and NT-3 in the regulation of cortical neurogenesis. *Neuron* 1995;15(1):89-103.

153. Qian X, Davis AA, Goderie SK, Temple S. FGF2 concentration regulates the generation of neurons and glia from multipotent cortical stem cells. *Neuron* 1997;18(1):81-93.
154. d'Avis PY, Robertson SC, Meyer AN, Bardwell WM, Webster MK, Donoghue DJ. Constitutive activation of fibroblast growth factor receptor 3 by mutations responsible for the lethal skeletal dysplasia thanatophoric dysplasia type I. *Cell Growth Differ* 1998;9(1):71-8.
155. Vaccarino FM, Schwartz ML, Raballo R, Nilsen J, Rhee J, Zhou M, et al. Changes in cerebral cortex size are governed by fibroblast growth factor during embryogenesis. *Nat Neurosci* 1999;2(3):246-53.
156. Armstrong RJ, Watts C, Svendsen CN, Dunnett SB, Rosser AE. Survival, neuronal differentiation, and fiber outgrowth of propagated human neural precursor grafts in an animal model of Huntington's disease. *Cell Transplant* 2000;9(1):55-64.
157. Raballo R, Rhee J, Lyn-Cook R, Leckman JF, Schwartz ML, Vaccarino FM. Basic fibroblast growth factor (FGF2) is necessary for cell proliferation and neurogenesis in the developing cerebral cortex. *J Neurosci* 2000;20(13):5012-23.
158. Osterhout DJ, Ebner S, Xu J, Ornitz DM, Zazanis GA, McKinnon RD. Transplanted oligodendrocyte progenitor cells expressing a dominant-negative FGF receptor transgene fail to migrate in vivo. *J Neurosci* 1997;17(23):9122-32.

159. Peters K, Ornitz D, Werner S, Williams L. Unique expression pattern of the FGF receptor 3 gene during mouse organogenesis. *Dev Biol* 1993;155(2):423-30.
160. Yazaki N, Hosoi Y, Kawabata K, Miyake A, Minami M, Satoh M, et al. Differential expression patterns of mRNAs for members of the fibroblast growth factor receptor family, FGFR-1-FGFR-4, in rat brain. *J Neurosci Res* 1994;37(4):445-52.
161. Deng C, Bedford M, Li C, Xu X, Yang X, Dunmore J, et al. Fibroblast growth factor receptor-1 (FGFR-1) is essential for normal neural tube and limb development. *Dev Biol* 1997;185(1):42-54.
162. Hebert JM, Lin M, Partanen J, Rossant J, McConnell SK. FGF signaling through FGFR1 is required for olfactory bulb morphogenesis. *Development* 2003;130(6):1101-11.
163. Coumoul X, Shukla V, Li C, Wang RH, Deng CX. Conditional knockdown of FGFR2 in mice using Cre-LoxP induced RNA interference. *Nucleic Acids Res* 2005;33(11):e102.
164. Oh LY, Denninger A, Colvin JS, Vyas A, Tole S, Ornitz DM, et al. Fibroblast growth factor receptor 3 signaling regulates the onset of oligodendrocyte terminal differentiation. *J Neurosci* 2003;23(3):883-94.
165. Karoui M, Hofmann-Radvanyi H, Zimmermann U, Couvelard A, Degott C, Faridoni-Laurens L, et al. No evidence of somatic FGFR3 mutation in various types of carcinoma. *Oncogene* 2001;20(36):5059-61.

166. Klint P, Claesson-Welsh L. Signal transduction by fibroblast growth factor receptors. *Front Biosci* 1999;4:D165-77.
167. Bellus GA, Bamshad MJ, Przylepa KA, Dorst J, Lee RR, Hurko O, et al. Severe achondroplasia with developmental delay and acanthosis nigricans (SADDAN): phenotypic analysis of a new skeletal dysplasia caused by a Lys650Met mutation in fibroblast growth factor receptor 3. *Am J Med Genet* 1999;85(1):53-65.
168. Bellus GA, Spector EB, Speiser PW, Weaver CA, Garber AT, Bryke CR, et al. Distinct missense mutations of the FGFR3 lys650 codon modulate receptor kinase activation and the severity of the skeletal dysplasia phenotype. *Am J Hum Genet* 2000;67(6):1411-21.
169. Muenke M, Schell U. Fibroblast-growth-factor receptor mutations in human skeletal disorders. *Trends Genet* 1995;11(8):308-13.
170. Rousseau F, Bonaventure J, Legeai-Mallet L, Pelet A, Rozet JM, Maroteaux P, et al. Mutations in the gene encoding fibroblast growth factor receptor-3 in achondroplasia. *Nature* 1994;371(6494):252-4.
171. Tavormina PL, Shiang R, Thompson LM, Zhu YZ, Wilkin DJ, Lachman RS, et al. Thanatophoric dysplasia (types I and II) caused by distinct mutations in fibroblast growth factor receptor 3. *Nat Genet* 1995;9(3):321-8.
172. Naski MC, Wang Q, Xu J, Ornitz DM. Graded activation of fibroblast growth factor receptor 3 by mutations causing achondroplasia and thanatophoric dysplasia. *Nat Genet* 1996;13(2):233-7.

173. Tavormina PL, Bellus GA, Webster MK, Bamshad MJ, Fraley AE, McIntosh I, et al. A novel skeletal dysplasia with developmental delay and acanthosis nigricans is caused by a Lys650Met mutation in the fibroblast growth factor receptor 3 gene. *Am J Hum Genet* 1999;64(3):722-31.
174. Webster MK, D'Avis PY, Robertson SC, Donoghue DJ. Profound ligand-independent kinase activation of fibroblast growth factor receptor 3 by the activation loop mutation responsible for a lethal skeletal dysplasia, thanatophoric dysplasia type II. *Mol Cell Biol* 1996;16(8):4081-7.
175. Webster MK, Donoghue DJ. Constitutive activation of fibroblast growth factor receptor 3 by the transmembrane domain point mutation found in achondroplasia. *Embo J* 1996;15(3):520-7.
176. Ornitz DM, Marie PJ. FGF signaling pathways in endochondral and intramembranous bone development and human genetic disease. *Genes Dev* 2002;16(12):1446-65.
177. Bellus GA, Gaudenz K, Zackai EH, Clarke LA, Szabo J, Francomano CA, et al. Identical mutations in three different fibroblast growth factor receptor genes in autosomal dominant craniosynostosis syndromes. *Nat Genet* 1996;14(2):174-6.
178. Hevner RF. The cerebral cortex malformation in thanatophoric dysplasia: neuropathology and pathogenesis. *Acta Neuropathol (Berl)* 2005;110(3):208-21.

179. Goutieres F, Aicardi J, Farkas-Bargeton E. [An unusual cerebral malformation associated with thanatophoric dwarfism]. *Rev Neurol (Paris)* 1971;125(6):435-40.
180. Dode C, Levilliers J, Dupont JM, De Paepe A, Le Du N, Soussi-Yanicostas N, et al. Loss-of-function mutations in FGFR1 cause autosomal dominant Kallmann syndrome. *Nat Genet* 2003;33(4):463-5.
181. Gonzalez-Martinez D, Hu Y, Bouloux PM. Ontogeny of GnRH and olfactory neuronal systems in man: novel insights from the investigation of inherited forms of Kallmann's syndrome. *Front Neuroendocrinol* 2004;25(2):108-30.
182. Eswarakumar VP, Lax I, Schlessinger J. Cellular signaling by fibroblast growth factor receptors. *Cytokine Growth Factor Rev* 2005;16(2):139-49.
183. Fioretos T, Panagopoulos I, Lassen C, Swedin A, Billstrom R, Isaksson M, et al. Fusion of the BCR and the fibroblast growth factor receptor-1 (FGFR1) genes as a result of t(8;22)(p11;q11) in a myeloproliferative disorder: the first fusion gene involving BCR but not ABL. *Genes Chromosomes Cancer* 2001;32(4):302-10.
184. Yoshimura N, Sano H, Hashiramoto A, Yamada R, Nakajima H, Kondo M, et al. The expression and localization of fibroblast growth factor-1 (FGF-1) and FGF receptor-1 (FGFR-1) in human breast cancer. *Clin Immunol Immunopathol* 1998;89(1):28-34.
185. Kobrin MS, Yamanaka Y, Friess H, Lopez ME, Korc M. Aberrant expression of type I fibroblast growth factor receptor in human pancreatic adenocarcinomas. *Cancer Res* 1993;53(20):4741-4.

186. Kwabi-Addo B, Ropiquet F, Giri D, Ittmann M. Alternative splicing of fibroblast growth factor receptors in human prostate cancer. *Prostate* 2001;46(2):163-72.
187. Yamaguchi F, Saya H, Bruner JM, Morrison RS. Differential expression of two fibroblast growth factor-receptor genes is associated with malignant progression in human astrocytomas. *Proc Natl Acad Sci U S A* 1994;91(2):484-8.
188. Jang JH, Shin KH, Park JG. Mutations in fibroblast growth factor receptor 2 and fibroblast growth factor receptor 3 genes associated with human gastric and colorectal cancers. *Cancer Res* 2001;61(9):3541-3.
189. Cappellen D, De Oliveira C, Ricol D, de Medina S, Bourdin J, Sastre-Garau X, et al. Frequent activating mutations of FGFR3 in human bladder and cervix carcinomas. *Nat Genet* 1999;23(1):18-20.
190. van Rhijn BW, Lurkin I, Radvanyi F, Kirkels WJ, van der Kwast TH, Zwarthoff EC. The fibroblast growth factor receptor 3 (FGFR3) mutation is a strong indicator of superficial bladder cancer with low recurrence rate. *Cancer Res* 2001;61(4):1265-8.
191. Onose H, Emoto N, Sugihara H, Shimizu K, Wakabayashi I. Overexpression of fibroblast growth factor receptor 3 in a human thyroid carcinoma cell line results in overgrowth of the confluent cultures. *Eur J Endocrinol* 1999;140(2):169-73.

192. Wu R, Connolly D, Ngelangel C, Bosch FX, Munoz N, Cho KR. Somatic mutations of fibroblast growth factor receptor 3 (FGFR3) are uncommon in carcinomas of the uterine cervix. *Oncogene* 2000;19(48):5543-6.
193. Jang JH, Shin KH, Park YJ, Lee RJ, McKeehan WL, Park JG. Novel transcripts of fibroblast growth factor receptor 3 reveal aberrant splicing and activation of cryptic splice sequences in colorectal cancer. *Cancer Res* 2000;60(15):4049-52.
194. Yagasaki F, Wakao D, Yokoyama Y, Uchida Y, Murohashi I, Kayano H, et al. Fusion of ETV6 to fibroblast growth factor receptor 3 in peripheral T-cell lymphoma with a t(4;12)(p16;p13) chromosomal translocation. *Cancer Res* 2001;61(23):8371-4.
195. Chesi M, Nardini E, Brents LA, Schrock E, Ried T, Kuehl WM, et al. Frequent translocation t(4;14)(p16.3;q32.3) in multiple myeloma is associated with increased expression and activating mutations of fibroblast growth factor receptor 3. *Nat Genet* 1997;16(3):260-4.
196. Streit S, Bange J, Fichtner A, Ihrler S, Issing W, Ullrich A. Involvement of the FGFR4 Arg388 allele in head and neck squamous cell carcinoma. *Int J Cancer* 2004;111(2):213-7.
197. Alberts B. *Molecular Biology of The Cell*. 4th ed.
198. Broek D, Bartlett R, Crawford K, Nurse P. Involvement of p34cdc2 in establishing the dependency of S phase on mitosis. *Nature* 1991;349(6308):388-93.

199. Hahn WC, Counter CM, Lundberg AS, Beijersbergen RL, Brooks MW, Weinberg RA. Creation of human tumour cells with defined genetic elements. *Nature* 1999;400(6743):464-8.
200. Druker BJ, Mamon HJ, Roberts TM. Oncogenes, growth factors, and signal transduction. *N Engl J Med* 1989;321(20):1383-91.
201. Pawson T. Protein modules and signalling networks. *Nature* 1995;373(6515):573-80.
202. Campbell SL, Khosravi-Far R, Rossman KL, Clark GJ, Der CJ. Increasing complexity of Ras signaling. *Oncogene* 1998;17(11 Reviews):1395-413.
203. Lewis TS, Shapiro PS, Ahn NG. Signal transduction through MAP kinase cascades. *Adv Cancer Res* 1998;74:49-139.
204. Kouhara H, Hadari YR, Spivak-Kroizman T, Schilling J, Bar-Sagi D, Lax I, et al. A lipid-anchored Grb2-binding protein that links FGF-receptor activation to the Ras/MAPK signaling pathway. *Cell* 1997;89(5):693-702.
205. Donohue PJ, Alberts GF, Hampton BS, Winkles JA. A delayed-early gene activated by fibroblast growth factor-1 encodes a protein related to aldose reductase. *J Biol Chem* 1994;269(11):8604-9.
206. Dan I, Watanabe NM, Kusumi A. The Ste20 group kinases as regulators of MAP kinase cascades. *Trends Cell Biol* 2001;11(5):220-30.
207. Chen Z, Gibson TB, Robinson F, Silvestro L, Pearson G, Xu B, et al. MAP kinases. *Chem Rev* 2001;101(8):2449-76.

208. Seger R, Seger D, Lozeman FJ, Ahn NG, Graves LM, Campbell JS, et al. Human T-cell mitogen-activated protein kinase kinases are related to yeast signal transduction kinases. *J Biol Chem* 1992;267(36):25628-31.
209. Lee HY, Suh YA, Robinson MJ, Clifford JL, Hong WK, Woodgett JR, et al. Stress pathway activation induces phosphorylation of retinoid X receptor. *J Biol Chem* 2000;275(41):32193-9.
210. Sherr CJ. Cancer cell cycles. *Science* 1996;274(5293):1672-7.
211. DeGregori J. The genetics of the E2F family of transcription factors: shared functions and unique roles. *Biochim Biophys Acta* 2002;1602(2):131-50.
212. Gille H, Kortenjann M, Thomae O, Moomaw C, Slaughter C, Cobb MH, et al. ERK phosphorylation potentiates Elk-1-mediated ternary complex formation and transactivation. *Embo J* 1995;14(5):951-62.
213. Kim HJ, Bar-Sagi D. Modulation of signalling by Sprouty: a developing story. *Nat Rev Mol Cell Biol* 2004;5(6):441-50.
214. Hacohen N, Kramer S, Sutherland D, Hiromi Y, Krasnow MA. sprouty encodes a novel antagonist of FGF signaling that patterns apical branching of the *Drosophila* airways. *Cell* 1998;92(2):253-63.
215. Zhang S, Lin Y, Itaranta P, Yagi A, Vainio S. Expression of Sprouty genes 1, 2 and 4 during mouse organogenesis. *Mech Dev* 2001;109(2):367-70.
216. Hall AB, Jura N, DaSilva J, Jang YJ, Gong D, Bar-Sagi D. hSpry2 is targeted to the ubiquitin-dependent proteasome pathway by c-Cbl. *Curr Biol* 2003;13(4):308-14.

217. Hanafusa H, Torii S, Yasunaga T, Nishida E. Sprouty1 and Sprouty2 provide a control mechanism for the Ras/MAPK signalling pathway. *Nat Cell Biol* 2002;4(11):850-8.
218. Fong CW, Leong HF, Wong ES, Lim J, Yusoff P, Guy GR. Tyrosine phosphorylation of Sprouty2 enhances its interaction with c-Cbl and is crucial for its function. *J Biol Chem* 2003;278(35):33456-64.
219. Dickinson RJ, Eblaghie MC, Keyse SM, Morriss-Kay GM. Expression of the ERK-specific MAP kinase phosphatase PYST1/MKP3 in mouse embryos during morphogenesis and early organogenesis. *Mech Dev* 2002;113(2):193-6.
220. Engelhardt CM, Bundschu K, Messerschmitt M, Renne T, Walter U, Reinhard M, et al. Expression and subcellular localization of Spred proteins in mouse and human tissues. *Histochem Cell Biol* 2004;122(6):527-38.
221. Furthauer M, Lin W, Ang SL, Thisse B, Thisse C. Sef is a feedback-induced antagonist of Ras/MAPK-mediated FGF signalling. *Nat Cell Biol* 2002;4(2):170-4.
222. Lupas A. Coiled coils: new structures and new functions. *Trends Biochem Sci* 1996;21(10):375-82.
223. Harbury PB, Zhang T, Kim PS, Alber T. A switch between two-, three-, and four-stranded coiled coils in GCN4 leucine zipper mutants. *Science* 1993;262(5138):1401-7.
224. Crick. The packing of α -helices: simple coiled coils. *Acta Crystallographica* 1953;6:689.

225. Fuchs E, Weber K. Intermediate filaments: structure, dynamics, function, and disease. *Annu Rev Biochem* 1994;63:345-82.
226. Crick FH. Is alpha-keratin a coiled coil? *Nature* 1952;170(4334):882-3.
227. Herrmann H, Aebi U. Structure, assembly, and dynamics of intermediate filaments. *Subcell Biochem* 1998;31:319-62.
228. Burkhard P, Stetefeld J, Strelkov SV. Coiled coils: a highly versatile protein folding motif. *Trends Cell Biol* 2001;11(2):82-8.
229. Wolkoff AW, Klausner RD, Ashwell G, Harford J. Intracellular segregation of asialoglycoproteins and their receptor: a prelysosomal event subsequent to dissociation of the ligand-receptor complex. *J Cell Biol* 1984;98(2):375-81.
230. Bomsel M, Parton R, Kuznetsov SA, Schroer TA, Gruenberg J. Microtubule- and motor-dependent fusion in vitro between apical and basolateral endocytic vesicles from MDCK cells. *Cell* 1990;62(4):719-31.
231. Vale RD. The molecular motor toolbox for intracellular transport. *Cell* 2003;112(4):467-80.
232. Vale RD, Reese TS, Sheetz MP. Identification of a novel force-generating protein, kinesin, involved in microtubule-based motility. *Cell* 1985;42(1):39-50.
233. Paschal BM, Vallee RB. Retrograde transport by the microtubule-associated protein MAP 1C. *Nature* 1987;330(6144):181-3.
234. Robb MJ, Wilson MA, Vierula PJ. A fungal actin-related protein involved in nuclear migration. *Mol Gen Genet* 1995;247(5):583-90.

235. Sapir T, Elbaum M, Reiner O. Reduction of microtubule catastrophe events by LIS1, platelet-activating factor acetylhydrolase subunit. *Embo J* 1997;16(23):6977-84.
236. Sapir T, Cahana A, Seger R, Nekhai S, Reiner O. LIS1 is a microtubule-associated phosphoprotein. *Eur J Biochem* 1999;265(1):181-8.
237. Karcher RL, Deacon SW, Gelfand VI. Motor-cargo interactions: the key to transport specificity. *Trends Cell Biol* 2002;12(1):21-7.
238. Nguyen MD, Shu T, Sanada K, Lariviere RC, Tseng HC, Park SK, et al. A NUDEL-dependent mechanism of neurofilament assembly regulates the integrity of CNS neurons. *Nat Cell Biol* 2004;6(7):595-608.
239. Smith DS, Niethammer M, Ayala R, Zhou Y, Gambello MJ, Wynshaw-Boris A, et al. Regulation of cytoplasmic dynein behaviour and microtubule organization by mammalian Lis1. *Nat Cell Biol* 2000;2(11):767-75.
240. Niethammer M, Smith DS, Ayala R, Peng J, Ko J, Lee MS, et al. NUDEL is a novel Cdk5 substrate that associates with LIS1 and cytoplasmic dynein. *Neuron* 2000;28(3):697-711.
241. Sasaki S, Shionoya A, Ishida M, Gambello MJ, Yingling J, Wynshaw-Boris A, et al. A LIS1/NUDEL/cytoplasmic dynein heavy chain complex in the developing and adult nervous system. *Neuron* 2000;28(3):681-96.
242. Hilfiker S, Greengard P, Augustine GJ. Coupling calcium to SNARE-mediated synaptic vesicle fusion. *Nat Neurosci* 1999;2(2):104-6.

243. Safieddine S, Ly CD, Wang YX, Wang CY, Kachar B, Petralia RS, et al. Ocsyn, a novel syntaxin-interacting protein enriched in the subapical region of inner hair cells. *Mol Cell Neurosci* 2002;20(2):343-53.
244. Cyr JL, Brady ST. Molecular motors in axonal transport. Cellular and molecular biology of kinesin. *Mol Neurobiol* 1992;6(2-3):137-55.
245. Zhai RG, Vardinon-Friedman H, Cases-Langhoff C, Becker B, Gundelfinger ED, Ziv NE, et al. Assembling the presynaptic active zone: a characterization of an active one precursor vesicle. *Neuron* 2001;29(1):131-43.
246. Su Q, Cai Q, Gerwin C, Smith CL, Sheng ZH. Syntabulin is a microtubule-associated protein implicated in syntaxin transport in neurons. *Nat Cell Biol* 2004;6(10):941-53.
247. Kammerer RA, Schulthess T, Landwehr R, Lustig A, Engel J, Aebi U, et al. An autonomous folding unit mediates the assembly of two-stranded coiled coils. *Proc Natl Acad Sci U S A* 1998;95(23):13419-24.
248. Spek EJ, Bui AH, Lu M, Kallenbach NR. Surface salt bridges stabilize the GCN4 leucine zipper. *Protein Sci* 1998;7(11):2431-7.
249. O'Shea EK, Klemm JD, Kim PS, Alber T. X-ray structure of the GCN4 leucine zipper, a two-stranded, parallel coiled coil. *Science* 1991;254(5031):539-44.
250. Landschulz WH, Johnson PF, McKnight SL. The leucine zipper: a hypothetical structure common to a new class of DNA binding proteins. *Science* 1988;240(4860):1759-64.

251. O'Shea EK, Rutkowski R, Kim PS. Evidence that the leucine zipper is a coiled coil. *Science* 1989;243(4890):538-42.
252. Lumb KJ, Carr CM, Kim PS. Subdomain folding of the coiled coil leucine zipper from the bZIP transcriptional activator GCN4. *Biochemistry* 1994;33(23):7361-7.
253. Vinson C, Myakishev M, Acharya A, Mir AA, Moll JR, Bonovich M. Classification of human B-ZIP proteins based on dimerization properties. *Mol Cell Biol* 2002;22(18):6321-35.
254. Gonzalez GA, Montminy MR. Cyclic AMP stimulates somatostatin gene transcription by phosphorylation of CREB at serine 133. *Cell* 1989;59(4):675-80.
255. Eferl R, Wagner EF. AP-1: a double-edged sword in tumorigenesis. *Nat Rev Cancer* 2003;3(11):859-68.
256. Zhu S, Yoon K, Sterneck E, Johnson PF, Smart RC. CCAAT/enhancer binding protein-beta is a mediator of keratinocyte survival and skin tumorigenesis involving oncogenic Ras signaling. *Proc Natl Acad Sci U S A* 2002;99(1):207-12.
257. la Cour T, Gupta R, Rapacki K, Skriver K, Poulsen FM, Brunak S. NESbase version 1.0: a database of nuclear export signals. *Nucleic Acids Res* 2003;31(1):393-6.
258. Wozniak RW, Rout MP, Aitchison JD. Karyopherins and kissing cousins. *Trends Cell Biol* 1998;8(5):184-8.

259. Talcott B, Moore MS. Getting across the nuclear pore complex. *Trends Cell Biol* 1999;9(8):312-8.
260. Nigg EA. Nucleocytoplasmic transport: signals, mechanisms and regulation. *Nature* 1997;386(6627):779-87.
261. Bogerd HP, Fridell RA, Benson RE, Hua J, Cullen BR. Protein sequence requirements for function of the human T-cell leukemia virus type 1 Rex nuclear export signal delineated by a novel in vivo randomization-selection assay. *Mol Cell Biol* 1996;16(8):4207-14.
262. Wen W, Meinkoth JL, Tsien RY, Taylor SS. Identification of a signal for rapid export of proteins from the nucleus. *Cell* 1995;82(3):463-73.
263. Fischer U, Huber J, Boelens WC, Mattaj IW, Luhrmann R. The HIV-1 Rev activation domain is a nuclear export signal that accesses an export pathway used by specific cellular RNAs. *Cell* 1995;82(3):475-83.
264. Fornerod M, Ohno M, Yoshida M, Mattaj IW. CRM1 is an export receptor for leucine-rich nuclear export signals. *Cell* 1997;90(6):1051-60.
265. Fukuda M, Asano S, Nakamura T, Adachi M, Yoshida M, Yanagida M, et al. CRM1 is responsible for intracellular transport mediated by the nuclear export signal. *Nature* 1997;390(6657):308-11.
266. Adachi Y, Yanagida M. Higher order chromosome structure is affected by cold-sensitive mutations in a *Schizosaccharomyces pombe* gene *crm1+* which encodes a 115-kD protein preferentially localized in the nucleus and its periphery. *J Cell Biol* 1989;108(4):1195-207.

267. Meissner T, Krause E, Vinkemeier U. Ratjadone and leptomycin B block CRM1-dependent nuclear export by identical mechanisms. *FEBS Lett* 2004;576(1-2):27-30.
268. Kudo N, Wolff B, Sekimoto T, Schreiner EP, Yoneda Y, Yanagida M, et al. Leptomycin B inhibition of signal-mediated nuclear export by direct binding to CRM1. *Exp Cell Res* 1998;242(2):540-7.
269. Fukuda M, Gotoh I, Gotoh Y, Nishida E. Cytoplasmic localization of mitogen-activated protein kinase kinase directed by its NH₂-terminal, leucine-rich short amino acid sequence, which acts as a nuclear export signal. *J Biol Chem* 1996;271(33):20024-8.
270. Stommel JM, Marchenko ND, Jimenez GS, Moll UM, Hope TJ, Wahl GM. A leucine-rich nuclear export signal in the p53 tetramerization domain: regulation of subcellular localization and p53 activity by NES masking. *Embo J* 1999;18(6):1660-72.
271. Xiao Z, Brownawell AM, Macara IG, Lodish HF. A novel nuclear export signal in Smad1 is essential for its signaling activity. *J Biol Chem* 2003;278(36):34245-52.
272. Kallstrom H, Lindqvist A, Pospisil V, Lundgren A, Rosenthal CK. Cdc25A localisation and shuttling: characterisation of sequences mediating nuclear export and import. *Exp Cell Res* 2005;303(1):89-100.
273. Karin M, Hunter T. Transcriptional control by protein phosphorylation: signal transmission from the cell surface to the nucleus. *Curr Biol* 1995;5(7):747-57.

274. Lenormand P, Sardet C, Pages G, L'Allemain G, Brunet A, Pouyssegur J. Growth factors induce nuclear translocation of MAP kinases (p42mapk and p44mapk) but not of their activator MAP kinase kinase (p45mapkk) in fibroblasts. *J Cell Biol* 1993;122(5):1079-88.
275. Fukuda M, Gotoh Y, Nishida E. Interaction of MAP kinase with MAP kinase kinase: its possible role in the control of nucleocytoplasmic transport of MAP kinase. *Embo J* 1997;16(8):1901-8.
276. Tanaka TS, Jaradat SA, Lim MK, Kargul GJ, Wang X, Grahovac MJ, et al. Genome-wide expression profiling of mid-gestation placenta and embryo using a 15,000 mouse developmental cDNA microarray. *Proc Natl Acad Sci U S A* 2000;97(16):9127-32.
277. FitzGerald UF, Gilbey T, Brodie S, Barnett SC. Transcription factor expression and cellular redox in immature oligodendrocyte cell death: effect of Bcl-2. *Mol Cell Neurosci* 2003;22(4):516-29.
278. Patterson GH, Knobel SM, Sharif WD, Kain SR, Piston DW. Use of the green fluorescent protein and its mutants in quantitative fluorescence microscopy. *Biophys J* 1997;73(5):2782-90.
279. Biederbick A, Kern HF, Elsasser HP. Monodansylcadaverine (MDC) is a specific in vivo marker for autophagic vacuoles. *Eur J Cell Biol* 1995;66(1):3-14.
280. Serrano M, Lin AW, McCurrach ME, Beach D, Lowe SW. Oncogenic ras provokes premature cell senescence associated with accumulation of p53 and p16INK4a. *Cell* 1997;88(5):593-602.

281. Bayne EH, Allshire RC. RNA-directed transcriptional gene silencing in mammals. *Trends Genet* 2005;21(7):370-3.
282. Temple S, Qian X. bFGF, neurotrophins, and the control of cortical neurogenesis. *Neuron* 1995;15(2):249-52.
283. Pellicano F, Inglis-Broadgate SL, Pante G, Ansorge W, Iwata T. Expression of coiled-coil protein 1, a novel gene downstream of FGF2, in the developing brain. *Gene Expr Patterns* 2005.
284. Gama-Carvalho M, Carmo-Fonseca M. The rules and roles of nucleocytoplasmic shuttling proteins. *FEBS Lett* 2001;498(2-3):157-63.
285. Farazi TA, Waksman G, Gordon JI. The biology and enzymology of protein N-myristoylation. *J Biol Chem* 2001;276(43):39501-4.
286. Vescovi AL, Reynolds BA, Fraser DD, Weiss S. bFGF regulates the proliferative fate of unipotent (neuronal) and bipotent (neuronal/astroglial) EGF-generated CNS progenitor cells. *Neuron* 1993;11(5):951-66.
287. Hevner RF, Daza RA, Rubenstein JL, Stunnenberg H, Olavarria JF, Englund C. Beyond laminar fate: toward a molecular classification of cortical projection/pyramidal neurons. *Dev Neurosci* 2003;25(2-4):139-51.
288. Caceres A, Banker G, Steward O, Binder L, Payne M. MAP2 is localized to the dendrites of hippocampal neurons which develop in culture. *Brain Res* 1984;315(2):314-8.
289. Soltysik-Espanola M, Rogers RA, Jiang S, Kim TA, Gaedigk R, White RA, et al. Characterization of Mayven, a novel actin-binding protein predominantly expressed in brain. *Mol Biol Cell* 1999;10(7):2361-75.

290. Hancock JF. Ras proteins: different signals from different locations. *Nat Rev Mol Cell Biol* 2003;4(5):373-84.
291. Homewood CA, Warhurst DC, Peters W, Baggaley VC. Lysosomes, pH and the anti-malarial action of chloroquine. *Nature* 1972;235(5332):50-2.
292. Lie SO, Schofield B. Inactivation of lysosomal function in normal cultured human fibroblasts by chloroquine. *Biochem Pharmacol* 1973;22(23):3109-14.
293. Cameron PL, Sudhof TC, Jahn R, De Camilli P. Colocalization of synaptophysin with transferrin receptors: implications for synaptic vesicle biogenesis. *J Cell Biol* 1991;115(1):151-64.
294. Dunn KW, McGraw TE, Maxfield FR. Iterative fractionation of recycling receptors from lysosomally destined ligands in an early sorting endosome. *J Cell Biol* 1989;109(6 Pt 2):3303-14.
295. Mu FT, Callaghan JM, Steele-Mortimer O, Stenmark H, Parton RG, Campbell PL, et al. EEA1, an early endosome-associated protein. EEA1 is a conserved alpha-helical peripheral membrane protein flanked by cysteine "fingers" and contains a calmodulin-binding IQ motif. *J Biol Chem* 1995;270(22):13503-11.
296. Yamashiro DJ, Tycko B, Fluss SR, Maxfield FR. Segregation of transferrin to a mildly acidic (pH 6.5) para-Golgi compartment in the recycling pathway. *Cell* 1984;37(3):789-800.
297. Fulton AB. How crowded is the cytoplasm? *Cell* 1982;30(2):345-7.
298. Klionsky DJ, Emr SD. Autophagy as a regulated pathway of cellular degradation. *Science* 2000;290(5497):1717-21.

299. Mizuno K, Kitamura A, Sasaki T. Rabring7, a novel Rab7 target protein with a RING finger motif. *Mol Biol Cell* 2003;14(9):3741-52.
300. Jadot M, Dubois F, Wattiaux-De Coninck S, Wattiaux R. Supramolecular assemblies from lysosomal matrix proteins and complex lipids. *Eur J Biochem* 1997;249(3):862-9.
301. Jockusch BM, Rudiger M. Crosstalk between cell adhesion molecules: vinculin as a paradigm for regulation by conformation. *Trends Cell Biol* 1996;6(8):311-5.
302. Weis K. Regulating access to the genome: nucleocytoplasmic transport throughout the cell cycle. *Cell* 2003;112(4):441-51.
303. van Hengel J, Vanhoenacker P, Staes K, van Roy F. Nuclear localization of the p120(ctn) Armadillo-like catenin is counteracted by a nuclear export signal and by E-cadherin expression. *Proc Natl Acad Sci U S A* 1999;96(14):7980-5.
304. Harbers M, Nomura T, Ohno S, Ishii S. Intracellular localization of the Ret finger protein depends on a functional nuclear export signal and protein kinase C activation. *J Biol Chem* 2001;276(51):48596-607.
305. Roux PP, Blenis J. ERK and p38 MAPK-activated protein kinases: a family of protein kinases with diverse biological functions. *Microbiol Mol Biol Rev* 2004;68(2):320-44.
306. Crews CM, Alessandrini A, Erikson RL. The primary structure of MEK, a protein kinase that phosphorylates the ERK gene product. *Science* 1992;258(5081):478-80.

307. Gross I, Bassit B, Benezra M, Licht JD. Mammalian sprouty proteins inhibit cell growth and differentiation by preventing ras activation. *J Biol Chem* 2001;276(49):46460-8.
308. Heerssen HM, Segal RA. Location, location, location: a spatial view of neurotrophin signal transduction. *Trends Neurosci* 2002;25(3):160-5.
309. Ferguson IA, Johnson EM, Jr. Fibroblast growth factor receptor-bearing neurons in the CNS: identification by receptor-mediated retrograde transport. *J Comp Neurol* 1991;313(4):693-706.
310. Blottner D, Stapf C, Meisinger C, Grothe C. Localization, differential expression and retrograde axonal transport suggest physiological role of FGF-2 in spinal autonomic neurons of the rat. *Eur J Neurosci* 1997;9(2):368-77.
311. Feng Y, Walsh CA. Protein-protein interactions, cytoskeletal regulation and neuronal migration. *Nat Rev Neurosci* 2001;2(6):408-16.
312. Feng Y, Walsh CA. Mitotic spindle regulation by Nde1 controls cerebral cortical size. *Neuron* 2004;44(2):279-93.
313. Johnson DG, Schwarz JK, Cress WD, Nevins JR. Expression of transcription factor E2F1 induces quiescent cells to enter S phase. *Nature* 1993;365(6444):349-52.
314. Matsuda S, Kawamura-Tsuzuku J, Ohsugi M, Yoshida M, Emi M, Nakamura Y, et al. Tob, a novel protein that interacts with p185erbB2, is associated with anti-proliferative activity. *Oncogene* 1996;12(4):705-13.

315. Kawamura-Tsuzuku J, Suzuki T, Yoshida Y, Yamamoto T. Nuclear localization of Tob is important for regulation of its antiproliferative activity. *Oncogene* 2004;23(39):6630-8.
316. Adachi M, Fukuda M, Nishida E. Nuclear export of MAP kinase (ERK) involves a MAP kinase kinase (MEK)-dependent active transport mechanism. *J Cell Biol* 2000;148(5):849-56.
317. Humbert P, Russell S, Richardson H. Dlg, Scribble and Lgl in cell polarity, cell proliferation and cancer. *Bioessays* 2003;25(6):542-53.
318. Fuchs E, Karakesisoglou I. Bridging cytoskeletal intersections. *Genes Dev* 2001;15(1):1-14.
319. Etienne-Manneville S, Hall A. Rho GTPases in cell biology. *Nature* 2002;420(6916):629-35.
320. Hall A, Nobes CD. Rho GTPases: molecular switches that control the organization and dynamics of the actin cytoskeleton. *Philos Trans R Soc Lond B Biol Sci* 2000;355(1399):965-70.
321. Lukaszewicz A, Savatier P, Cortay V, Kennedy H, Dehay C. Contrasting effects of basic fibroblast growth factor and neurotrophin 3 on cell cycle kinetics of mouse cortical stem cells. *J Neurosci* 2002;22(15):6610-22.
322. Cavanagh JF, Mione MC, Pappas IS, Parnavelas JG. Basic fibroblast growth factor prolongs the proliferation of rat cortical progenitor cells in vitro without altering their cell cycle parameters. *Cereb Cortex* 1997;7(4):293-302.
323. Tissir F, Goffinet AM. Reelin and brain development. *Nat Rev Neurosci* 2003;4(6):496-505.

324. Sequier JM, Hunziker W, Andressen C, Celio MR. Calbindin D-28k Protein and mRNA Localization in the Rat Brain. *Eur J Neurosci* 1990;2(12):1118-1126.
325. Marin O, Rubenstein JL. A long, remarkable journey: tangential migration in the telencephalon. *Nat Rev Neurosci* 2001;2(11):780-90.
326. McConnell SK, Kaznowski CE. Cell cycle dependence of laminar determination in developing neocortex. *Science* 1991;254(5029):282-5.
327. Ferguson KL, McClellan KA, Vanderluit JL, McIntosh WC, Schuurmans C, Polleux F, et al. A cell-autonomous requirement for the cell cycle regulatory protein, Rb, in neuronal migration. *Embo J* 2005;24(24):4381-91.
328. Brose K, Tessier-Lavigne M. Slit proteins: key regulators of axon guidance, axonal branching, and cell migration. *Curr Opin Neurobiol* 2000;10(1):95-102.
329. Yuan W, Zhou L, Chen JH, Wu JY, Rao Y, Ornitz DM. The mouse SLIT family: secreted ligands for ROBO expressed in patterns that suggest a role in morphogenesis and axon guidance. *Dev Biol* 1999;212(2):290-306.
330. Conover JC, Doetsch F, Garcia-Verdugo JM, Gale NW, Yancopoulos GD, Alvarez-Buylla A. Disruption of Eph/ephrin signaling affects migration and proliferation in the adult subventricular zone. *Nat Neurosci* 2000;3(11):1091-7.
331. Wong A, Lamothe B, Lee A, Schlessinger J, Lax I. FRS2 alpha attenuates FGF receptor signaling by Grb2-mediated recruitment of the ubiquitin ligase Cbl. *Proc Natl Acad Sci U S A*. 2002;99(10):6684-9.

332. Hicke L. A new ticket for entry into budding vesicles-ubiquitin.
Cell. 2001 Sep 7;106(5):527-30.
- 333 Marmor MD, Yarden Y. Role of protein ubiquitylation in regulating
endocytosis of receptor tyrosine kinases.Oncogene. 2004 Mar
15;23(11):2057-70.
334. Maxfield FR, McGraw TE. Endocytic recycling. Nat Rev Mol Cell Biol. 2004
Feb;5(2):121-32.